PREPARATION OF SOME SEMI-SYNTHETIC SAPONIN ANALOGS AND INVESTIGATION OF THEIR MECHANISM OF ACTION ON NECROTIC CELL DEATH

A Thesis Submitted to
The Graduate School of Engineering and Sciences of
İzmir Institute of Technology
in Partial Fulfilment of the Requirements for the Degree of

MASTER OF SCIENCE

in Biotechnology

by
Göklem ÜNER

June 2019
İZMİR

We approve the thesis of **Göklem ÜNER**

Examining Committee Members:

_____

Prof. Dr. Erdal BEDİR
Department of Bioengineering, İzmir Institute of Technology

_____

Assoc. Prof. Dr. Yasemin ERAÇ
Department of Pharmacology, Ege University

_____

Asst. Prof. Dr. Çiğdem TOSUN
Department of Molecular Biology and Genetic, İzmir Institute of Technology

16 July 2019

_____

Prof. Dr. Erdal BEDİR
Supervisor, Department of Bioengineering
İzmir Institute of Technology

_____

Prof. Dr. Petek BALLAR
Co-Supervisor, Department of
Pharmacology, Ege University

_____

Assoc. Prof. Dr. Engin ÖZÇİVİCİ
Head of the Department of Biotechnology
and Bioengineering

_____

Prof. Dr. Aysun SOFUOĞLU
Dean of the Graduate School of
Engineering and Sciences

ACKNOWLEDGMENTS

I am deeply grateful to my advisor Prof. Dr. Erdal BEDİR and to my co-advisor Prof. Dr. Petek BALLAR-KIRMIZIBAYRAK for continuous support of my master thesis and related research, for their all the encouragement, patience and immense knowledge. I'm very lucky to have the chance to carry out my thesis with their guidance.

My sincere thanks to my labmates of Natural Product Chemistry Laboratory and Laboratory of BALLAR for the sleepless nights we were working together and also all the fun and friendship. Besides, I must especially thank Sinem Yılmaz for everything she taught me and her valuable support. I cannot explain how important her support was. I also thank to Ünver KURT for all support and showing patience and tolerance during my working-times.

I would like to thank to 118S709 project supported by The Scientific and Technological Research Council of Turkey (TÜBİTAK), and the Scientific Research Project 2017IYTE71 by İzmir Institute of Technology.

Finally, I would like to thank my parents and Ferruh SOLAK for providing me with unfailing support and continuous encouragement throughout my years of study

ABSTRACT

PREPARATION OF SOME SEMI-SYNTHETIC SAPONIN ANALOGS AND INVESTIGATION OF THEIR MECHANISM OF ACTION ON NECROTIC CELL DEATH

Since antitumor potency of saponins is relatively weak, researchers focus on semi-synthetic modification of saponins to obtain highly potent structures. With the same motivation, we prepared cytotoxic sapogenol (AG-08), from cycloastragenol. Our preliminary studies revealed that AG-08 was inducing necrotic cell death together with autophagic inhibition. Furthermore, immunoblotting experiments suggested that AG-08 promoted cleavage of various proteins. A continuation study was performed in this thesis with aims of: i) verifying previous studies; ii) identifying molecular mechanism of AG-08; iii) preparing further analogs of AG-08 and deduce structure activity relationships(SAR).

Accordingly, necrotic cell death and autophagic inhibition via AG-08 was verified, and cytotoxicity of AG-08 on 13 cell lines was examined. Furthermore, inhibitors of calpain-1, general caspases, cathepsin B/L/S, and caspase-8 were found to partially alleviate cell death, whereas cathepsin D/E inhibitor were not able to do. Additionally, lysosomal impairment due to loss of acidic nature was demonstrated. Later data and effect of cathepsin inhibitor on AG-08 mediated cell death suggest lysosomal membrane permeabilization.

In synthesis part, 15 AG-08 analogs were prepared, three of which were cytotoxic. Additionally, active analogs triggered similar cell death mechanism with AG-08. SAR evaluation reveals that presence of tosyl, and tetrahydrofuran ring are required for activity, while double bond at C-6 is not essential.

Consequently, this thesis provides important data on mechanism of necrotic cell death and autophagic inhibition via AG-08 treatment as well as relationship between structure and activity. However, further studies are warranted to clarify complete mechanism of AG-08 and substantiate structure activity relationship deductions.

ÖZET

BAZI YARI-SENTETİK SAPONİN ANALOGLARININ HAZIRLANMASI VE BUNLARIN NEKROTİK HÜCRE ÖLÜMÜ ÜZERİNDEKİ AKTİVİTE MEKANİZMALARININ ARAŞTIRILMASI

Yarı-sentez çalışmaları, göreceli olarak düşük anti-tümör aktiviteye sahip saponinlerden yüksek potansiyele sahip yeni moleküller elde etmek için sıklıkla kullanılır. Bu amaçlar ile yürüttüğümüz bir proje kapsamında sikloastragenolden sitotoksik bir sapogenol analoğu olan AG-08 elde edilmiştir. Ön çalışmalarımız AG-08'in nekrotik hücre ölümüne ve otofaji inhibisyonuna neden olduğunu göstermiştir. Ayrıca immunoblotlama çalışmaları PARP-1, p62 ve ATG proteinlerinin AG-08 uygulaması ile kesildiğini işaret etmiştir. Bu tezin temel amaçları; i) ön dataları doğrulamak, ii) AG-08'in moleküler mekanizmasını aydınlatmak, iii) AG-08 analogları hazırlayıp yapı-aktivite ilişkisi kurmaktır. Bu kapsamda yapılan çalışmalar ile AG-08 aracılı nekrotik hücre ölümü ve otofaji inhibisyonu kanıtlanmıştır. Ayrıca 13 insan hücre hattı ile sitotoksisite taraması yapılarak AG-08'in seçiciliği araştırılmıştır. Çalışmalarımızın devamında kalpain, genel kaspaz, katepsin B/L/S ve kaspaz-8 inhibitörlerinin AG-08 aracılı hücre ölümünü zayıflatırken, katepsin D/E inhibitörünün etkilemediği görülmüştür. Lysotracker boyaması ile AG-08'in lizozomun asidik pH'sını kaybetmesine neden olduğu gösterilmiştir. Katepsin inhibitörlerinin hücre ölümü üzerine etkisi ve lizozomal bazifikasyon, AG-08'in lizozomal membran geçirgenliğine neden olduğunu işaret etmektedir. Yarı-sentez çalışmalarında ise 15 AG-08 analoğu sentezlenmiş ve bunlardan üç tanesi sitotoksik bulunmuştur. Devam çalışmaları üç analoğunda AG-08 ile benzer bir moleküler yolağı aktive ettiğini kanıtlamıştır. Oluşturulan yapı-aktivite ilişkisi, tosil grubunun ve tetrafuran halkasının aktivite için önemli olduğunu ancak C-6 ve C-7 arasındaki çift bağın önemli olmadığını ortaya koymuştur. Sonuç olarak, bu tez ile hem AG-08 aracılı hücre ölümünün moleküler yolağı ile ilgili hem de AG-08 ve analoglarının yapı-aktivite ilişkisi ile ilgili önemli bilgiler elde edilmiştir. Bununla birlikte, moleküler mekanizmanın tam olarak aydınlatılması ve yapı-aktivite ilişkisinin doğrulanması için ileri çalışmalar gerektiği açıktır.

TABLE OF CONTENTS

LIST OF FIGURES ix

LIST OF TABLES xi

LIST OF SPECTRA xii

ABBREVIATIONS xv

CHAPTER 1. INTRODUCTION 1

1.1. Regulated Cell Death 3

1.1.1. Apoptosis 4

1.1.2. Autophagy and Autophagy-Dependent Cell Death 5

1.1.3. Regulated Necrosis 7

1.1.3.1. Regulated Necrosis and Cancer Treatment 10

1.1.4. Crosstalk of RCD Types 11

1.2. Lysosome in Cell Death 13

1.3. Proteases Taking Role in Cell Death 16

1.4. Saponins and Cell Death 19

CHAPTER 2. MATERIALS AND METHODS 22

2.1. MATERIALS 22

2.1.1. Materials and Instruments for Synthesis 22

2.1.2. Materials for Bioactivity Studies 22

2.1.2.1. Antibodies 23

2.1.2.2. Chemical Agents and Kits 23

2.1.2.3. Buffers 23

2.2. Methods 24

2.2.1. Semi-Synthesis Studies 24

2.2.1.1. Separation and Purification of Semi-Synthetic Analogs 25
2.2.2. Bioactivity Studies 29
2.2.2.1. Mammalian Cell Culture Condition and Cell Passaging 29
2.2.2.2. Cell Freezing 29
2.2.2.3. Cytotoxicity Assay for Determination of IC_{50} values 29
2.2.2.4. Immunoblotting Studies 30
2.2.2.5. Inhibition of Proteases 31
2.2.2.6. Lysotracker Staining 32
2.2.2.7. LDH Assay 32

CHAPTER 3. RESULTS AND DISCUSSION 33
3.1. Biological Activity of AG-08 33
3.1.1. Cytotoxicity of AG-08 33
3.1.2. Effect of AG-08 on Autophagy 34
3.1.3. Effect of Proteas Inhibitors on AG-08-mediated Cell Death 38
3.1.4. Effect of AG-08 on Lysosome 40
3.2. Structural Elucidation of Semi-synthetic Derivatives 42
3.2.1. Structural Elucidation of Compound AG-02 42
3.2.2. Structural Elucidation of Compound AG-03 47
3.2.3. Structural Elucidation of Compound AG-04 52
3.2.4. Structural Elucidation of Compound AG-05 57
3.2.5. Structural Elucidation of Compound CG-02 62
3.2.6. Structural Elucidation of Compound CG-03 67
3.2.7. Structural Elucidation of Compound CG-04 72
3.2.8. Structural Elucidation of Compound CG-05 77
3.2.9. Structural Elucidation of Compound SCG-01 82
3.2.10. Structural Elucidation of Compound SCG-02 87
3.2.11. Structural Elucidation of Compound SCG-03 91
3.2.12. Structural Elucidation of Compound SCG-04 96
3.2.13. Structural Elucidation of Compound SCG-05 101

3.2.14. Structural Elucidation of Compound SCG-06 106
3.2.15. Structural Elucidation of Compound SCG-07 110
3.3. Biological Activity of AG-08 Derivatives 115
3.3.1. Cytotoxic Activity of Semi-Synthetic Derivatives 116
3.3.2. Molecular Mechanism of Action of Cytotoxic AG-08 Analogs .. 119

CHAPTER 4. CONCLUSION 122

REFERENCES 127

APPENDIX A. PREVIOUS RESULTS OF AG-08 151

LIST OF FIGURES

Figure **Page**

Figure 1. Semi-synthesis of AG-08 from CG. 2
Figure 2. Schematic illustration of autophagy 6
Figure 3. Different complexes by death receptor 9
Figure 4. Relationship between autophagy and apoptosis 12
Figure 5. Inducer of lysosomal membrane permeabilization. 15
Figure 6. Mechanism of main protease group. 17
Figure 7. Isolation Procedure of AG reaction with p-TsCl at room temperature. 26
Figure 8. Isolation Procedure of CG reaction with p-TsCl at room temperature. 26
Figure 9. Isolation Procedure of CG reaction with MsCl at room temperature..... 25
Figure 10. Isolation Procedure of SCG reaction with p-TsCl..... 27
Figure 11. Isolation Procedure of SCG reaction with p-TsCl..... 27
Figure 12. Isolation Procedure of SCG reaction with MsCl. 28
Figure 13. Isolation Procedure of AG reaction with MsCl. 28
Figure 14. Release of LDH by AG-08 treatment. 34
Figure 15. Effect of AG-08 on autophagic proteins.. 36
Figure 16. Effect of IC_{50} treatment on the autophagic protein levels 37
Figure 17. Co-treatment of CHX and AG-08. 37
Figure 18. The effect of protease inhibitors on AG-08 mediated cell death. 39
Figure 19. Lysotracker staining of AG-08 exposed cells. 41
Figure 20. Chemical Structure of AG-02..... 42
Figure 21. Chemical Structure of AG-03..... 47
Figure 22. Chemical Structure of AG-04..... 52
Figure 23. Chemical Structure of AG-05..... 57
Figure 24. Chemical Structure of CG-02. 62
Figure 25. Chemical Structure of CG-03. 67
Figure 26. Chemical Structure of CG-04. 72
Figure 27. Chemical Structure CG-05. 77
Figure 28. Chemical Structure of SCG-01..... 82
Figure 29. Chemical Structure of SCG-02..... 87
Figure 30. Chemical Structure of SCG-03..... 91

Figure **Page**

Figure 31. Chemical Structure of SCG-04..... 96
Figure 32. Chemical Structure of SCG-05..... 101
Figure 33. Chemical Structure of SCG-06..... 106
Figure 34. Chemical Structure of SCG-07..... 110
Figure 35. Structure of AG derivatives..... 115
Figure 36. Structure of CG derivatives..... 115
Figure 37. Structure of SCG derivatives..... 116
Figure 38. Release of LDH with AG-08 analogs..... 120
Figure 39. Immuno-blotting studies with cytotoxic analogs. 121
Figure 40. Structures of cytotoxic analogs and their parent compounds with their IC_{50} values (μM) versus HCC1937 cell line..... 124
Figure 41. 7-AAD/ Annexin V staining in flow cytometry (A) and acridine orange/ ethidium bromide fluorescent staining (B) of AG-08 treated..... 151
Figure 42. Immunoblotting image which show cleavage of PARP-1 with AG-08 151
Figure 43. Investigation of caspases activation with AG-08 152
Figure 44. Effect of AG-08 on autophagic marker 152

LIST OF TABLES

Table **Page**

Table 1. Starting materials and reagents with reaction conditions. 24
Table 2. Preparation of stacking and resolving gel. 31
Table 3. IC_{50} values of AG-08 versus 13 human cell lines 35
Table 4. The ^{13}C and ^{1}H NMR data of AG-02 (100/500 MHz, δ ppm, in $CDCl_3$) 43
Table 5. The ^{13}C and ^{1}H NMR data of AG-03 (100/500 MHz, δ ppm, in $CDCl_3$). 48
Table 6. The ^{13}C and ^{1}H NMR data of AG-04 (100/500 MHz, δ ppm, in $CDCl_3$). 53
Table 7. The ^{13}C and ^{1}H NMR data of AG-05 (100/400 MHz, δ ppm, in $CDCl_3$). 58
Table 8. The ^{13}C and ^{1}H NMR data of CG-02 (100/500 MHz, δ ppm, in $CDCl_3$). 63
Table 9. The ^{13}C and ^{1}H NMR data of CG-03 (100/500 MHz, δ ppm, in $CDCl_3$). 68
Table 10. The ^{13}C and ^{1}H NMR data of CG-04 (100/500 MHz, δ ppm, in $CDCl_3$). 73
Table 11. The ^{13}C and ^{1}H NMR data of CG-05 (100/500 MHz, δ ppm, in $CDCl_3$). 78
Table 12. The ^{13}C and ^{1}H NMR data of SCG-01 (100/500 MHz, δ ppm, in $CDCl_3$). 82
Table 13. The ^{13}C and ^{1}H NMR data of SCG-02 (100/500 MHz, δ ppm, in $CDCl_3$). 87
Table 14. The ^{13}C and ^{1}H NMR data of SCG-03 (100/500 MHz, δ ppm, in $CDCl_3$). 92
Table 15. The ^{13}C and ^{1}H NMR data of SCG-04 (100/400 MHz, δ ppm, in $CDCl_3$). 97
Table 16. The ^{13}C and ^{1}H NMR data of SCG-05 (100/500 MHz, δ ppm, in $CDCl_3$). ... 101
Table 17. The ^{13}C and ^{1}H NMR data of SCG-06 (100/500 MHz, δ ppm, in $CDCl_3$). ... 106
Table 18. The ^{13}C and ^{1}H NMR data of SCG-07 (100/500 MHz, δ ppm, in $CDCl_3$). ... 111
Table 19. IC_{50} values (μM) of analogs and parent molecules. 117
Table 20. IC_{50} values (μM) of cytotoxic analogs and AG-08. 119

LIST OF SPECTRA

Spectrum **Page**

Spectrum 1. HR-ESI-MS Spectrum of AG-02 (positive mode) 44
Spectrum 2. ^{1}H NMR Spectrum of AG-02. 44
Spectrum 3. ^{13}C NMR Spectrum of AG-02. 45
Spectrum 4. DEPT135 spectrum of AG-02. 45
Spectrum 5. COSY spectrum of AG-02 46
Spectrum 6. HMQC spectrum of AG-02. 46
Spectrum 7. HMBC spectrum of AG-02. 47
Spectrum 8. HR-ESI-MS Spectrum of AG-03 (positive mode). 49
Spectrum 9. ^{1}H NMR Spectrum of AG-03. 49
Spectrum 10. ^{13}C NMR Spectrum of AG-03. 50
Spectrum 11. DEPT135 spectrum of AG-03. 50
Spectrum 12. COSY spectrum of AG-03. 51
Spectrum 13. HMQC spectrum of AG-03. 51
Spectrum 14. HMBC spectrum of AG-03. 52
Spectrum 15. HR-ESI-MS Spectrum of AG-04 (positive mode). 54
Spectrum 16. ^{1}H NMR Spectrum of AG-04. 54
Spectrum 17. ^{13}C NMR Spectrum of AG-04. 55
Spectrum 18. DEPT135 spectrum of AG-04. 55
Spectrum 19. COSY spectrum of AG-04. 56
Spectrum 20. HMQC spectrum of AG-04 56
Spectrum 21. HMBC spectrum of AG-04 57
Spectrum 22. HR-ESI-MS Spectrum of AG-05 (positive mode). 59
Spectrum 23. ^{1}H NMR Spectrum of AG-05. 59
Spectrum 24. ^{13}C NMR Spectrum of AG-05. 60
Spectrum 25. COSY spectrum of AG-05. 60
Spectrum 26. HSQC spectrum of AG-05. 61
Spectrum 27. HMBC spectrum of AG-05. 61
Spectrum 28. HMBC spectrum of AG-05. 62
Spectrum 29. HR-ESI-MS Spectrum of CG-02 (positive mode). 64
Spectrum 30. ^{1}H NMR Spectrum of CG-02. 64
Spectrum 31. ^{13}C NMR Spectrum of CG-02. 65
Spectrum 32. DEPT135 spectrum of CG-02. 65
Spectrum 33. COSY spectrum of CG-02. 66
Spectrum 34. HMQC spectrum of CG-02. 66
Spectrum 35. HMBC spectrum of CG-02. 67
Spectrum 36. HR-ESI-MS Spectrum of CG-03 (positive mode). 69

Spectrum **Page**

Spectrum 37. ^{1}H NMR Spectrum of CG-03. 69
Spectrum 38. ^{13}C NMR Spectrum of CG-03. 70
Spectrum 39. DEPT135 spectrum of CG-03. 70
Spectrum 40. COSY spectrum of CG-03. 71
Spectrum 41. HMQC spectrum of CG-03. 71
Spectrum 42. HMBC spectrum of CG-03. 72
Spectrum 43. HR-ESI-MS Spectrum of CG-04 (positive mode). 74
Spectrum 44. ^{1}H NMR Spectrum of CG-04. 74
Spectrum 45. ^{13}C NMR Spectrum of CG-04. 75
Spectrum 46. DEPT135 spectrum of CG-04**.** 75
Spectrum 47. COSY spectrum of CG-04. 76
Spectrum 48. HMQC spectrum of CG-04. 76
Spectrum 49. HMBC spectrum of CG-04. 77
Spectrum 50. ^{1}H NMR Spectrum of CG-05. 79
Spectrum 51. ^{13}C NMR Spectrum of CG-05. 79
Spectrum 52. DEPT135 spectrum of CG-05. 80
Spectrum 53. COSY spectrum of CG-05. 80
Spectrum 54. HMQC spectrum of CG-05. 81
*S*pectrum 55. HMBC spectrum of CG-05. 81
Spectrum 56. HR-ESI-MS Spectrum of SCG-01 (positive mode). 83
Spectrum 57. ^{1}H NMR Spectrum of SCG-01 84
Spectrum 58. ^{13}C NMR Spectrum of SCG-01. 84
Spectrum 59. DEPT135 spectrum of SCG-01. 85
Spectrum 60. COSY spectrum of SCG-01. 85
Spectrum 61. HMQC spectrum of SCG-01. 86
Spectrum 62. HMBC spectrum of SCG-01. 86
Spectrum 63. ^{1}H NMR Spectrum of SCG-02. 88
Spectrum 64. ^{13}C NMR Spectrum of SCG-02. 89
Spectrum 65. DEPT135 spectrum of SCG-02. 89
Spectrum 66. COSY spectrum of SCG-02. 90
Spectrum 67. HSQC spectrum of SCG-02. 90
Spectrum 68. HMBC spectrum of SCG-02. 91
Spectrum 69. HR-ESI-MS Spectrum of SCG-03 (positive mode). 93
Spectrum 70. ^{1}H NMR Spectrum of SCG-03. 93
Spectrum 71. ^{13}C NMR Spectrum of SCG-03. 94
Spectrum 72. DEPT135 spectrum of SCG-03. 94
Spectrum 73. COSY spectrum of SCG-03. 95
Spectrum 74. HMQC spectrum of SCG-03. 95

Spectrum **Page**

Spectrum 75. HMBC spectrum of SCG-03. 96
Spectrum 76. ^{1}H NMR Spectrum of SCG-04. 98
Spectrum 77. ^{13}C NMR Spectrum of SCG-04. 98
Spectrum 78. COSY spectrum of SCG-04. 99
Spectrum 79. HMQC spectrum of SCG-04. 99
Spectrum 80. HMBC spectrum of SCG-04. 100
Spectrum 81. HMBC spectrum of SCG-04. 100
Spectrum 82. ^{1}H NMR Spectrum of SCG-05. 102
Spectrum 83. HR-ESI-MS Spectrum of SCG-05 (positive mode). 103
Spectrum 84. ^{13}C NMR Spectrum of SCG-05. 103
Spectrum 85. DEPT135 spectrum of SCG-05. 104
Spectrum 86. COSY spectrum of SCG-05. 104
Spectrum 87. HMQC spectrum of SCG-05. 105
Spectrum 88. HMBC spectrum of SCG-05. 105
Spectrum 89. ^{1}H NMR Spectrum of SCG-06. 107
Spectrum 90. ^{13}C NMR Spectrum of SCG-06. 108
Spectrum 91. DEPT135 spectrum of SCG-06. 108
Spectrum 92. COSY spectrum of SCG-06. 109
Spectrum 93. HMQC spectrum of SCG-06. 109
Spectrum 94. HMBC spectrum of SCG-06. 110
Spectrum 95. HR-ESI-MS Spectrum of SCG-07 (positive mode). 111
Spectrum 96. ^{1}H NMR Spectrum of SCG-07. 112
Spectrum 97. ^{13}C NMR Spectrum of SCG-07. 112
Spectrum 98. DEPT135 spectrum of SCG-07. 113
Spectrum 99. COSY spectrum of SCG-07. 113
Spectrum 100. HMQC spectrum of SCG-07. 114
Spectrum 101. HMBC spectrum of SCG-07. 114

ABBREVIATIONS

^{13}C NMR	Carbon Nuclear Magnetic Resonance
1D-NMR	One-Dimensional Nuclear Magnetic Resonance
^{1}H NMR	Proton Nuclear Magnetic Resonance
2D-NMR	Two-Dimensional Nuclear Magnetic Resonance
AG	Astragenol
AIF1	Apoptosis inducing factor mitochondria associated 1
Amu	Atomic mass unit
Apaf-1	Apoptosis protease-activating factor 1
Baf A1	Bafilomycin A1
brs	Broad singled
CAT-I	Cathepsin Inhibitor I
CDDO	2-cyano-3,12-dioxoolean-1,9-dien-28-oic acid
CG	Cycloastragenol
$CHCl_3$	Chloroform
CHX	Cycloheximide
COSY	Correlation Spectroscopy
CyloHXN	Cyclohexane
CYPD	Cyclophylline D (CYPD)
d	Doubled
DCM	Dichloromethane
dd	Doubled-doubled
DISC	Death-inducing signaling complex
DMSO	Dimethyl sulfoxide
EtOAc	Ethyl Acetate
FADD	Fas-associated death domain
HMBC	Heteronuclear Multiple Bond Coherence
HSQC	Heteronuclear Single Quantum Coherence
Hxn	n-Hexane
m	Multiplied
MeOH	Methanol
MIF	Macrophage migration inhibitory factor (MIF)

MLKL	Mixed lineage kinase domain like pseudokinase
MsCl	Methanesulfonyl chloride
PARP-1	Poly(ADP-ribose) polymerase 1 (PARP1)
PBS	Phosphate Buffered Saline
PCD	Programmed cell death
PE	Petroleum ether
Pep A	Pepstatin A
p-TsCl	p-Toluenesulfonyl chloride
RCD	Regulated cell death
RN	Regulated necrosis
s	Singled
SCG	20(27)-octanor cycloastragenol
SDS	Sodium dodecyl sulfate
Sta	Staurosporin
Si	Silica
t	Tripled
td	Tripled of doubled
TEA	Triethylamine
TNF	Tumor necrosis factor
UV	Ultraviolet

CHAPTER 1

INTRODUCTION

Saponins are secondary metabolites exhibiting diverse biological activities. Anti-tumor effect of saponins has been demonstrated in numerous studies. However, in many cases, the potency of saponins is relatively weak. Therefore, anticipating highly potent novel structures, scientists have begun bioassay-directed drug design and synthesis. One of the most recent studies has revealed that semi-synthetic oleanane-type saponin, 2-cyano-3,12-dioxoolean-1,9-dien-28-oic acid (CDDO) is a multi-functional molecule with promising clinical potential as a chemopreventive agent and as a therapeutic agent for the treatment of cancer. Up to 10.000-fold activity increase of CDDO compared to the starting molecule (oleanolic acid) has proven that semi-synthesis studies might be a promising approach to discover and develop saponin-based anti-cancer drugs.

Semi-synthetic anticancer drug-discovery programs focusing on the saponin group have mainly engaged with commercially available triterpenoids such as oleanolic acid and ursolic acid, not including less common miscellaneous aglycons such as cycloartanes, lanostanes, and hopanes. Our group carried out a TUBITAK project (109S345) with cycloartanes and aimed to prepare new anti-tumor agents from cycloastragenol (CG) and cyclocanthogenol (SKG), which are the main aglycones of many cycloartane-type glycosides, via semi-synthesis and biotransformation studies. In the project, 71 new compounds were synthesized from CG and its commercial production artifact astragenol (AG). Also, 15 new compounds were produced from CG, AG, and SKG by biotransformation studies. Seven of the semi-synthetic derivatives were found to be cytotoxic versus cancer and normal cell lines in MTT assays. In our subsequent studies, one of the active substances, namely AG-08, showed non-canonical cell death and became a molecule of interest due to its unexpected feature (results of studies were given in Appendices section).

AG-08 exhibited cytotoxicity against HeLa and HCC1937 cell lines with IC_{50} values less than 10 μM. 7-AAD/Annexin V and ethidium bromide/acridine orange staining of AG-08 treated HCC1937 cells suggested that AG-08 induced necrotic cell death instead of apoptosis (Figure 40). Also, formation of 50 kDa fragments of PARP-1

supported necrotic cell death (Figure 41). Overriding basis for this deduction is that the cleavage of PARP-1 into 89 kDa and 24 kDa by caspases is a widely used biomarker for apoptosis, and 50 kDa fragments of PARP-1 indicates necrotic cell death as reported previously (Gobeil et al. 2001, Chaitanya, Steven, and Babu 2010). In these studies, by Gobeil and Chaitanya et al., it was shown that lysosomal cathepsins were responsible for 50 kDa fragments of PARP-1 during necrotic cell death. Based on this crucial data, it is likely that AG-08 mediated cell death involves cathepsins. Furthermore, in our studies, observation of caspase 8 and 3 activations but not caspase 9 was exciting finding as these caspases are well-known apoptotic effectors and generally are not related to necrotic cell death (Figure 42).

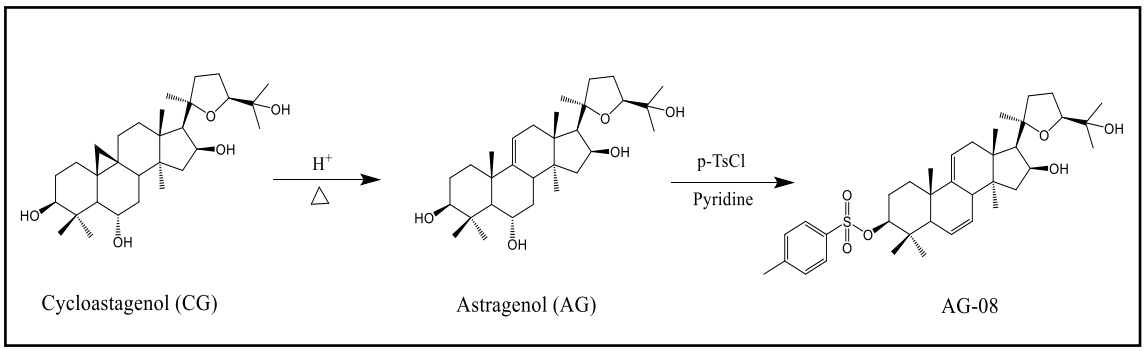

Figure 1. Semi-synthesis of AG-08 from CG.

Moreover, AG-08 had effects on autophagy involving two steps. Firstly, increase in LC3-II level suggested vacuole accumulation due to autophagic flux inhibition. Interestingly, decrease in full-length p62 was observed which was accompanied with the formation of 20 kDa fragments (Figure 43). P62 is usually accumulated during autophagic flux inhibition and decreased level of p62 shows autophagic activation. But several studies have shown that cleavage of p62 with proteases may lead to a decrease in protein level even in the case of autophagic inhibition (Klionsky et al. 2016). Correspondingly, the formation of 20 kDa fragments via cleavage of p62 explained that the full-length protein accumulation was not the case upon AG-08 treatment. In the second phase of autophagy inhibition, we observed reduction of various Atg proteins, probably due to proteases activation (Figure 43). Calpains and caspases have been reported to be able to cleave ATGs (Norman, Cohen, and Bampton 2014). Since autophagy required the

presence of ATGs, the formation of autophagic vacuole was abolished by AG-08 in this stage.

Intriguing results of our preliminary studies prompted us to investigate the death mechanism of AG-08 more intensely. Thus, in this thesis, further molecular studies were carried out to verify necrotic cell death and autophagic inhibitory properties of AG-08. In the second part, analogs of AG-08 were prepared synthetically, and their biological activities were investigated to understand structure-activity relationship (SAR).

1.1. Regulated Cell Death

Cell death is an essential process for multicellular organisms. Beside passive cell death triggered by critical structural damage which cells cannot protect their integrity, active cell death is modulated by one or more signal transduction modules. Active cell death plays a critical role in tissue turnover, cell number balancing, development, morphogenesis, and elimination of harmful cells. While most of the sources used programmed cell death (PCD), active cell death was named as regulated cell death (RCD) by Nomenclature Committee on Cell Death 2018 and they defined PCD as a particular type of RCD (Galluzzi et al. 2018, Ashkenazi and Salvesen 2014, Chen, Kang, and Fu 2018). PCD is directly related with physiological process and occur without exogenous environmental stress signals. In addition to PCD, however, RCD also includes stress-induced cell death caused by intracellular or extracellular signals that the cell cannot overcome (Galluzzi et al. 2018).

Due to the function in physiological and pathophysiological processes, any deregulation of RCD lead to various diseases such as cancer and neurodegenerative disorders (Chen, Kang, and Fu 2018, Fulda 2013). Especially cancer is related with RCD at numerous points. Firstly, cancer formation and progression simply depend on imbalance between cell death and proliferation. Additionally, almost all cancer treatment strategies rely on induction of RCD in cancer cells. Therefore, RCD is critical in cancer treatment and protection from carcinogenesis (Mishra et al. 2018).

Several specific RCD forms have been identified by numerous studies. Despite different classifications of them, RCD can be classified into apoptosis, autophagic cell death and regulated necrosis depending on morphological features. They are not

completely irrelevant mechanisms and may share similar molecular pathways (Chen, Kang, and Fu 2018).

1.1.1. Apoptosis

Apoptosis, which is the best characterized RCD type, provoke various morphological changes such as cell shrinkage, formation of apoptotic bodies, nuclear condensation and fragmentation and plasma membrane blebbing. In addition to that, cytoplasm is dense, cell size is smaller, and organelles are more tightly packed in apoptotic cells (Elmore 2007). As for biochemical change, exposure of phosphatidyl-l-serine on the outer plasma membrane and fragmentation of DNA etc. occurs during (Saraste and Pulkki 2000, Chen, Kang, and Fu 2018).

Caspases, are cysteine proteases family, are generally effectors of apoptosis. They can be categorized into apoptotic and inflammatory caspases. Apoptotic caspases can also be divided into two groups as initiator and effector caspases depending on mechanism of action. Initiator caspases such as caspase 8 and 9 initiate caspase cascade and activate effector caspases like caspase 3 (McIlwain, Berger, and Mak 2013, Li and Yuan 2008).

Intrinsic, extrinsic, and perforin/granzyme pathway are three molecular signaling pathways of apoptosis. In perforin/ granzyme pathway; cytotoxic T cells, which are immune system cells, use perforin and/or granzyme to induce apoptosis in virus-infected or transformed cells (Trapani and Smyth 2002). Extrinsic apoptosis triggered by binding of death ligands to death receptors which are members of tumor necrosis factor (TNF) receptor gene superfamily on the cell membrane. FasL/FasR, TNF-α/TNFR1, Apo3L/DR3 can be example for ligand/receptor interaction. When a ligand binds to the death receptor, pro-caspase 8 and FADD (Fas-associated death domain) form a complex named as DISC (death-inducing signaling complex), and caspase 8 is autocatalytically activated (Jin and El-Deiry 2014). Intrinsic apoptosis is induced by intercellular signals instead of extracellular ligand and involves mitochondrial outer membrane permeabilization (MOMP) (Elmore 2007). Pro-apoptotic protein such as cytochrome c, Smac/DIABLO, and serine protease HtrA2/Omi etc. are released to cytoplasm from mitochondria through MOMP. Cytochrome c, Apaf-1 (apoptosis protease-activating factor 1) and procaspase-9 form a complex named apoptosome and caspases cascade

starts with activation of caspase 9 in this complex (Chen, Kang, and Fu 2018, Lawen 2003).

Mitochondrial change during apoptosis controlled by Bcl-2 protein family. Bcl-2 protein can act as anti-apoptotic (Bcl-2, Bcl-x, Bcl-XL, Bcl-XS etc.) or pro-apoptotic (Bax, Bak, Bid, Bad, Bim etc.). When pro-apoptotic Bcl-2 protein dominate, MOMP is promoted. Meanwhile, MOMP can also occur during extrinsic pathway. Activated caspase 8 can activate Bid and this protein initiate MOMP process (Campbell and Tait 2018, Nikoletopoulou et al. 2013).

Both in extrinsic and intrinsic pathway, initiator caspases cleave and activate effector caspases like caspase 3 which culminating with starting final pathway of apoptosis. Effector caspases and some other proteases activated by effector caspases cleave various structural proteins, PARP-1, the nuclear protein NuMA etc. to kill cell. Lastly, apoptotic bodies, which are membrane bound vesicles, form. This cell fragments are eliminated by macrophage through phagocytosis. Macrophages recognize apoptotic cells by specific signals like phosphatidylserine translocation from inner membrane to outer membrane of cells (Jin and El-Deiry 2014).

1.1.2. Autophagy and Autophagy-Dependent Cell Death

Autophagy may be defined as a lysosome-mediated intracellular degradation process. Autophagy is used for recycling of long-lived proteins and organelles as well as degradation of damaged ones. Autophagy plays a pivotal role in maintaining cell survival under various stress conditions (Jacquin et al. 2017).

There are three different types of autophagy: macro-autophagy, microautophagy, and chaperone-mediated autophagy. In micro-autophagy, the cytosolic components to be degraded are taken directly by the lysosome through invasion of the lysosomal membrane (Mizushima and Komatsu 2011). Chaperone-mediated autophagy involves selective translocation of the cytoplasmic proteins to lysosome by chaperones such as Hsp-70. Chaperons are recognized by lysosomal receptors called lysosomal-associated membrane protein 2A and lysosome takes cytoplasmic cargo for degradation (Kaminskyy and Zhivotovsky 2012). In macro-autophagy, cytoplasmic cargo is translocated to lysosome by double membrane-bound vesicle called autophagosome (Mizushima 2007b). Autophagy is often used to describe macro-autophagy, while other types of autophagy

should be specified with names. Hence, autophagy from now on will be used to indicate macro-autophagy in this thesis.

Activation of AMPK and/or inhibition of mTOR induce beginning of autophagy mechanism. The first step of autophagy is formation of phagophore (isolation membrane). Although phagophores are mainly generated from ER membrane, exact source of phagophore in mammalian is not precise. Several pieces of evidence indicated that the Golgi complex, the mitochondria membrane, and the plasma membrane may contribute to the formation of phagophore (Mizushima and Komatsu 2011). Formed phagophore starts sequestering cytoplasmic cargo and membrane of phagophore elongate to form autophagosome. Autophagosome then fuses with lysosome to form new vacuole called autolysosome. Hydrolases in lysosome degrade cytoplasmic material in autophagosome along with inner membrane of autophagosome (Figure 2) (Mizushima 2007a). Autophagy is controlled by ATG proteins like Beclin-1, Atg-5, Atg-3 etc. There are more than 30 ATG proteins playing a major role in different steps of autophagic pathway. Most of ATG proteins take role in formation of autophagosome (Shimizu et al. 2014).

Autophagy is mostly activated in starvation to provide energy. In this case, autophagosome non-selectively sequesters part of cytoplasm and degrade its content to obtain energy. However, autophagy also plays an important role in protecting hemostasis by selectively degradation of aggregated protein or damaged organelles in non-starved cells (Zaffagnini and Martens 2016).

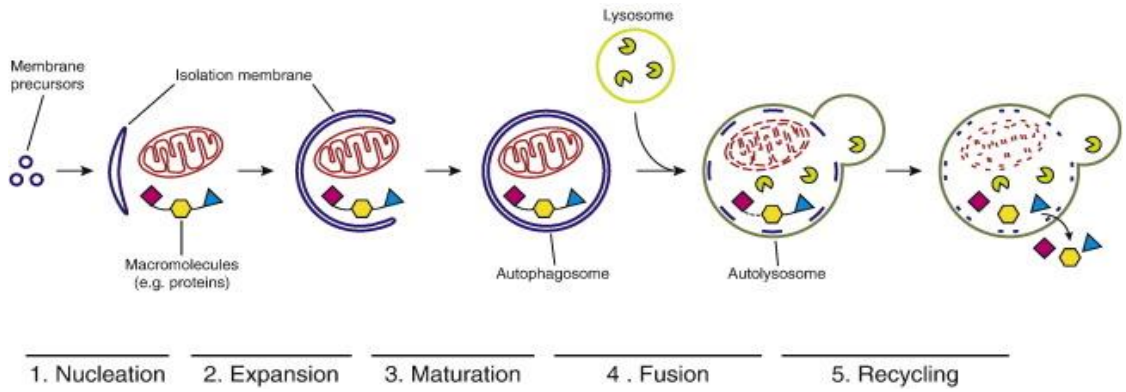

Figure 2. Schematic illustration of autophagy (Source: Zaffagnini and Martens 2016)

Autophagy usually provides cell survival and inhibition of autophagy makes cells susceptible to death. However, in some conditions, activation of autophagy mediate a certain type of cell death, called autophagic cell death or autophagy-dependent cell death (ODCD) (Shimizu et al. 2014, Bialik, Dasari, and Kimchi 2018). Autophagy is often activated during stress-driven cell death as protection mechanism or sometimes it may accelerate different type of cell death. However, autophagic cell death does not mean a cell death involving autophagic activation. Nomenclature Committee on Cell Death 2018 defined ODCD as cell death that relies on autophagic machinery and is ceased by inhibition of autophagy (Galluzzi et al. 2018). Though autophagic vacuole accumulation is a major morphological changing during autophagic cell death, it is necessary but not sufficient to detect ODCD since another main reason of autophagic vacuole accumulation is inhibition of autophagy (Vegliante and Ciriolo 2018).

Although role of ODCD in development of Drosophila and *Caenorhabditis elegans* as well as pathological conditions such as neonatal hypoxia-ischemia and myocardial infarction were reported (Galluzzi et al. 2018), molecular mechanism of ODCD has not been fully identified yet. However evidences indicated that OCDC were triggered in apoptosis resistance cells through MAPK c-Jun N-terminal kinase (JNK) dependent pathway (Shimizu et al. 2010). Moreover, prolonged exposure of hypoxia trigger autophagic cell death even with intact apoptotic machinery (Azad et al. 2008).

1.1.3. Regulated Necrosis

In contrast with necrosis that is accidental and uncontrollable cell death, regulated necrosis (RN) is controlled by complex cell signals and takes role in both physiological and pathological processes (Galluzzi et al. 2014, Kim 2017). RN may be defined as regulated cell death which eventually ends with cellular leakage. Unlike apoptosis, necrotic cells release pro-inflammatory signals. Cellular and organelle swelling, loss of membrane integrity, mitochondria swelling, and cytoplasmic granulation are morphological characteristics of RN. (Soriano et al. 2017). There are several cell death pathways involving the morphological features of RN and they are considered to be subtype of RN namely necroptosis, ferroptosis, parthanatos, pyroptosis and mitochondrial permeability transition (MPT)-driven necrosis (Conrad et al. 2016).

Necroptosis is most well-studied form of regulated necrosis. After its discovery, this term improperly used as synonym of RN. But now, necroptosis is defined as a type of RN which depend on RIP3, MLKL (mixed lineage kinase domain like pseudokinase) and RIP1 (mostly but not always) (Galluzzi et al. 2014). Necroptosis is triggered by binding death receptor to death ligands. When death ligands bind their receptor, RIPK3 is activated by RIPK1. However, there are alternative ways to activate RIP3 in case of RIP1 independent necroptosis. Activated RIP3 phosphorylate MLKL and it is translocated to plasma membrane. Although MLKL is main player of necroptosis, exact mechanism of its role is not fully understood yet. Even so, numerous laboratory studies have shown that MLKL promote activation of cell-surface proteases of the ADAM family and increase the sodium influx when located in plasma membrane (Cai et al. 2016b, Chen et al. 2014).

Mostly binding of death ligand and death receptor cause formation of complex IIa or IIb which cause apoptosis and RIP1 dependent apoptosis, respectively. But condition like caspases inhibition or increasing protein level of RIP3 results in complex IIc, in other name necrosome, formation and beginning of necroptosis. While complex IIa and IIb dependent on caspase 8 activation, caspase 8 inactivate necroptosis via cleavage of RIP1 and RIP3 (Figure 3) (Conrad et al. 2016).

Ferroptosis is a lipid peroxidation dependent and caspases independent RCD form. Whereas ferroptosis is accepted as a type of regulated necrosis in most sources, some articles refer to ferroptosis as a different cell death mechanism from main 3 RCD types. But ferroptosis is considered to be a kind of RN in this thesis because of its necrotic morphotypes such as electron-dense ultrastructure, outer mitochondrial membrane rupture and immune reaction (Galluzzi et al. 2018). Enzymatic and non-enzymatic reaction may control ferroptosis by lipid peroxidation. Non-enzymatic reactions are stems from iron, which is known as one of the main inducers of ferroptosis. İron accumulation results in lipid peroxidation through lysosomal fenton type reaction (Xie et al. 2016, Torii et al. 2016). Enzymatic reaction involves inactivation of GPX4 (Glutathione Peroxidase 4) which is known as an endogenous inhibitor of ferroptosis. GSH (glutathione) depletion is main reason for losing activity of GPX4 since it catalyzes GSH dependent reduction of lipid peroxidation. Therefore, GSH is also other important player of ferroptosis. Obstruction of GSH synthesis via inactivation of cystine/glutamate antiporter system X^c which provide cysteine to cells is one of main pathways of ferroptosis induction (Yang and Stockwell 2016).

Parthanatos is another RN type that relies on over-activation of poly (ADP-ribose) polymerase 1 (PARP1). Since PARP-1 use NAD^+ (Nicotinamide adenine dinucleotide) for its function, over-activity of PARP1 lead to depletion of NAD+ and eventually, depletion of ATP. As a result, cells die due to lack of energy (David et al. 2009). Parthanatos mechanism includes apoptosis-inducing factor mitochondria associated 1 (AIF1 or AIF) and macrophage migration inhibitory factor (MIF). Binding of PARP1 to AIF results in releasing of AIF from the mitochondria to the cytosol, followed by translocation into the nucleus. In addition, AIF lead translocation of MIF into the nucleus. They mediate DNA cleavage and chromatin condensation during parthanatos (Wang et al. 2016). MPT-driven necrosis is type of cell death that based on increasing the permeability of the inner mitochondrial membrane to small solutes. In contrast to MOMP inducing MPT in apoptosis, permeability transition pore complex (PTPC) which is supramolecular complex formed between inner and outer mitochondrial membranes, is responsible for MPT in MPT-driven necrosis (Izzo et al. 2016, Galluzzi et al. 2014). Although extensive research has been carried out on MPT-driven necrosis, cyclophylline D (CYPD) is the only protein determined to play an important role in this cell death type (Nakagawa et al. 2005, Galluzzi et al. 2018).

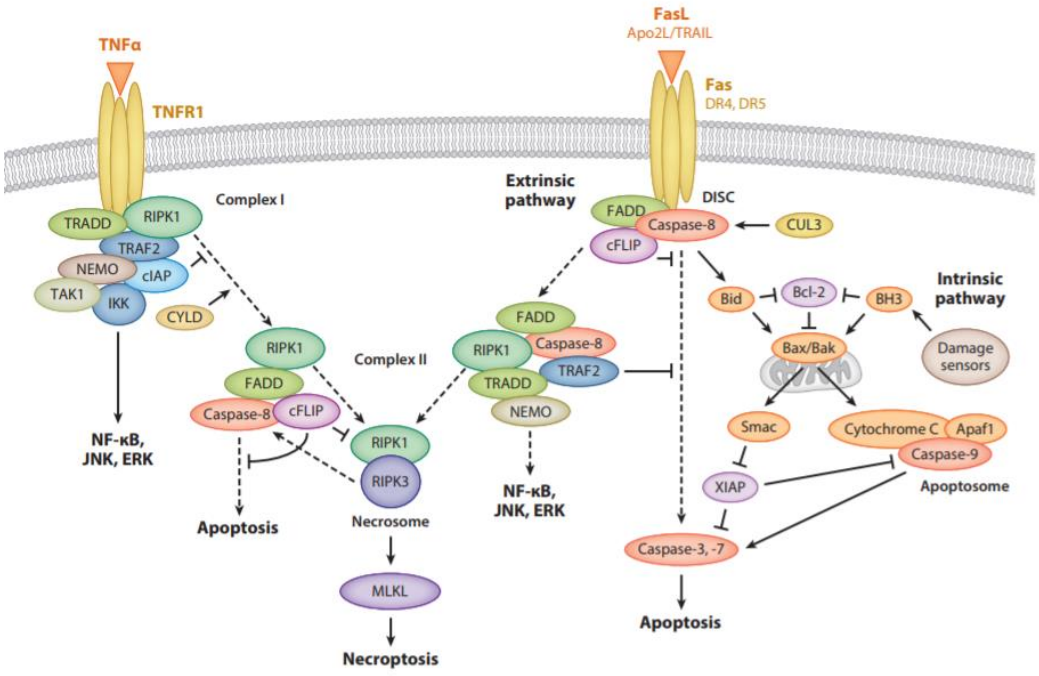

Figure 3. Different complexes by death receptor (Source: Ashkenazi and Salvesen 2014)

Pyroptosis may be defined as a regulated necrosis type that relies on gasdermin protein family especially gasdermin D. Cell swelling and membrane rupture during pyroptosis are compatible morphological changes with necrotic cell death. Additionally, peculiar form of chromatin condensation and pyroptotic bodies similar to apoptotic bodies are seen in pyroptotic cell death. Both pyroptotic bodies and chromatin condensatation are different from those occurring in apoptosis (Chen et al. 2016, Jorgensen and Miao 2015). Molecular mechanism of pyroptosis usually include inflammatory caspases namely caspase 1, caspase 4, caspase 5, and caspase 11. Inflammatory caspases cleave gasdermin family and form pyroptotic fragments which oligomerize to generate pores on cell membrane (Kovacs and Miao 2017). Pyroptosis involve inflammasome formation as well as releasing cytokines IL-1β and IL-18 (Man, Karki, and Kanneganti 2017). Although first studies indicated that only monocytes undergo pyroptosis, non-monocytes cells also having inflammatory caspases may die with pyroptosis (Shi et al. 2014).

1.1.3.1. Regulated Necrosis and Cancer Treatment

OCDC has lowest killing potential due to survival role of autophagy while the regulated necrosis is reported as the RCD type with the most killing potential (Chen, Kang, and Fu 2018). Thus, after discovery of regulated necrosis, induction of necrotic cell death in anti-cancer treatment become the one of main topic of conversation. The most controversial issue about RN is the immune reaction that is widely considered tumor supporting process (Hanahan and Weinberg 2011). However, necrosis also may induce anti-tumor immunity which enhance treatment (Amaravadi and Thompson 2007). Therefore, more researhes especially clinical studies are required to determine effect of immun response via necrosis on cancer treatment.

There are no drug which approved as necrotic cell death inducer in market. But studies uncovered that some approved anti-cancer drug induce necrosis. Imatinib which is inhibitor of ABL tyrosine kinase was approved by FDA at 2001 for cancer treatment. Three years later, Okada and friends (2004) reported that imatinib exposed cells exhibit necrotic morphology independent from caspases. Cell death triggered by imatinib relies on serine protease Omi/HtrA2 that released from mitochondria (Okada et al. 2004). Sorafenib, is another FDA approved tyrosine kinase inhibitor for cancer treatment, induce

ferroptosis. While iron chaletor namely deferoxamine, abrogated cell death, do not inhibite tyrosine kinesa inhibition. Therefore sorafenib induce ferroptosis and tyrosine kinase inhibition via independent pathway (Louandre et al. 2013, Lachaier et al. 2014). DNA alkylating/damaging agents were demonstrated that induce necrotic cell death due to over activation of PARP-1. Along similar lines, necrotic cell death via Oxaliplatin, is one of DNA damaging agents approved by FDA, were reported. Oxaliplatin trigger ATP depletion due to over-activation of PARP-1. Also, it was shown that oxaliplatin mediated cell death depend on RIP-1but not RIP-3 (Wu et al. 2015).

Not only small molecules, approved monocular antibodies (mAb) were reported as necrotic inducer. Type II anti-CD20 mAbs (tositumomab and GA101) and anti-HLA DR mAbs (L243, 1D10, and WR18) induce non-apoptotic cell death which have necrotic features. Cell death mediated by mAb is independent from Bcl-2 protein and caspases. These mAbs cause ROS generation via nicotinamide adenine dinucleotide phosphate (NADPH) oxidase and subsequently lysosomal membrane permeabilization (see section 1.2.) (Ivanov et al. 2009, Honeychurch et al. 2012)

1.1.4. Crosstalk of RCD Types

Forms of RCD are controlled by specific cell signals. However, it has been demonstrated that molecular pathway of them may overlap (Nikoletopoulou et al. 2013). Relationship of autophagy and apoptosis is complex and situation dependent. Anti-apoptotic Bcl-2 protein and Beclin-1, is key protein for autophagy, are well-known intersection of apoptosis and autophagy. Beclin-1 and Bcl-2 protein bind each other under normal condition and autophagy cannot be activated in this circumstance. Some apoptotic inducer signals result in releasing of Beclin-1 and consequently activation of autophagy. In contrast, caspase-3 activated during apoptosis cleave Beclin-1 culminating with autophagic inhibition. (Gump and Thorburn 2011). Atg-12 which is autophagic protein is another intersection point having dual role. Conjugation of ATG12 to ATG3 result in enhanced BCL-XL expression and apoptosis inhibition. However, unconjugated ATG12 may induce mitochondrial-dependent apoptosis (Tait, Ichim, and Green 2014). These molecular connections represent complex and changeable interaction of apoptosis and autophagy

Autophagy and apoptosis may control activity of each other through degradation of critical proteins of other. Several studies revealed that autophagy is antagonized by apoptosis activation due to cleavage of autophagic proteins with caspases (Cho et al. 2009, Djavaheri-Mergny, Maiuri, and Kroemer 2010). Moreover, calpain, another proteases family which may be activated during apoptosis, inhibit autophagy by cleavage of Atg-5 (Yousefi et al. 2006). Vice versa is also possible. Some cell type can evade apoptosis whereby autophagy mediated degradation of active caspase 8. For example, treatment with trail to Bax $^{-/--}$ Hct116 colon carcinoma cells (having resistance to Trial mediated apoptosis) cause autophagy activation. Activated autophagy degrades active form of caspase 8 which result in apoptosis inhibition. Prognosticatively, inhibition of autophagy leads to caspase-dependent apoptosis in same situation (Hou et al. 2010).

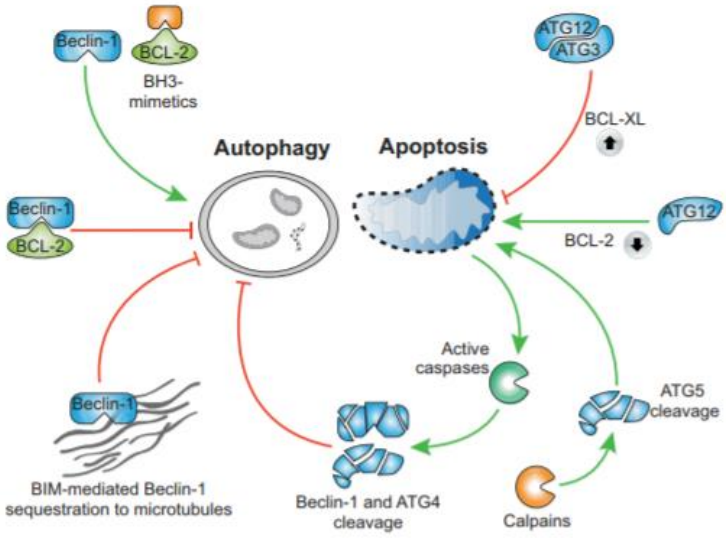

Figure 4. Relationship between autophagy and apoptosis (Source: Tait, Ichim, and Green 2014)

As for relationship between autophagy and RN forms, a number of studies have postulated a convergence between ferroptosis and autophagy. Simultaneous activation of autophagy with ferroptosis lead to degradation of cellular iron stock protein, ferritin, by specific autophagic pathway called ferritinophagy. Lacking ferritin increase cell death via ferroptosis as a result of cells being susceptible to iron related ROS accumulation (Gao et al. 2016, Masaldan et al. 2018). Opposite relationship was reported in simultaneously activation of parthanatos and autophagy under oxidative stress. Autophagy play a pre-

survival role in this case and inactivation of autophagy enhance cell death by parthanatos (Jiang et al. 2018). Necroptosis is also directly associated with autophagy. A recent study has shown that binding of p62 to RIP1 is necessary for TRAIL-induced necroptosis and lacking p62 cause switching of necroptosis to apoptosis. Interestingly inhibition of late stage autophagy enhances necroptosis while inhibition of early step cease cell death. Therefore, autophagic machinery may have effect on necroptosis independent from its degradation function (Goodall et al. 2016). Additionally, autophagic dependent RIP-1 degradation may culminate with necroptosis inhibition (Tait, Ichim, and Green 2014).

RN and apoptosis usually accepted as opposite mechanism. RN activation is largely displayed in case of apoptosis malfunction. A well-characterized example of it is that Tnf-α induced necroptosis. As mention previously, binding Tnf-α to death receptor may lead formation three different complexes. While two of them end up with apoptosis, formation of third complex in case of harmed apoptotic machines cause necroptosis (Conrad et al. 2016). Furthermore, as previously mentioned, degradation of RIP3 and RIP1 by caspase 8 activation leads to inhibition of necroptosis. Hereby, apoptosis negatively control necroptosis due to cleavage of critical proteins (Lin et al. 1999, Feltham, Vince, and Lawlor 2017). Switching apoptosis to necrosis-like cell death (not necroptosis) by Tnf-α induction was reported at low extracellular pH (Meurette et al. 2005). Further studies demonstrate that this necrotic cell death depend on caspase activation and RIP1. Interestingly, caspase 8 cannot degrade RIP1 in acidic condition, but do it in the neutral state as in the inhibition of necroptosis by caspase 8 (Meurette et al. 2007).

1.2. Lysosome in Cell Death

Lysosome, an acidic organelle, is responsible for degradation of extracellular cargo as well as cellular components. Lysosome contains more than 50 hydrolases including glycosidases, lipase, and proteases which show action in acidic environment (pH is 4.5–5). Lysosome membrane is protecting from acidic environment and hydrolases through high glycosylation of lysosomal membrane proteins namely lysosomal integral membrane proteins (LIMPs) and lysosomal associated membrane proteins (LAMPs). Additionally, heat shock protein 70 kDa (Hsp70) and cholesterol play a role in stabilization of lysosome membrane (Kavcic, Pegan, and Turk 2017, Serrano-Puebla and

Boya 2016). Lysosome membrane also protects cytosol from lysosomal enzymes. Rupture of lysosomal membrane cause acidification of cytosol and massive degradation of cellular component. But selective permeabilization of lysosomal membrane called lysosomal membrane permeabilization (LMP) also culminate with released in number of hydrolases. Though most of lysosomal enzymes are only active in low pH and are inactivated in neutral pH of cytosol, activation of some proteases for a very short period of time is sufficient to cause damage to the cell (Kavcic, Pegan, and Turk 2017). Cathepsins, particularly cathepsins B, L, and D are main proteases responsible for LMP-related damage (Repnik, Hafner Cesen, and Turk 2014).

Lysosomotropic detergents one of LMP stimulants. They are generally weak bases and passively pass through lysosome membrane. They are trapped into lysosome by protonation and dissolve membrane of lysosome with their detergent-like properties (Giraldo et al. 2014). O-methyl-serine dodecylamine hydrochloride and L-leucyl-L-leucine methyl ester (Leu-Leu-OMe) are well-known lysosomotropic detergents causing LMP (Repnik et al. 2017, Li et al. 2000). Also, changing content of lysosome membrane may result in destabilization of membrane. Activation of PLA2, phospholipase C and sphingomyelinase (aSMase) effect composition of lysosomal membrane (Johansson et al. 2010). For example, conversion of sphingomyelin to sphingosine by sequential action of aSMase and acid ceramidase in lysosomal membrane induce LMP since sphingomyelin promote stabilization of lysosomal membrane, while sphingosine act as endogenous lysosomotropic detergents (Giraldo et al. 2014). Lysosome is highly sensitive to ROS (reactive oxygen species) due to lack of antioxidant enzymes and ROS were reported as one of main inducer of LMP. High amount of iron content in lysosome due to degradation of iron containing proteins lead to formation of highly reactive hydroxyl radicals through catalyzing Fenton reaction. Formed hydroxyl radical critically harm lysosomal membrane (Lin, Epstein, and Liton 2010). Zhang et al. (2012) showed that cell death inflicted by (-)-epigallocatechin-3-gallate, known as anti-cancer tea polyphenol, relies on ROS-mediated LMP (Zhang et al. 2012).

It was demonstrated that several proteases may trigger LMP. Caspase 8 and 2 may amplify apoptosis via releasing of cathepsin from lysosome (Gyrd-Hansen et al. 2006, Guicciardi et al. 2000, Aits and Jaattela 2013). Other proteases causing LMP are calpains which mediates LMP through cleavage of lysosome-associated membrane protein-2 (LAMP-2) (Villalpando Rodriguez and Torriglia 2013). Calpain activation by Ca^{+2} elevation cause releasing of cathepsin to cytosol in ischemic neuronal cell death.

(Yamashima et al. 2003). Additionally, cathepsin itself may contribute LMP. Studies shown that lacking cathepsins cease sphingosine or TNF-a induced LMP (Werneburg et al. 2002). Degradation of proteins that sustain stability of lysosomal membrane after minor leakage of cathepsin or cleavage of highly glycosylated proteins of inner lysosomal membrane by cathepsin may be reason of cathepsin mediated LMP although exact mechanism is not determined yet. (Aits and Jaattela 2013, Fehrenbacher et al. 2008).

Other stimuli of LMP is Bcl-2 proteins which are regulators of apoptosis. BAX, pro-apoptotic Bcl-2 protein, may locate in lysosome membrane to induce pore formation. With similar context, BAX is responsible for pore formation on mitochondrial outer membrane during apoptosis. Another Bcl-2 protein, Bid, also take role in LMP via activating BAX (Kågedal et al. 2005). Beside all these, several factors such as viral and bacterial proteins, p53 and some kinases may induce LMP.

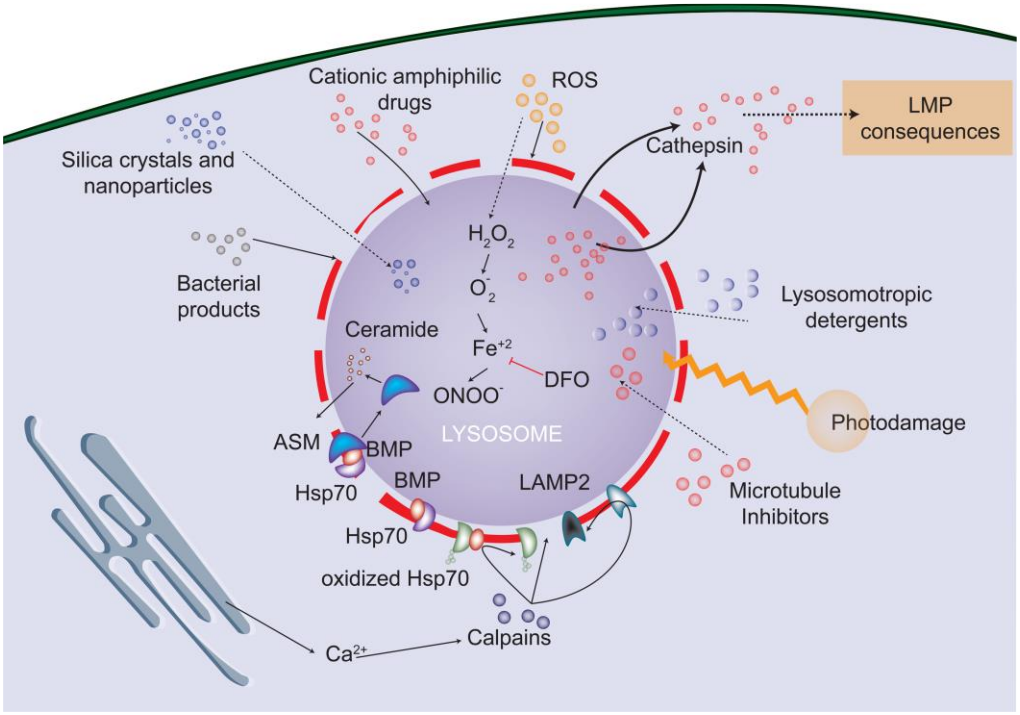

Figure 5. Inducer of lysosomal membrane permeabilization (Source: Serrano-Puebla and Boya 2018)

LMP has been shown to be associated with cell death. Although LMP generally amplify cell death, it may be inducer of cell death (Repnik, Hafner Cesen, and Turk 2014). Cell death which initiated with LMP is defined as a different form of cell death mechanism called lysosome-dependent cell death (LDCD) according to some sources.

However, molecular mechanism of LDCD is not precise yet (Wang, Gomez-Sintes, and Boya 2018). Therefore, it is quite tricky to distinguish LDCD from other cell death forms included LMP.

Contribution of LMP to apoptosis has demonstrated by various studies (Hsu et al. 2009, Dunlop, Brunk, and Rodgers 2011, Liu et al. 2017). BID, is a Bcl-2 protein, serve as sensor role in LMP involving apoptosis. Lysosomal proteases especially papain like cathepsins cleave and activate BID in order to initiate mitochondrial pathway of apoptosis (Stoka et al. 2001). Playing role of LMP in necrotic cell death was often reported. In 2019, Chen et al. demonstrated that 27-Hydroxycholesterol induce NLRP3-dependent pyroptosis by cathepsin B releasing through LMP (Chen et al. 2019). Lysosomal membrane is disrupted at later stage of pyroptosis and released cathepsin take a role in IL-1β secretion and also cell death. Interestingly, Lima Jr. et al. have shown that alum, is an adjuvant, and LLOMe stimulate necrotic cell death having similar characteristics to pyroptosis. But diametrically, lysosome rupture occurs at early point of treatment in this case. Although Alum and LLOME induce minor Nlrp3, caspase 1 activation and IL-1β releasing, caspase 1 do not play role in this cell death. In addition, these agents trigger cathepsin-mediated proteolysis of cytosol content, including pro-inflammatory proteins, although they cause minor inflammations. Therefore, at first glance, pyroptosis inducers and lysosomal destabilization agents namely, alum and LLOME seem to share similar result. But while LMP is result of pyroptosis, it is reason of cell death for second (Lima et al. 2013). Bupivacaine is another compound which induce LMP and necroptosis. Cathepsin inhibitors and necroptosis inhibitors attenuated cell death inflicted by Bupivacaine. Also ROS was determined as reason of LMP as well as cell death (Cai et al. 2018). As mention above calpain mediated LMP take role in neurodegeneration. Calpain–cathepsin hypothesis suggest that activated calpains by calcium elevation lead lysosomal membrane permeabilization and subsequently cathepsin releasing to cytosol. These molecular steps end up with necrotic neuronal cell death in several neurogenerative diseases. (Vosler, Brennan, and Chen 2008, Yamashima 2004).

1.3. Proteases Taking Role in Cell Death

Proteases are enzymes that catalyze cleavage of peptide bonds of proteins. Proteases can be categorized into 4 main groups according to catalytic mechanism; serine,

cysteine, aspartyl and metalloproteases. Aspartyl and metalloproteases activate water molecules via active-site residues for nucleophilic attack whereas cysteine and serine proteases use directly nucleophilic active-site residues for hydrolyzation (Figure 6) (Erez, Fass, and Bibi 2009, Sanman and Bogyo 2014). Proteases regulate many biological processes such as cell cycle, development and immune response. Besides, proteases are very effective player in cell death as the function of proteases is irreversible. They take a critical role in cell death during neurodegeneration, cardiovascular diseases, and cancer treatment. (Divya, Vasudevan, and Sudhandiran 2017). Among the large protease families, calpain, cathepsins and caspases are widely associated with the cell death.

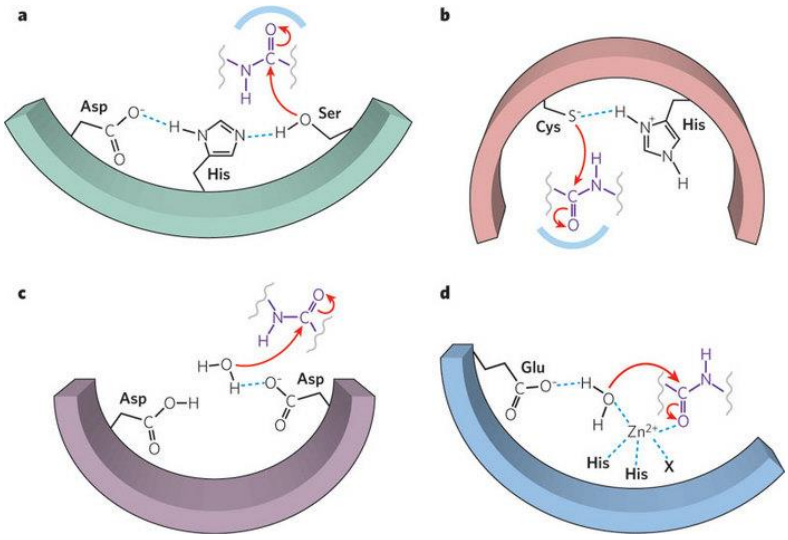

Figure 6. Mechanism of main protease group. a-) serine proteases, b-) cysteine proteases, c-) aspartyl proteases, d-) metalloproteases (Source: Erez, Fass, and Bibi 2009)

Caspases are cysteine proteases family which cleave aspartic acid peptide bonds. eighteen mammalian caspases were defined, and placental mammals contain fifteen of them. As mentioned earlier, caspases are one of main player of extrinsic and intrinsic apoptosis. Apoptotic caspases subdivided as initiator and effector caspases. Initiator caspases, caspase 8, 10, 2, 9, 1 and 11 are activated by dimerization and subsequently autocatalytic cleavage. Activated initiator caspases cleave effector caspases (caspases 3, 6, and 7) culminated with bringing their two active side together to form dimer. Additionally, effector can activate other effector caspases and proteases (Shalini et al. 2015).

Cathepsins are protease family that mostly found in lysosome. Aspartic (cathepsins D and E), serine (cathepsins A and G), and cysteine cathepsins were defined.

They are synthesized as inactive zymogens and activated in late endosome during transportation into lysosome. A largest group of cathepsins, cysteine cathepsins, composed of 11 members; cathepsins B, C, F, H, K, L, O, S, V, W and X. While cathepsin B, L, C and H are expressed continuously, expression of others is strictly controlled. Although extended binding site of cathepsin determine their substrate, they exhibit broad specificity (Reiser, Adair, and Reinheckel 2010, Turk 1999). As mention in lysosome and cell death section, releasing cathepsins from lysosome cause degradation of critical cytoplasmic protein and cell death. Cathepsin may induce apoptosis similar with caspases. But unlike caspases, only a small number of substrates which related with apoptosis were determined. Most-known apoptotic substrate of cathepsins is Bid and most of cathepsins can activate this protein to induce apoptosis. Also cathepsin can promote apoptosis by degradation of anti-apoptotic Bcl-2 protein (Droga-Mazovec et al. 2008). Castro et al. have shown that cathepsin B cause switching from necrosis to apoptosis by this pathway in case of NDI-induced lysosomal rupture. Further, cathepsin b promote apoptosis via inhibition of undefined cysteine protease, which induce necrosis. Also, this undefined protease inhibits apoptosis via degradation of BAX. Lacking cathepsin B resulted in necrotic cell death via undefined cysteine proteases in this situation. Therefore two cysteine proteases have opposite function in NDI-induced lysosomal rupture (de Castro, Bunt, and Wouters 2016). Pacheco et al. demonstrated that cathepsin L cleave topoisomerase I during necrotic cell death which by induced Tnf-a and caspase inhibition (Pacheco et al. 2005). In other study, cathepsin C is demonstrated as main player of Leu-Leu-OMe-induced necrosis and adjuvant effect (Jacobson, Lima, Goldberg, Gocheva, Tsiperson, Sutterwala, Joyce, Gapp, Blomen, and Chandran 2013).

Calpains are calcium dependent cysteine protease family. They recognize bond between domain of substrates rather than specific sequence. Calpain family are composed of 14 members (Suzuki et al. 2004). However, calpain-1 (μ-calpain) and calpain-2 (m-calpains) are ubiquitously expressed and most known calpains. They are named according to calcium dependence; calpain-1 is activated at micromoles per liter of Ca^{2+}, but calpain-2 at millimoles (Storr et al. 2011). Both are found in cytosol as inactive form. When calcium concentration increase, they translocated to plasma membrane and autocatalytically activated. Phosphorylation of calpain by protein kinase A may also cause activation of calpains (Suzuki et al. 2004). Several studies have demonstrated that apoptosis may involve calpain activation. Yousefi et al. shown that apoptotic inducers activate calpains and cause Atg-5 cleavage dependent autophagy inhibition. Also

truncated Atg-5 translocated to mitochondria and associate with Bcl-xL which is anti-apoptotic protein. This association has resulted in releasing cytochrome c from mitochondria and subsequent apoptosis. It was suggested that all apoptosis involves calpain activation in this study (Yousefi et al. 2006). However, another study has shown that only some of apoptosis contain calpain activation and even they shown protection effect of calpain against TNF-a induced apoptosis (Lu et al. 2002).

These 3 different proteases family can be co-work during cell death. Most simple example is activation of caspases and cathepsin or caspases and calpain during apoptosis. Besides, they can regulate activity of each other. In section of Lysosome and Cell Death, roles of calpain and caspases on LMP was mentioned. Therefore, activity of calpain or caspase can lead cathepsin releasing into cytoplasm. Also, caspase activation by cathepsin were reported. Especially cathepsin D can cleave caspase 8 and cause activation via dimerization (Katunuma et al. 2001, Conus et al. 2012). Similar condition is observed with calpain and caspases. Caspase 7 activation by calpain 1 was shown with *in vitro* experiment. Moreover, calpain-1 activated caspase 7 show different activity, localization and binding affinity from caspase 7 that activated by caspase (Gafni et al. 2009). Conflictingly, Chua et al. (2000) found that calpain may directly cleave and inhibit caspases. Inactive truncated caspase 9 whereby calpain-1 is not able to activate effector caspases and releasing cytochrome c form mitochondria (Chua, Guo, and Li 2000).

Beside 3 main cell death related proteases, other proteases like granzyme, ADAM protease family, Omi/HtrA2 etc. was associated with cell death (Suzuki et al. 2003, Lieberman 2010, Cai et al. 2016a).

1.4. Saponins and Cell Death

Saponins are secondary metabolites having sugar units on triterpenoid or steroidal aglycone. They are found in higher plants as well as marine organism. Saponins can be subdivided into two groups based on aglycone structure (known as sapogenin); triterpenoid and the steroid saponins. Both derived from oxidosqualene containing 30 carbon atoms. However, while triterpene saponins have all 30 carbon, steroid saponins contain 27 carbon due to 3 methyl losses (Vincken et al. 2007). Additionally, triterpene saponins can be divided into ten as dammaranes, lanostanes, ursanes, oleananes, curcubitanes, cycloartanes, lupanes and hopanes, taraxasteranes, and tirucallanes

(Escobar-Sánchez, Sánchez-Sánchez, and Sandoval-Ramírez 2015). Saponins have broad biological activities such as antifungal, anti-inflammatory, neuroprotective, immunomodulatory, hypoglycaemic, anti-cancer etc. (Podolak, Galanty, and Sobolewska 2010).

Anti-cancer activity of saponins was demonstrated with various studies. Beside natural saponins, semi-synthetic derivatization is used to enhance anti-cancer activity and obtain information about structure activity relationship (SAR). Synthetic studies with betulinic acid and lupeol generated more potent molecules for anti-cancer activity (Jacobson, Lima, Goldberg, Gocheva, Tsiperson, Sutterwala, Joyce, Gapp, Blomen, Chandran, et al. 2013, Zhang et al. 2015). An oleanic acid derivative namely 2-cyano-3,12-dioxoolean-1,9-dien-28-oic acid (CDDO) is one of most exiting examples for semi-synthesis of saponin. CDDO suppress nitric oxide synthase and cyclooxiganese-2 by showing upto1000 times more potential than oleanic acid (Watson 2011). Ongoing clinical studies support anti-cancer potential of CDDO and its methyl esters. Additionally, CDDO and its derivative was reported as multitargeting molecules because of Nrf-2 activation at lower dose. In contrast with anti-cancer activity, Nrf-2 enhance cell survival and cell protection via antioxidant effect. CDDO was entered clinical studies as Nrf-2 activator for chronic kidney disease and type 2 diabetes. But studies were terminated at stage III due to severe adverse effects and mortality in patients (Moses, Papadopoulou, and Osbourn 2014).

While cytotoxic screening of isolated saponins often reported, studies about molecular activity mechanism of saponin is limited. However, different cell death signals which induced by saponin was demonstrated even with limited studies. Lots of saponins such as Lupeol (Saleem 2009),Frondoside A (Li et al. 2008) as well as CDDO are reported as apoptotic inducer. Saponin-mediated apoptosis involve various well known cell death signal like cell arrest, ROS formation, endoplasmic reticulum stress (ER-stress), mitochondrial damage etc. (Lv et al. 2013, Xu et al. 2009, Choi, Kim, and Singh 2009). But also, uncommon cell death pathway may be induced in saponin mediated cell death. For instance, 24-methylenelanosta-7,9(11)-diene-3b,15adiol-21-oic acid (MMHO1), were isolated from *Antrodia cinnamomea,* induce apoptosis and mitotic catastrophe in U937 cell line. Mitotic catastrophe is an antiproliferative mechanism, which occurs when cells enter early or inappropriately mitosis and cannot complete mitosis (Vakifahmetoglu, Olsson, and Zhivotovsky 2008).

Some of saponin induce autophagy accompanied by apoptosis. Although autophagy is generally activated as a mechanism for protection from saponin-induced cell death, induction of autophagic cell death by saponins has also been reported. As an example, akebia saponin PA isolated from *Dipsacus asperoides* induce apoptosis involved caspase 3 and autophagic cell death. Cell death and caspase 3 activation was alleviated by autophagic inhibitor whereas caspase 3 inhibitor do not effect cell death and autophagic activation (Xu et al. 2013). In other study, treatment with Eclalbasaponin I result in activation of apoptosis and autophagic cell death by regulation of JNK, p38, and mTOR (Cho et al. 2016).

Inducing necrotic cell death by saponin were also shown. Betulinic acid (BA) is one of most studies saponin for anti-cancer activity. BA induce apoptosis on wide range of cancer cell line (Kessler et al. 2007, Fulda and Kroemer 2009). A semi-synthetic derivative of BA, B10, induce necrotic cell death which include lysosomal membrane permeabilization and caspase 3 activation. Although autophagic flux inhibited due to lysosomal dysfunction, autophagosome accumulation is play a role in cell death by B10 (Gonzalez et al. 2012). Albiziabioside A is another saponin which more cytotoxic semi-synthetic derivative's produced. A derivative of Albiziabioside A which produced according to SARs was determined that simultaneously induce apoptosis and ferroptosis. While disruption of mitochondrial membrane potential and ROS generation cause apoptosis, lipid peroxidation due to GPX4 inhibition result in ferroptosis (Wei et al. 2018). Polyphyllin D induce apoptotic cell death in NB-69 cells involving caspase activation while it stimulates necroptosis in IMR-32 and LA-N-2 without caspase activation. Unsurprisingly, polyphyllin D-mediated cell death is antagonized by necroptosis inhibitor (Watanabe et al. 2017).

CHAPTER 2

MATERIALS AND METHODS

2.1. Materials

The materials used in thesis were explain briefly in this section.

2.1.1. Materials and Instruments for Synthesis

p-TsCl (*p*-Tosyl Chloride, Acros Organics), MsCl (Methanesulfonyl chloride, Acros Organics), pyridine (Carlo Erba), TEA (triethylamine, Sigma-Aldrich) were purchased for semi-synthesis studies. Chloroform (VWR Chemicals) , methanol (Carlo Erba), ethyl acetate (VWR Chemicals), n-hexane (VWR Chemicals), cyclohexane (VWR Chemicals), dichloromethane (VWR Chemicals), Silica gel (Kiesegel 60, 70-230 mesh, Sigma-Aldrich), Silica gel RP-18 (Fluka), Silica gel aluminum sheets (Kiesegel 60 F_{254}, 0.2 mm, Merck) and RP silica gel aluminum sheets (Kiesegel 60 RP-18 F_{254}, 0.2 mm, Merck) were purchased for chromatography studies. Lyophilizer (Christ, Alpha1-2LDplus), Rotavapor (Heidolph), UV Lamp (Vilber Lourmat), SpeedVac Concentrator (Thermo Scientific Savant SPD 121P) were used as instruments during semi-synthesis studies. Also, Nuclear Magnetic Resonance Spectrometer (Varian MERCURY plus-AS 400 (400 MHz); Bruker (500 MHz)) and mass spectrometer (Agilent 1200/6539 Instrument- HRTOF MS) were used for spectral characterization of isolated molecules.

2.1.2. Materials for Bioactivity Studies

MTT, WST-1 (Rosche), RPMI 1640 medium (BI), DMEM (Gibco, USA), EMEM (Gibco, USA), Fetal Bovine Serum (FBS) (Panbiotech), 2-Mercaptoethanol (Sigma-Aldrich), L-glutamine (Thermo Scientific), Ammonium persulfate (Amresco), SDS (Amresco), Mammalian Protease Inhibitor Cocktail (Promega), Sodium azide (Sigma-Aldrich) were purchased for bioactivity studies. Tween-20, Triton X-100, Nonidet P-40,

Ponceau S Stain, glycerol, Tris, TEMED, 2-mercaptoethanol, Ethylenediaminetetraacetic acid (EDTA), Ethylenglycol Tetraacetic Acid (EGTA), sodium chloride, sodium phosphate monobasic anhydrate, sodium phosphate dibasic anhydride were purchased from Amresco.

2.1.2.1. Antibodies

Anti-Atg-5, Anti-Atg-7, Anti-Atg3, Anti-LC3 and Anti-caspase 3 purchased from Cell Signaling Technology. Also, Anti-p62 (BD Bioscience) and Anti-β-Actin (Sigma-Aldrich) was used during thesis studies.

2.1.2.2. Chemical Agents and Kits

Pepstatin A (Enzo; ALX-260-085-M025) as cathepsin D/E inhibitor, Cathepsin inhibitor I (Calbiochem®, 219415) as cathepsin B, L, S inhibitor, Z-VAD-fmk (Enzo; ALX-260-020-M001) a pan-caspase inhibitor, Z-IETD-fmk (Abcam; ab141382), caspase 8 inhibitor were used in inhibitor studies. Bafilomycin A1 (Baf A1) (Cell signaling; 54645), LysoTracker™ Red DND-99 (Invitrogen; L7528), Cycloheximide (Calbiochem; CAS 66-81-9) were purchased for other studies. LDH-Cytotoxicity Colorimetric Assay Kit II (Biovision, K313) assay were kindly given by Assoc. Prof. Dr. Güliz ARMAĞAN.

2.1.2.3. Buffers

a-) 10x PBS (phosphate buffered saline): 87.5 g sodium chloride, 11.5 g sodium monohydrogen phosphate and 2.3 g sodium dihydrogen phosphate were dissolved in 1-liter distilled water.
b-) 2x RIPA: 40 mg SDS (sodium dodecyl sulfate) and 200 mg deoxycholic acid were dissolved in 7 ml 10xPBS containing 0.4 ml NP-40. Then the solution was completed with distilled water to 20 ml.
c-) Resolving Buffer: 1.5 M Tris HCl (90.855 g), 0.4% h/h TEMED (2 ml) and 0.4% a/h SDS (2 g) were dissolved in 500 ml distilled water and pH of the solution was adjusted to 8.9.

d-) Stacking Buffer: 0.5 M Tris HCl (30.285 g), 0.4% h/h TEMED (2 ml), 0.4% a/h SDS (2 g) were dissolved in 500 ml distilled water and pH of the solution was adjusted to 6.8.

e-) 10x SDS-PAGE Running Buffer: 30.2 g Tris Base, 144 g Glysin and 10 g SDS were dissolved in 1-liter distilled water.

f-) 10x SDS-PAGE Transfer Buffer: 30.33 g Tris base and 144 g Glysin were dissolved in 1-liter distilled water.

g-) Washing Buffer for SDS-PAGE: 100 ml 10x PBS was completed to 1 liter with distilled water and 1 ml Tween-20 was added.

2.2. Methods

The methods used in thesis were explain briefly in this section.

2.2.1. Semi-Synthesis Studies

Table 1**.** Starting materials and reagents with reaction conditions.

Reactant	**Reagents**	**Solvent/ Addition**	**Condition**	**Time**
100 mg AG	450 mg *p*-TsCl	Pyridine	Room temp.	5 h
150 mg AG	140 µl MsCl	DCM/ 150 µl TEA	at 0 °C	3 h
200 mg CG	450 mg p-TsCl	Pyridine/5 mg DMAP	At reflux	6 h
350 mg CG	140 µl MsCl	DCM / 294 µl TEA	at 0 °C	3 h
150 mg SCG	130 µl MsCl	Pyridine	at 0 °C	4 h
500 mg SCG	1000 mg *p*-TsCl	Pyridine	at reflux	6 h
30 mg AG-01	200 mg *p*-TsCl	Pyridine	Room temp.	12 h
25 mg CG-01	200 mg *p*-TsCl	Pyridine	Room temp.	12 h

Semi-synthesis studies were performed with AG (astragenol), CG (cycloastragenol) and SCG. Moreover AG-6(oxo) and CG-6(oxo), referred to as AG-01 and CG-01, respectively, were used as starting materials. While SCG, AG-01 and CG-01 were found in our molecule library, cycloastragenol was donated by Bionorm Natural Products Production & Marketing Co., Izmir, TURKEY. As for AG, it was synthesized

from CG through acid hydrolysis. In briefly, 20 g CG was dissolved with 400 ml methanol and 10 ml concentrated sulfuric acid were added to this solution. Reaction was continued 6 h at reflux. Then reaction mixture was neutralized with NaOH and dried with evaporator at 60 ^{o}C. Firstly, acetonitrile precipitation and then RP gel column with 60:40 acetone: water was used to purified AG.

Table 1. shown condition of conducted reaction to produce analogs of AG-08. TLC was used to follow progression of reactions and determination of reaction time. All reaction mixtures were quenched by addition of distilled water and extracted 3 times with ethyl acetate and evaporated at 50°C in rotary evaporator for further separation and purification steps.

2.2.1.1 Separation and Purification of Semi-Synthetic Analogs

Separation and purification steps of reaction fractions carried out by using silica gel as stationary phase for column chromatography. Silica gel and RP silica gel coated commercial plates were used for TLC to follow column chromatography. Bands of TLC were marked under the UV light at 254 and 365 nm, and then sprayed with 20% aq. H_2SO_4 and heated for 5 minutes to visualize the bands. Isolation procedure of molecules shown in Figure 7, Figure 8, Figure 9, Figure 10, Figure 11, Figure 12 and Figure 13.

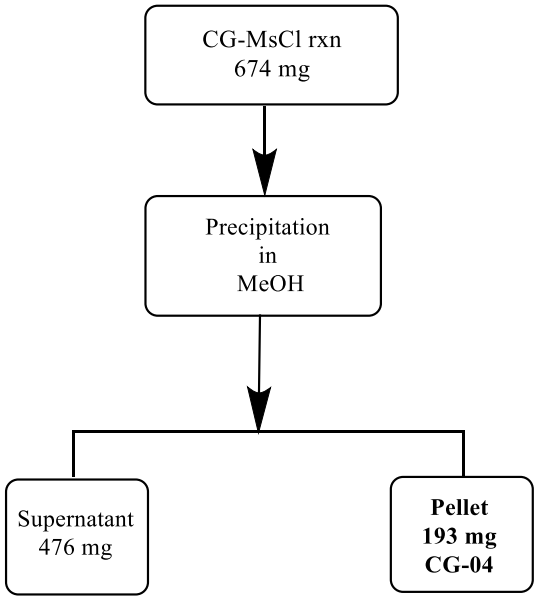

Figure 7. Isolation procedure of CG reaction with MsCl at room temperature.

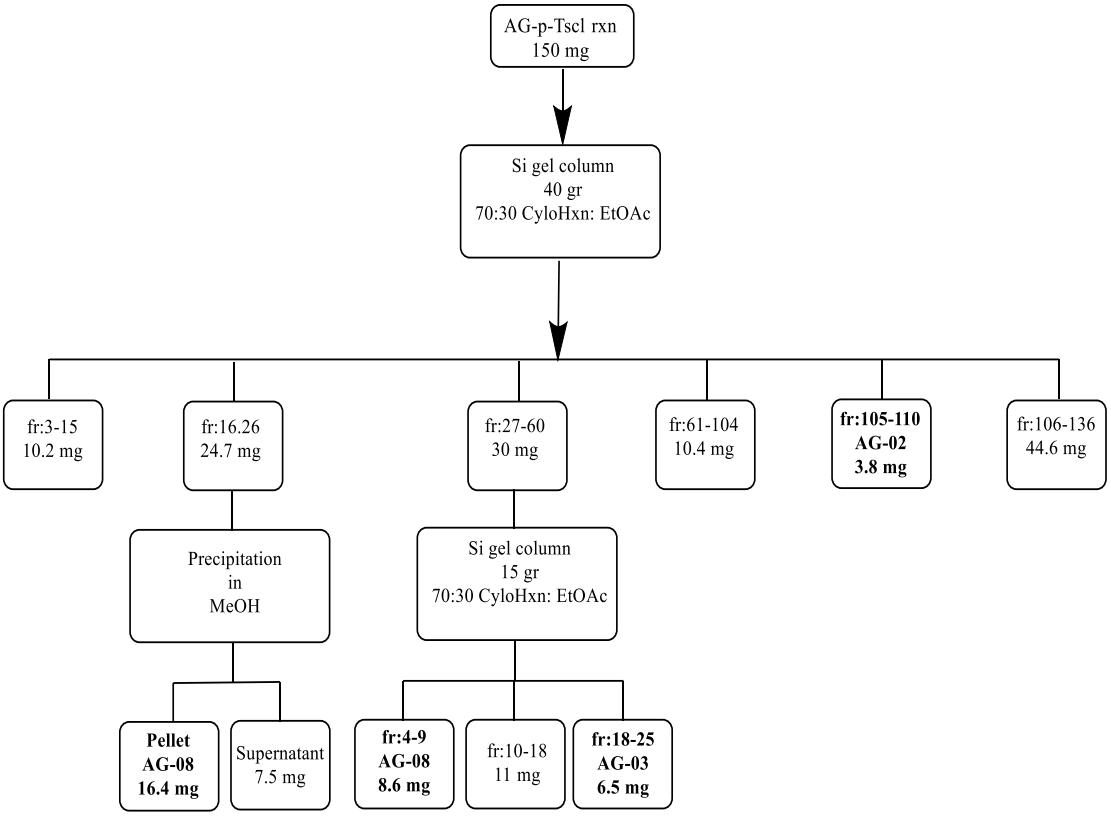

Figure 8. Isolation procedure of AG reaction with *p*-TsCl at room temperature.

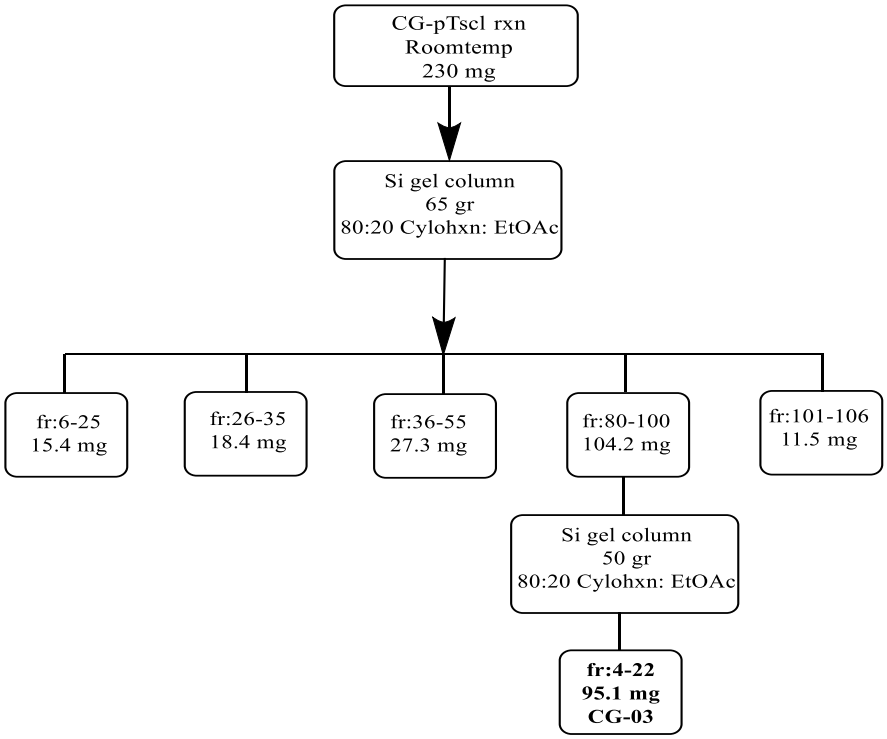

Figure 9. Isolation procedure of CG reaction with *p*-TsCl at room temperature.

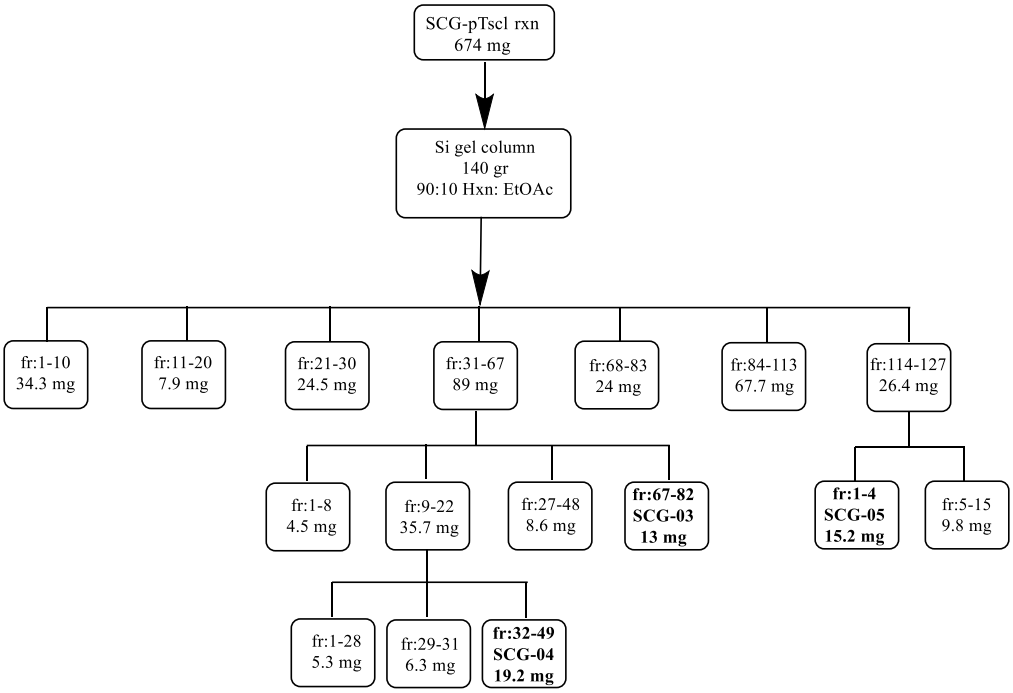

Figure 10. Isolation procedure of SCG reaction with *p*-TsCl.

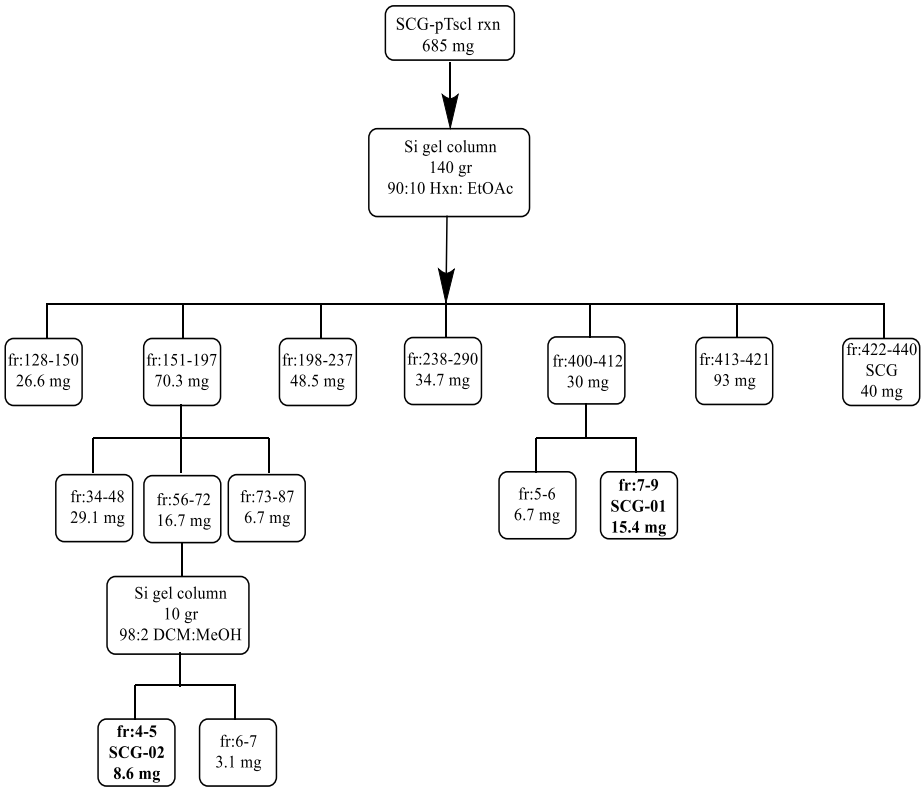

Figure 11. Isolation procedure of SCG reaction with *p*-TsCl.

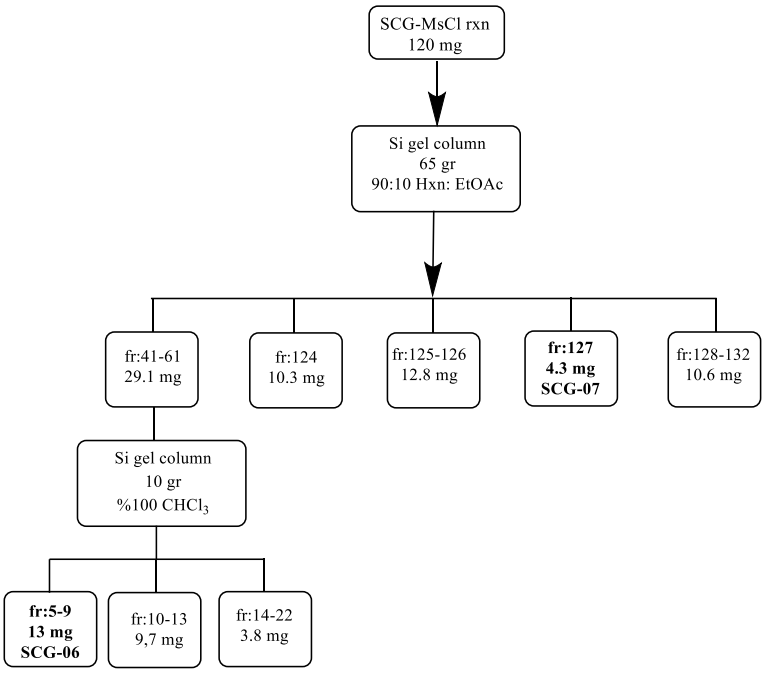

Figure 12. Isolation procedure of SCG reaction with MsCl.

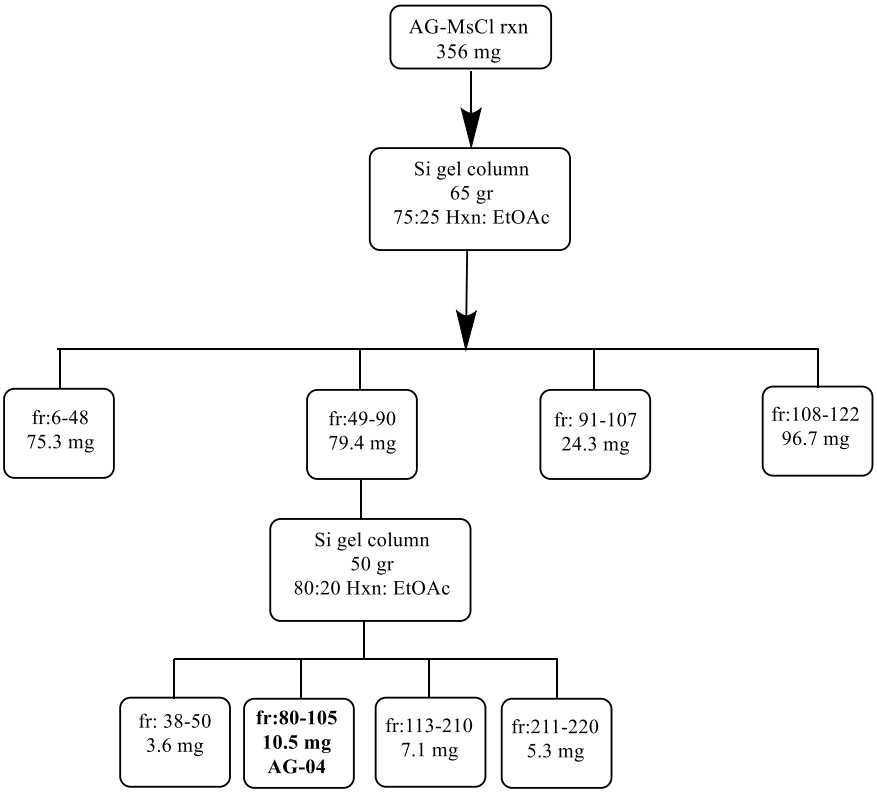

Figure 13. Isolation procedure of AG reaction with MsCl.

2.2.2. Bioactivity Studies

The methods used in biological studies of thesis were explain briefly in this section.

2.2.2.1. Mammalian Cell Culture Condition and Cells Passaging

Cells were maintained with appropriate cell media with 10% FBS (DMEM high glucose for HeLa, MCF7, HK-2, PC3, A549, SHSY-5Y, DU145, HepG2, IMR-90, and U2OS cell lines; EMEM for MRC-5; DMEM F12 for H295r and RPMI-1640 for HCC1937 cells). Cells were incubated in incubator containing 5% CO2 at 37 °C. When cells reach 70% confluence, old medium was removed, and cell surface was washed with 0.05% trypsin. Subsequently, cells were treated with 0.25% trypsin at 37 °C until detaching from surface. Cells were collected with fresh medium and appropriate amount of cells suspension was transferred to new culture dish containing fresh medium.

2.2.2.2. Cells Freezing

After cells were detached via trypsin as mentioned above, they were collected with freezing buffer consisting of FBS, and 5% cryoprotectant namely DMSO. Then cell suspension was distributed to cryovials to contain 2×10^6 cells/ml each. Cryovials were stored at -80 ° C for one day and transferred to liquid nitrogen tank.

2.2.2.3. Cytotoxicity Assay for Determination of IC_{50} values

Cells were seeded homogenously in 96 well plates (7000 cells/well for HeLa, MCF7, PC3, A549, HepG2; 8500 cells/well for HCC1937, U2OS, DU145; 10000 cells/well for HK-2, MRC-5, IMR-90, H295r and 20000 cells/well for SHSY-5Y) and allowed to adhere overnight. Various concentrations of molecules which dissolved in DMSO were added to wells as triplicate. Following incubation in incubator for 48 h, whole medium was poured off and fresh media containing 10% MTT was added to each well. Living cells convert MTT to formazan crystals by mitochondrial activity, and

colorimetric detection of formazan crystals is used to determine percentage of living cells. Then plates incubated 4 h in incubator. Again, whole medium pulled out and DMSO was added to solve formed formazan crystals. Finally, photometric absorbance was measured at wavelength of 590/690 nm by using Varioscan flash spectrophotometer by Thermo Scientific. Data were analyzed by using GraphPad Prism to determine IC_{50} value of molecules.

2.2.2.4. Immunoblotting Studies

Cells were seeded into 6 or 12 well plates for immunoblotting studies. After the indicated treatment time, cells were detached by trypsinization and harvested with 1xPBS in eppendorf. Subsequently, cell suspension was centrifuged for 3 minutes at 10000 g at 4 °C and supernatant was removed. Same process was repeated 2 times for 2 and 1 minutes. 1x PBS and 2x RIPA (1:1 ratio) that involve 50x PIC (protein inhibitor cocktail) were used as lysis buffer. Samples containing appreciate amount lysis buffer were vortexed vigorously for 5 times after every 5 minutes. Then samples were centrifuged at 14000 g at 4 °C for 10 minutes and supernatant part was transferred to clean eppendorf.

Total protein content of samples is determined by using BCA assay in order to equal loading. 190 µl BCA solution (reagent A and B in 50:1 ratio) were added to 2 µl samples and 8 µl distilled water. Following incubation at 37 °C for 30 minutes, photometric absorbance was measured at 562 nm wavelength. Samples were prepared according to the data of the BCA assay and 4x loading buffer was added to each with a final concentration of 1x. Dry bath was used to denature samples at 95°C for 5 min.

Samples were run with 10%, 12% or 15% SDS gels which prepared as shown in Table 2. by using running buffer. Firstly, they were run at 60 V for 40 min, then 120V was used to complete running process.

Following running process, proteins on gels were transferred to PVDF (Polyvinylidene difluoride) membrane. A sandwich containing sponge, two filter paper, gel, PVDF membrane, two filter paper, and sponge sequentially was assembled in transfer cassette for transfer process at 200 mA for 90 min (in ice) or 20 mA for overnight.

PVDF membranes that proteins were transferred on, were treated with 5% milk for 1 h before blotting with primer antibodies. Antibodies were incubated for 1 h or overnight depending on the type of antibody used. Then membranes were washed with

wash buffer for 30 min and appropriate secondary antibodies were used for 1 h. After last washing step for 30 min, chemiluminescence images were taken by using ECL with Vilber Lourmat Fx-7 imaging system.

Table 2. Preparation of stacking and resolving gel.

Resolving gel			
Gel percentage	**10%**	**12%**	**15%**
Acrylamide (30%)	3.33 ml	4 ml	5 ml
4x Resolving Buffer	2.5 ml	2.5 ml	2.5 ml
Distilled water	4.1 ml	3.5 ml	2.5 ml
AP (10%)	75 µl		

Stacking Gel	
Acrylamide (30%)	0.35 ml
4x Stacking Buffer	0.75 ml
Distilled water	1.9 ml
AP (10%)	25 µl

2.2.2.5. Inhibition of Proteasis

Cells were pre-treated for 1h with 100 µM Pepstatin A (PepA), 50 µM Cathepsin inhibitor I (CatI), 70 µM Z-VAD-fmk, 30 µM Z-IETD-fmk, and 30 µM Calpeptin which were dissolved in DMSO. 8 µM (~2 x IC_{50} value) AG-08 was applied for 24 h to cells. The dosage and treatment time with AG-08 were selected for the killing of approximately 50% of cells by AG-08 during experiment. Medium was taken out and fresh medium containing 10% WST-1 was added each well. Working principle of WST-1 is similar with MTT assay but WST-1 was used to obtain more selective results. Photometric absorbance at a wavelength of 440 nm was measured per h for 4 h. Data were analyzed using GraphPad Prism to determine the percentage of living cells.

2.2.2.6. Lysotracker Staining

LysoTracker® Red DND-99 was used to labeling lysosome. HCC1937 ($1.5x10^5$ cells/well) were seeded on coverslips in 6 well plates. After 24-h incubation, cells were treated with AG-08 for 16h. Then cells incubated with 50 nM lysotracker in pre-warmed fresh medium for 40 min at 37 °C and 5% CO2. Cells were washed with 1xPBS and mounted. Lastly, cells were observed immediately using a fluorescence microscope (Olympus FX7).

2.2.2.7. LDH Assay

LDH-Cytotoxicity Colorimetric Assay Kit II (Biovision) were used to detection LDH releasing. HCC1937 (8500 cells/well) were seeded on 96 well plate. After 24-h incubation, cells were treated with AG-08 for 24 h. Then cells were centrifuged at 600 x g for 10 min. 10 µl/well were transferred to clean 96 well plate and added 100 µl LDH Reaction Mix which composed of WST Substrate Mix LDH Assay Buffer. Fallowing 30 min incubation at room temperature, 10 µl stop solution were added and absorbance were measured at 450 nm.

CHAPTER 3

RESULTS AND DISCUSSION

3.1. Biological Activity of AG-08

The results of biological studies of thesis were explain in this section.

3.1.1. Cytotoxicity of AG-08

The 7-AAD/ Annexin V and ethidium bromide/acridine orange staining in our preliminary studies suggested AG-08 mediated cell death might have necrotic feature. LDH assay, which is another method to detect necrotic cell death, were performed to verify these data. LDH is normally intracellular enzyme and released to the extracellular space in case of damaged cell membrane. Therefore, LDH release is a well-known feature of necrotic cell death (Chan, Moriwaki, and De Rosa 2013, Rayamajhi, Zhang, and Miao 2013). As shown in Figure 14, LDH activity in cell culture supernatants were increased significantly with AG-08 treatment even at the lowest concentration. Additionally, staurosporine, an apoptosis inducer, did not cause LDH release as expected. Consequently, necrotic cell death induction by AG-08 was verified with the third methodology (LDH). It needs to be stressed that LDH assay is easier and faster than the other necrosis confirmation methods; therefore, selected semi-synthetic compounds have been tested in subsequent studies with LDH assay after cytotoxicity screenings.

Cytotoxic activity against HeLa and HCC1937 cell lines were reported in preliminary studies. Herein, IC_{50} values of AG-08 on 13 human cell lines including HeLa and HCC1937 were determined employing MTT assay in order to see selectivity of AG-08. MRC-5, IMR-90, and HK-2 are normal (non-cancerous) cells, whereas the others are cancer cell lines. As seen in the Table 3, AG-08 displayed a potent inhibitory activity against all cell lines. Among them, AG-08 showed the highest cytotoxicity against A549 with an IC_{50} of 2.3±0.035 µM, while the least cytotoxicity was observed versus HK-2 (IC_{50}: 10.18±0.509 µM). Although the cytotoxic effect of AG-08 on HK-2, a normal cell

line, is slightly lower than cancer cells, it is not rational to suggest selectivity for AG-08 between cancer and normal cell lines.

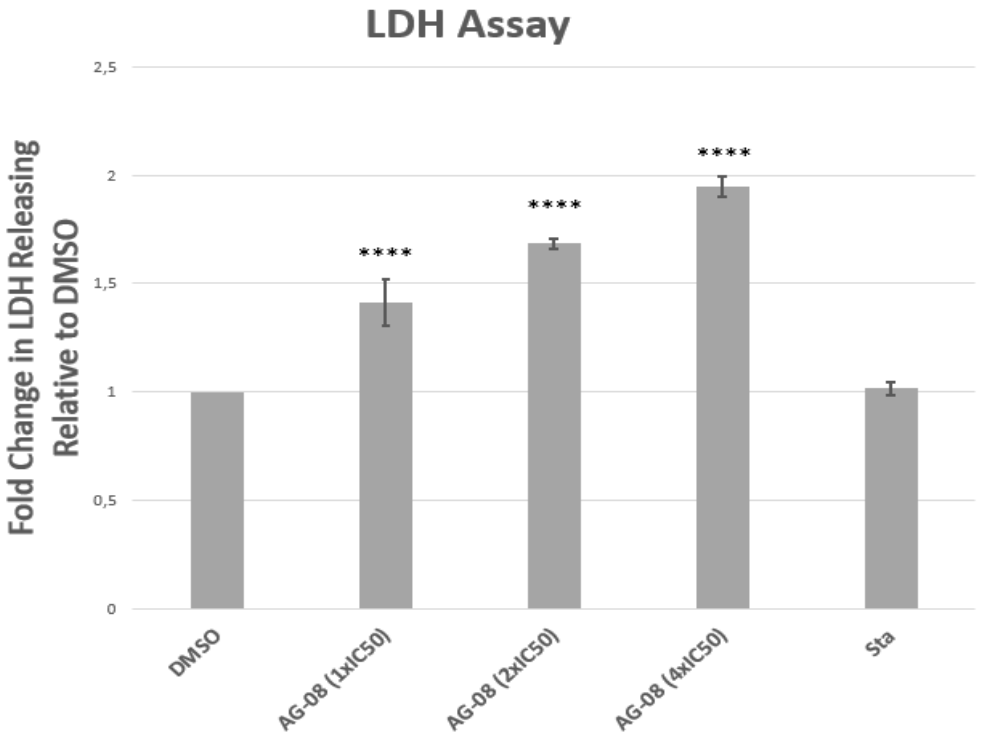

Figure 14. Release of LDH by AG-08 treatment. Cells were treated with 1, 2 and 4-fold of IC_{50} values of AG-08 for 24 h. 0.5 µM staurosporine (sta) was used to induce apoptosis as negative control. Release of LDH was calculated as fold change relative to DMSO. Error bars are the standard deviations. One-way ANOVA was used to analyze the statistical significance. The significant difference is defined between DMSO and treatments.

3.1.2. Effect of AG-08 on Autophagy

AG-08 has been shown to affect various autophagic proteins. In the scope of this thesis, protein levels of ATGs, p62, and LC3-I/II were determined again to confirm the previous data. As shown in Figure 15B, immunoblotting studies revealed that Atg-5, Atg-7, Atg-12, Atg-16L1, and Atg-9a decreased dose-dependently. Additionally, LC3-II accumulation was observed. However, p62 level was increased at IC_{50} concentration, whereas 2 and 4-fold IC_{50} treatments decreased the protein level (Figure 15A). This data contradicted with our preliminary data, which exhibited steady decrease in p62 levels dose dependently.

Table 3. IC_{50} values of AG-08 versus 13 human cell lines. Data represents as mean ± standard error from the triplicate experiment (n: 3).

Cell lines	IC_{50} value of AG-08 (µM)
HeLa	5.7±0.447
HCC1937	3.81±0.272
MRC-5	2.58±0.044
MCF7	3.78±0.269
A549	2.3±0.035
SH-SY5Y	3.57±0.092
DU145	3.46±0.074
PC3	6.6±0.887
HK-2	10.18 ±0.509
U2OS	6.49±0.729
IMR-90	6.48±0.166
H295r	4.41±0.181
HepG2	6.4 ±0.673

Given the finding that showed increase in p62 protein levels at lower concentrations, we suggested that p62 was accumulated due to autophagic flux inhibition at early stage. Then, p62 was cleaved by activated proteases and a decrease in p62 was the case. Therefore, longer treatment with the IC_{50} value was expected to cause decrease in p62 levels. In this context, time course changes in autophagic protein levels were investigated with immunoblotting. p62 protein levels were augmented at 16 h, followed by a decrease at 36 h substantiating our suggestion (Fig 15A). Additionally, IC_{50} dosing of AG-08 caused LC3-II accumulation time-dependently as expected. Increase in LC3-II level started at 16 h similar with that of p62. The simultaneous increase in p62 and LC3-II supported that p62 accumulation stemmed from autophagic flux inhibition.

Here, we have complemented the findings of our preliminary studies by showing both LC3-II and p62 accumulation that occur during autophagic flux inhibition. However, the current data contradicted with the previous one in regard to the level of p62. The main difference was that the lowest concentration used in the preliminary study was 7 µM

compared to the 4 µM treatment in the latter. 7 µM is almost 2 fold of the IC_{50} value, which was shown to decrease p62. Therefore, unconformity between both data could be explained by that the dose used in the preliminary screenings was too high to observe p62 increase.

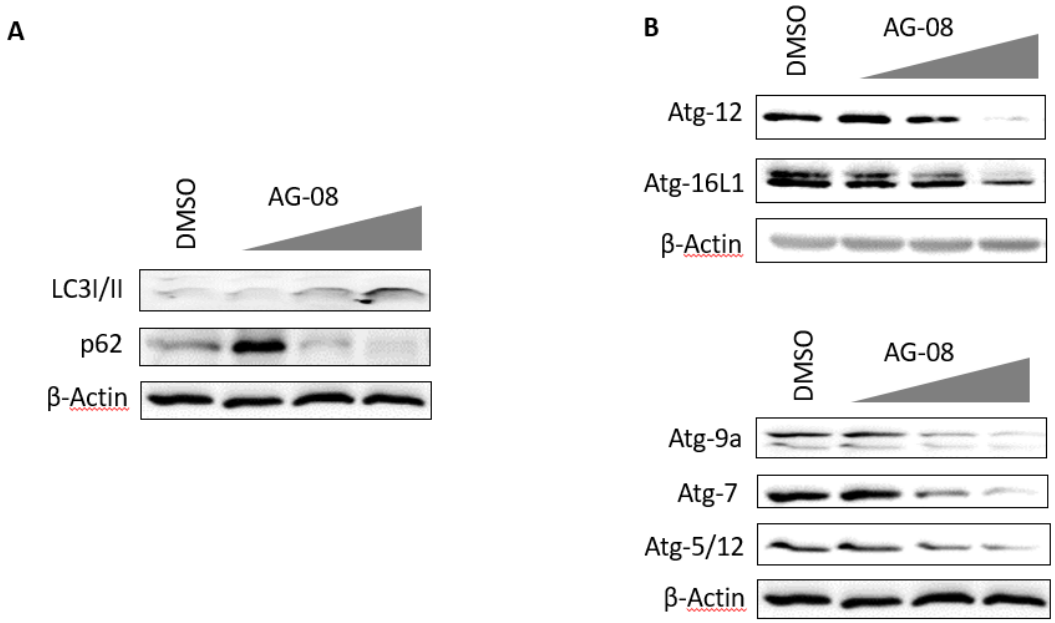

Figure 15**.** Effect of AG-08 on autophagic proteins. HCC1937 cells were treated with 1, 2 and 4-fold of IC50 value for 16 h. Immunoblotting of LC3I/II and p62 (A) and Atg-5/12, Atg-7, Atg12, Atg16L1 and Atg-9a (B). β-Actin was used as the loading control.

Strikingly, even though 2 and 4-fold IC_{50} concentrations decreased the Atg protein levels at 16 h (Fig 15), no change on their levels were detected with IC_{50} concentration with prolonged exposure up to 48 h (Fig 16). An explanation for this result might be that a minor posttranslational decrease in ATGs cannot be noticeable due to the high rate of newly synthesized proteins. To overcome this issue, cells might be co-treated with a protein synthesis inhibitor (Cycloheximide: CHX) in order to observe slight alterations in protein levels. Additionally, CHX is also widely used to sensitize cells to TNF-α or TRAIL inducing apoptosis through obstruction of anti-apoptotic pathway (Pajak, Gajkowska, and Orzechowski 2005). Intriguingly, Atg3 cleavage by activated caspase 8 with TRAIL or TNF-α treatment was only evidenced by CHX co-treatment (Oral et al. 2012). Therefore, we investigated effect of co-treatment of AG-08 and CHX on ATGs.

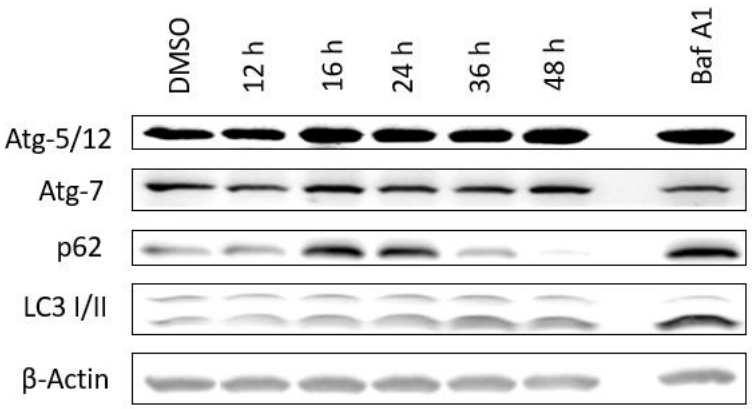

Figure 16. Effect of IC_{50} treatment on the autophagic protein levels. Western blot analysis of Atg-5, Atg-7, p62 and LC3I/II. HCC1937 cells were incubated with AG-08 for 12, 16, 24, 36 and 48 h. While Baf A1 was used as a positive control, DMSO was negative control. β-Actin was used as the loading control.

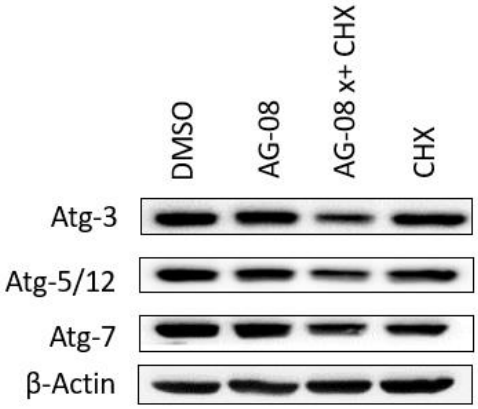

Figure 17. Co-treatment of CHX and AG-08. Immunoblotting of Atg3, Atg-5, and Atg-7 with AG-08 and CHX combination. HCC1937 cells were pre-treated with 0.5 µg/ml CHX for 1 h and then incubated with AG-08 for 24 h. β-Actin was used as the loading control.

Significant decrease in Atg-5 and Atg-3 levels was observed with the co-treatment, while no substantial change was noted with single treatments of AG-08 or CHX. Likewise, Atg-7 decreased with AG-08 and CHX combination; however, CHX treatment alone also resulted in Atg-7 decline. Since CHX is widely used to detect half-

life of proteins, the observed decrease in Atg-7 level by CHX treatment might be due to its short half-life. Nevertheless, consistent with other results, AG-08 treatment produced additional reduction in Atg-7 level. In summary, these experiments show that the IC_{50} concentrations of AG-08 indeed decreases ATG protein levels, as evidenced by cleavage of ATGs with AG-08 and CHX co-treatment.

3.1.3. Effect of Proteas Inhibitors on AG-08-mediated Cell Death

Since protease activation via AG-08 treatment was suggested based on the cleavage of p62, PARP-1 and ATG proteins, the effect of several protease inhibitors on the cell death was evaluated. Caspases were inhibited by Z-VAD-fmk (general caspase inhibitor) and Z-IETD-fmk (caspase 8 inhibitor) due to the activation of caspases by AG-08. Additionally, PepA (cathepsin D/E) and CatI (cathepsin B, L, and S) were used since cathepsins were reported to cleave PARP-1 to 50-kDa fragment. Finally, calpeptin was inhibited by calpains because it was shown that calpains was able to cleave ATGs.

Figure 18 shows that all inhibitors except PepA significantly alleviate cell death with different extent. Calpeptin and Z-VAD-fmk showed the most potent protective effect with approximately 1.5-fold change as compared to the cells treated by AG-08 alone. Also, it was found that CatI effectively prevented cell death by 1.38-fold, whereas the lowest protective effect was observed with Z-IETD-fmk (1.24-fold).

The effect of CatI on cell death might imply the cleavage of PARP-1 by cathepsins. Furthermore, this finding suggests release of cathepsin into cytosol from lysosome. Interestingly our data indicated that cathepsins B, L and S inhibition attenuated cell death, however, cathepsins D and E inhibition via pepstatin A treatment did not seem to affect the extent of cell death. This finding might stipulate selective release of cathepsin B, L and/or S into the cytosol but not cathepsins D and/or E. On the other hand, Wang et al. stated that although cathepsin D is released to the cytosol prior to cathepsin B, specific cathepsin B inhibitor but not PepA effectively prevented cell death induced with some cationic nanoparticles (Wang, Salvati, and Boya 2018). Similar with their findings, cathepsin D might be also released by AG-08 treatment but had no significant impact on the molecular mechanism leading to cell death. However, to substantiate this proposition, more data is warranted such as immunostaining of cathepsins.

Our preliminary experiments demonstrated caspase activation with AG-08, however the contribution of caspases in cell death was not precise. In this thesis, Z-VAD-fmk, a general caspases' inhibitor, was found to be the most protective one among tested inhibitors, while specific caspase 8 inhibitor possessed minimal effect. Although activation of caspase 3 via caspase 8 was expected, the lesser effect of Z-IETD-fmk was noteworthy suggesting other paths to be involved in activation of caspase 3. Firstly, caspase 3 could be activated by another initiator caspase turned on by AG-08, and inhibition of this caspase and caspase 3 provides higher protection in the case of Z-VAD-fmk treatment. In addition, alternative pathways such as cathepsin D release might be of importance for mediation of caspase 3 activation independent of caspase 8.

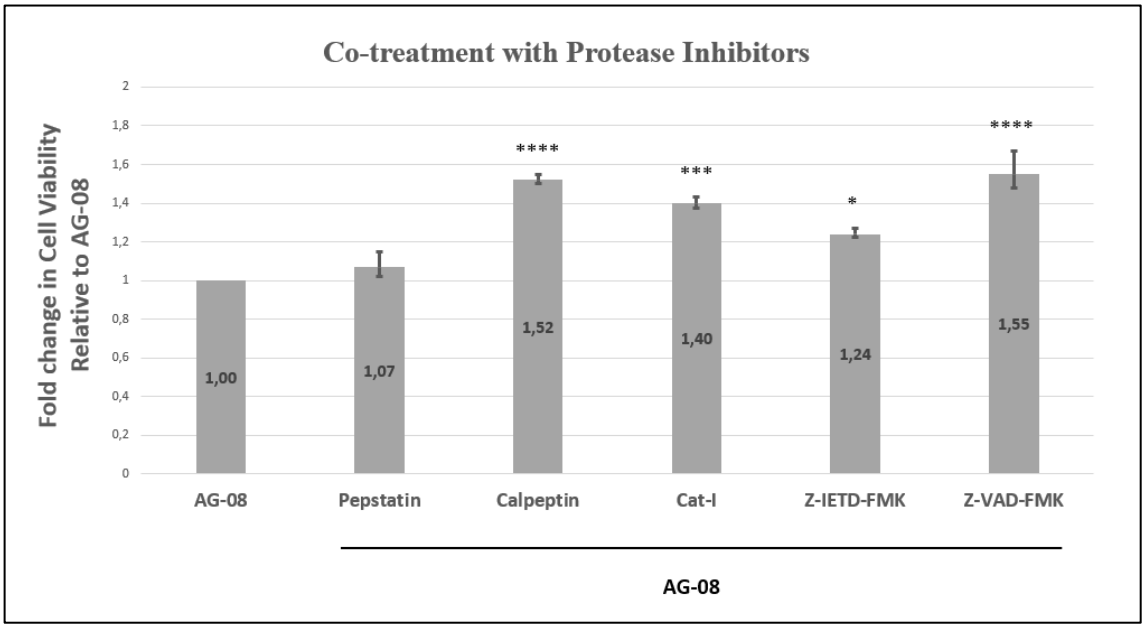

Figure 18. The effect of protease inhibitors on AG-08 mediated cell death. HCC1937 cells were pre-treated 1 h with stated inhibitors and incubated with 8 µM AG-08 for 24 h. After incubation, WST-1 reagent was used to determine percentage of living cells. Recovery from cell death was calculated as fold change compared to only AG-08 treatment. Error bars represent standard deviations. One-way ANOVA was used to analyze the statistical significance. The significant difference was defined between AG-08 and inhibitor treatments.

Caspases 3 and 8 are well-known apoptotic proteases, and they are generally inactive in necrotic cell death. None of the established necrosis pathways reports involvement of these caspases. There are only a few non-classified necrotic cell death cases including apoptotic caspases in the literature. One of them is B10 that is shown to

induce both necrosis and caspase 3 activation (Gonzalez et al. 2012). Nonetheless, contribution of these caspases to necrosis mechanism is still unclear. Thus, our findings verifying activation of caspases are quite significant for the literature, and further studies with AG-08 and caspases may provide important data to find the link between apoptotic caspases and regulated necrosis.

Notably, the cleavage of ATGs by caspases and calpains were well reported in the literature. Cleavage of Atg-5 with calpains or Beclin-1 with caspases have been reported to result in inactivation of autophagy (Zhu et al. 2010, Yousefi et al. 2006). Fluspirilene, which is an autophagy inducer, blocks activation of calpain by reducing intracellular Ca^{+2} and hinder cleavage of Atg-5. In the same study, it was demonstrated that silencing calpain-1 expression afforded greater autophagy induction. Based on their findings, (Xia et al. 2010) state that calpains are one of the modulators of autophagy (Xia et al. 2010). As for AG-08, co-activation of calpain and caspases may result in the cleavage of most of ATGs and effective autophagy inhibition at later stage(s) of the treatment.

3.1.4. Effect of AG-08 on Lysosome

Lysosome is a main player of autophagic machinery. Our results indicate that cathepsin inhibition lessens cell death implying lysosomal membrane leakage. To justify this finding, the effect of AG-08 on lysosomal leakage was investigated. Cells were stained with LysoTracker® Red DND-99, a lysosomotropic dye specifically staining lysosome and late endosome due to their acidic nature. Staining with lysotracker reduced in dose-dependent manner as shown in Fig. 19. In particular, 3 and 4-fold of IC_{50} caused a dramatic decrease in staining, which indicated lysosomal impairment by AG-08 treatment. In the test, lysosome staining means undamaged structure, while no coloring implies a possible leakage. Additionally, inhibition of V-ATPase, responsible for the acidic pH of the lysosome, leads to loss of pH-gradient (Repnik, Cesen, and Turk 2016). Despite these two different mechanisms affecting the acidity of the lysosome, AG-08 mediated cell death is probably linked with lysosomal membrane permeabilization due to the effect of cathepsin inhibitors on AG-08 mediated cell death. As mentioned before, leakage of cathepsin to the cytosol may result in cleavage of critical proteins leading to cell death. If the leakage from lysosome is massive, it results in uncontrollable degradation of cytosol content and eventually necrotic cell death. But specific leakage of

proteases from lysosome also occurs during necrosis; however, such incident usually triggers mitochondria dependent apoptosis (Messner et al. 2012, Aits and Jaattela 2013, Brojatsch et al. 2014). In the case of AG-08, it is plausible to suggest that whether selective permeabilization or massive rupture of lysosomal membrane plays significant role in necrotic profile of AG-08.

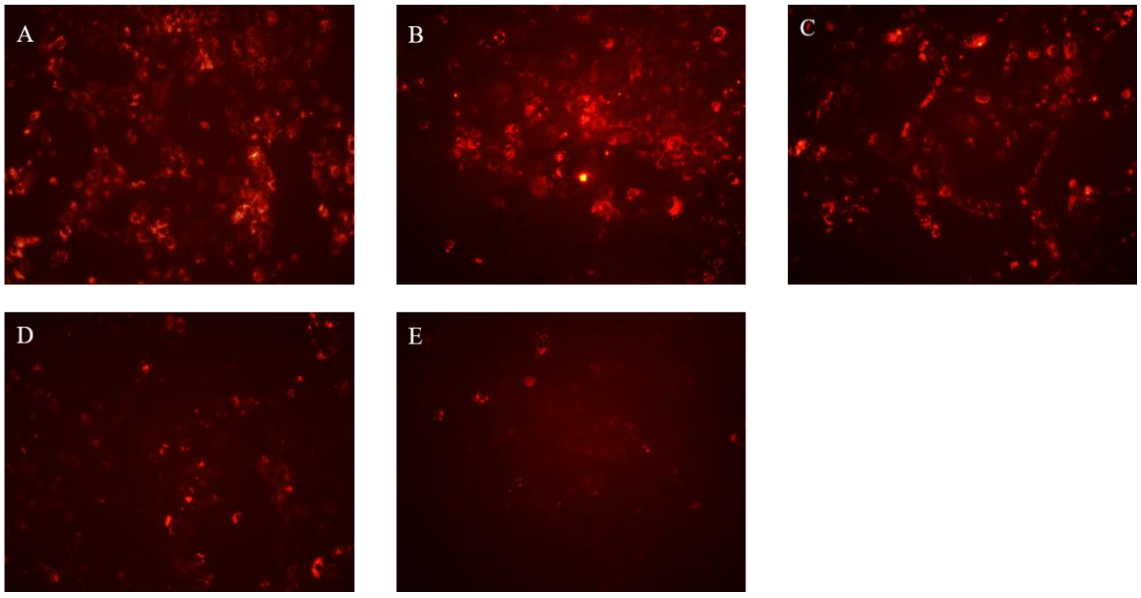

Figure 19. Lysotracker staining of AG-08 exposed HCC1937 cells. Cells were treated with 1, 2, 3 and 4-fold IC50 value of AG-08. Lysosome of dead cell do not be stained by lysotracker. Therefore, cells were stained with lysotracker after 16 h incubation with AG-08 since most of cells are still alive in this time point. DMSO (A), IC_{50} value of AG-08 (B), 2-fold of IC_{50} of AG-08 (C), 3-fold of IC_{50} of AG-08 (D), 4-fold of IC_{50} of AG-08 (E).

We have previously suggested that AG-08 affected autophagy in two steps. Impairment of lysosomal function might be the first step of autophagic inhibition in AG-08 treated cells. As autophagic vacuoles cannot be degraded as a consequence of non-acidic lysosome, p62 and LC3-II accumulate because of the inhibited autophagic flux. The blockage of autophagic flux via lysosomal impairment was previously reported in various studies. Indomethacin is used to sensitize cancer cells to cytotoxic agents as well as to inhibit autophagic flux that leads to increase in p62 and LC3-II levels. Lysosomal basification was demonstrated to be overriding basis of indomethacin induced autophagic flux inhibition (Vallecillo-Hernández et al. 2018).

Herein, lysosomal impairment via AG-08 treatment was demonstrated. Nevertheless, it is not clear whether lysosomal impairment initiates the cell death or is a

consequence of the cell death. Further studies are needed to clarify exact role of lysosomal dysfunction in AG-08 triggered cell death.

3.2. Structural Elucidation of Semi-synthetic Derivatives

Semi-sythetic analogs of AG-08 was produced to strucuture activity releationship, while molecular studies to determined activity mechanism of AG-08 carried out. Fifteen AG-08 analogs were produced and structural eleducation the compounds was performed based on spectroscopic methods (1D NMR, 2D NMR and MS spectra).

3.2.1. Structural Elucidation of Compound AG-02

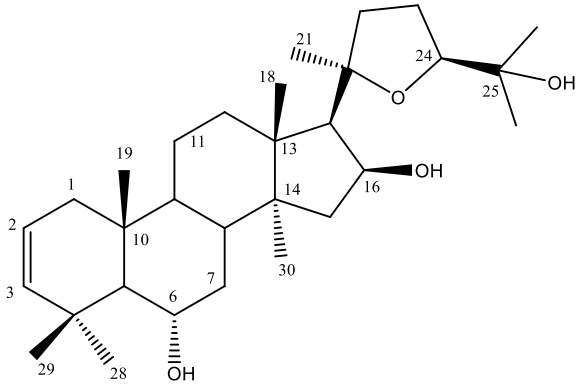

Figure 20. Chemical Structure of AG-02

Compound AG-02 was obtained from reaction of AG with *p*-TsCl. A major ion peak was observed at *m/z* 495.34667 $[M+Na]^+$ in the HR-ESI-MS spectrum of AG-02, indicating molecular formula as $C_{30}H_{48}O_4$. When the MS data of AG-02 was compared with AG, 18 amu (atomic mass unit) difference implied elimination of a water molecule. Also, initial inspection of the ^{1}H NMR spectrum revealed that the characteristic H-3 resonance was lacking. Moreover, a disubstituted double bond system was apparent in the ^{1}H, ^{13}C NMR and DEPT135 spectra (δ_{C-3} 139.6, d; δ_{C-2} 120.3, d; δ_{H-2} 5.50 and δ_{H-3} 5.31, each 1H) suggesting that the dehydration reaction took place at C-3(OH). To justify this proposition, 2D NMR spectra of AG-02 were taken. All the spectral data given in the

Table 4 were assigned thoroughly by interpreting COSY, HSQC and HMBC spectra. The key long-range correlations from C-3 (δ_C 139.6) to H_3-28 and H_3-29 verified the position of the double bond at C-2. Thus, the structure of AG-02 was established as 20(*R*),24(*S*)-epoxy-6α,16β,25-trihydroxy lanosta-2,9(11)-diene.

Table 4. The ^{13}C and ^{1}H NMR data of AG-02 (*100/500 MHz, δ ppm, in $CDCl_3$*)

H/C	**δ_C (ppm)**	**δ_H (ppm), *J* (Hz)**
1	37.9 t	2.04 m, 2.11 m
2	120.3 d	5.5 ddd (10.1, 5.4, 3)
3	139.6 d	5.31 m
4	36 s	-
5	55.4 d	1.28 m
6	70.2 d	4.06 ddd (10.8, 10.8, 3.9)
7	38.6 t	1.44 m, 1.86 m
8	40.9 d	2.4 m
9	145.8 s	-
10	40.3 s	-
11	116.3 d	5.3 m
12	37.8 t	1.89 m, 2.14 m
13	44.3 s	-
14	43.9 s	-
15	45.1 t	1.51 dd (12.8, 6.2), 2.05 m
16	73.4 d	4.72 ddd (7.9, 7.9, 6.3)
17	56.2 d	2.36 d (7.8)
18	18.1 q	0.94 s
19	23.75 q	1.05 s
20	87.2 s	-
21	28 q	1.23 s
22	34.6 t	1.6 m, 2.59 q (10.4)
23	25.9 t	2 m
24	81.51 d	3.75 dd (8.1, 6.2)
25	72 s	-
26	26.7 q	1.14 s
27	27.81 q	1.3 s
28	34.9	1.2 s
29	23.0 q	1.17 s
30	19.2 q	0.79 s

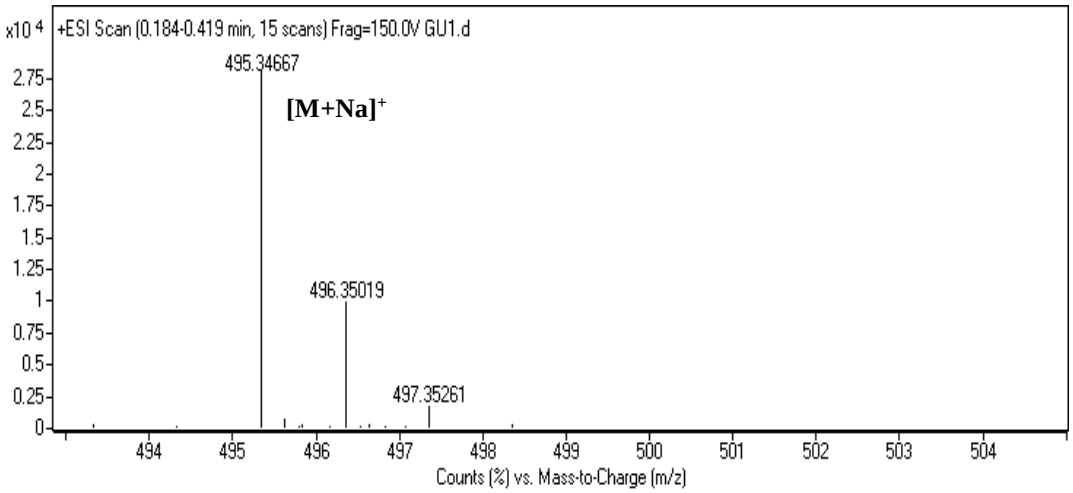

Spectrum 1. HR-ESI-MS Spectrum of AG-02 (positive mode)

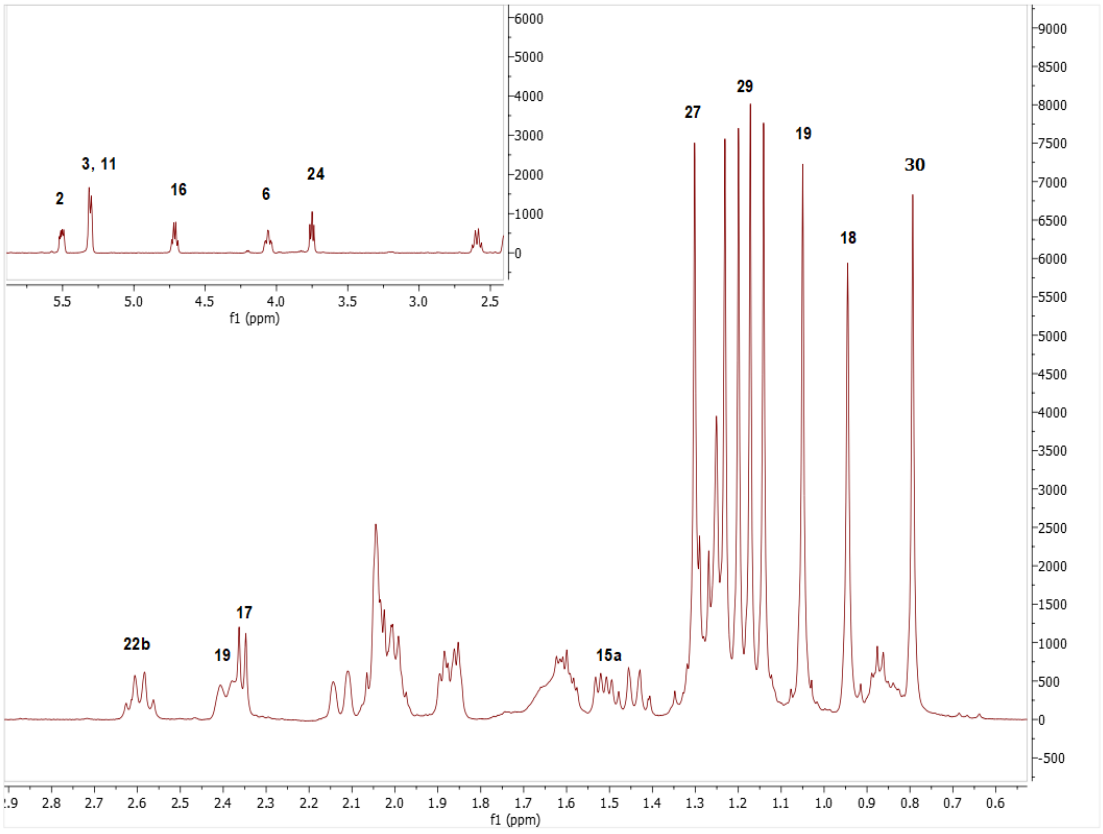

Spectrum 2. ^{1}H NMR Spectrum of AG-02.

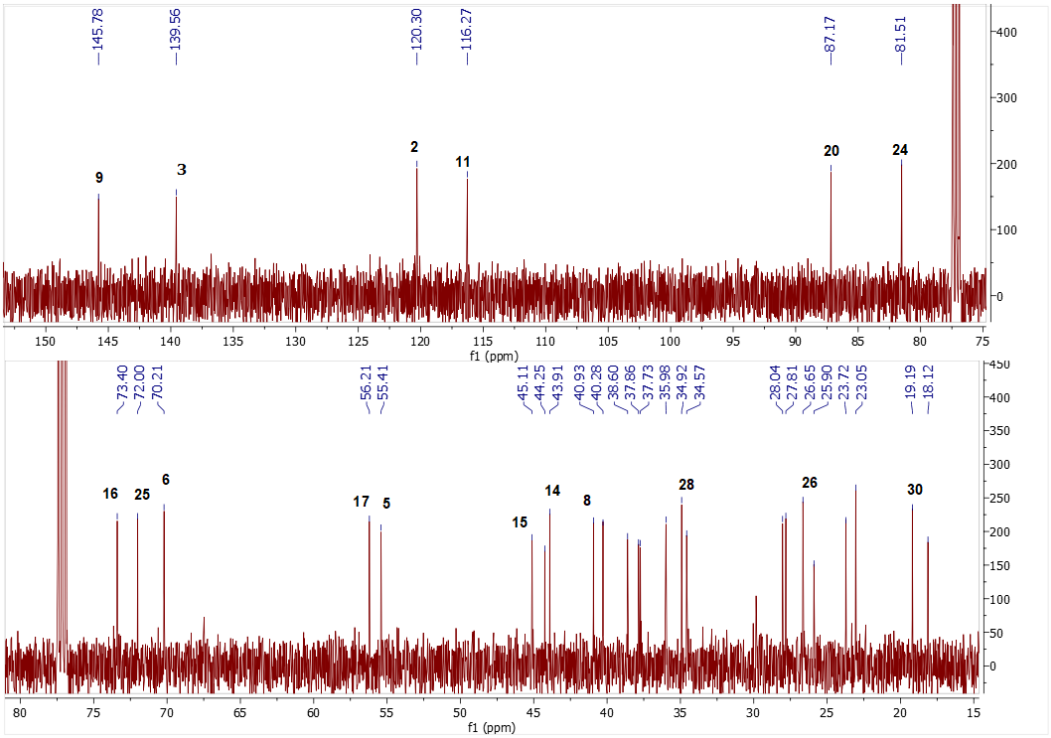

Spectrum 3. ^{13}C NMR Spectrum of AG-02.

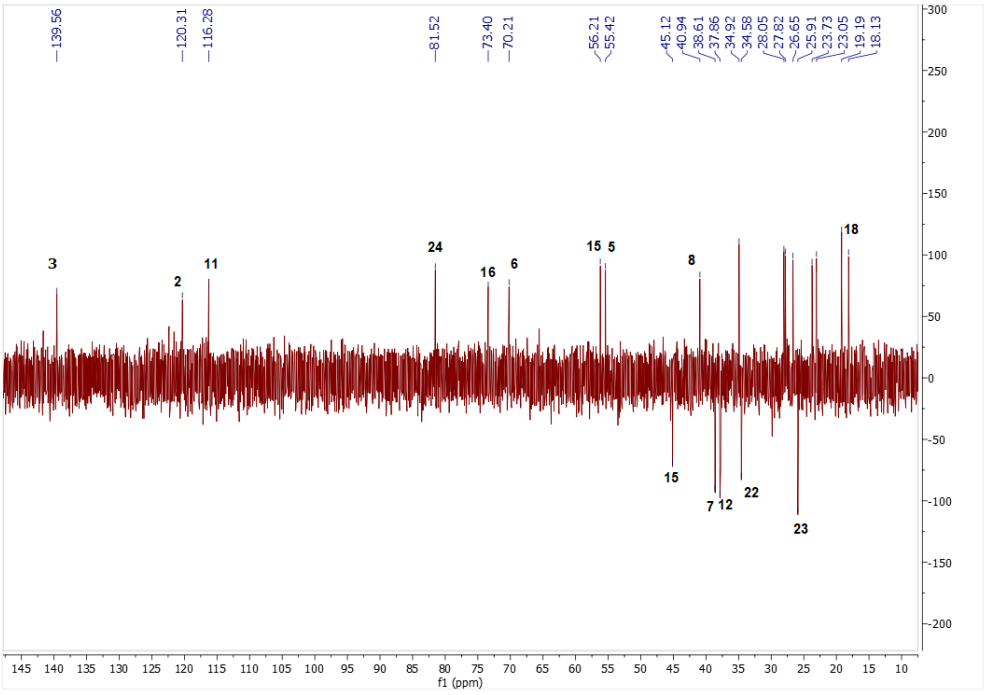

Spectrum 4. DEPT135 spectrum of AG-02.

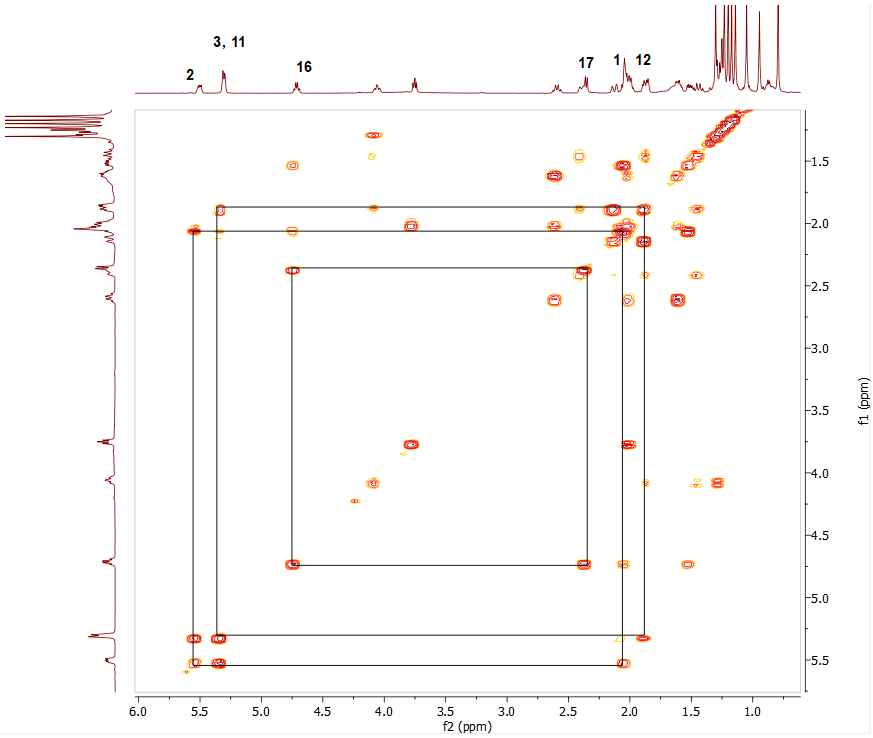

Spectrum 5. COSY spectrum of AG-02

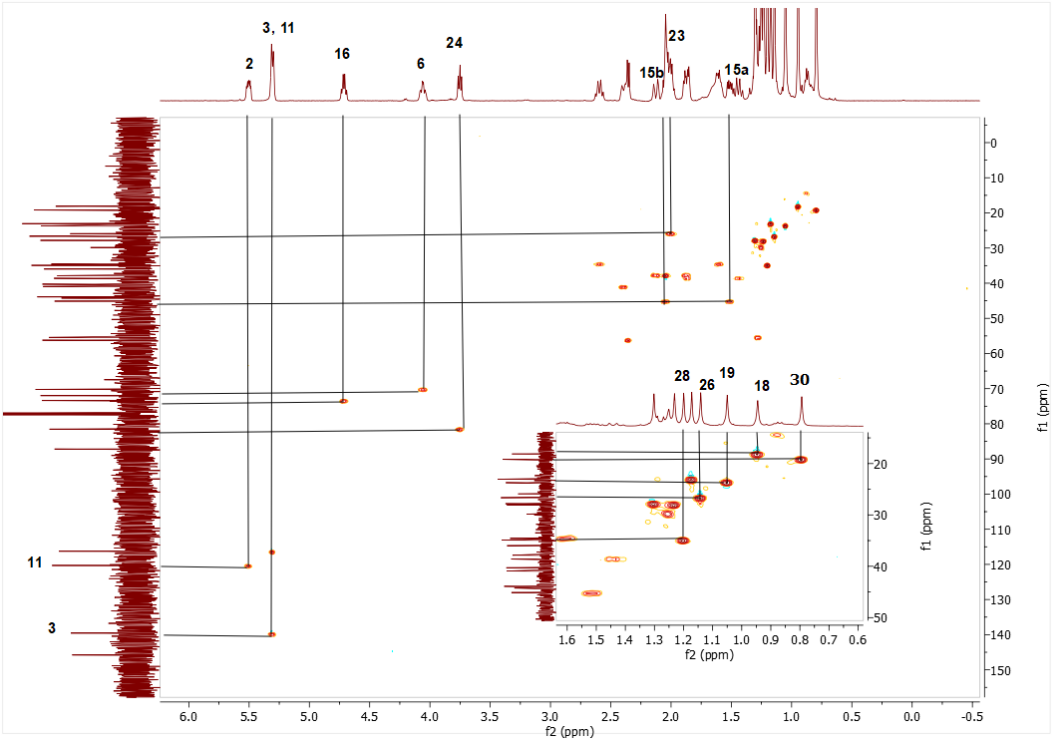

Spectrum 6. HMQC spectrum of AG-02.

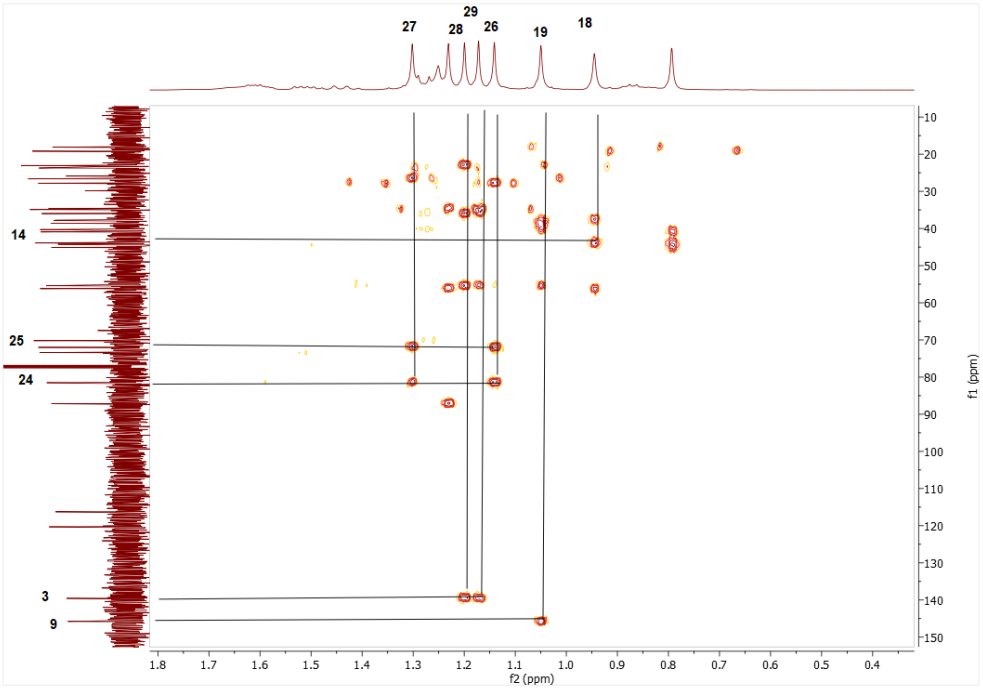

Spectrum 7. HMBC spectrum of AG-02.

3.2.2. Structural Elucidation of Compound AG-03

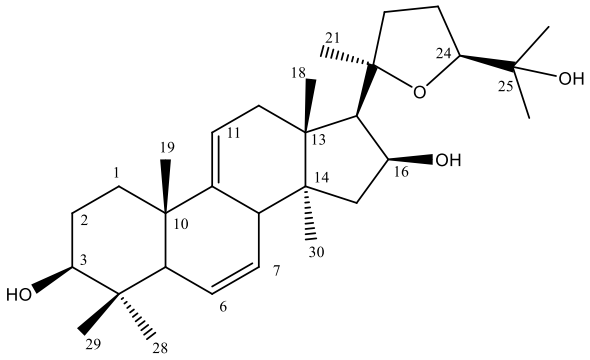

Figure 21. Chemical Structure of AG-03.

AG-03 was the other analog obtained via AG and *p*-TsCl reaction. HR-ESI-MS spectrum showing a major ion peak at *m/z* 495.34894 ($[M + Na]^+$) indicated a molecular formula of $C_{30}H_{48}O_4$. Similar with AG-02, MS spectrum showed 18 amu difference compared to AG suggesting elimination of a water molecule. Moreover, the presence of a disubstituted double bond system was apparent in the ^1H, ^{13}C NMR and DEPT135 spectra ($\delta_{C\text{-}7}$: 128.9, d; $\delta_{C\text{-}6}$: 127.3, d; $\delta_{H\text{-}6}$: 5.71 and $\delta_{H\text{-}7}$: 5.57, each 1H). The characteristic

resonances deriving from H-3 (δ_H 3.23, dd, 11.8, 4.8) and H-16 (δ_H 4.69 m) were observed in the low-field of the ^{1}H NMR spectrum, revealing that the dehydration reaction took place at C-6(OH). In the COSY spectrum, H-6 and H-7 coupled with two different methine protons which were assigned readily to H-5 (δ_H 1.70) and H-8 (δ_H 2.84) protons. The carbon signal attributed to C-5 (δ_C 52.2) based on the HSQC spectrum exhibited long-range correlations with H-7, H_3-28 and H_3-29, whereas C-8 (δ_C 43.9) showed cross peaks with H_3-30 in the HMBC spectrum. Thus, the double bond unambiguously was located at C-6. As a result, the structure of AG-03 was defined as 20(*R*),24(*S*)-epoxy-16β,25-dihydroxy lanosta-6,9(11)-diene.

Table 5. The ^{13}C and ^{1}H NMR data of AG-03 *(100/500 MHz, δ ppm, in $CDCl_3$).*

H/C	**δ_C (ppm)**	**δ_H (ppm), *J* (Hz)**
1	34.4 t	1.59 m
2	28.2 t	1.78 m
3	79.3 d	3.23 dd (11.8, 4.8)
4	38.8 s	-
5	52.2 d	1.70 d (12.2)
6	127.3 d	5.71 m
7	128.9 d	5.57 dt (10.2, 3.2)
8	43.9 d	2.84 brs
9	145.9 s	-
10	39.2 s	-
11	113.6 d	5.16 brs
12	38.2 t	2.04 m, 1.92 m
13		
	43.8 s	-
14	44.8 s	-
15	44.3 t	2.07 m, 1.57 m
16	73.6 d	4.69 m
17	56.6 d	2.24 dd (11.8, 6.1)
18	19.1 q	0.98 s
19	20.4 q	1.01
20	87.3 s	-
21	28.2 d	1.23 s
22	34.8 d	1.58 m, 2.56 m
23	26.1 t	2 m
24	81.8 d	3.75 t (7.2)
25	72.2 s	-
26	28.2 q	1.29 s
27	26.9 q	1.14 s
28	28.2 q	1.01 s
29	16 q	0.83 s
30	18.91	0.64 s

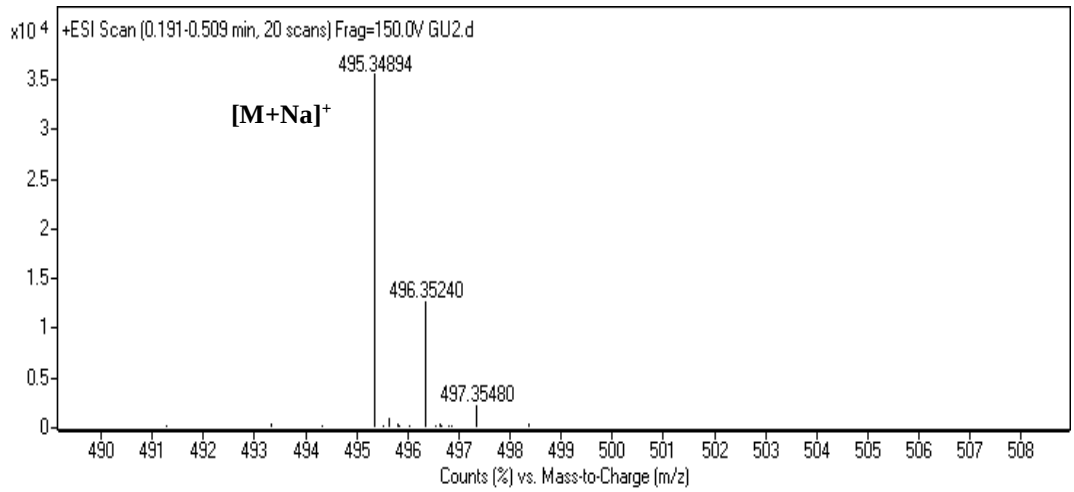

Spectrum 8. HR-ESI-MS Spectrum of AG-03 (positive mode).

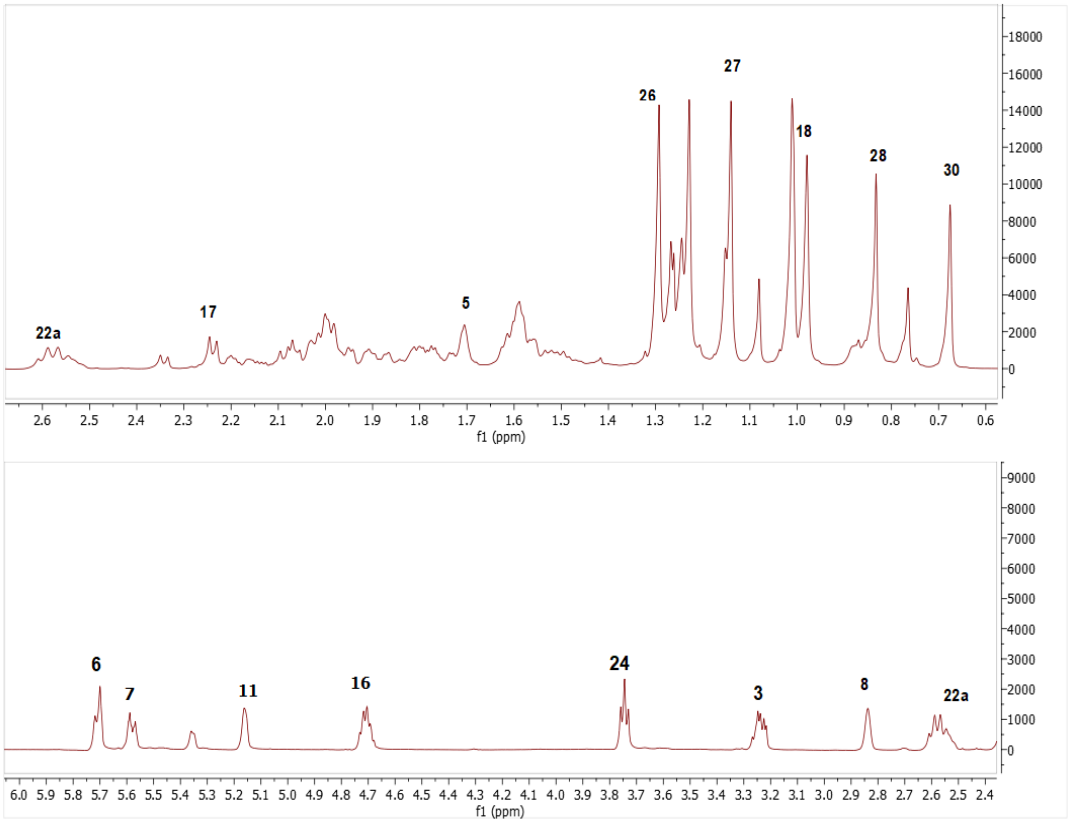

Spectrum 9. ^{1}H NMR Spectrum of AG-03.

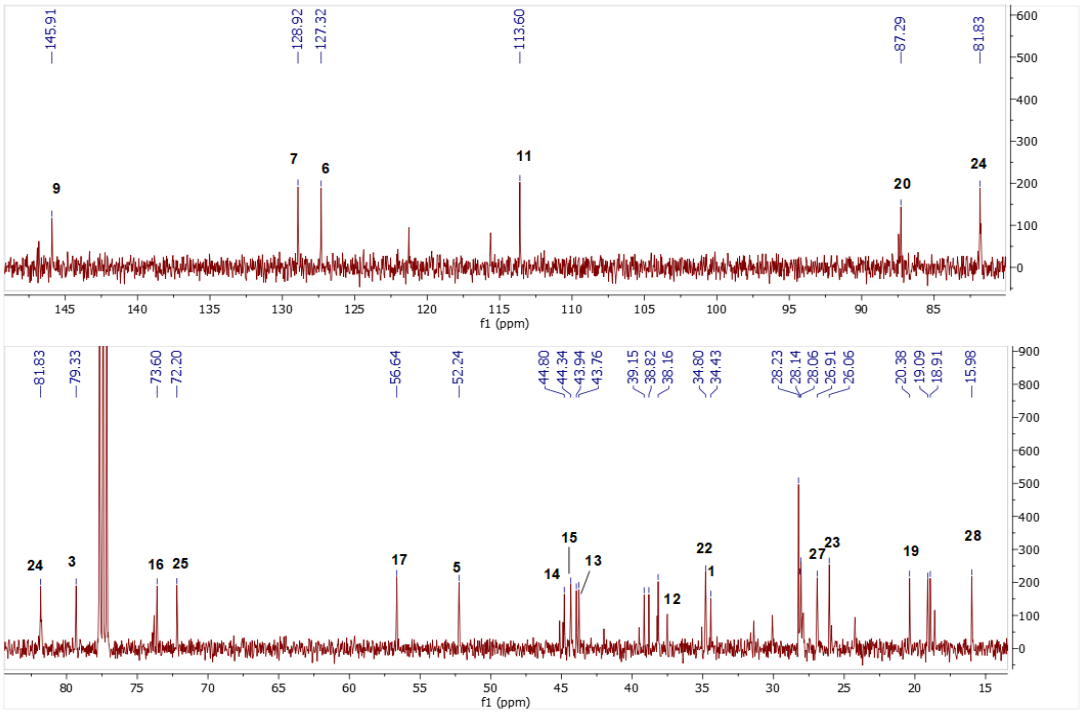

Spectrum 10. ^{13}C NMR Spectrum of AG-03.

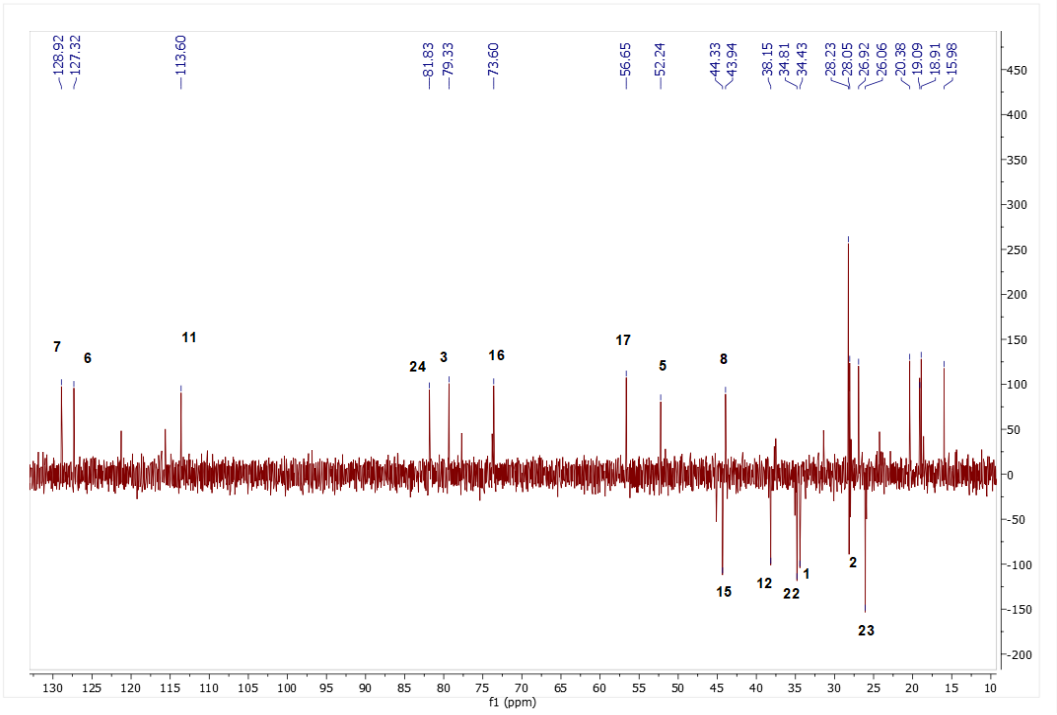

Spectrum 11. DEPT135 spectrum of AG-03.

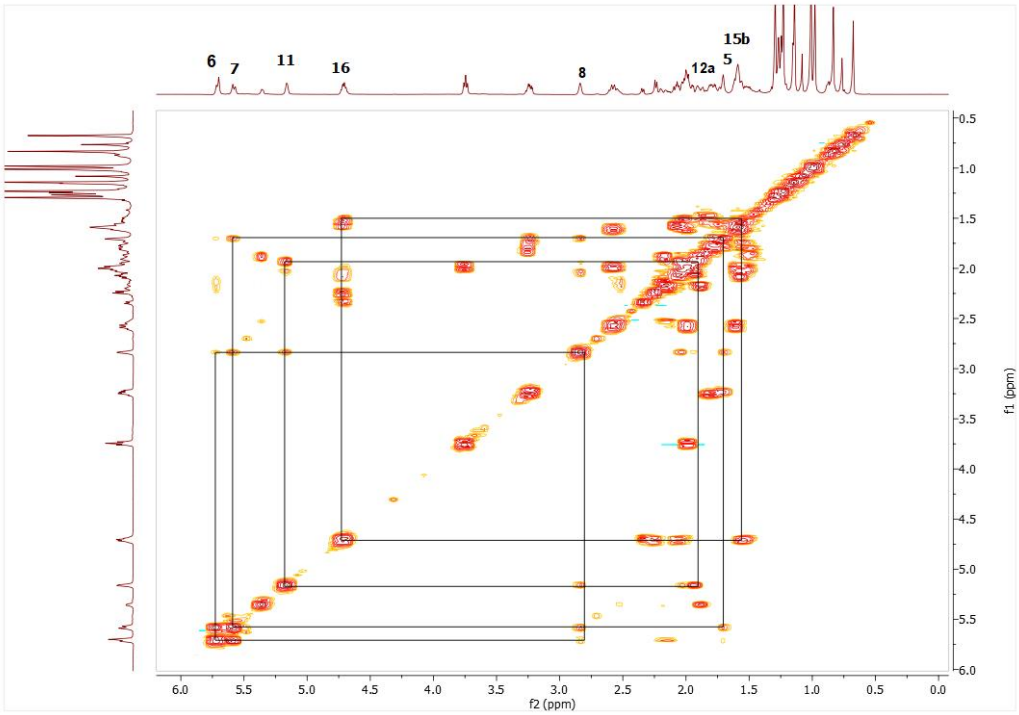

Spectrum 12. COSY spectrum of AG-03.

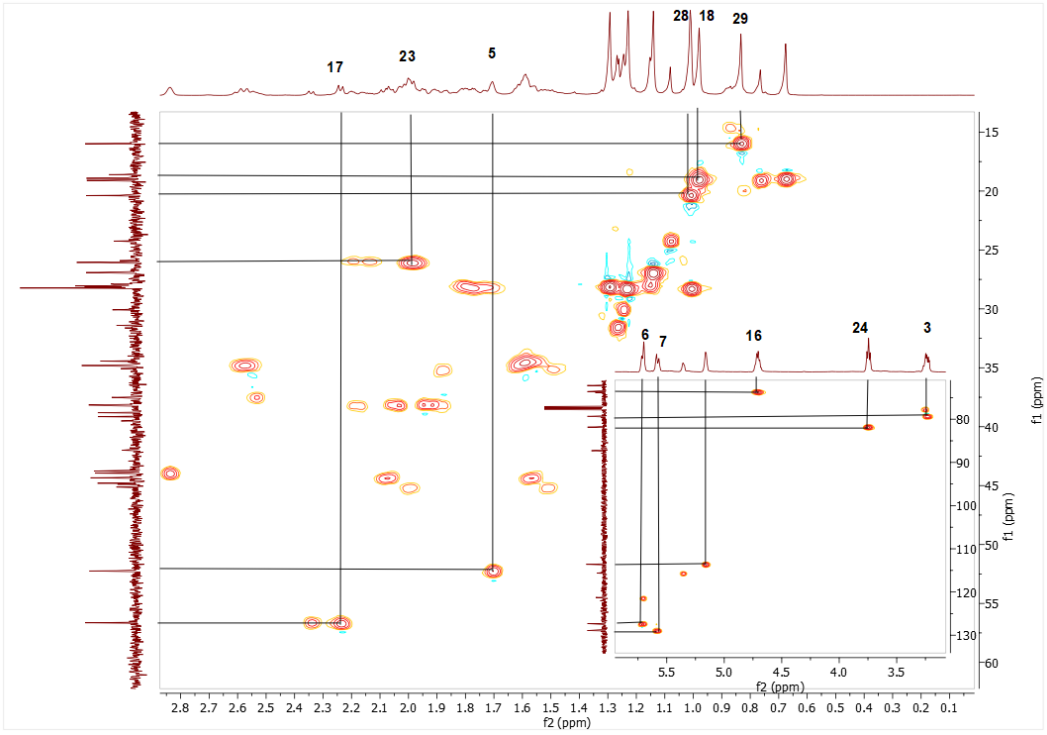

Spectrum 13. HMQC spectrum of AG-03.

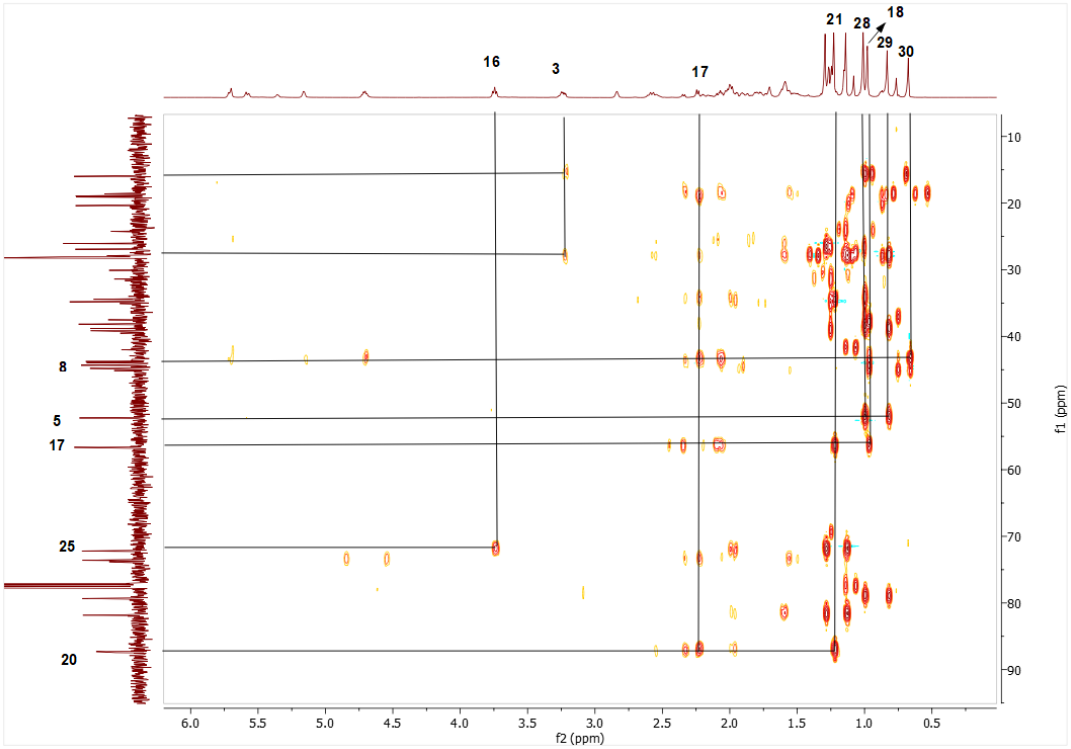

Spectrum 14. HMBC spectrum of AG-03.

3.2.3. Structural Elucidation of Compound AG-04

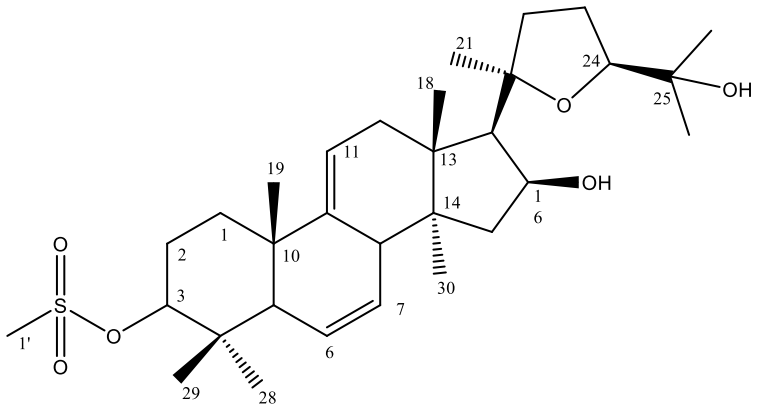

Figure 22. Chemical Structure of AG-04.

The molecular formula of compound AG-04 was established as $C_{31}H_{50}O_6S$ by HR-ESI-MS analysis (*m/z* 573.32873 ([M + Na]$^+$)). Initial inspection of the ^{1}H NMR spectrum of compound revealed presence of new methyl protons (δ_H 3.03) at low-field which demonstrated presence of mesylate. Moreover, disubstituted double bond was

observed in structure (δ_C 128.4, d and 126.1, d; δ_H 5.67 and 5.63; deduced by DEPT135, ^1H and ^{13}C and HSQC). In ^1H NMR spectrum, characteristic H-3 signal (δ_H 4.35) shifted to low-field, showing that mesylation occur at 3-OH. Moreover, absence of characteristic H-6 (δ_H 5.67) signal in ^1H NMR spectrum indicated double bond at C-6. When 2D spectra were inspected in detail to confirm double bond positions, correlation from olefinic proton (H-7; δ_H 5.63) with H-8 (δ_H 2.85) and H-5 (δ_H 1.81) in COSY spectrum were noted. Consequently, AG-04 was deduced to be 20(*R*),24(*S*)-epoxy-3(O)-Mesyl-16β,25-dihydroxy lanosta-6,9(11)-diene.

Table 6. The ^{13}C and ^1H NMR data of AG-04 *(100/500 MHz, δ ppm, in $CDCl_3$).*

H/C	**δ_C (ppm)**	**δ_H (ppm), *J* (Hz)**
1	44.0 t	1.65 m
2	25.74 t	2.06 m, 2.2 m
3	90.2 d	4.35 dd (11.6, 4.9)
4	38.6 s	-
5	52.2 d	1.81 brs
6	126.1 d	5.67 dt (10.1, 2.1)
7	128.4 d	5.63 m
8	43.7 d	2.85 brs
9	144.8 s	-
10	38.3 s	-
11	113.9 d	5.17 dt (5.3, 2.5)
12	37.9 t	1.96 m, 2.05 m
13	44.6 s	-
14	43.5 s	-
15	44.0 t	1.57 m, 2.08 m
16	73.3 d	4.71 ddd (7.7, 7.7, 5.9)
17	56.4 d	2.24 d (7.6)
18	18.7 q	0.67 s
19	20.1 q	1.05 s
20	87.0 s	-
21	27.9 q	1.24 s
22	34.6 t	1.64 m, 2.57 q (10.6)
23	25.81 t	2 m
24	81.6 d	3.76 dd (7.2, 7.2)
25	72 s	-
26	27.8 q	1.3 s
27	26.7 q	1.15 s
28	28.1 q	1.05 s
29	16.5 q	0.92 s
30	18.84 q	0.98 s
1'	39 q	3.03 s

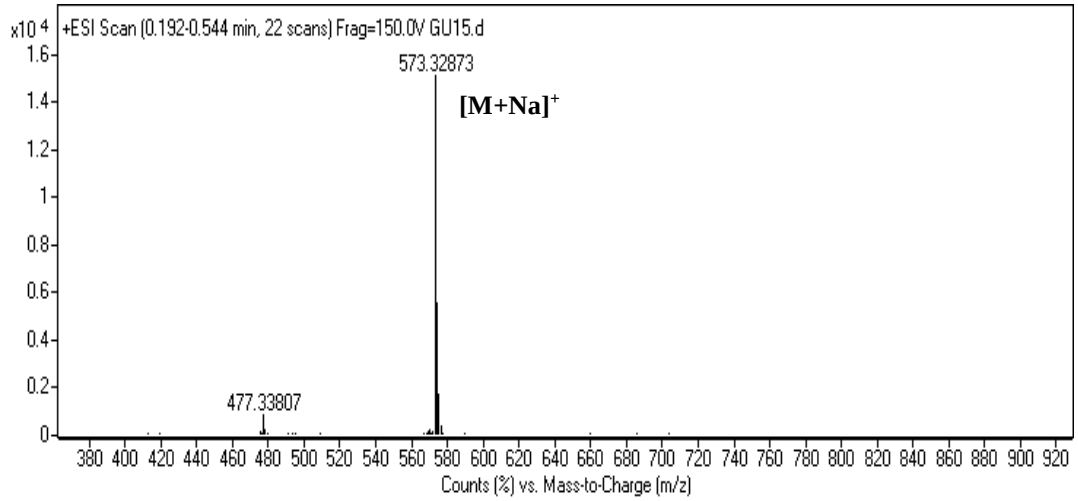

Spectrum 15. HR-ESI-MS Spectrum of AG-04 (positive mode).

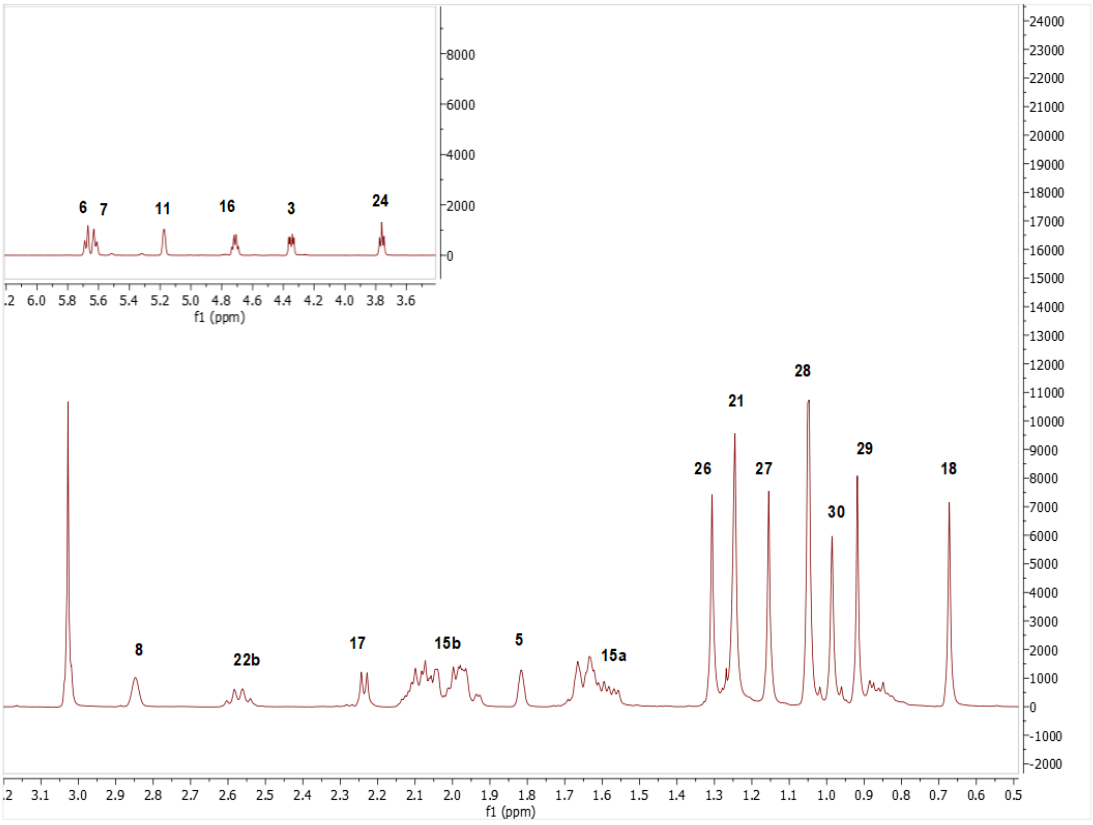

Spectrum 16. ^{1}H NMR Spectrum of AG-04.

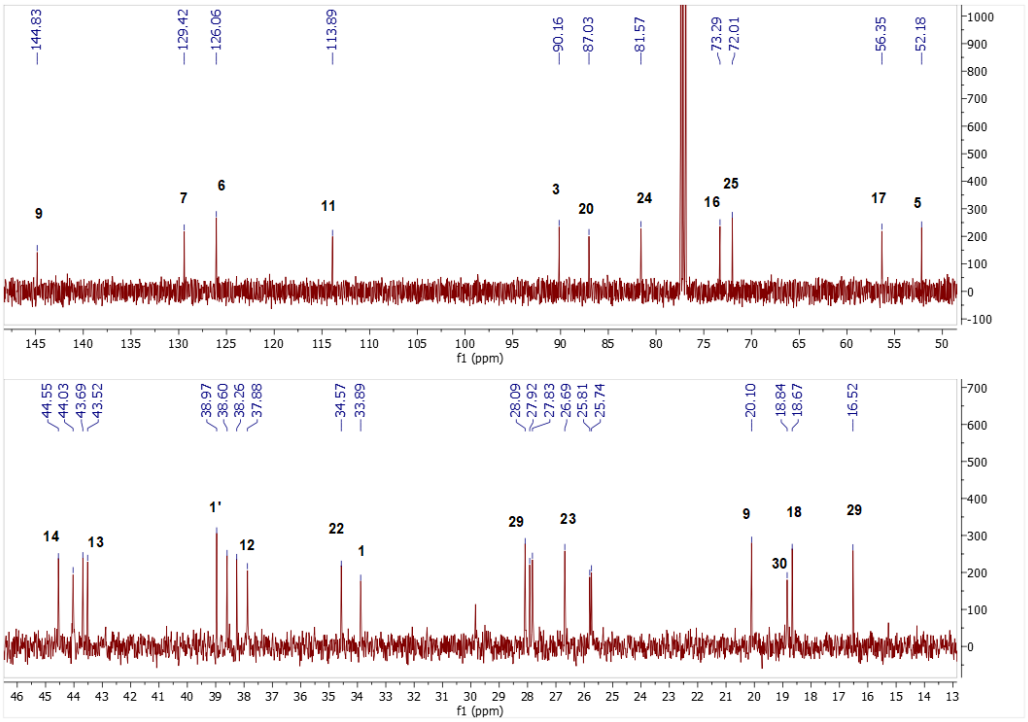

Spectrum 17. ^{13}C NMR Spectrum of AG-04.

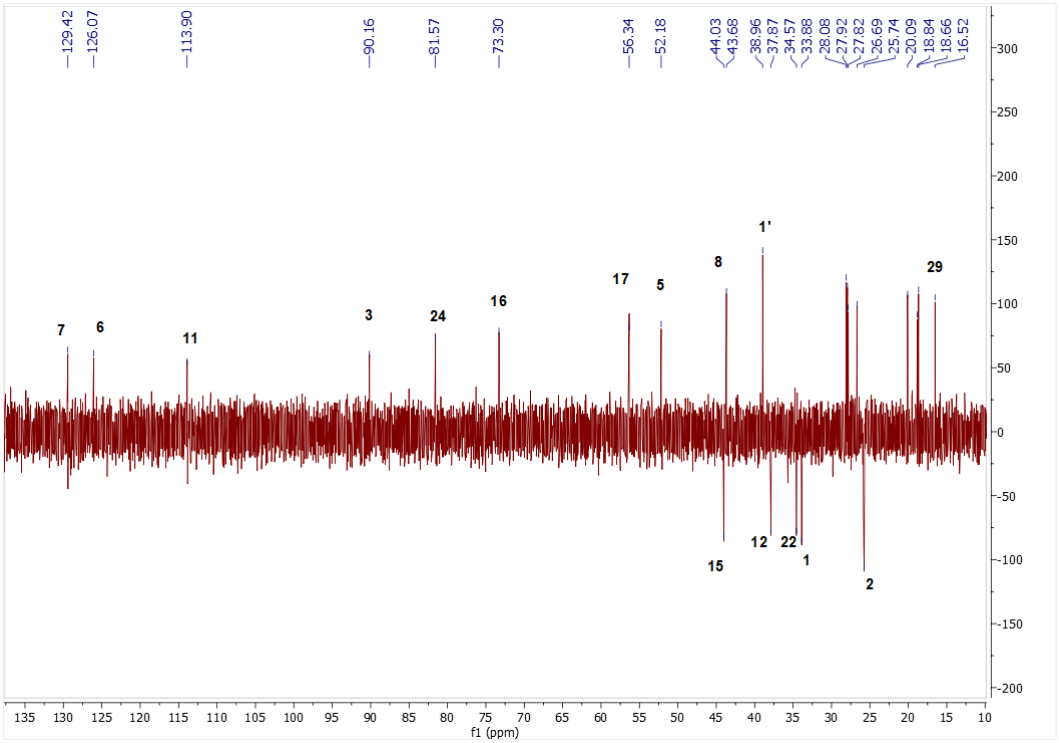

Spectrum 18. DEPT135 spectrum of AG-04.

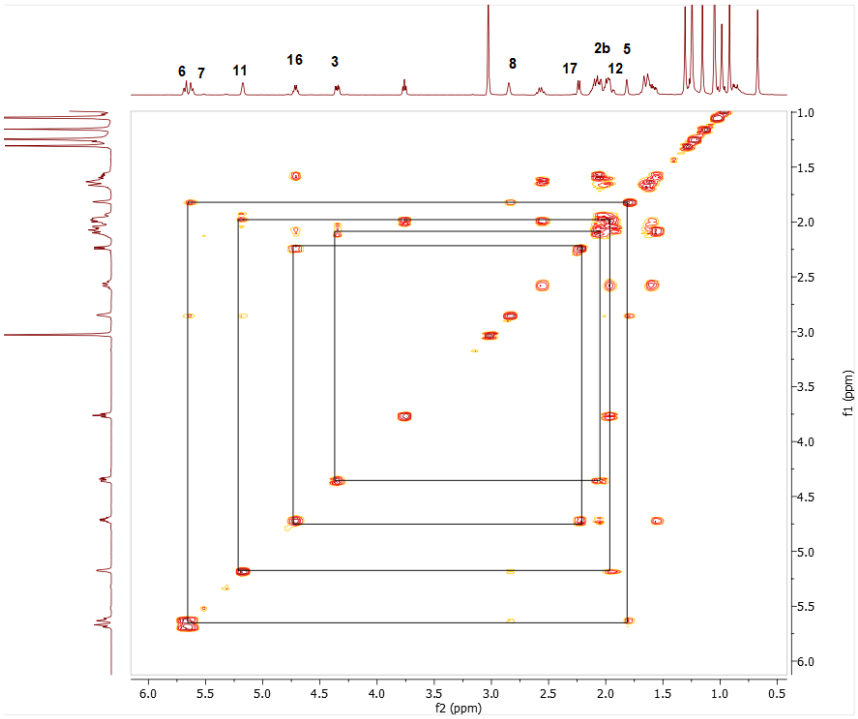

Spectrum 19. COSY spectrum of AG-04.

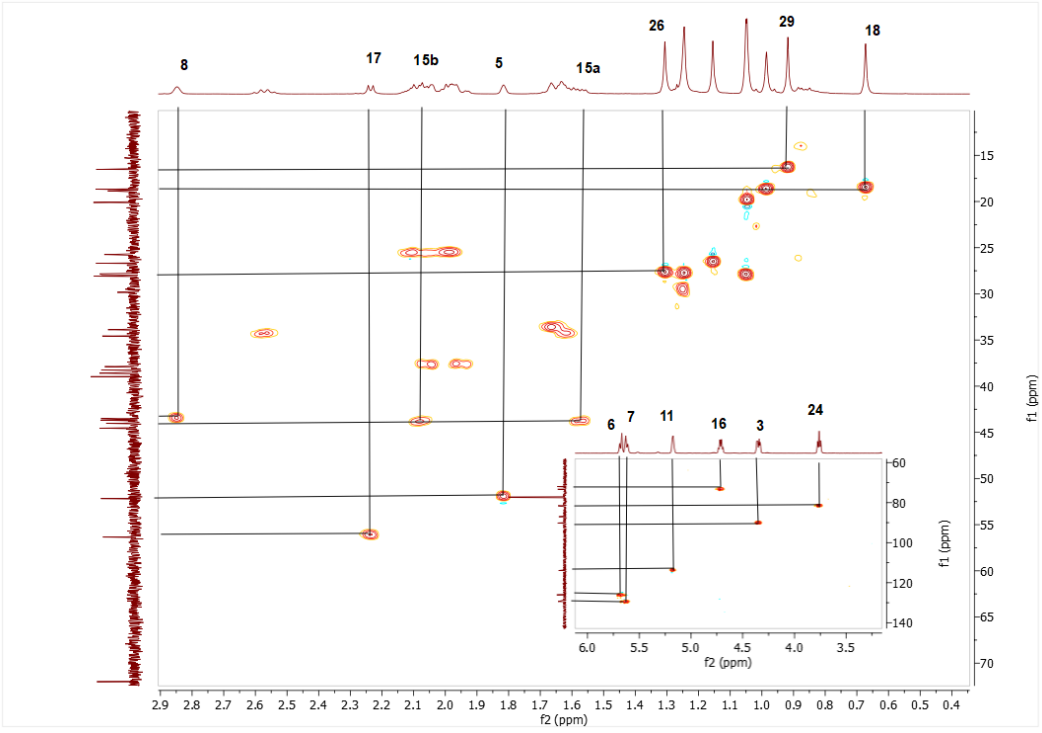

Spectrum 20. HMQC spectrum of AG-04

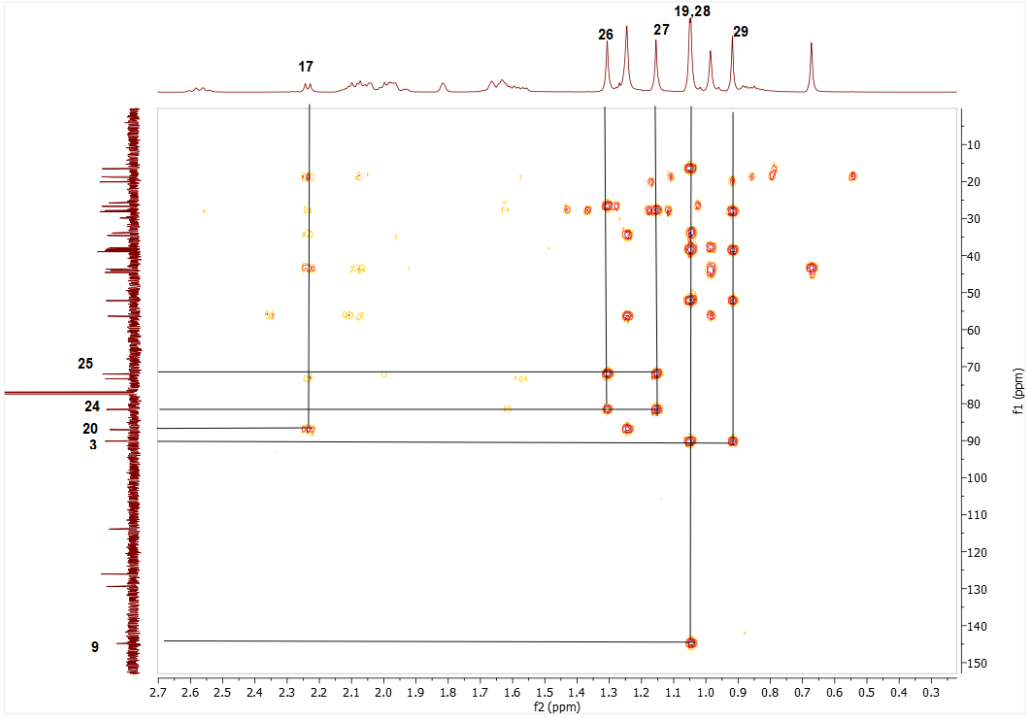

Spectrum 21. HMBC spectrum of AG-04

3.2.4. Structural Elucidation of Compound AG-05

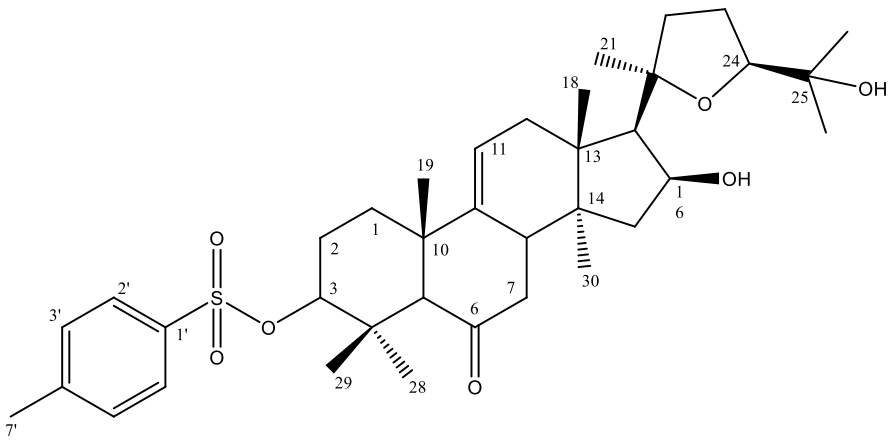

Figure 23. Chemical Structure of AG-05.

The HR-ESI-MS data of AG-05 (*m/z* 665.35653 $[M+Na]^+$) supported a molecular formula $C_{37}H_{54}O_7S$. ^1H and ^{13}C NMR spectra showed presence of carbonyl signal (δ_C 210.4) and disappearance of H-6 signal due to AG-01. Moreover, aromatic signals of

tosyl were noted in ^{1}H NMR spectrum (δ_H 7.77 and 7.32; each 2 H). When examined ^{1}H spectrum, characteristic H-16 (δ_H 4.68) signal was observed implying tosylation position is C-3(OH). Moreover, H-3 (δ_H 4.07) signal shifted to low-field, supporting this proposition. As a result, AG-05 was established as 20(*R*),24(*S*)-epoxy-3(O)-p-tosyl-6-one-16β,25-dihydroxy lanosta-9(11)-ene.

Table 7. The ^{13}C and ^{1}H NMR data of AG-05 *(100/400 MHz, δ ppm, in $CDCl_3$).*

H/C	**δ_C (ppm)**	**δ_H (ppm), *J* (Hz)**
1	35.9 t	1.68 m, 1.85 d (1,5)
2	25.1 t	1.91 m
3	89.4 d	4.07 m
4	37.7 s	-
5	61.7 d	2.17 brs
6	210.4 s	-
7	43.98 t	2.19 m, 2.34 d (5)
8	43.8 d	2.69 brs
9	144.5 s	-
10	44.3 s	-
11	118.1 d	5.44 dd (6.3, 1.7)
12	44.2 t	1.43 dd (12.9, 6.3), 1.88 d (4.24)
13	44.2 s	-
14	44.3 s	-
15	37.4 t	1.95 m, 2.15 m
16	73.0 d	4.68 q (6.8)
17	56.3 d	2.32 brs
18	18.2 q	0.9 s
19	23.8 q	1.04 s
20	86.9 s	-
21	28.0 q	1.22 s
22	34.5 t	1.56 dt (12,6), 2.56 q (10.4)
23	25.8 d	1,96 m
24	81.4 d	3.75 td (7.4, 1.6)
25	72.0 s	-
26	26.8 q	1.14 s
27	27.8 q	1.29 s
28	27.8 q	0.84 s
29	16.1 q	1.27 d (1.3)
30	18.9 q	0.84 s
1'	134.6 s	-
2'	127.8 d	7.77 dd (8.2, 1.7)
3'	129.8 d	7.32 dd (8.4, 1.8)
4'	144.6 s	-
5'	129.8 d	7.32 dd (8.4, 1.8)
6'	127.8 d	7.77 dd (8.2, 1.7)
7'	21.78 q	2.43 s

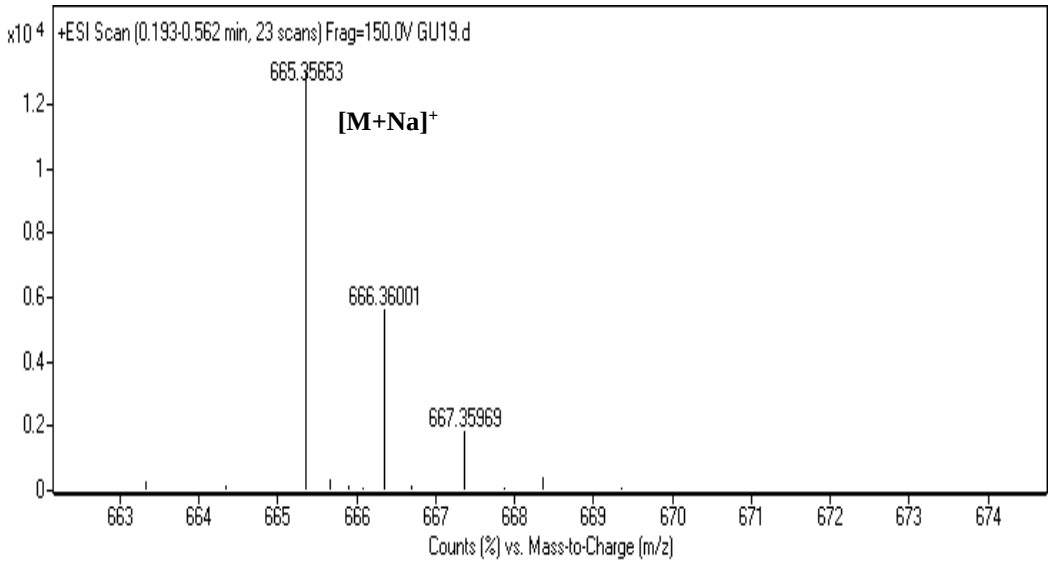

Spectrum 22. HR-ESI-MS Spectrum of AG-05 (positive mode).

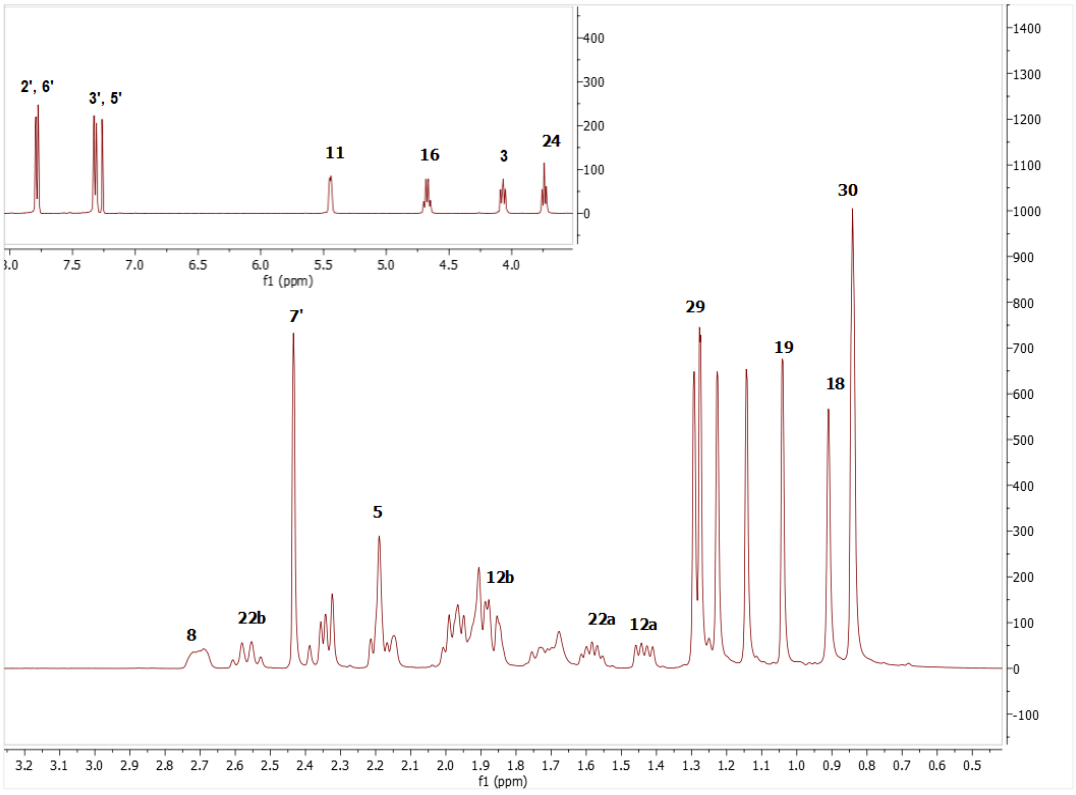

Spectrum 23. ^{1}H NMR Spectrum of AG-05.

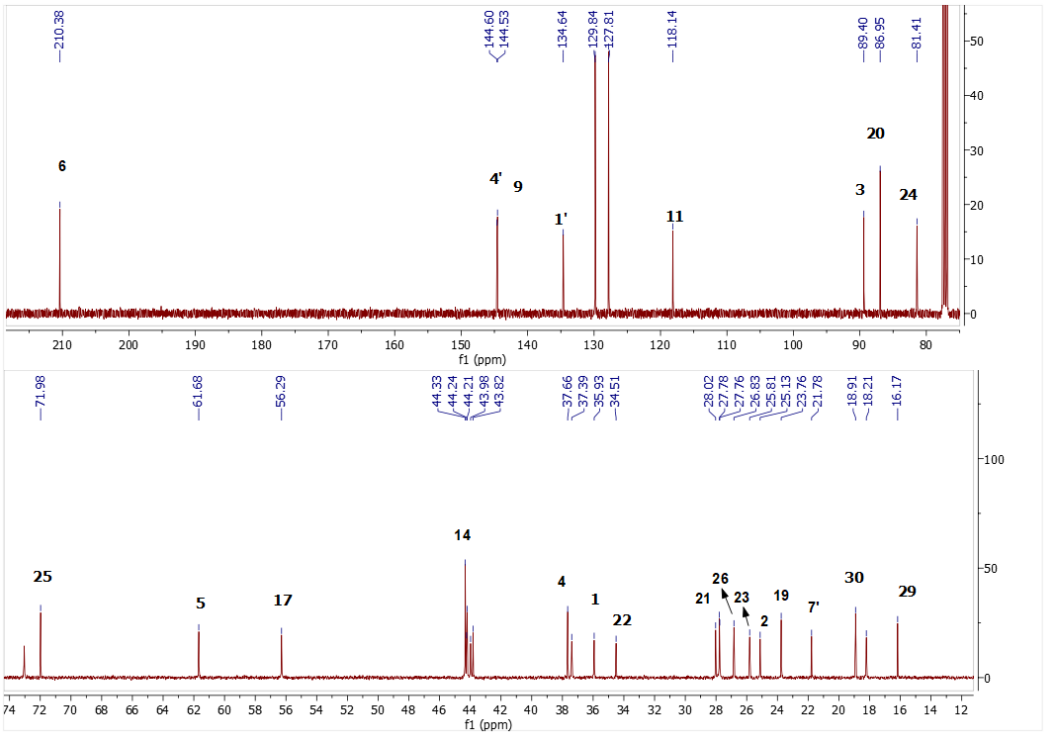

Spectrum 24. ^{13}C NMR Spectrum of AG-05**.**

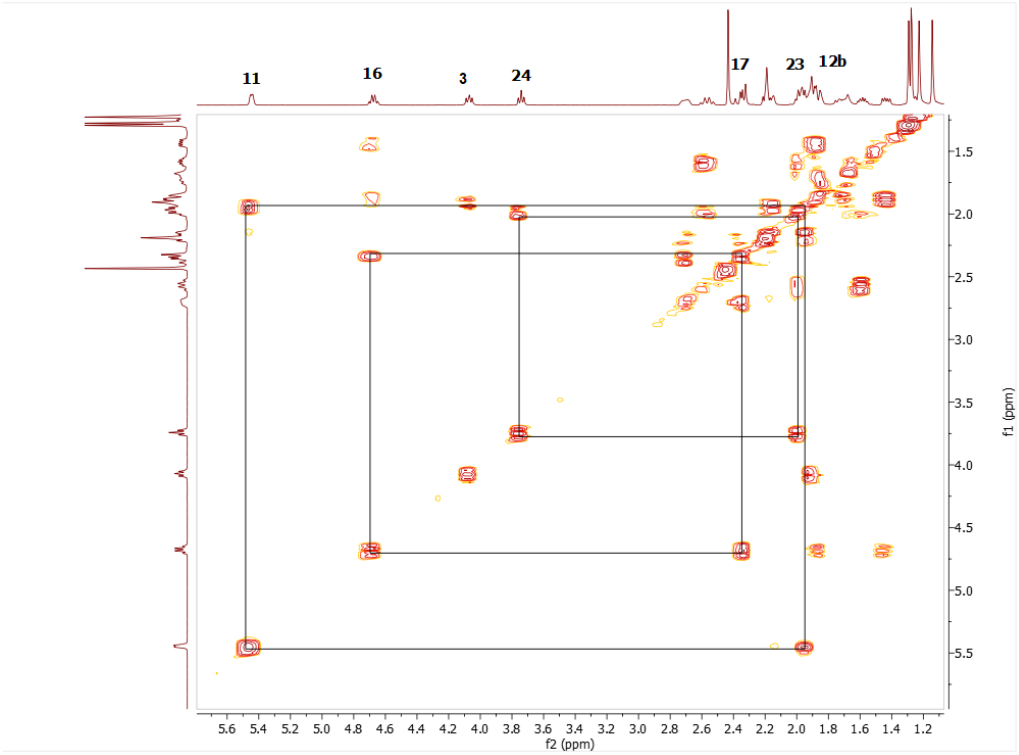

Spectrum 25. COSY spectrum of AG-05.

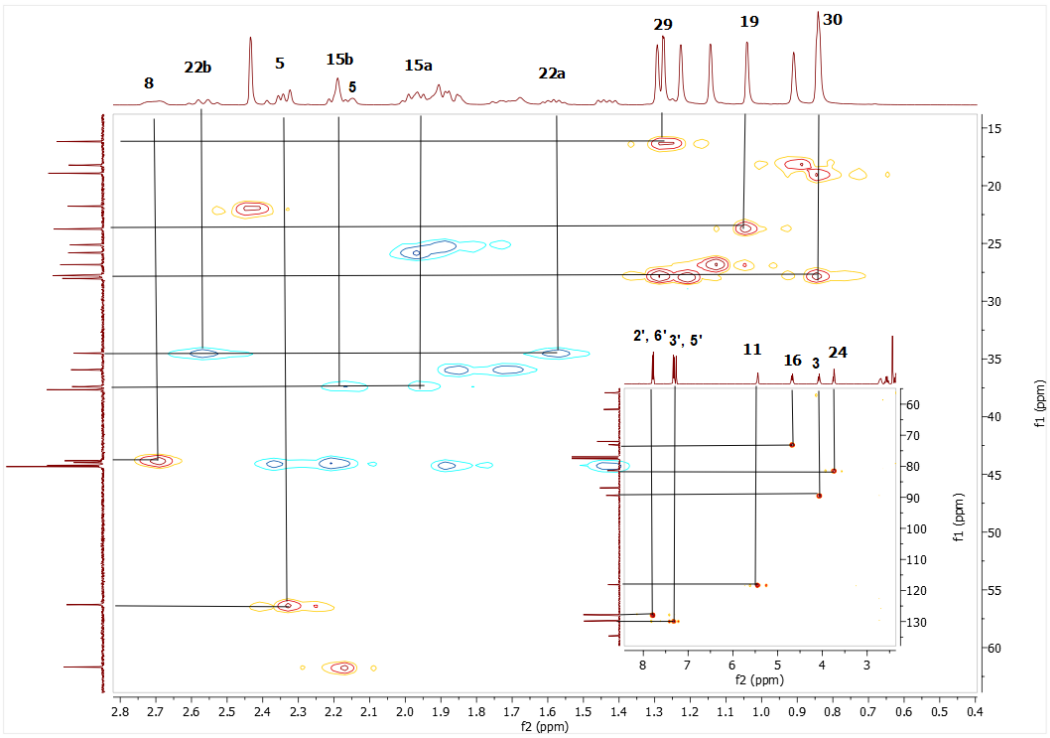

Spectrum 26. HSQC spectrum of AG-05.

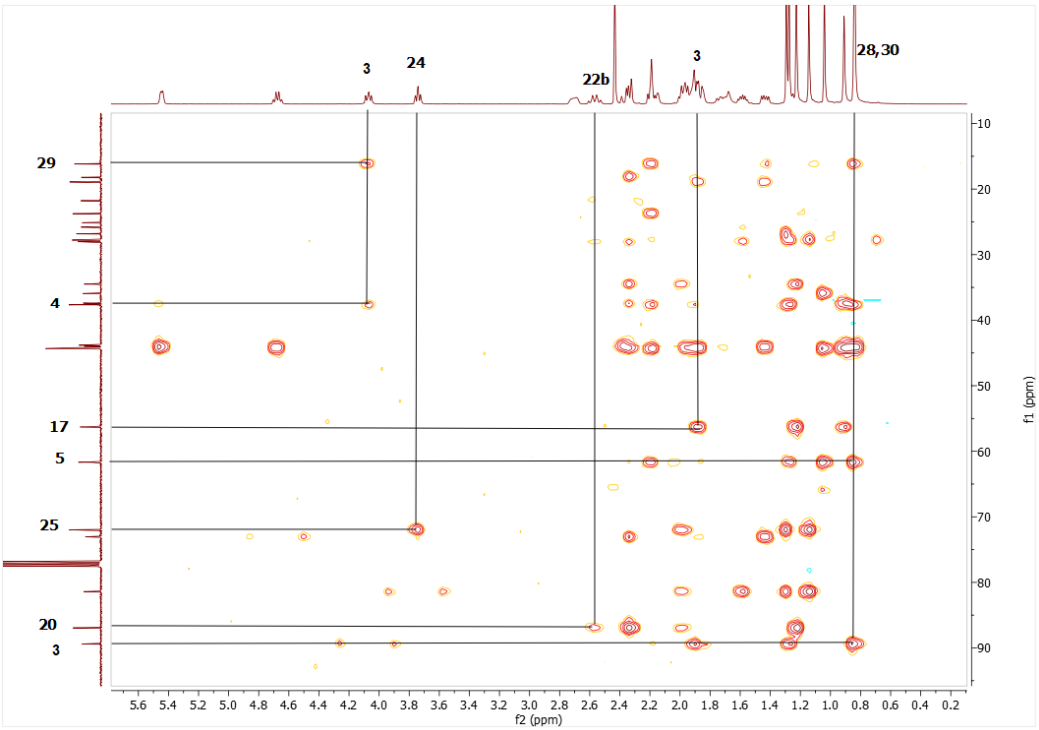

Spectrum 27. HMBC spectrum of AG-05.

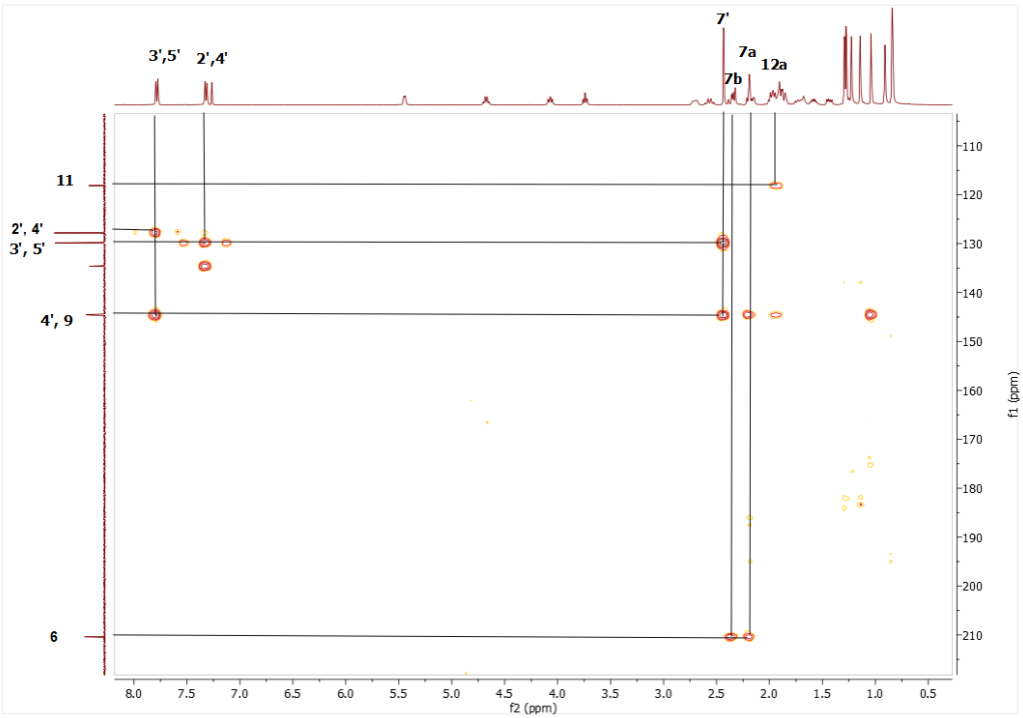

Spectrum 28. HMBC spectrum of AG-05.

3.2.5. Structural Elucidation of Compound CG-02

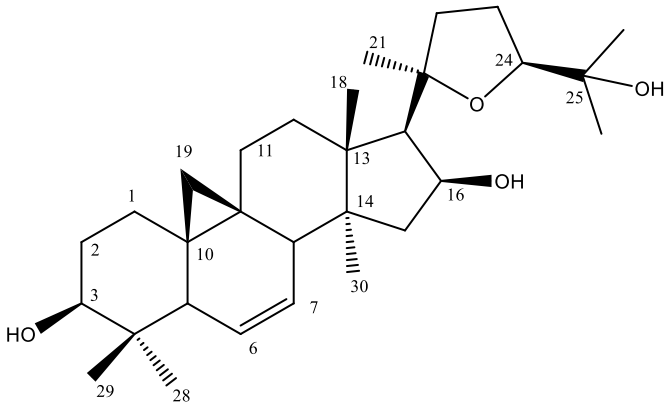

Figure 24. Chemical Structure of CG-02.

CG-02 was obtained from reaction of CG with *p*-TsCl. In the HR-ESI-MS of CG-02, the major ion peak was observed *m/z* 495.3498 $[M + Na]^+$ ($C_{30}H_{48}O_4$), indicating additional unsaturation as well as lack of water molecule due to 18 amu difference comparing to CG. The ^{1}H and ^{13}C NMR spectra of CG-02 were similar to those of AG-03, except absence of double bond at C-9(11) and presence of cyclopropane signal

derived from CG skeleton. All the proton and carbon resonances of CG-02 were secured by COSY, HSQC and HMBC spectra, verifying double bond location at C-6 like AG-03. Correlation of H-5 with H-6/ H-7 and H-8 with H-7 in COSY spectrum confirmed presence of double bond at C-6. Moreover, in ^{1}H and ^{13}C NMR spectra, characteristic cyclopropane carbon signal (δ_C 18.7) and one of its hydrogen (δ_H -0.16, H-19a) was observed at up-field, probably due to deshielding effect of double bond at C-6. In conclusion, the structure of the compound was determined to be 20(R),24(S)-epoxy-6α,16β,25-trihydroxy 9,19-cyclolanosta-6-ene.

Table 8. The ^{13}C and ^{1}H NMR data of CG-02 *(100/500 MHz, δ ppm, in $CDCl_3$).*

H/C	**δ_C (ppm)**	**δ_H (ppm), *J* (Hz)**
1	29.8 t	1.25 s, 1.41 m
2	30.1 t	1.82 m, 1.59 m
3	78.5 d	3.32 dd (11.4, 4.6)
4	40.3 s	-
5	46.6 d	1.85 m
6	126.6 d	5.63 d (10.6)
7	129.2 d	5.48 brs
8	43.4 d	2.71 d (7.9)
9	20.6 s	-
10	28.4 s	-
11	25.2 t	1.40 m, 1.88 m
12	33.4 t	1.62 m, 1.42 m
13	45.2 s	-
14	48.5 s	-
15	43.6 t	1.84 m, 1.52 m
16	73.5 d	4.69 q (7.2)
17	56.4 d	2.27 d (7.6)
18	18.1 q	1.23 s
19	18.7 t	-0.16 d (4.3), 0.74 m
20	87.3 s	-
21	28.1 q	1.22 s
22	34.6 t	1.6 m, 2.59 q (10.6)
23	25.9 t	2 m
24	81.4 d	3.74 dd (7.1, 7.1)
25	72.1 s	-
26	27.9 q	1.31 s
27	26.7 q	1.15 s
28	14.5 q	0.78 s
29	25.6	1.05 s
30	18.2	1.23 s

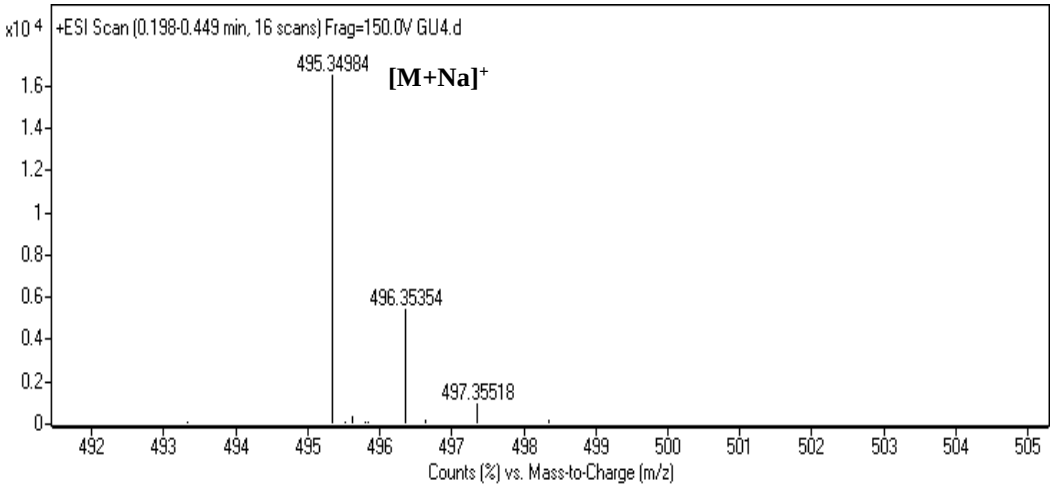

Spectrum 29. HR-ESI-MS Spectrum of CG-02 (positive mode).

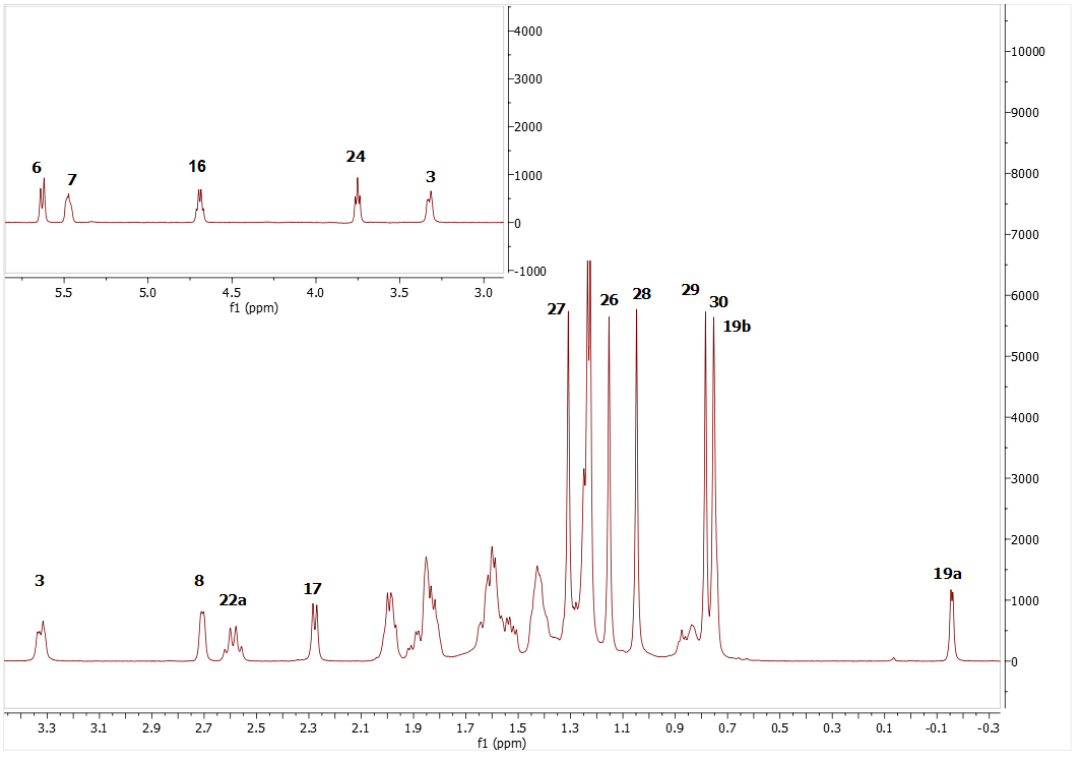

Spectrum 30. ^{1}H NMR Spectrum of CG-02.

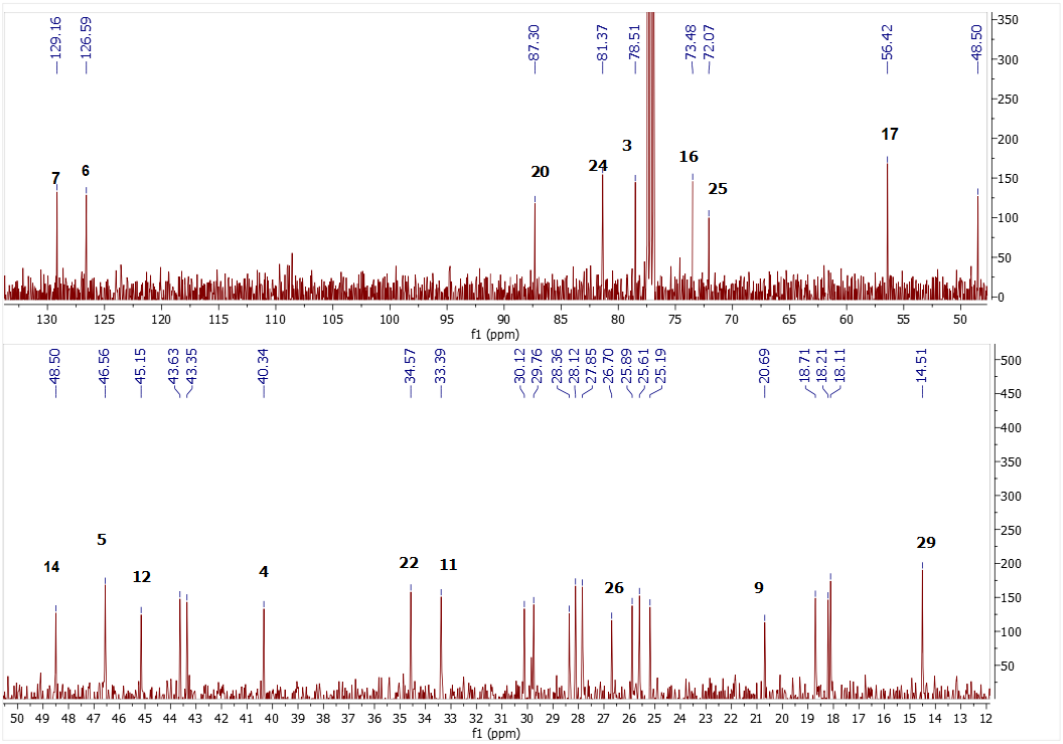

Spectrum 31. ^{13}C NMR Spectrum of CG-02.

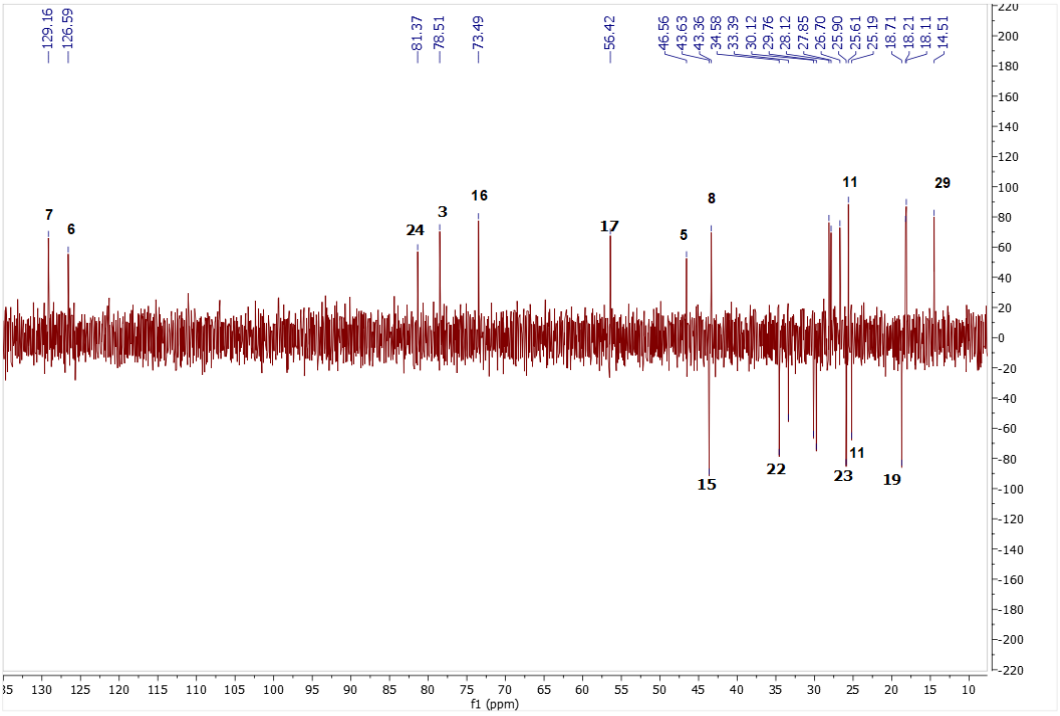

Spectrum 32. DEPT135 spectrum of CG-02.

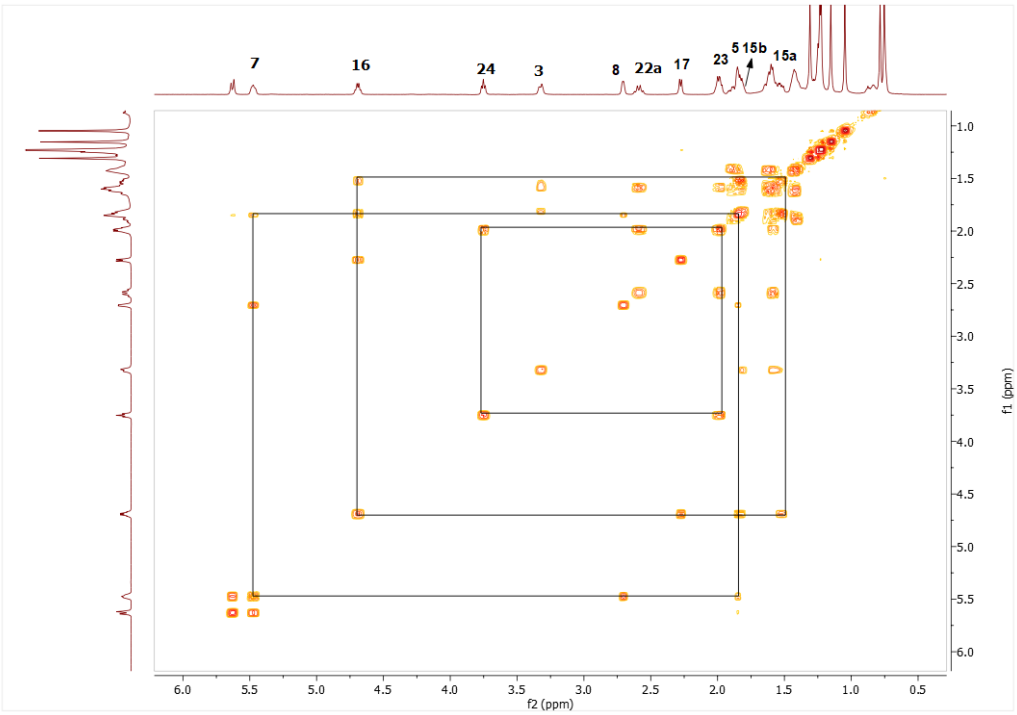

Spectrum 33. COSY spectrum of CG-02.

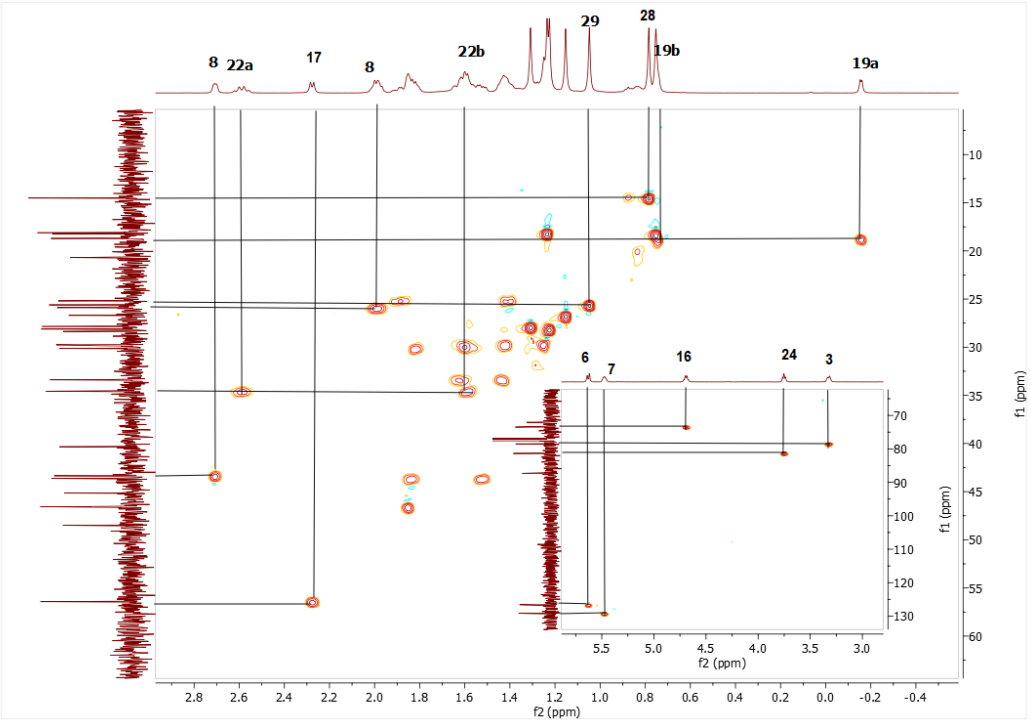

Spectrum 34. HMQC spectrum of CG-02.

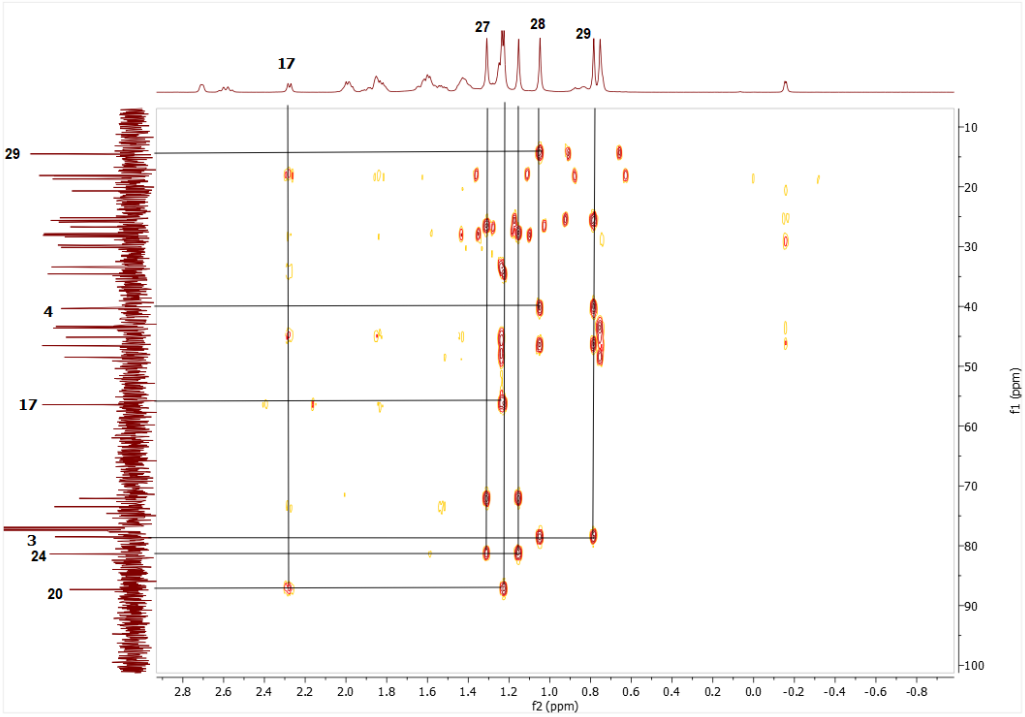

Spectrum 35. HMBC spectrum of CG-02.

3.2.6. Structural Elucidation of Compound CG-03

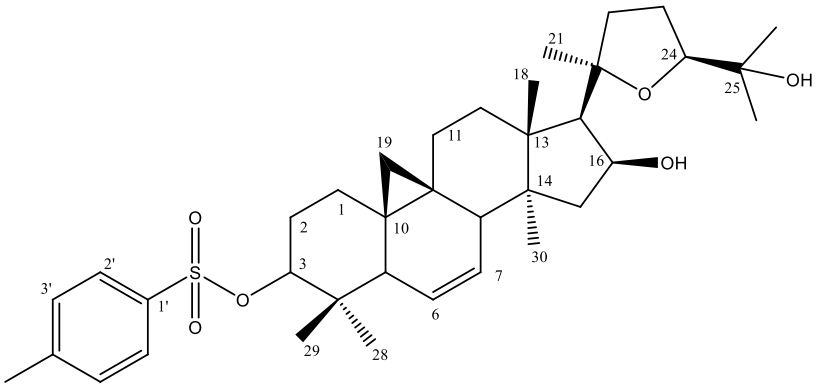

Figure 25. Chemical Structure of CG-03.

The HR-ESI-MS spectrum of CG-03 showed a major ion peak at *m/z* 649.36046, indicating a molecular formula is $C_{37}H_{54}O_6S$. Four protons (δ_H 7.79 and 7.32, each 2H) and additional methyl signals (δ_H 2.43, 3H) in the low-field region of the ^{1}H NMR spectrum demonstrated tosyl addition to CG skeleton. Also, ^{1}H, ^{13}C NMR, DEPT135 and HMQC spectra revealed disubstituted double bond system (δ_C 125.6, d and 129.8, d; δ_H

5.51 and 5.46, each 1H). While characteristic H-3 signal shifted to δ_H 4.31 implying tosylation position, lacking H-6 resonance indicated double bond location. Additionally, double bond location was supported by H-19a and C-19 signals which shifted to up-field like CG-02. This assumption was confirmed with the $^3J_{C\text{-}H}$ long-distance correlations in the HMBC spectrum (C-9 to H-7; C-10 to H-6; C-5 and C-8 to H-6). On the basis of these evidence, the structure of compound CG-03 was elucidated as 20(*R*),24(*S*)-epoxy-3(O)-*p*-tosyl-16β,25-dihydroxy 9,19-cyclolanosta-6-ene.

Table 9. The ^{13}C and ^{1}H NMR data of CG-03 *(100/500 MHz, δ ppm, in $CDCl_3$).*

H/C	**δ_C (ppm)**	**δ_H (ppm), *J* (Hz)**
1	29.5 t	1.38 m, 1.58 m
2	27.8 t	1.77 m, 1.89 m
3	90.2 s	4.31 dd (11.8, 4.6)
4	40 s	-
5	46.7 d	1.86 m
6	125.6 d	5.51 d (10.7)
7	129.8 d	5.46 ddd (10.7 ,6, 3)
8	43.3 d	2.68 dd (6, 2.5)
9	20.7 s	-
10	27.9 s	-
11	25.2 t	1.34 m, 1.85 m
12	33.3 t	1.41 m,1.57 m
13	48.6 s	-
14	45.1 s	-
15	43.5 t	1.48 m, 1.79 m
16	73.4 d	4.68 ddd (7.7, 7.7, 6.1)
17	56.4 d	2.26 d (7.7)
18	18.1 q	1.21 s
19	18.6 t	-0.17, 0.72 d (4.2)
20	87.2 s	-
21	28.2 q	1.19 s
22	34.5 t	1.56 m, 2.58 q (10.5)
23	25.9 t	2 td (10.5, 9, 5)
24	81.3 d	3.74 dd (7.1, 7.1)
25	72.0 s	-
26	28.8 q	1.29 s
27	26.7 q	1.13 s
28	25.4 q	0.81 s
29	15.4 q	0.8 s
30	18.2 q	0.71 s

(cont. on next page)

Table 9 (cont.).

H/C	δ_C (ppm)	δ_H (ppm), *J* (Hz)
1'	132.9 s	-
2'	127.8 d	7.79 d (8.2)
3'	129.8 d	7.32 d (8.2)
4'	144.5 s	-
5'	129.8 d	7.32 d (8.2)
6'	127.8 d	7.79 d (8.2)
7'	21.2 q	2.43 s

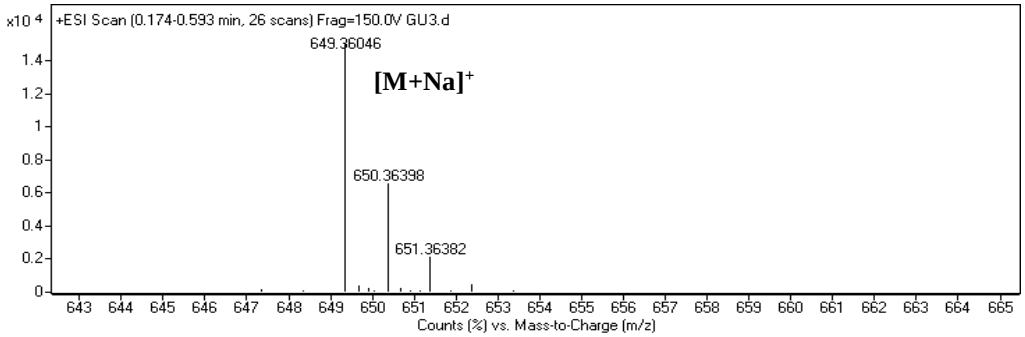

Spectrum 36. HR-ESI-MS Spectrum of CG-03 (positive mode).

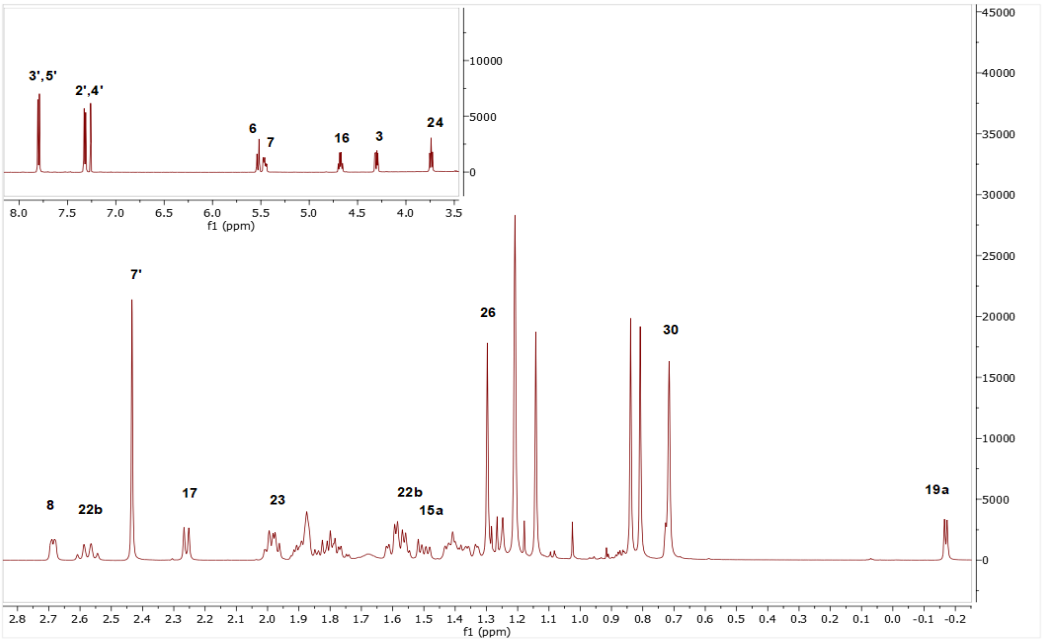

Spectrum 37. ^{1}H NMR Spectrum of CG-03.

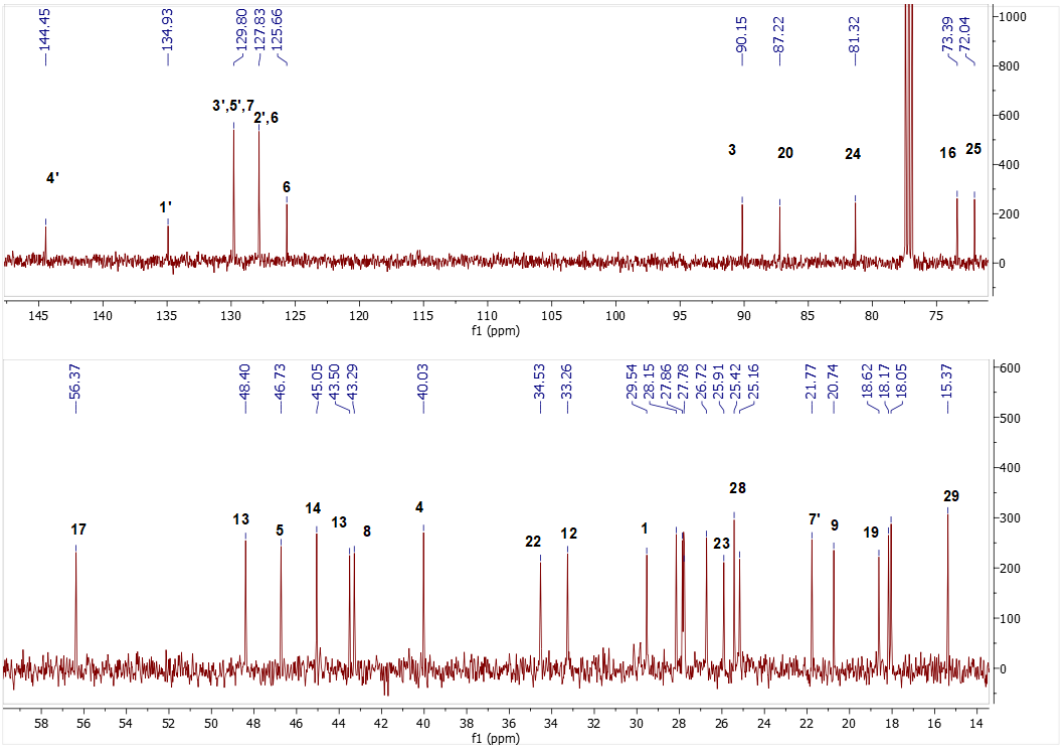

Spectrum 38. ^{13}C NMR Spectrum of CG-03.

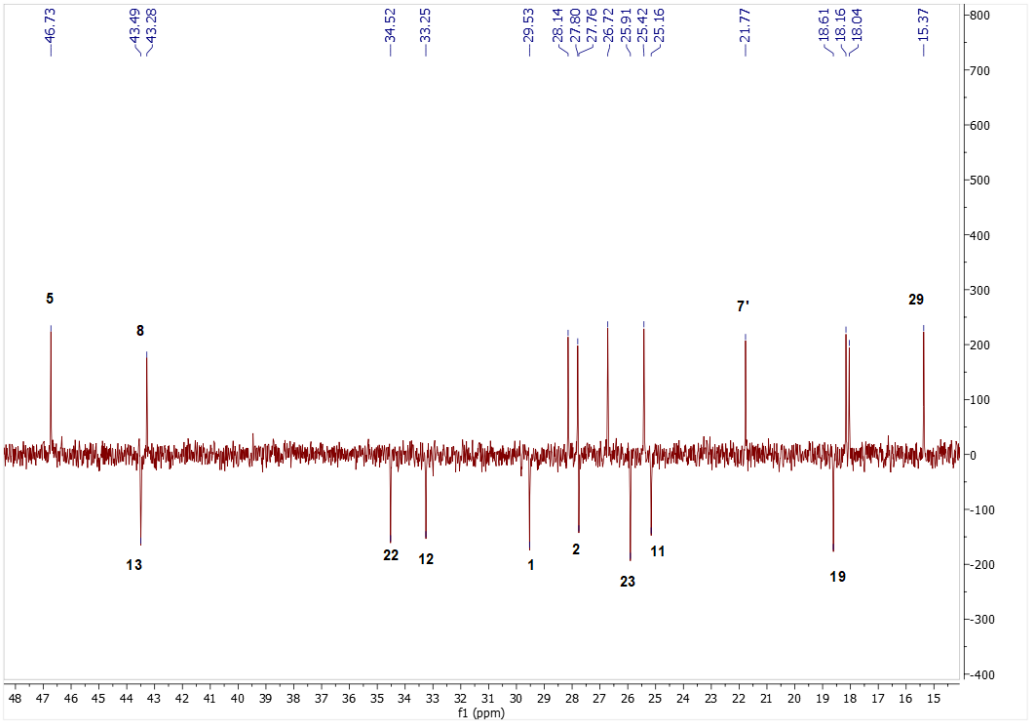

Spectrum 39. DEPT135 spectrum of CG-03.

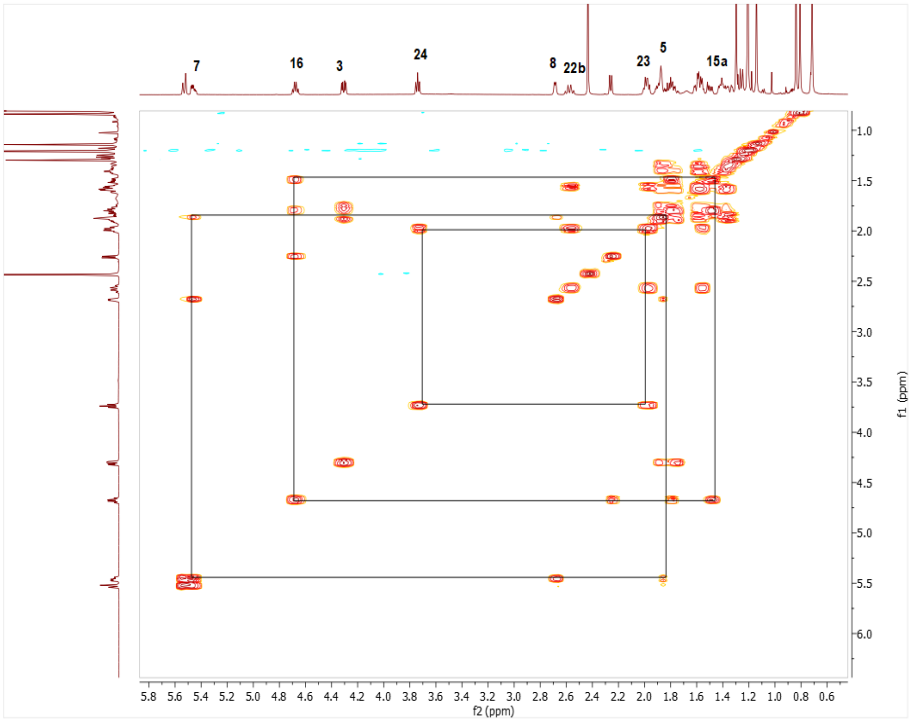

Spectrum 40. COSY spectrum of CG-03.

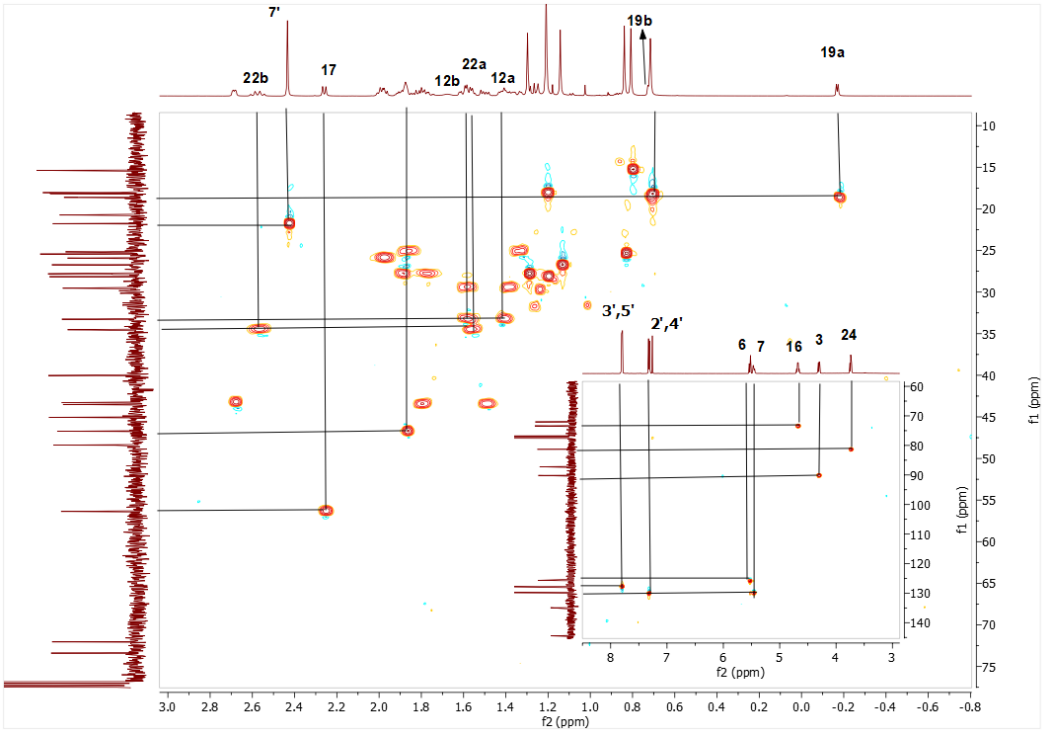

Spectrum 41. HMQC spectrum of CG-03.

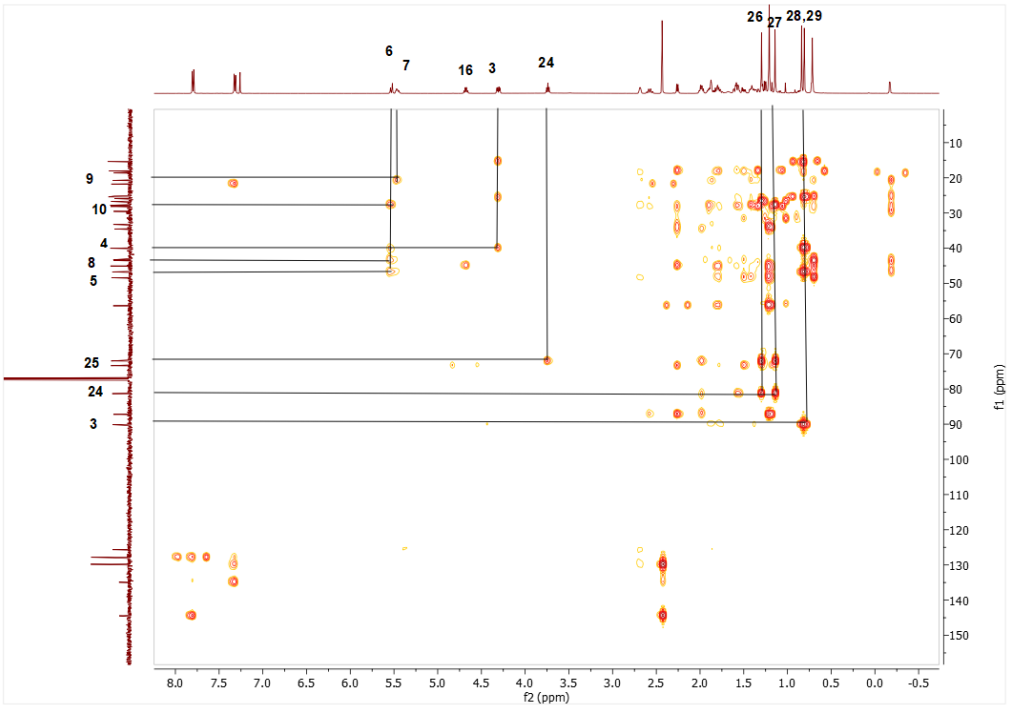

Spectrum 42. HMBC spectrum of CG-03.

3.2.7. Structural Elucidation of Compound CG-04

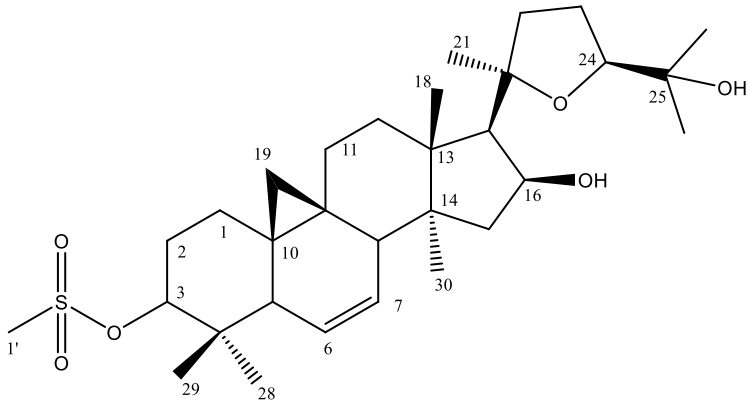

Figure 26. Chemical Structure of CG-04.

Compound CG-04 was prepared with reaction of CG with MsCl. The molecular formula was found to be $C_{31}H_{50}O_6S$ based on the major ion peak at *m/z* 573.32624 $[M+Na]^+$. Inspection of the ^1H, ^{13}C NMR and DEPT135 spectra showed disubstituted double bond system (δ_C 129.9, d and 125.6, d; δ_H 5.58 and 5.49, each 1H) and additional

methyl signal (δ_H 3.01) at low-field suggested mesylate additon to CG. Since charactresitic H-16 signals (δ_H 4.7 ddd; 7.7, 7.7, 6) were noted in ^{1}H spectra, it suggested that modificaitons occur at C-6(OH) and C-3(OH). In order to deduce modification positions, the 2D NMR spectra were inspected in detail. In COSY spectrum, corelation from an olefenic signal at δ_H 5.49 (H-7) with H-8 and H-5 confimed double bond at C-6. Also, characteric H-3 (δ_H 4.43) signal shifted to low-field suggesting mesylate addition position. On the basis of these results, the structure of CG-04 was established as 20(*R*),24(*S*)-epoxy-3(O)-Mesyl-16β,25-dihydroxy 9,19-cyclolanosta-6-ene.

Table 10. The ^{13}C and ^{1}H NMR data of CG-04 *(100/500 MHz, δ ppm, in $CDCl_3$).*

H/C	**δ_C (ppm)**	**δ_H (ppm), *J* (Hz)**
1	29.5 d	1.47 m, 1.68 m
2	28.2 t	1.9 m, 2.12 dd (12.5, 3.9)
3	89.7 d	4.43 dd (11.9, 4.6)
4	40.1 s	-
5	46.7 d	1.96 m
6	125.6 d	5.58 d (10.6)
7	129.9 d	5.49 ddd (10.6, 6.1, 3.1)
8	43.3 d	2.71 dd (6.2, 2.6)
9	20.8 s	-
10	27.9 s	-
11	25.2 t	1.38 m, 1.89 m
12	33.3 t	1.43 m, 1.61m
13	48.4 s	-
14	45.1 s	-
15	43.5 t	1.51m, 1.81m
16	73.4 d	4.7 ddd (7.7, 7.7, 6)
17	56.4 d	2.27 d (7.6)
18	18.1 q	1.22 s
19	18.6 t	-0.12 d (4.3), 0.77 d (3.6)
20	87.2 s	-
21	28.2 q	1.2 s
22	34.5 t	1.6 m, 2.58 d (10.6)
23	25.8 t	2 m
24	81.3 d	3.73 dd (7.1, 7.1)
25	72.0 s	-
26	27.8 q	1.29 s
27	26.7 q	1.14 s
28	25.7 q	1.05 s
29	15.4 q	0.86 s
30	18.2 q	0.74 s
1'	38.9 q	3.01 s

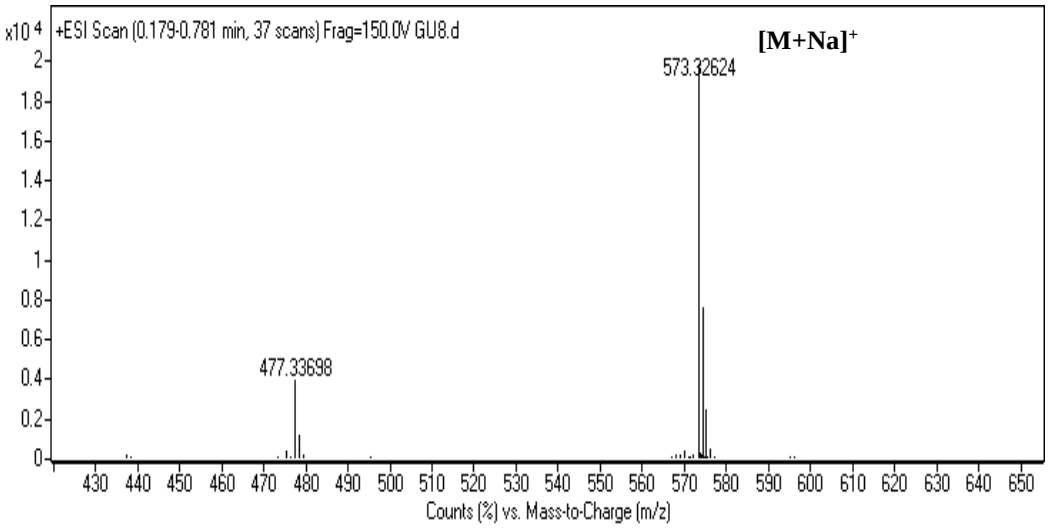

Spectrum 43. HR-ESI-MS Spectrum of CG-04 (positive mode).

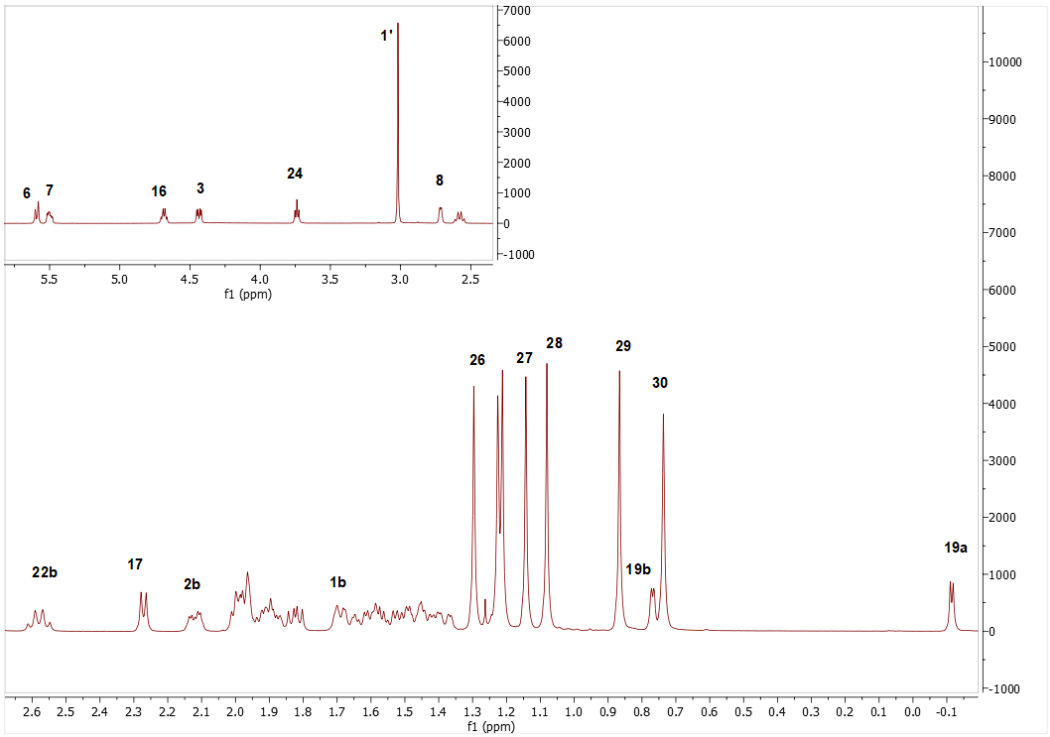

Spectrum 44. ^{1}H NMR Spectrum of CG-04.

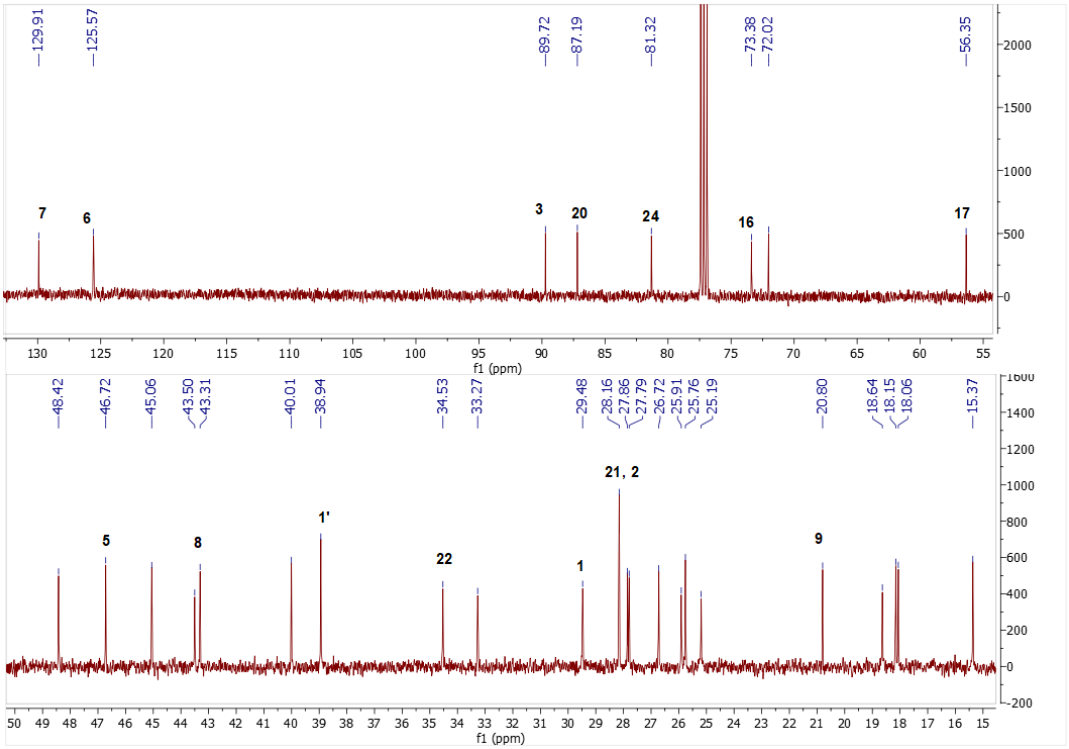

Spectrum 45. ^{13}C NMR Spectrum of CG-04.

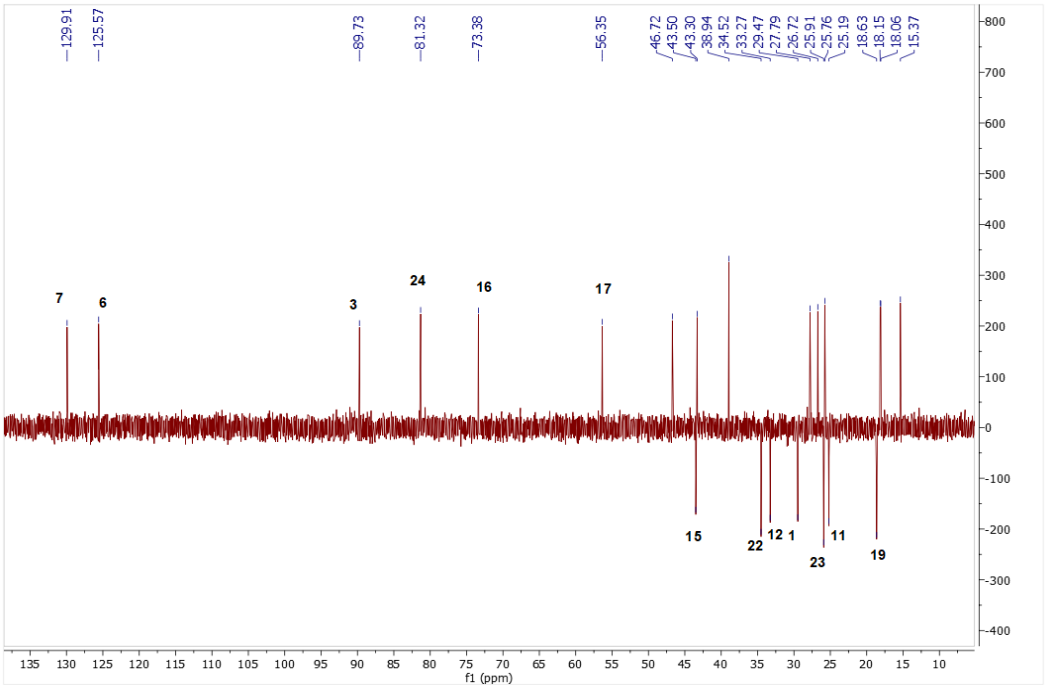

Spectrum 46. DEPT135 spectrum of CG-04**.**

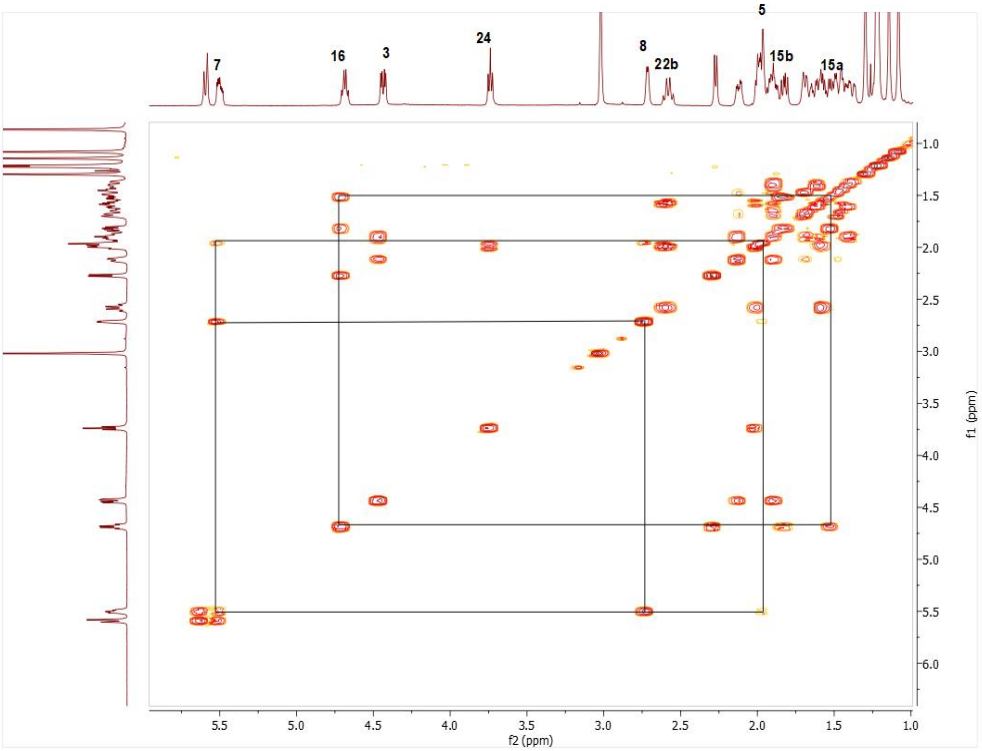

Spectrum 47. COSY spectrum of CG-04.

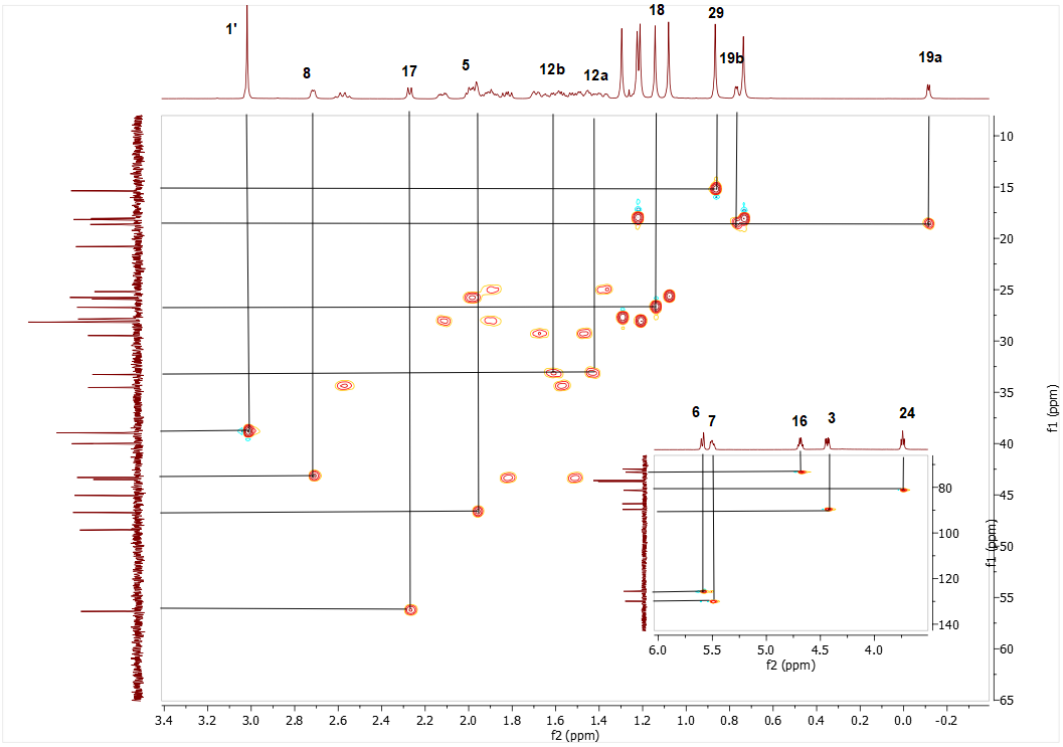

Spectrum 48. HMQC spectrum of CG-04.

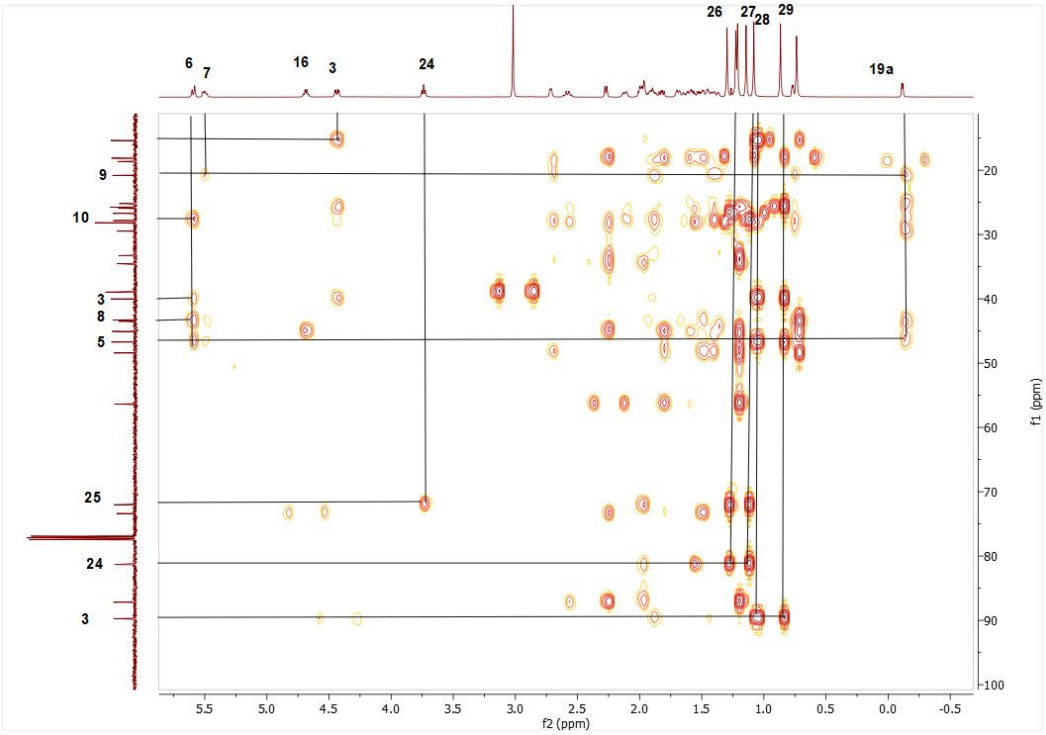

Spectrum 49. HMBC spectrum of CG-04.

3.2.8. Structural Elucidation of Compound CG-05

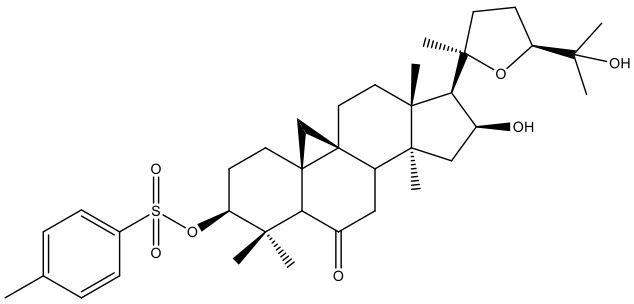

Figure 27. Chemical Structure CG-05.

Compound CG-05 was obtained from reaction of CG-01 with *p*-TsCl. In the ^{13}C spectrum, similar with AG-05, carbonyl signal at δ_C 210 originated from CG-01 was noted. Additionally, aromatic protons of tosyl structure were observed in ^{1}H spectrum. Location of the tosylation was assigned from investigation of ^{1}H spectrum. Characteristic H-3 signal shifted to low-field implying position of tosyl addition. Also, all the proton

and carbon resonances of CG-05 were assigned by COSY, HSQC and HMBC to verify this assumption. Consequently, the structure of CG-05 was determined to be 20(*R*),24(*S*)-epoxy-3(O)-p-Tosyl-6-one-16β,25-dihydroxy 9,19-cyclolanostan.

Table 11. The ^{13}C and ^{1}H NMR data of CG-05 *(100/500 MHz, δ ppm, in $CDCl_3$).*

H/C	**δ_C (ppm)**	**δ_H (ppm), *J* (Hz)**
1	30.0 t	1.42 m, 1.76 m
2	27.3 t	1.79 m, 1.94 m
3	89.3	4.21 m
4	40.0 s	-
5	57.2 d	2.3 brs
6	210 s	-
7	41.2 t	2.12 m, 2.17 m
8	42.4 d	2.66 dd (8.5, 4)
9	21.7 s	-
10	29.7 s	-
11	26.5 t	1.46 m, 1.85 m
12	33.0	1.47 m, 1.6 m
13	47.1 s	-
14	45.3 s	-
15	43.8 t	1.37 m, 1.84 m
16	72.9 d	4.69 ddd (7.8, 7.8, 6.1)
17	56.9 d	2.32 d (7.6)
18	18.4 q	1.21 m
19	22.2 t	0.21, 0.6 d (5.5)
20	87.1 s	-
21	28.1	1.21 s
22	34.5 t	1.57 m, 2.57 q (10.8)
23	25.91 t	1.98 m
24	81.26 d	3.75 dd (8.3, 6.1)
25	72.1 s	-
26	26.8 q	1.14 s
27	27.8 q	1.3 s
28	26.3 q	1.02 s
29	14.8 q	1 s
30	19.1 q	0.89 s
1'	134.7 s	-
2'	127.8 d	7.79 d (8.3)
3'	129.8 d	7.3 d (8.1)
4'	144.6 s	-
5'	129.8 d	7.3 d (8.1)
6'	127.8 d	7.79 d (8.3)
7'	21.8 q	2.43 s

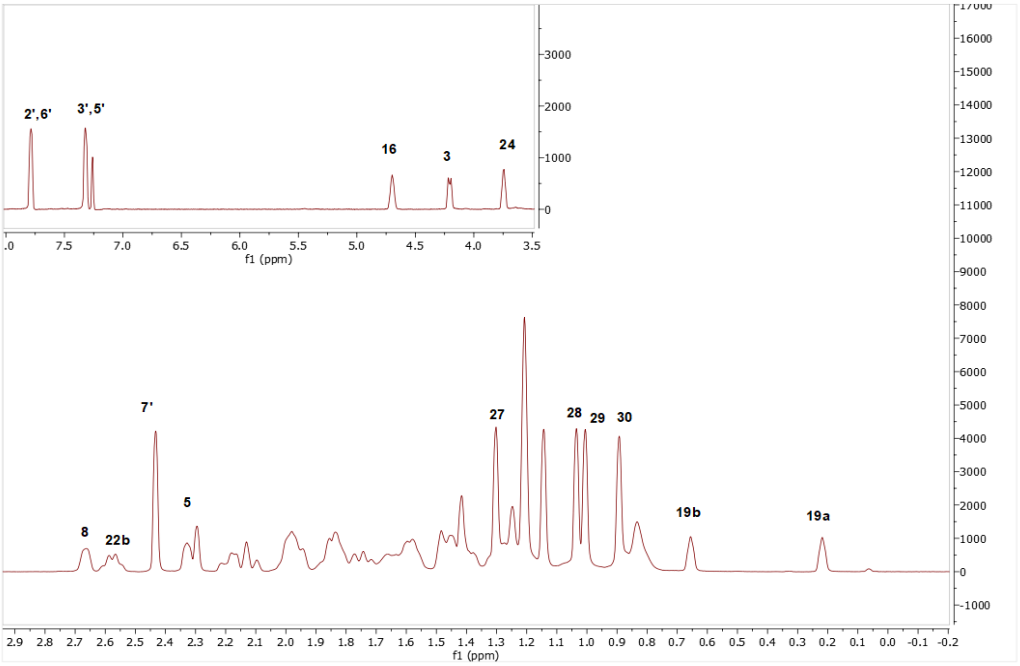

Spectrum 50. ^{1}H NMR Spectrum of CG-05.

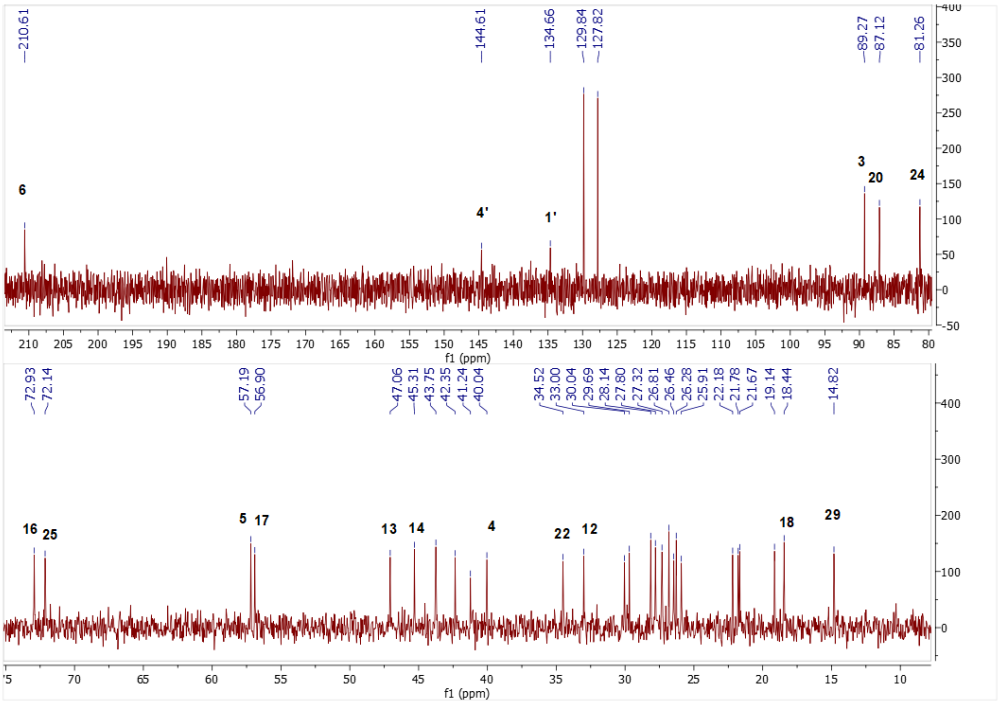

Spectrum 51. ^{13}C NMR Spectrum of CG-05.

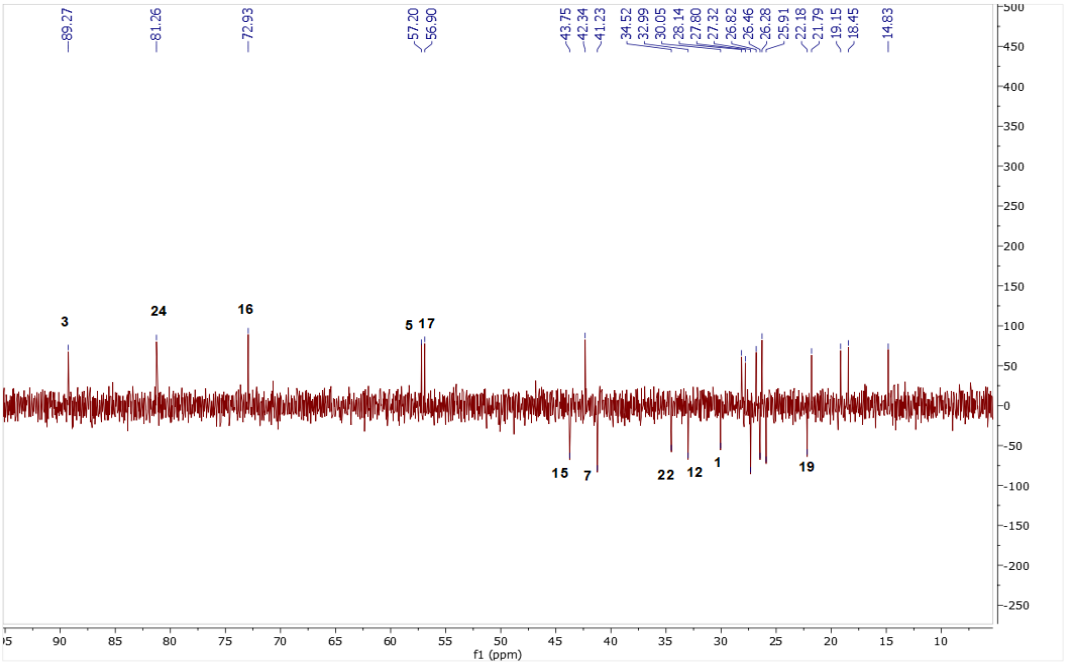

Spectrum 52. DEPT135 spectrum of CG-05.

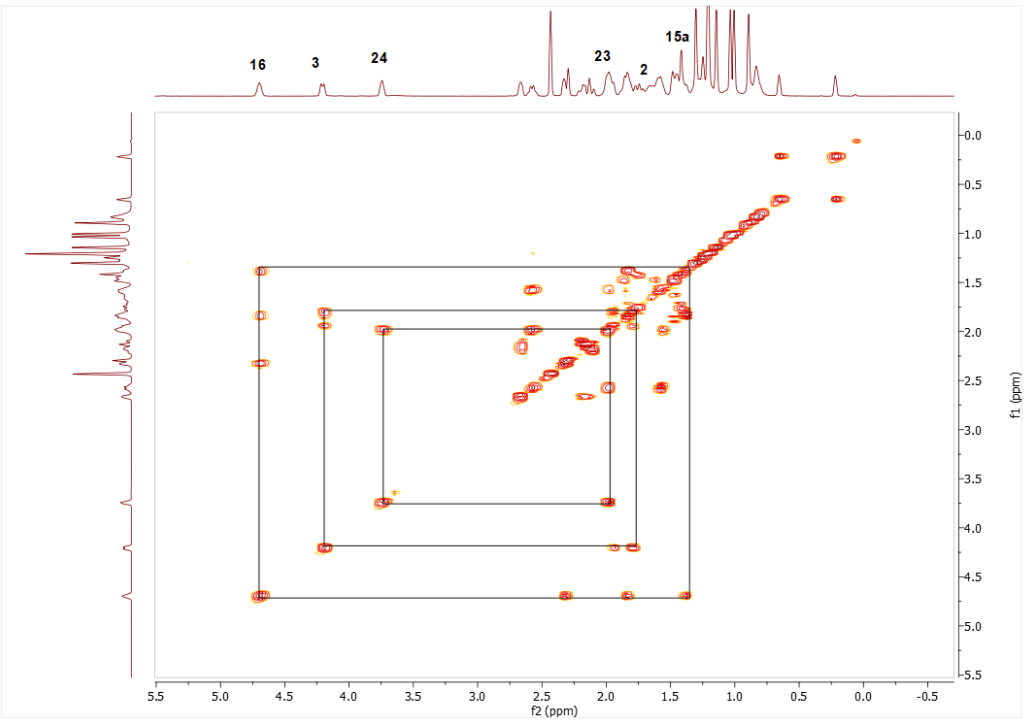

Spectrum 53. COSY spectrum of CG-05.

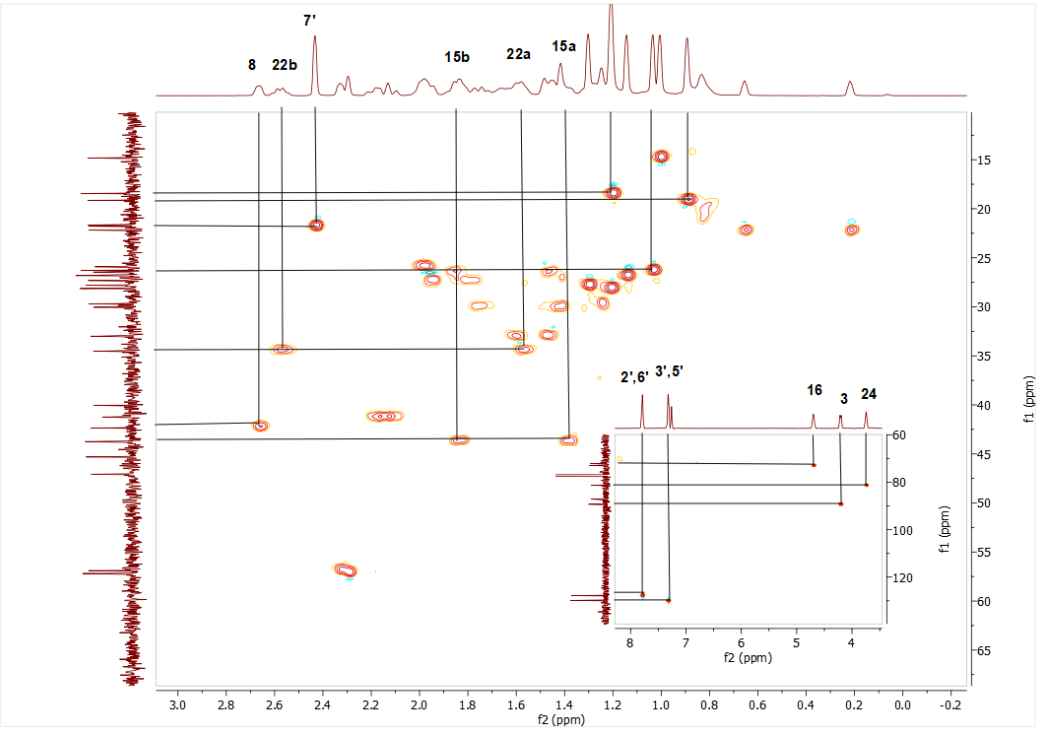

Spectrum 54. HMQC spectrum of CG-05.

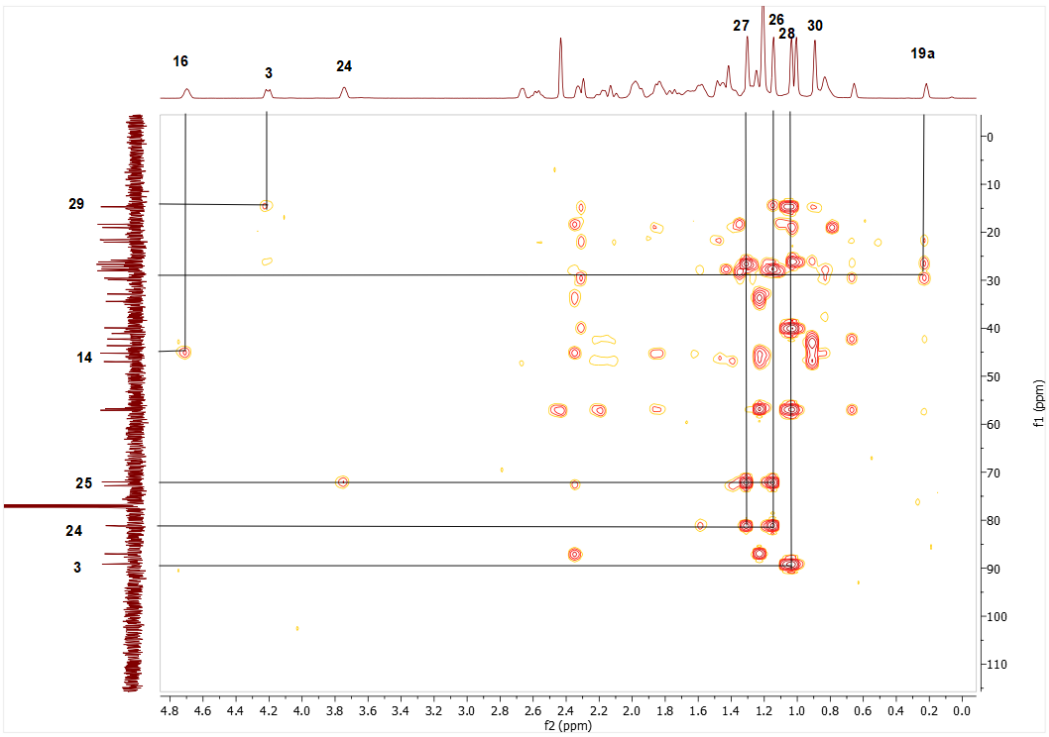

Spectrum 55. HMBC spectrum of CG-05.

3.2.9. Structural Elucidationof Compound SCG-01

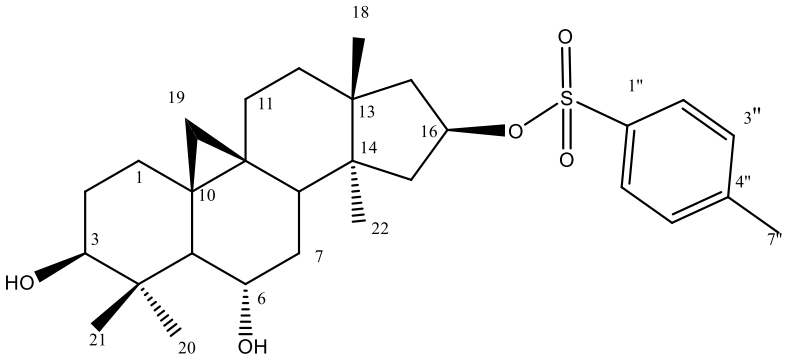

Figure 28. Chemical Structure of SCG-01.

Compound SCG-01 was obtained from reaction of SCG with *p*-TsCl. The HR-ESI-MS spectrum of SCG-01, exhibited a sodium adduct ion at *m/z* 525.2699 $[M + Na]^+$ and led to establishment of its molecular formula as $C_{29}H_{42}O_5S$. When compare with SCG, MS spectra displayed 154 amu difference showing tosyl addition and H removing. Also, aromatic signals (δ_C 129.9 d and 127.8 d each 2C; δ_H 7.75 and 5.31, each 2H) in the ^1H and ^{13}C NMR spectra verified addition of tosyl group. Characteristic signals of H-16 shifted to low-field which indicated tosylation location. Thus, the structure of SCG-01 was established as 16(O)-p-Tosyl-20,27-octanor cycloastragenol.

Table 12. The ^{13}C and ^1H NMR data of SCG-01 *(100/500 MHz, δ ppm, in $CDCl_3$).*

H/C	δ_C (ppm)	δ_H (ppm), *J* (Hz)
1	32 t	1.2 d (3.2), 1.57 m
2	30.3 t	1.56 m, 1.78 m
3	78.4 d	3.29 dd (11.3, 4.6)
4	41.6 s	-
5	53.5 d	1.34 d (1.97)
6	68.5 d	3.51 ddd (9.1, 9.1, 4.2)
7	37.5 t	1.3 m, 1.44 m
8	45.8 d	1.6 m
9	20.8 s	-
10	29.8 s	-
11	26.1 t	1.25 m, 1.92 m
12	30.3 t	1.4 m, 1.6 m

(cont. on next page)

Table 12 (cont.).

H/C	δ_C (ppm)	δ_H (ppm), *J* (Hz)
13	44.5 s	-
14	45.9 s	-
15	46 t	1.88 m
16	82.9 d	5.06 ddd (15.4, 7.9, 1.4)
17	44.4 t	1.86 m, 1.64 d (1.43)
18	25 q	0.95 s
19	30 t	0.28 d (0.46), 0.45 d (0.46)
28	28 q	1.22 s
29	15.3 q	0.92 s
30	19.8 q	1.04 s
1'	134.4	-
2'	127.8	7.75 d (8.2)
3'	129.9	7.31 d (8.2)
4'	144.6 s	-
5'	129.9	7.31 d (8.2)
6'	127.8	7.75 d (8.2)
7'	21.8 q	2.44 s

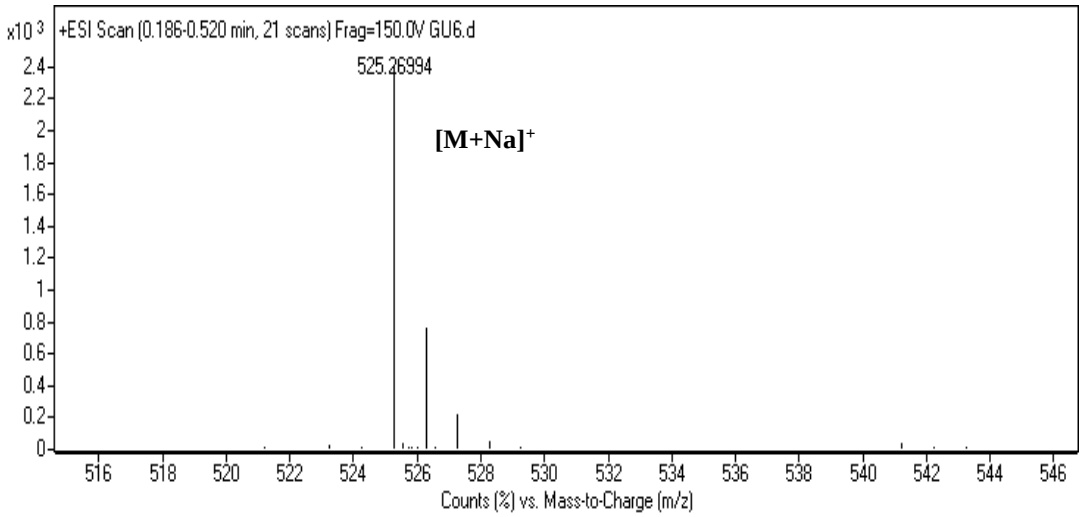

Spectrum 56. HR-ESI-MS Spectrum of SCG-01 (positive mode).

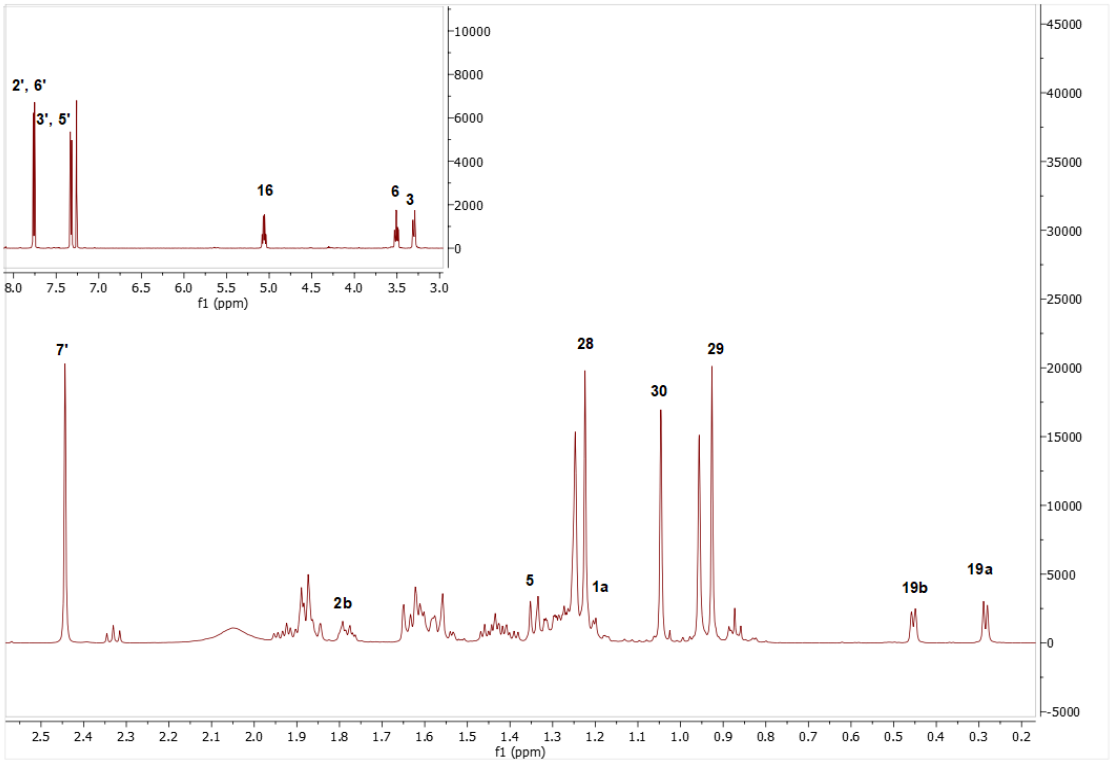

Spectrum 57. ^{1}H NMR Spectrum of SCG-01

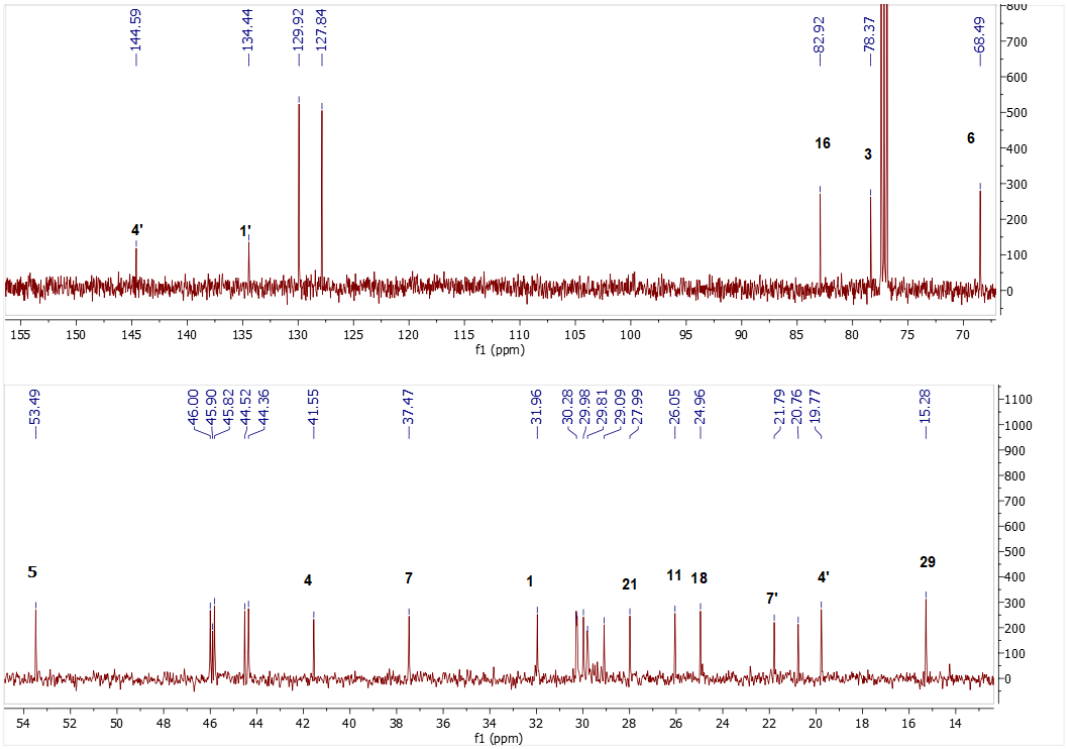

Spectrum 58. ^{13}C NMR Spectrum of SCG-01.

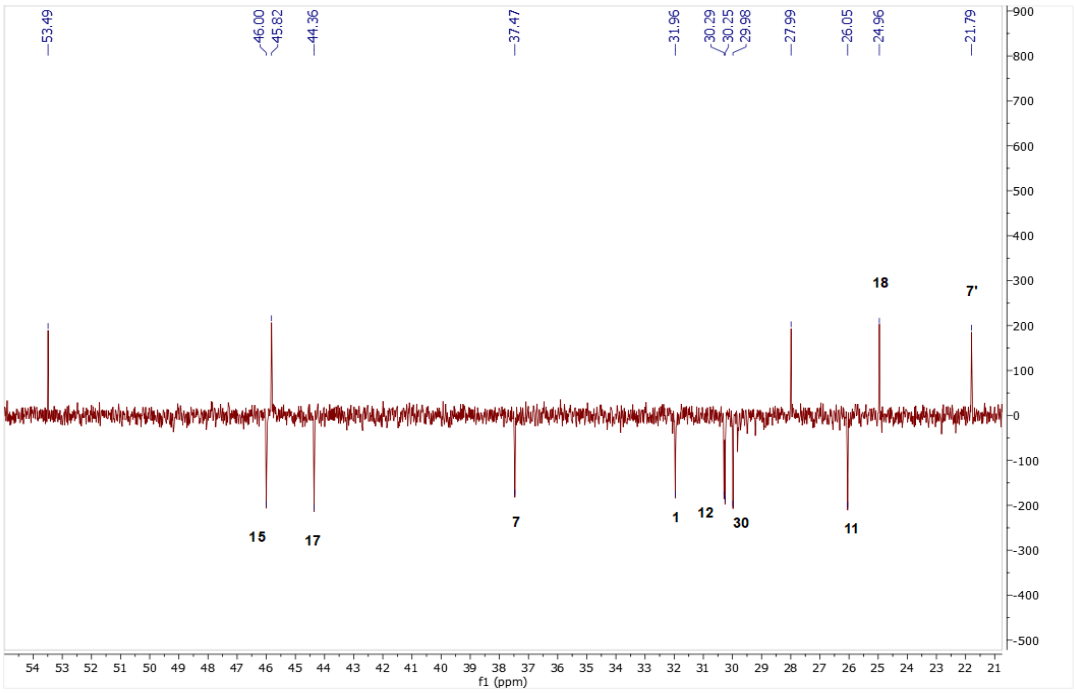

Spectrum 59. DEPT135 spectrum of SCG-01.

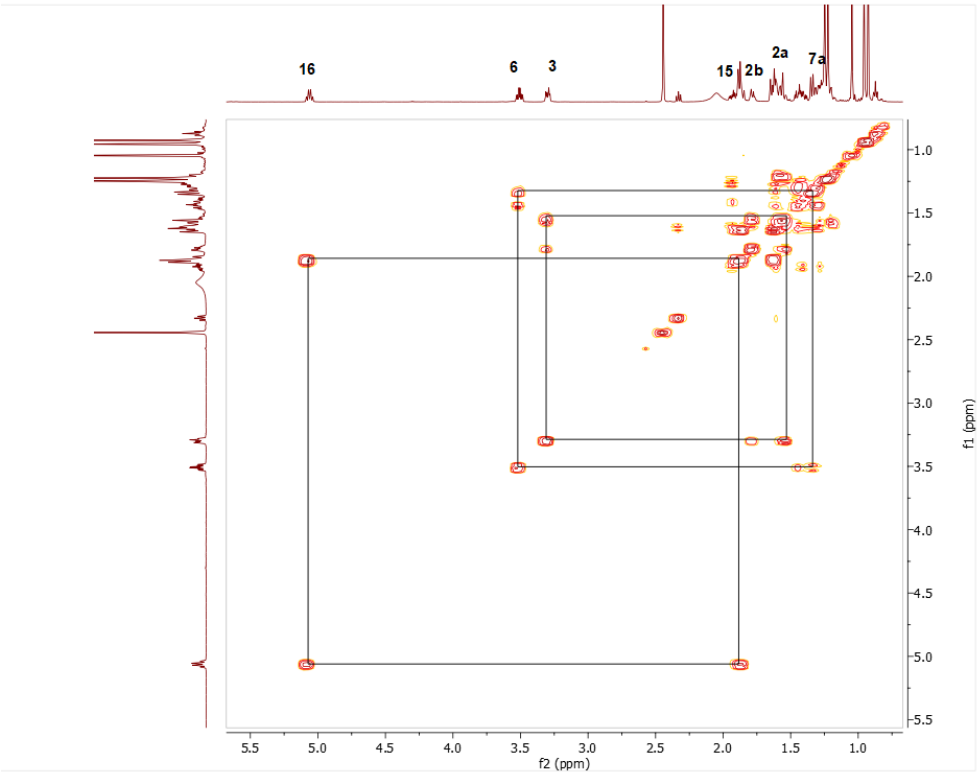

Spectrum 60. COSY spectrum of SCG-01.

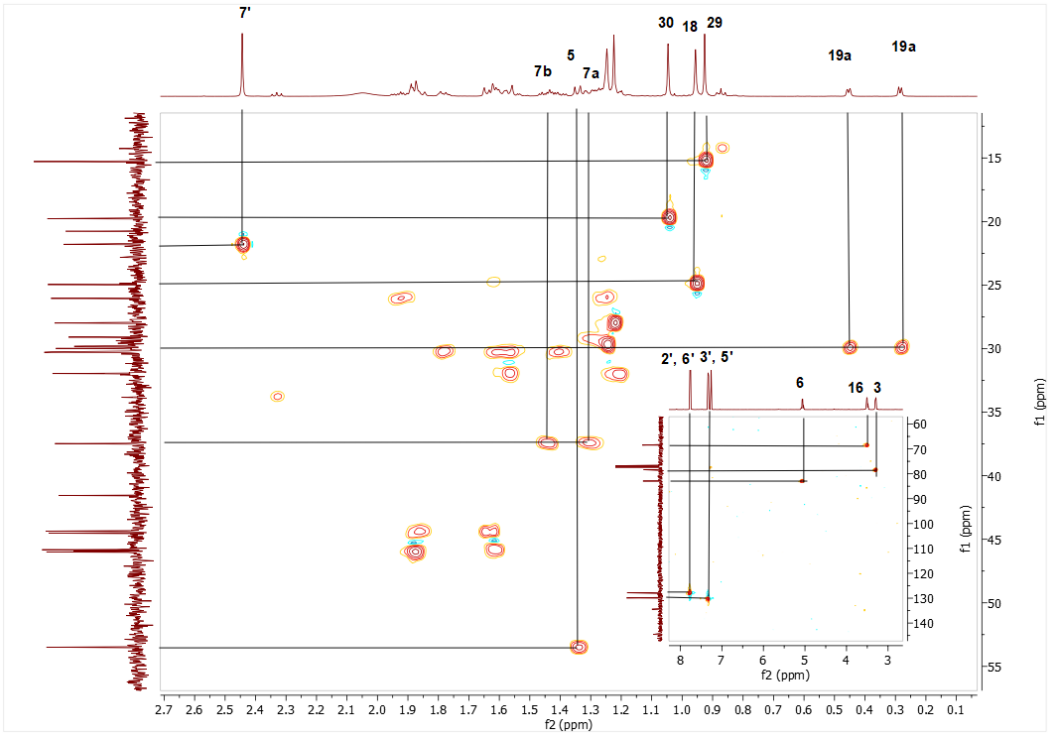

Spectrum 61. HMQC spectrum of SCG-01.

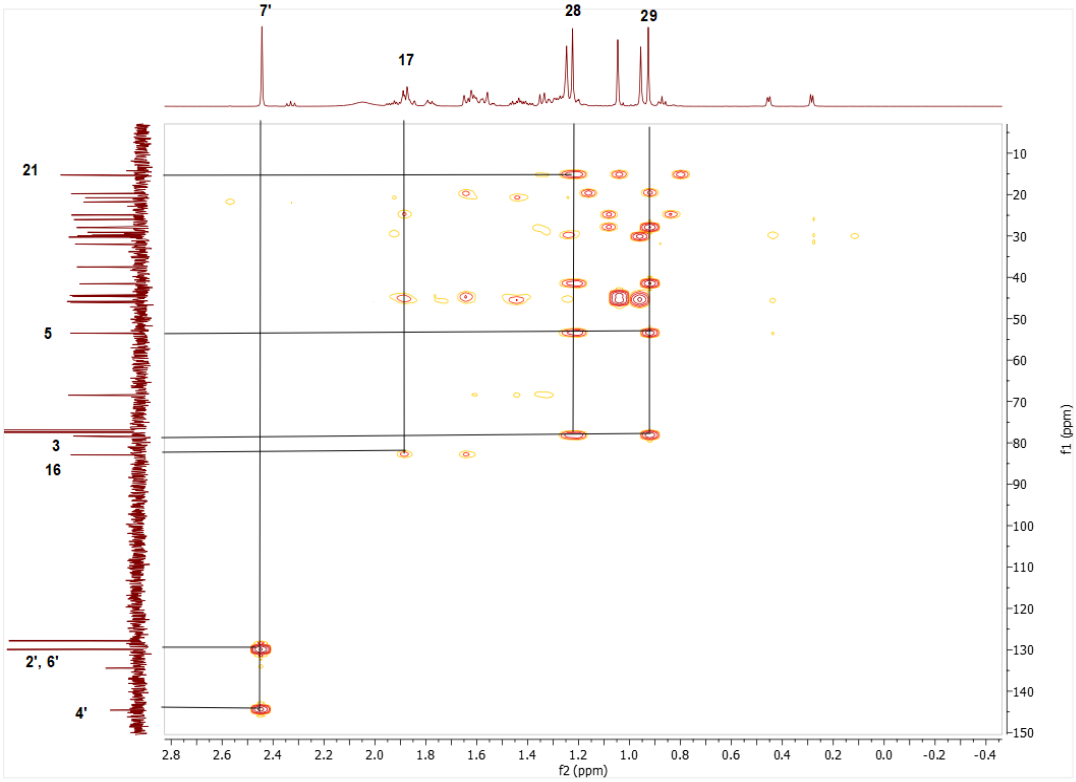

Spectrum 62. HMBC spectrum of SCG-01.

3.2.10. Structural Elucidation of Compound SCG-02

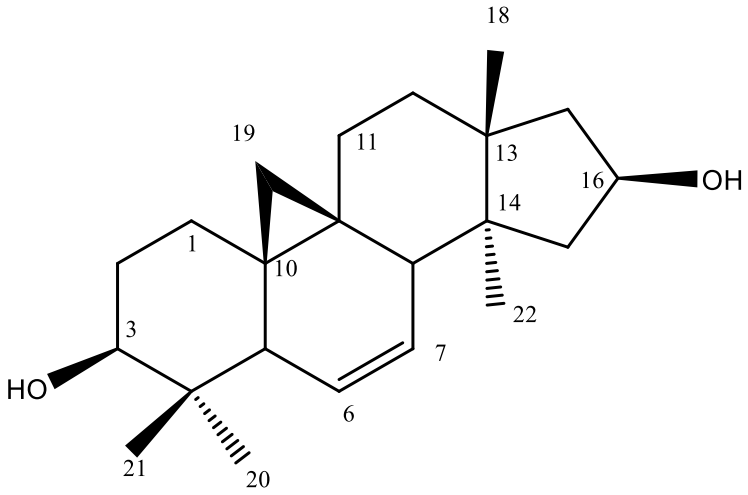

Figure 29. Chemical Structure of SCG-02.

Compound SCG-02 was obtained from reaction of SCG with *p*-TsCl. ^{1}H, ^{13}C NMR and DEPT135 spectra of compound revealed disubstituted double bond system (δ_C 120.0, d and 139.0, d; δ_H 5.50 and 5.30, each 1H). Like AG-03 and CG-02, compound SCG-02 displayed the 9,19-cyclopropane ring signals (δ_C 18.5; δ_H -0.15, 0.73) at low-field suggesting location of double bond at C-6. To verify proposition, all the proton and carbon resonances of SCG-02 were secured by 2D NMR. Signal of H-6 was apparent at low-field and ^{3}J-HMBC correlation from H-7 (δ_H 5.44) to C-9 (δ_C 21.2) and from H-6 (δ_H 5.62) to C-10 (δ_C 28.3) confirmed location of double bond. In conclusion, the structure of SCG-02 was determined to be 6-ene-20,27-octanor cycloastragenol.

Table 13. The ^{13}C and ^{1}H NMR data of SCG-02 *(100/500 MHz, δ ppm, in $CDCl_3$).*

H/C	**δ_C (ppm)**	**δ_H (ppm), *J* (Hz)**
1	29.8 t	1.25 m, 1.46 m
2	30.1 t	1.6 m, 1.82 m
3	78.5 d	3.3 dd (11.2, 4.4)
4	40.3 s	-
5	46.5 d	1.89 m
6	126.3 d	5.62 d (10.5)
7	129.1 d	5.44 ddd (10.6, 6.1, 3.2)
8	43.7 d	2.48 dd (6.2, 2.6)
9	21.2 s	-

(cont. on next page)

Table 13 (cont.).

H/C	δ_C (ppm)	δ_H (ppm), *J* (Hz)
10	28.3 s	-
11	25.2 t	1.42 m, 1.85 m
12	31.4 t	1.22 m, 1.69 m
13	48.5 s	-
14	45.3 s	-
15	45.4 t	1.27 m, 2.05 dd (13.7, 8.2)
16	72.2 d	4.55 ddd (14.5, 7.7, 1.4)
17	47.8 t	1.86 m, 1.62 m
18	22.2 q	0.96 s
19	18.5 t	-0.15 d (4.1), 0.73 d (4.5)
28	25.6 q	1.05 s
29	14.5 q	0.77 s
30	18.4 q	0.92 s

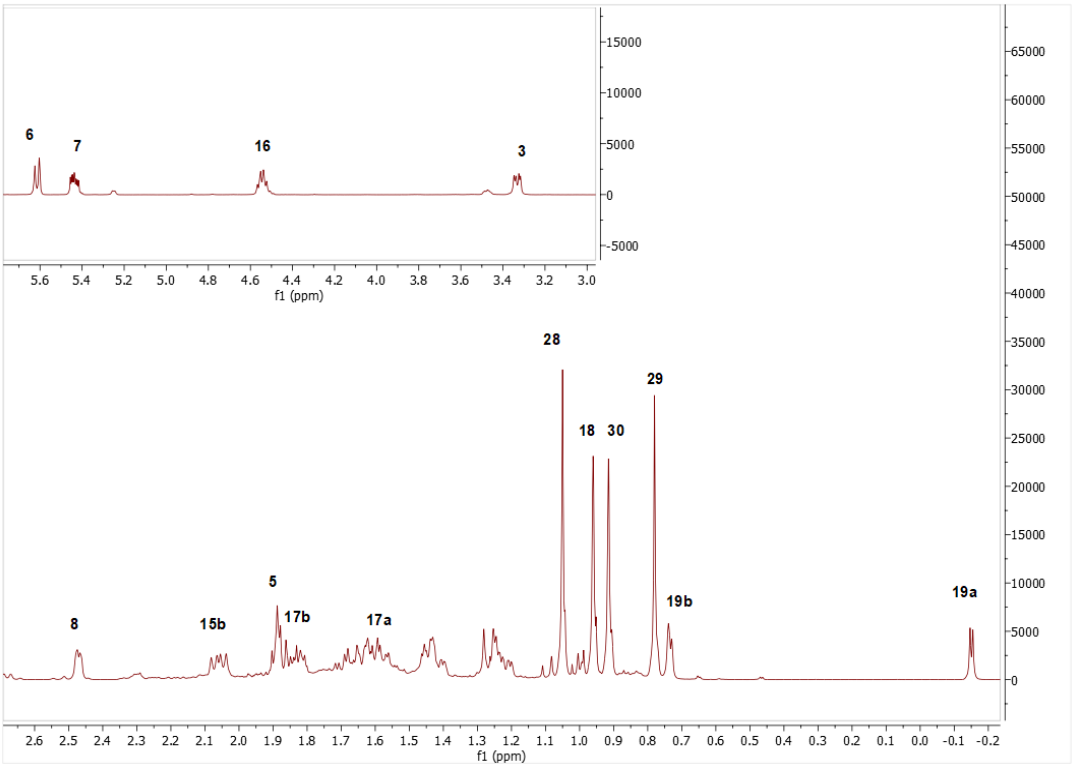

Spectrum 63. ^{1}H NMR Spectrum of SCG-02.

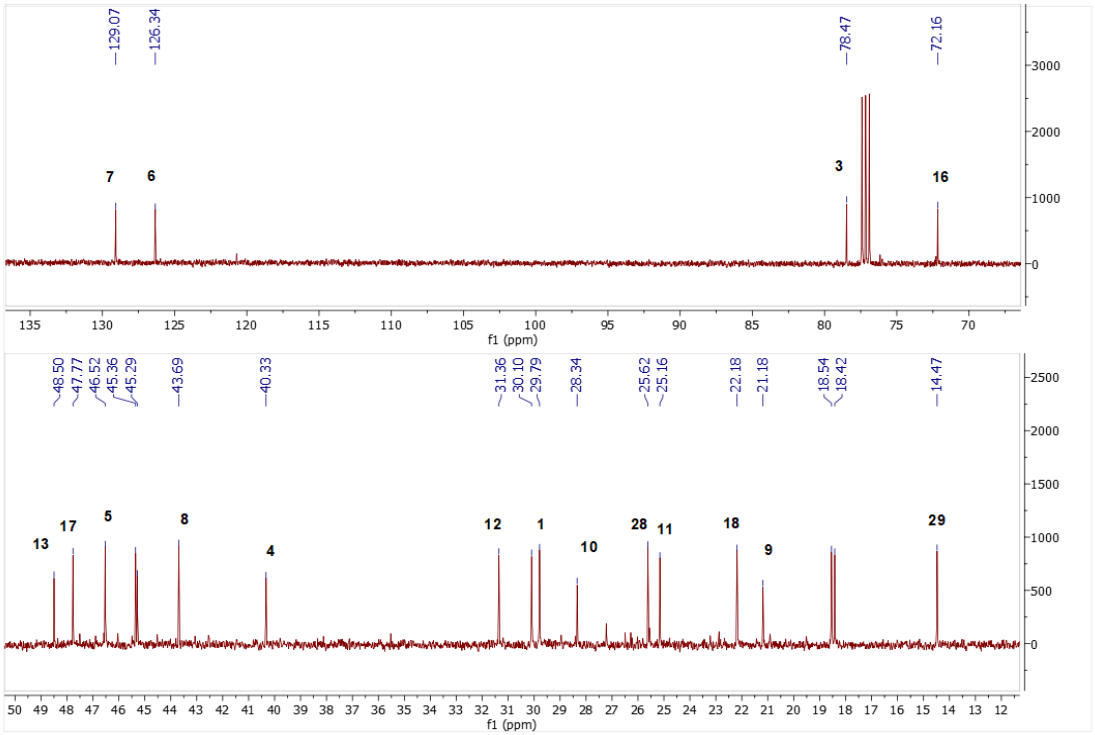

Spectrum 64. ^{13}C NMR Spectrum of SCG-02.

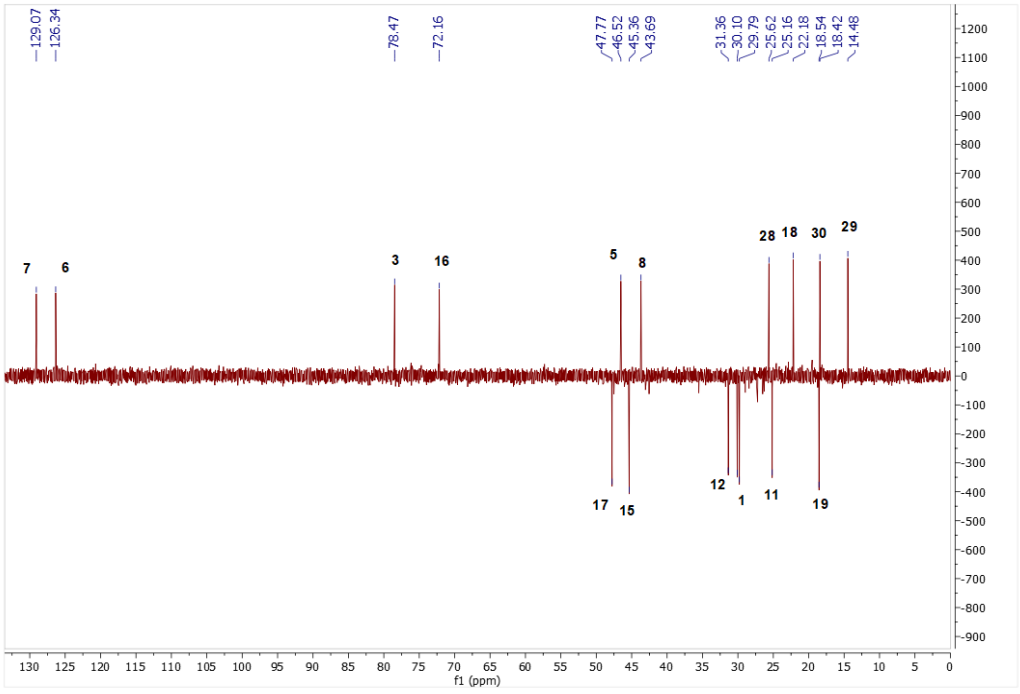

Spectrum 65. DEPT135 spectrum of SCG-02.

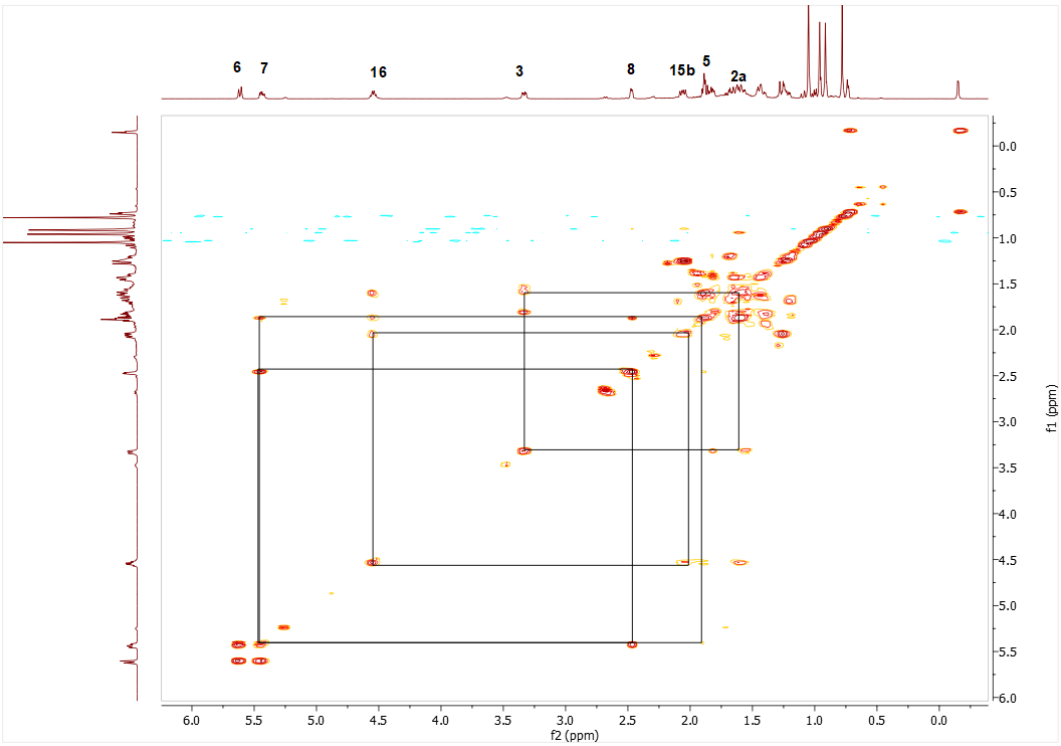

Spectrum 66. COSY spectrum of SCG-02.

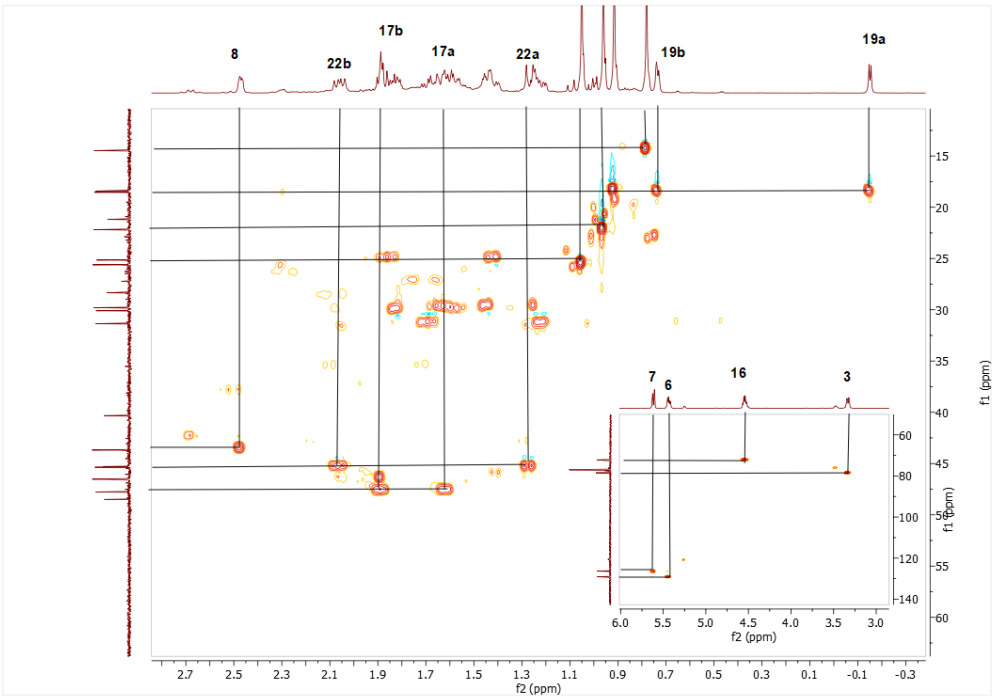

Spectrum 67. HSQC spectrum of SCG-02.

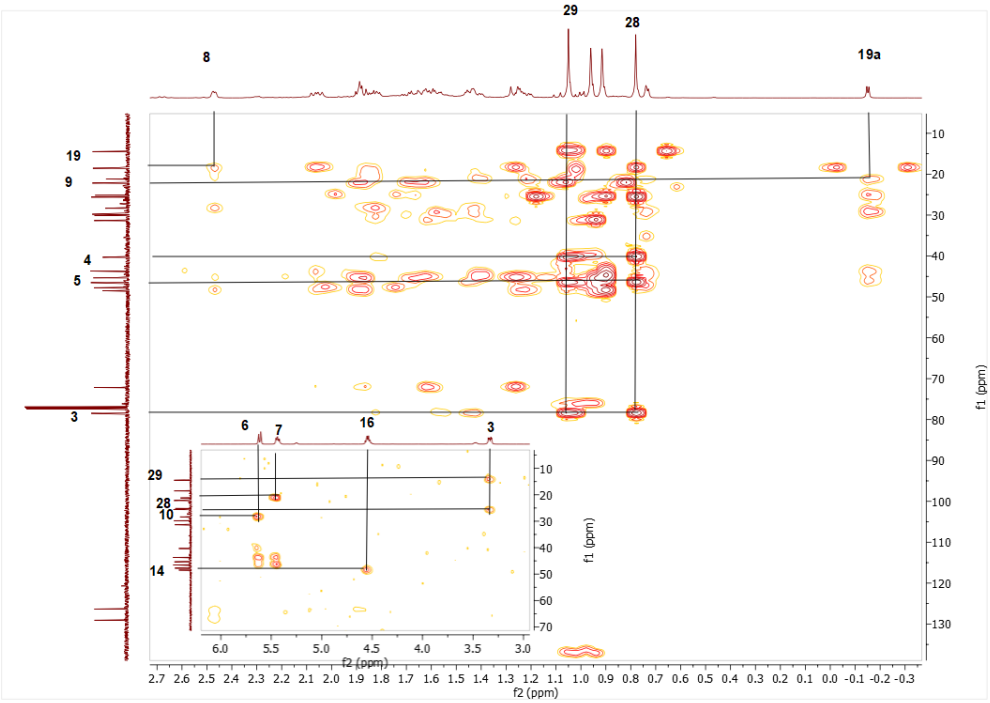

Spectrum 68. HMBC spectrum of SCG-02.

3.2.11. Structural Elucidation of Compound SCG-03

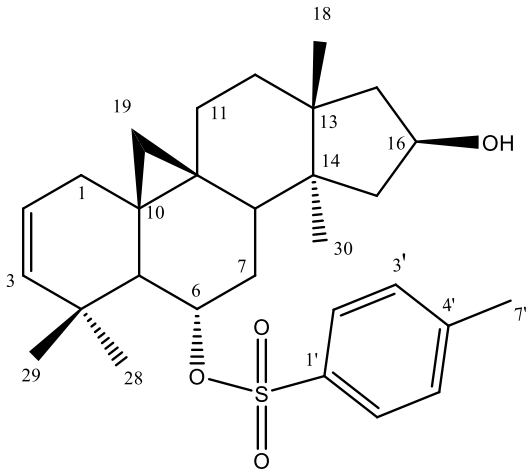

Figure 30. Chemical Structure of SCG-03.

The molecular formula of SCG-03 was established as $C_{29}H_{40}O_4S$ based on ^{13}C NMR and MS data (obsd $[M + Na]^+$, *m/z* 507.2578). ^1H, ^{13}C NMR and DEPT135 spectrum showed presence of disubstituted double bond (δ_C 140.7, 122.8; δ_H 5.49, 5.3; each 1H) and aromatic signals (δ_C 129.9, 127.8; δ_H 7.74, 7.31 each 2H). In ^1H spectra,

characteristic H-6 signal shifted to low-field suggesting tosylation position, while H-3 resonance was lacking. Based on this, it was suggested that dehydration took place at C-3(OH) and tosylation was occur at C-6(OH). To verify this proposition, 2D spectra was inspected in detail. The key long-range correlations from C-3 (δ_C 140.7) to H_3-28 and H_3-29 verified the position of the double bond at C-2. Consequently, SCG-03 was deduced to be 6-ene-3(O)-*p*-tosyl-20,27-octanor cycloastragenol.

Table 14. The ^{13}C and ^{1}H NMR data of SCG-03 *(100/500 MHz, δ ppm, in $CDCl_3$).*

H/C	**δ_C (ppm)**	**δ_H (ppm), *J* (Hz)**
1	34.9 t	1.39 m, 2.30 m
2	122.8 d	5.49 ddd (9.9, 5.8, 2)
3	140.7	5.3 dd (9.8, 2.7)
4	38.0 s	-
5	52.6 d	1.58 m
6	83 d	5.04 q (7.4)
7	28.4 t	1.34 m, 1.90 m
8	47.9 d	1.54 m
9	19.2 s	-
10	28.2 s	-
11	25.8 t	1.1 m, 2.07 m
12	30.16	1.47 m, 1.62 m
13	44.4 s	-
14	45.9 s	-
15	44.9 t	1.65 m, 1.87 m
16	70.7 d	3.45 td (9.8, 4.7)
17	46.1 t	1.88 m
18	25.7 q	0.99 s
19	31.7 q	0.34 d (4.5), 0.51 d (5)
28	33.1 q	1.23 s
29	23.5 q	1.05 s
30	20.2 q	1.03 s
1'	134.2 s	-
2'	127.8 d	7.74 dd (8.2, 3.6)
3'	129.9 d	7.31 dd (8.2, 3.6)
4'	144.6 s	-
5'	129.9 d	7.31 dd (8.2, 3.6)
6'	127.8 d	7.74 dd (8.2, 3.6)
7'	21.8 q	2.44 s

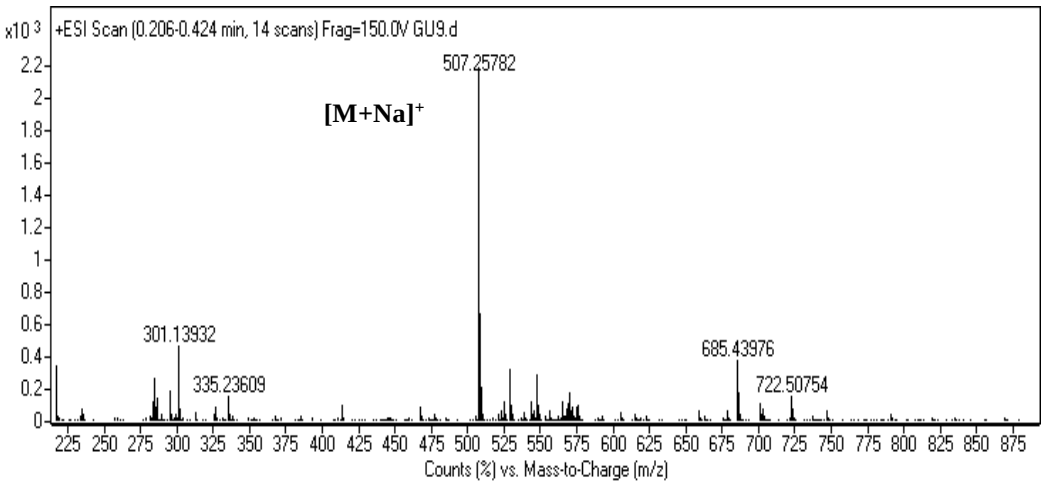

Spectrum 69. HR-ESI-MS Spectrum of SCG-03 (positive mode).

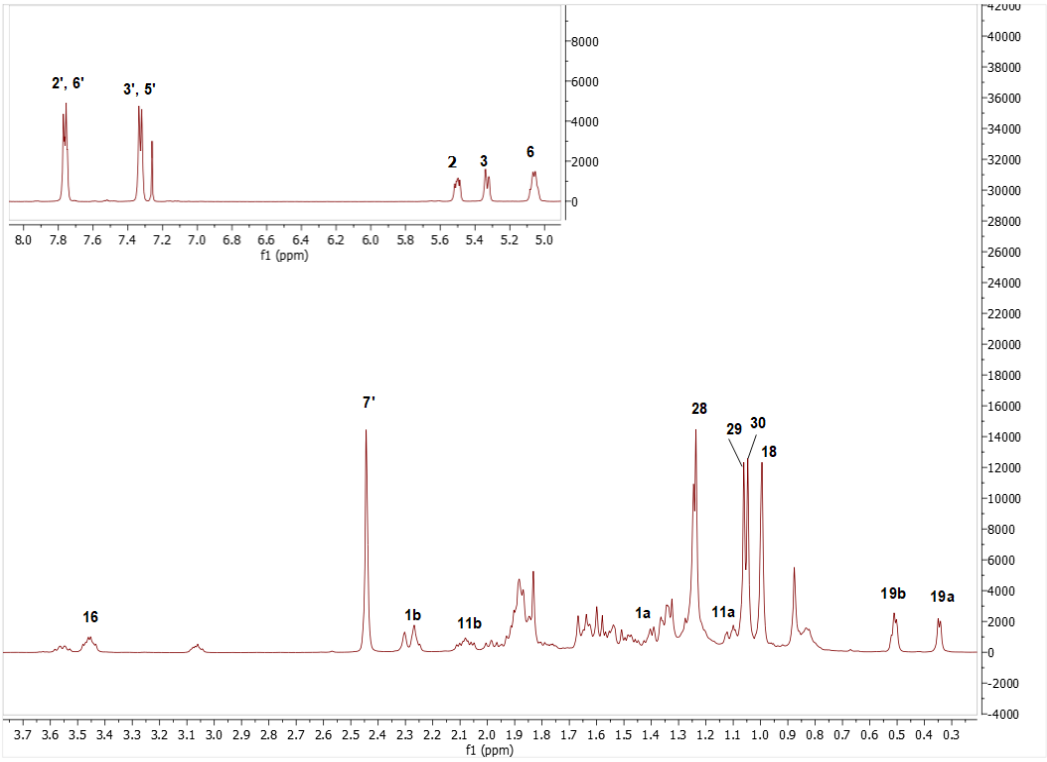

Spectrum 70. ^{1}H NMR Spectrum of SCG-03.

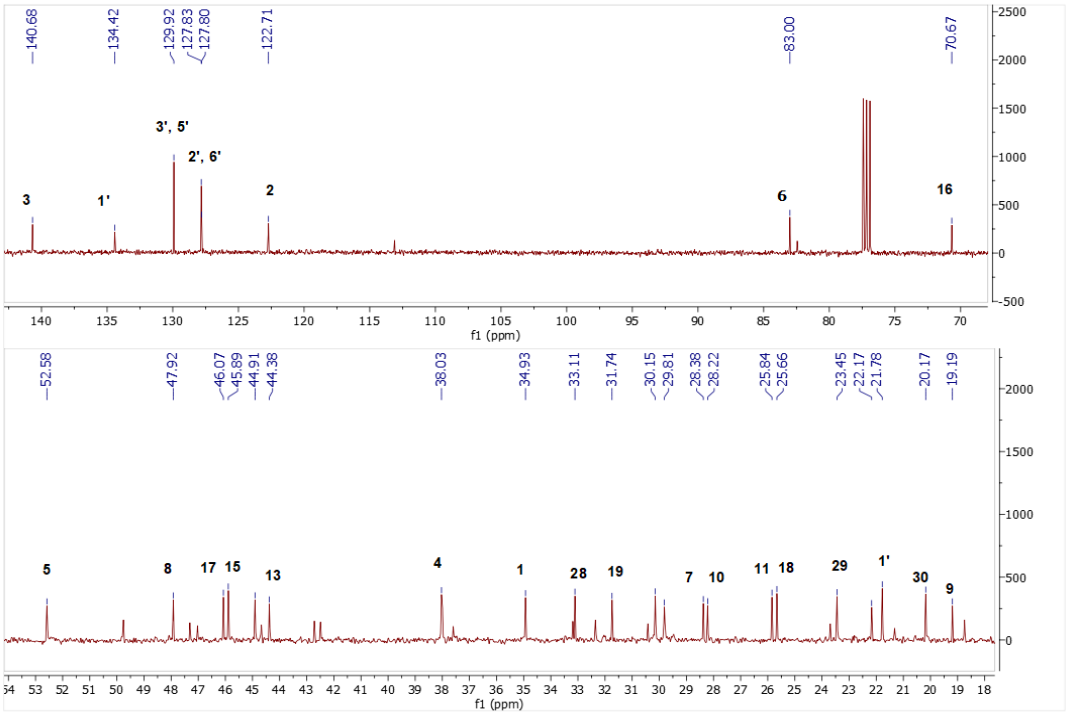

Spectrum 71. ^{13}C NMR Spectrum of SCG-03.

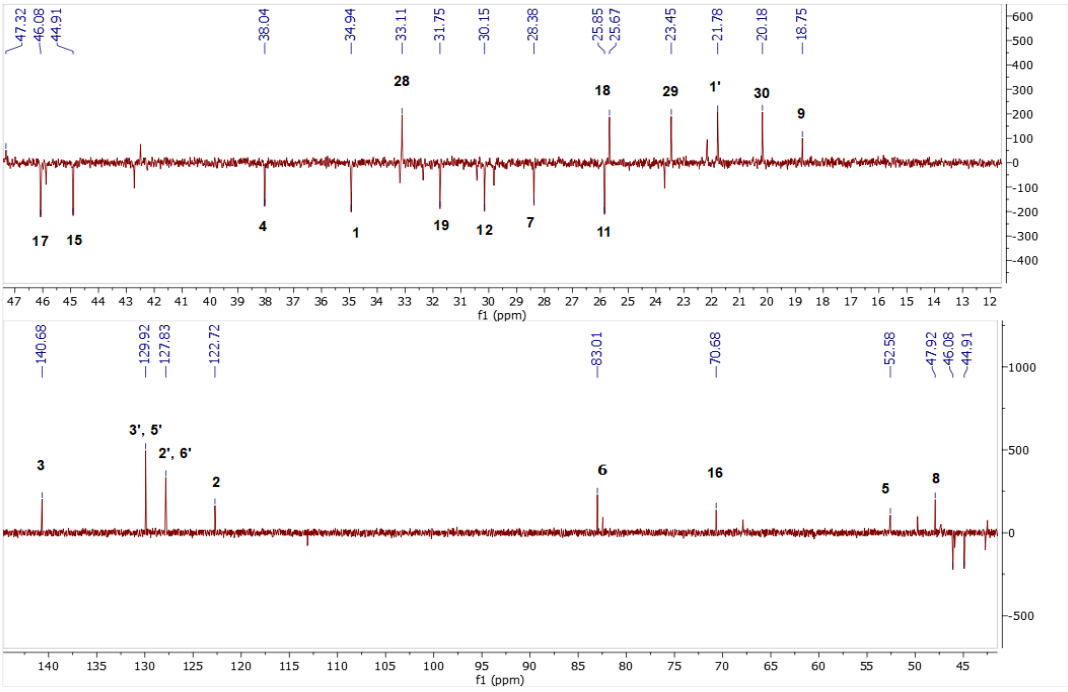

Spectrum 72. DEPT135 spectrum of SCG-03.

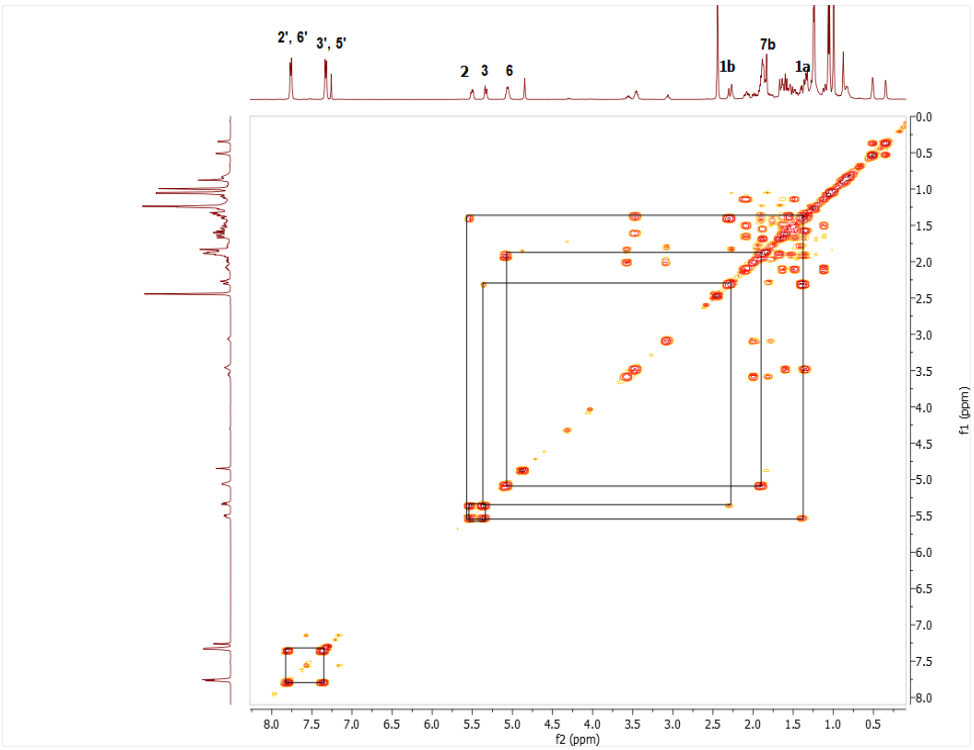

Spectrum 73. COSY spectrum of SCG-03.

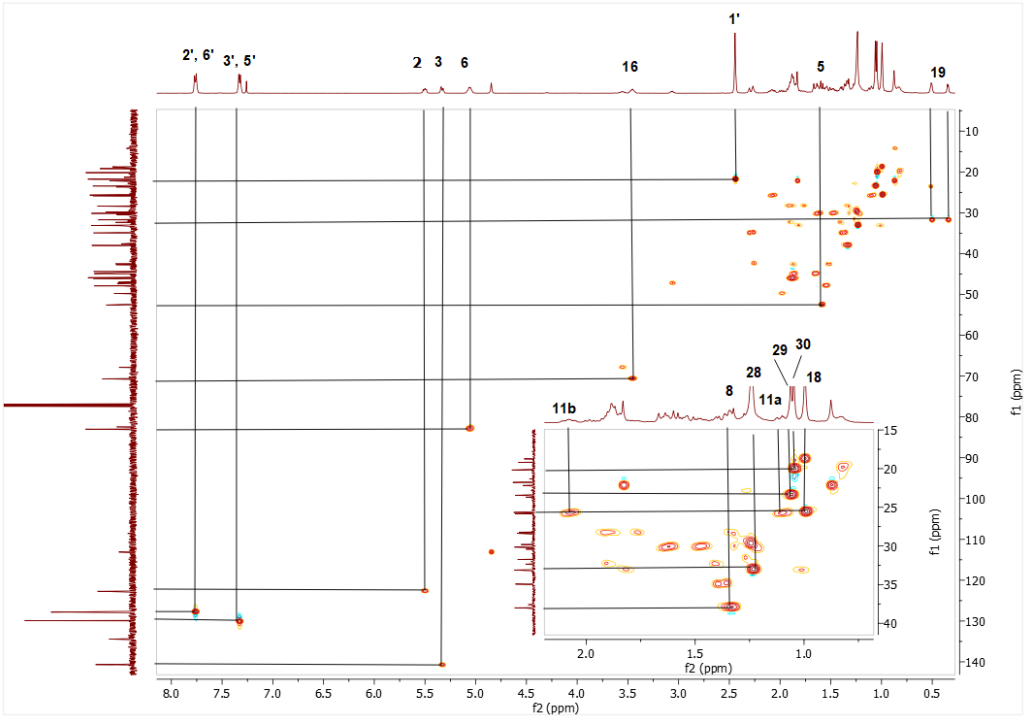

Spectrum 74. HMQC spectrum of SCG-03.

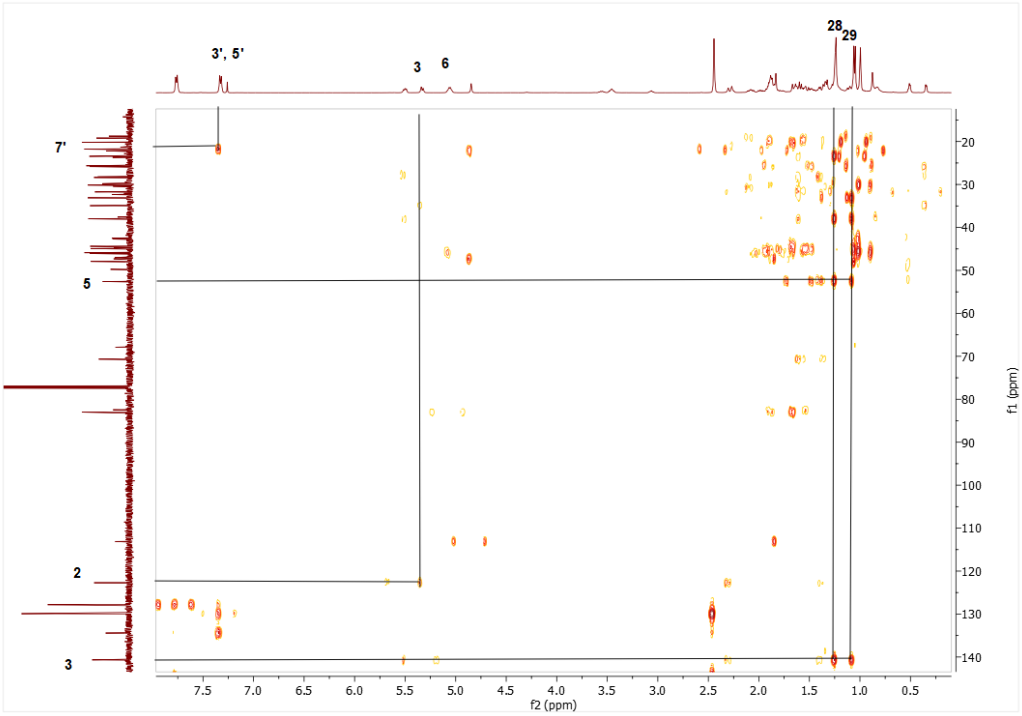

Spectrum 75. HMBC spectrum of SCG-03.

3.2.12. Structural Elucidation of Compound SCG-04

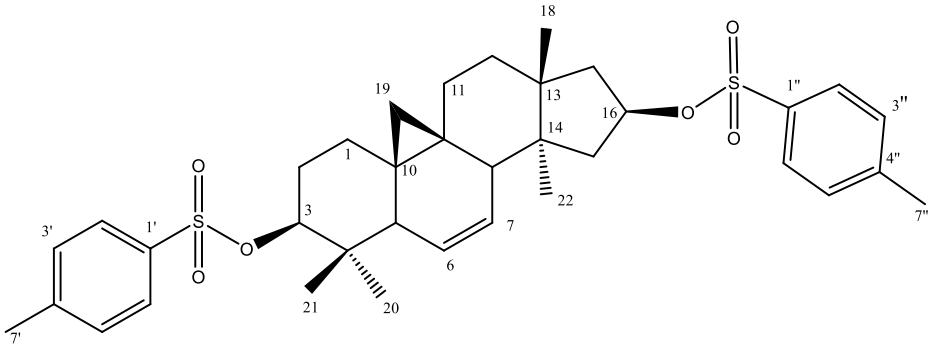

Figure 31. Chemical Structure of SCG-04.

In the ^{13}C and ^{1}H NMR spectrum of SCG-04, similar with metabolite SCG-03, tosyl and olefinic signals were noted. However, ^{1}H and ^{13}C spectra indicated two tosyl group in structure. ^{1}H spectrum revealed that one proton of cyclopropane (C-19) shifted up-field impling double bond at C-6. This assumption was substantiated by the long-range

HMBC correlation from H-6 (δ_H 5.52) to C-10 (δ_C 27.7) and C-8 (δ_C 43.1) and also from H-7 (δ_H 5.36) to C-9 (δ_C 20.9) and C-5 (δ_C 46.5). Additionaly, shifting of characterictic signals of H-3 and H-16 to low-field revealed 3(O) and 16(O) tosylation. Consequently, the structure of SCG-03 was determined to be 6-ene-16(O),3(O)-di-*p*-tosyl-20,27-octanor cycloastragenol.

Table 15. The ^{13}C and ^{1}H NMR data of SCG-04 (*100/400 MHz, δ ppm, in $CDCl_3$).*

H/C	**δ_C (ppm)**	**δ_H (ppm), *J* (Hz)**
1	29.4 t	1.4 m,1.6 m
2	27.6 t	1.8 m, 1.9 m
3	89.9 d	4.3 dd (11.6, 4.5)
4	39.8 s	-
5	46.5 d	1.89 m
6	125,7 d	5.52 d (10.7)
7	128.9 d	5.36 ddd (9.6, 5.9, 2.9)
8	43.1 d	2.41 m
9	20.9 s	-
10	27.7 s	-
11	24.79	1.8 m, 1.39 m
12	30.7	1.16 m, 1.61
13	44.4 s	-
14	48.1 s	-
15	44.9 t	1.81 m
16	82.4 d	5.06 q (7.5)
17	41.9 t	2 m, 1.5 m
18	21.8 q	0.88 s
19	18.3 t	-0.16 d (4.1), 0.71 d (4.1)
28	25.3 q	0.83 s
29	15.2 q	0.79 s
30	17.6 q	0.82 s
1'	134.7* s	-
2'	127.7 d	7.75+ d (7.8)
3'	129.7' d	7.32 d (7.8)
4'	144.4- s	-
5'	129.7' d	7.32 d (7.8)
6'	127.7 d	7.75+ d (7.8)
7'	21.6 q	2.44 s
1''	134.2* s	-
2''	127.7 d	7.8+ d (7.7)
3''	129.7' d	7.32 d (7.8)
4''	144.7- s	-
5''	129.7' d	7.32 d (7.8)
6''	127.7 d	7.8+ d (7.7)
7''	21.6 q	2.44 s

*,-,',+: changeable

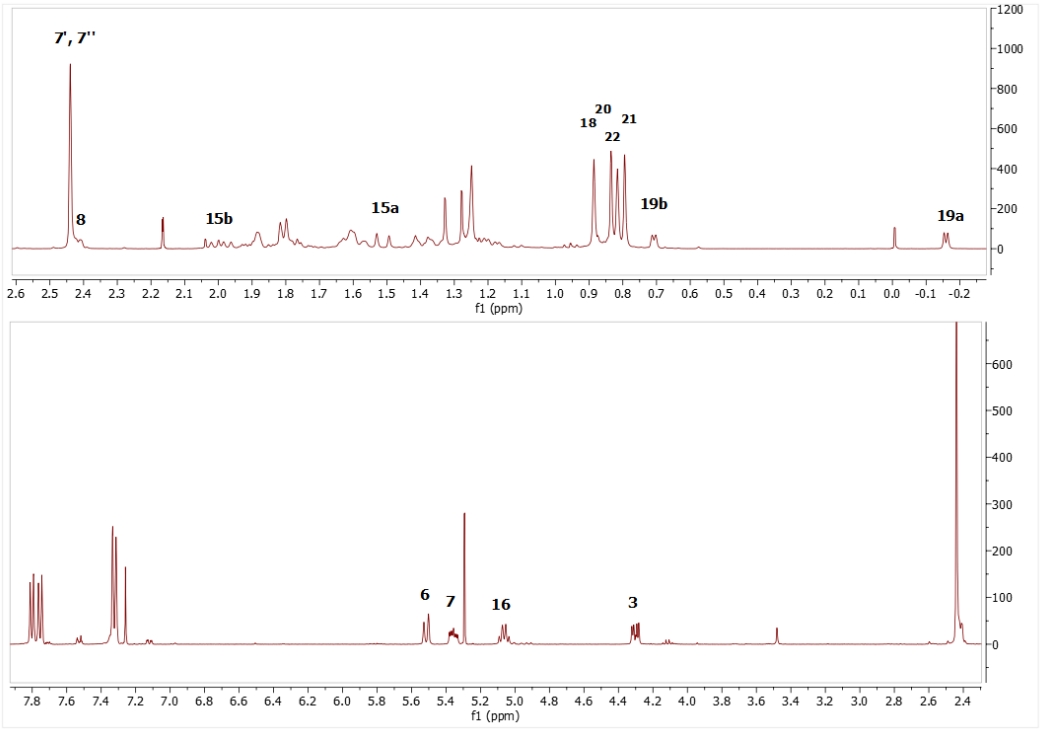

Spectrum 76. ^{1}H NMR Spectrum of SCG-04.

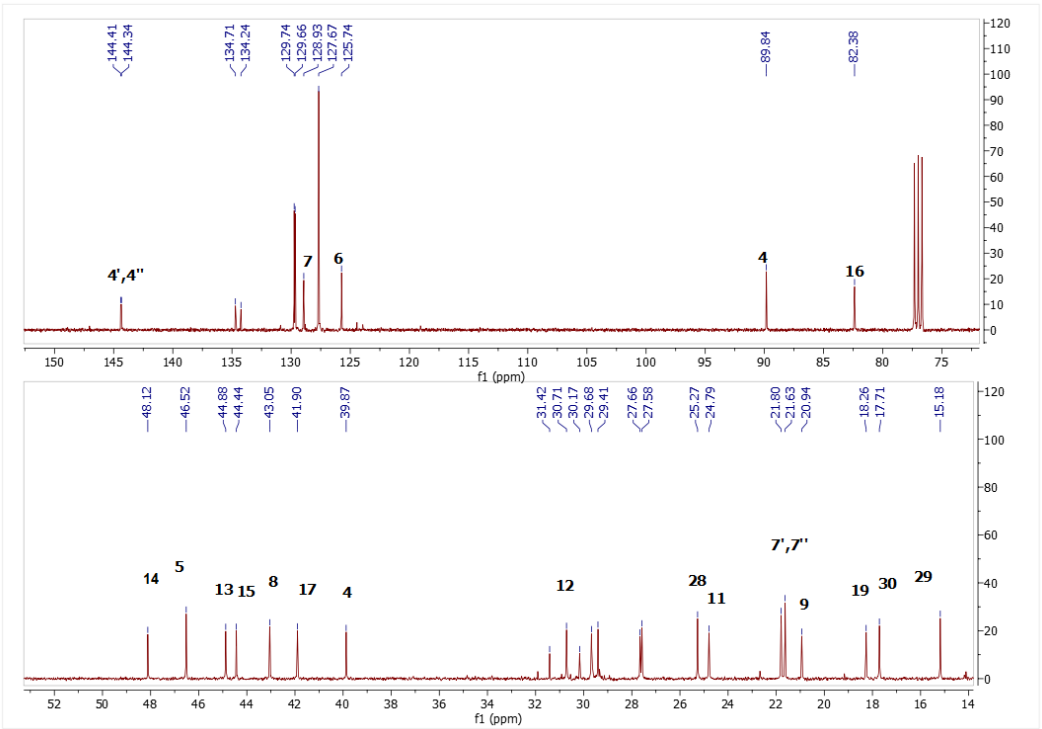

Spectrum 77. ^{13}C NMR Spectrum of SCG-04.

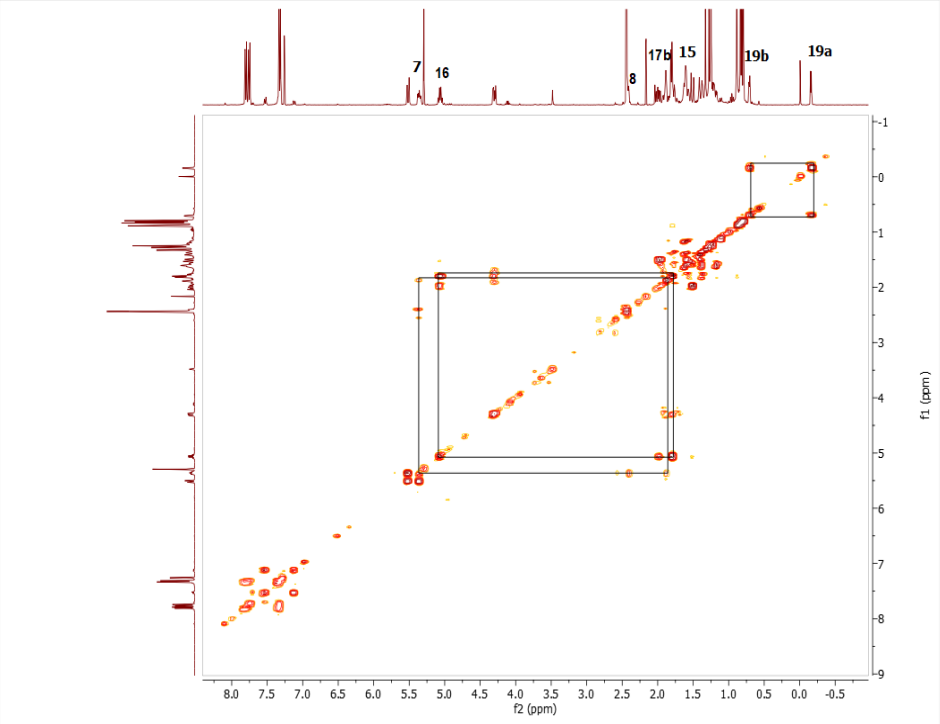

Spectrum 78. COSY spectrum of SCG-04.

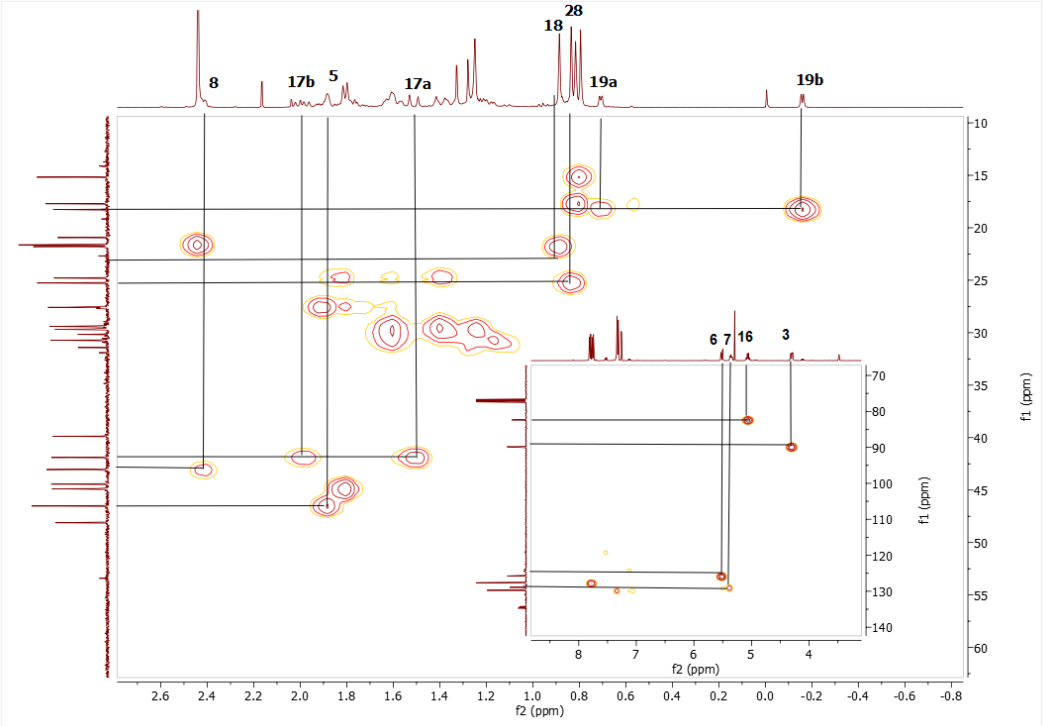

Spectrum 79. HMQC spectrum of SCG-04.

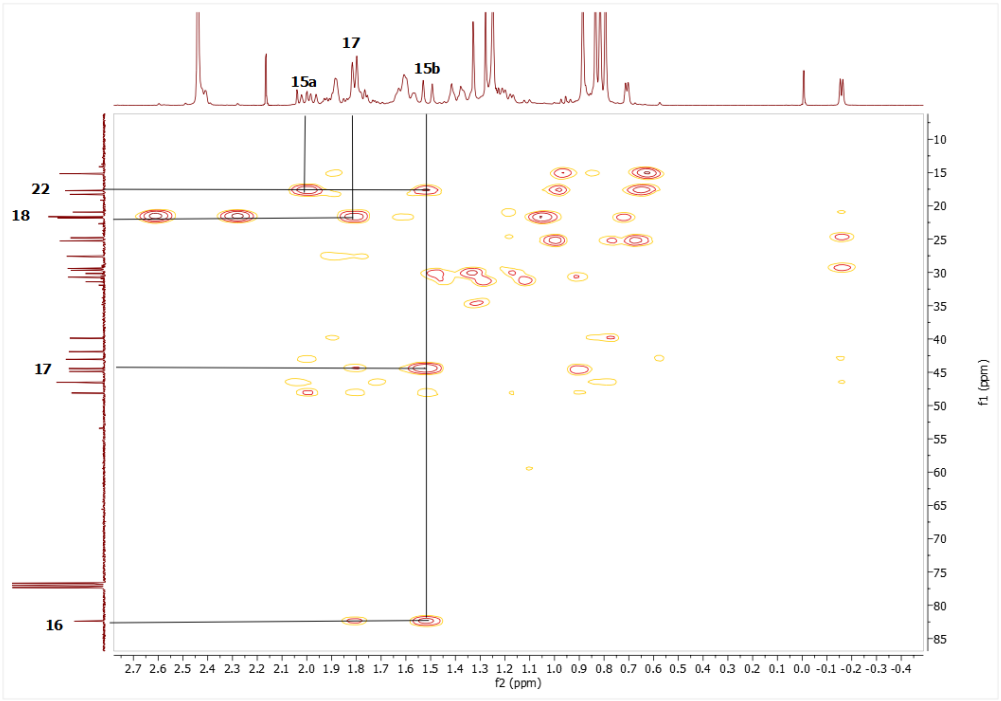

Spectrum 80. HMBC spectrum of SCG-04.

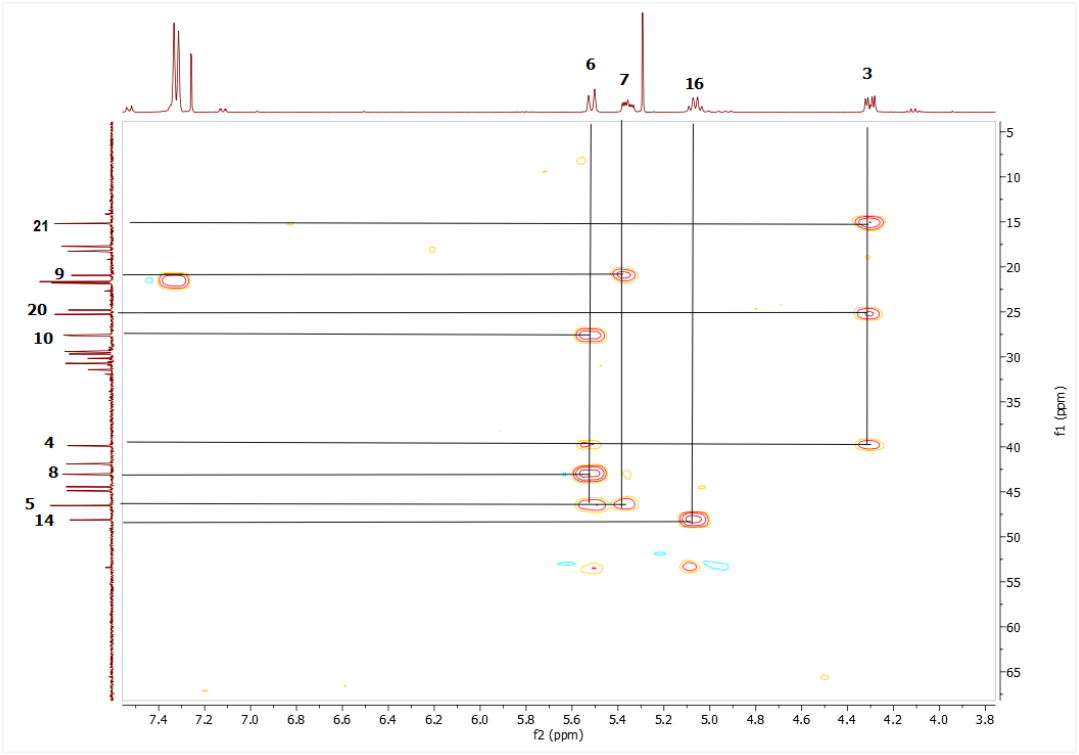

Spectrum 81. HMBC spectrum of SCG-04.

3.2.13. Structural Elucidation of Compound SCG-05

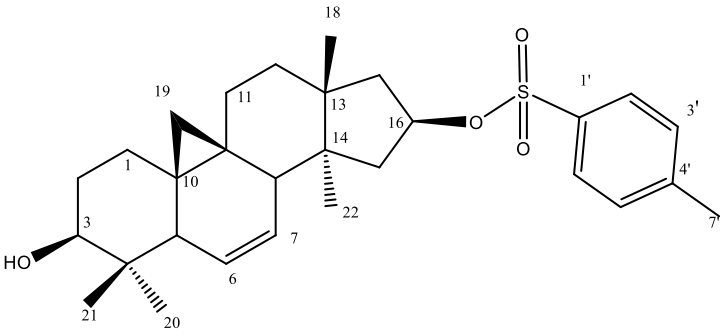

Figure 32. Chemical Structure of SCG-05.

HR-ESI-MS spectrum showing a major ion peak at *m/z* 502.2940 ($[M + NH_4]^+$) indicated a molecular formula of $C_{29}H_{40}O_4S$. Disubstituted double bond (δ_C 128.5, d and 126.9, d; δ_H 5.610 and 5.37, each 1H) and aromatic signals of tosyl was noted in in the ^1H, ^{13}C NMR and DEPT135 spectra. In ^1H spectrum, characteristic H-16 signal shifted to low-field demonstrating location of tosyl. In the COSY spectrum, correlation from olefinic signal at d 5.37 (H-7) with H-5 and H-8 suggested double bond between C-6 and C-7. Additionally, this assumption was substantiated by the long-range HMBC correlation from H-6 at δ_H 5.61 to C-8 (δ_C 43.3) and C-10 (δ_C 28.3). As a result, metabolite SCG-05 was established as 6-ene-16(O)-p-tosyl-20,27-octanor cycloastragenol.

Table 16. The ^{13}C and ^1H NMR data of SCG-05 (*100/500 MHz, δ ppm, in $CDCl_3$).*

H/C	**δ_C (ppm)**	**δ_H (ppm), *J* (Hz)**
1	29.8 t	1.23 s, 1.43 s
2	30.1 t	1.62 m, 1.82 s
3	78.5 d	3.33 dd (10.8, 3.9)
4	40.4 s	-
5	46.5 d	1.86 d (2.4)
6	126.9 d	5.61 d (10.5)
7	128.5 d	5.37 m
8	43.3 d	2.44 m
9	21.1 s	-
10	28.3 s	-
11	25.0 t	1.81 d (5.6), 1.42 m
12	31.0 t	1.63 d (12.9), 1.2 dd (12.7, 4.3)
13	48.4 s	-

(cont. on next page)

Table 16 (cont.).

H/C	δ_C (ppm)	δ_H (ppm), *J* (Hz)
14	44.6 s	-
15	45.2 t	1.83 s
16	82.7	5.07 dd (14.7, 7.2)
17	42.1 t	1.53 d (14.7), 2.01 dt (23.2, 11.6)
18	21.8 q	0.9 s
19	18.5 t	0.72d (3.1), -0.15d (3.9)
28	25.6 q	1.05 s
29	14.5 q	0.77 s
30	17.9 q	0.85 s
1'	134.5 s	-
2'	127.8 d	7.76 d (8.1)
3'	129.9 d	7.32 d (7.9)
4'	127.8 d	7.76 d (8.1)
5'	129.9 d	7.32 d (7.9)
6'	144.5 s	-
7'	21.6 q	2.44 s

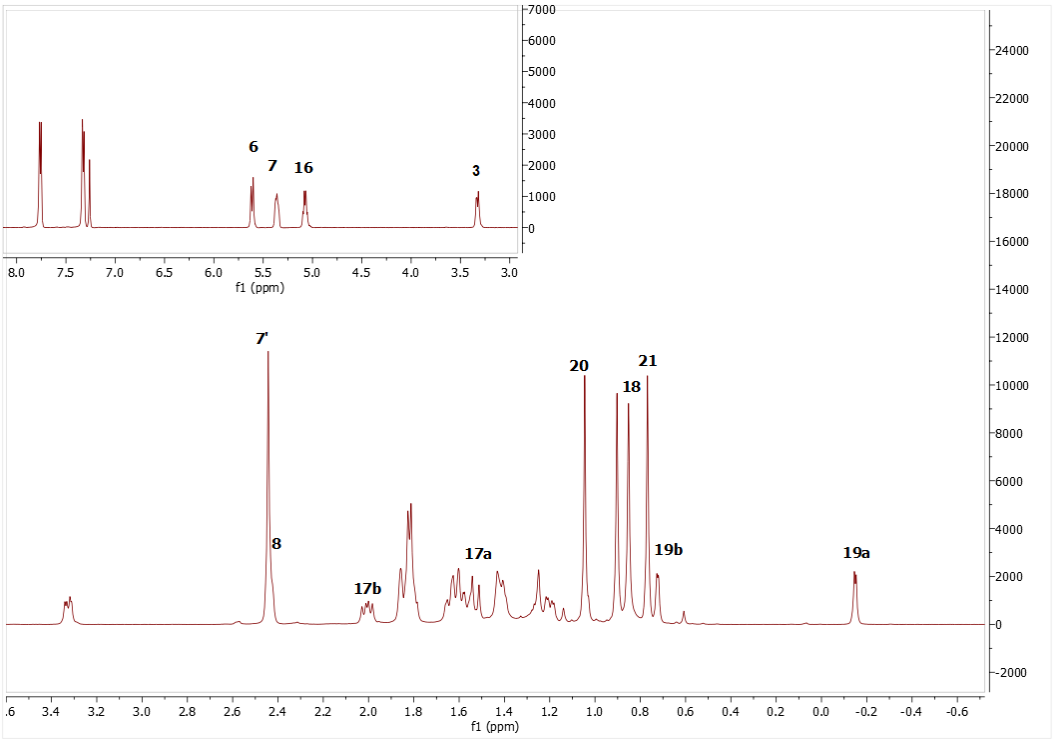

Spectrum 82. ^{1}H NMR Spectrum of SCG-05.

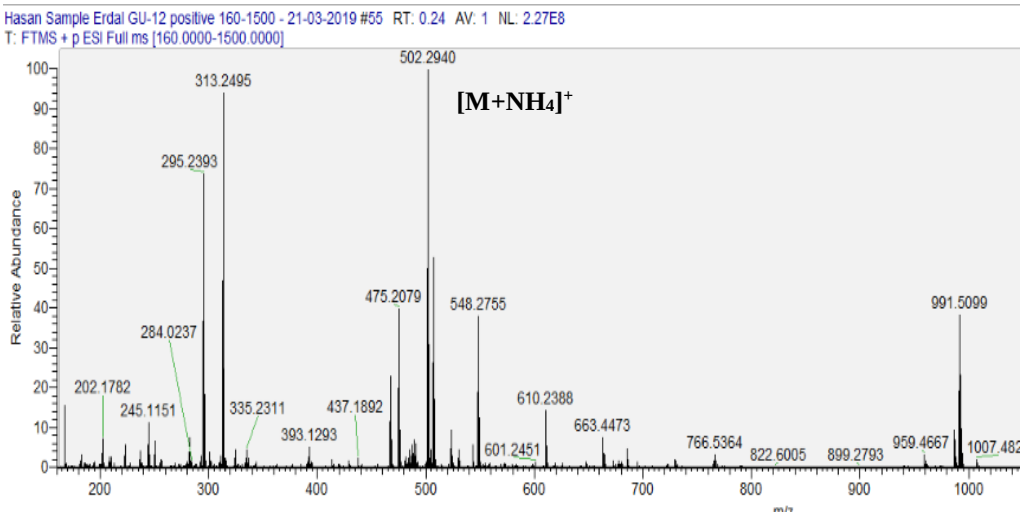

Spectrum 83. HR-ESI-MS Spectrum of SCG-05 (positive mode).

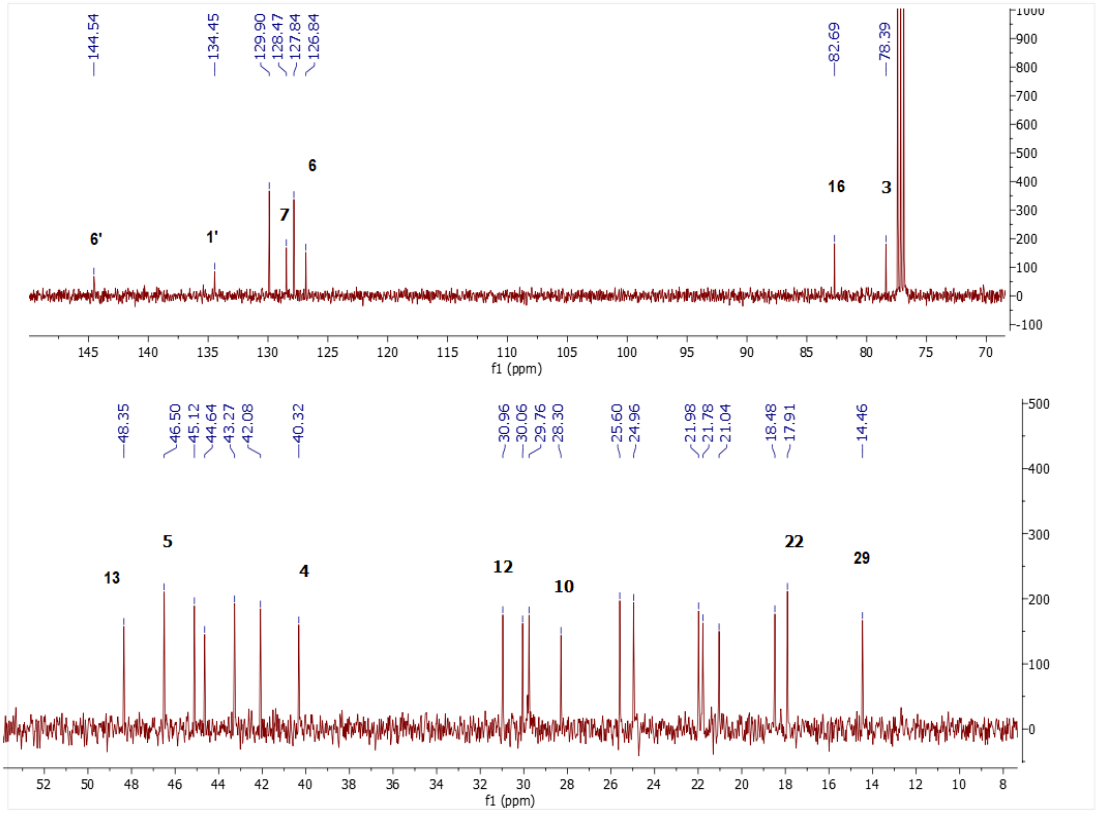

Spectrum 84. ^{13}C NMR Spectrum of SCG-05.

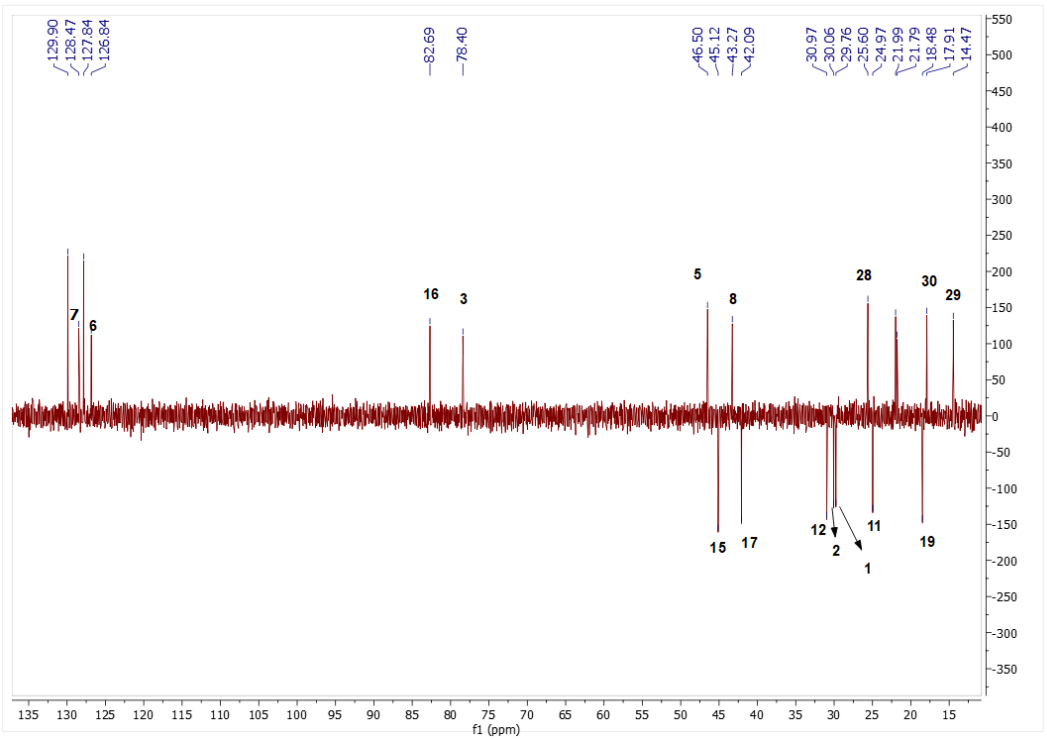

Spectrum 85. DEPT135 spectrum of SCG-05.

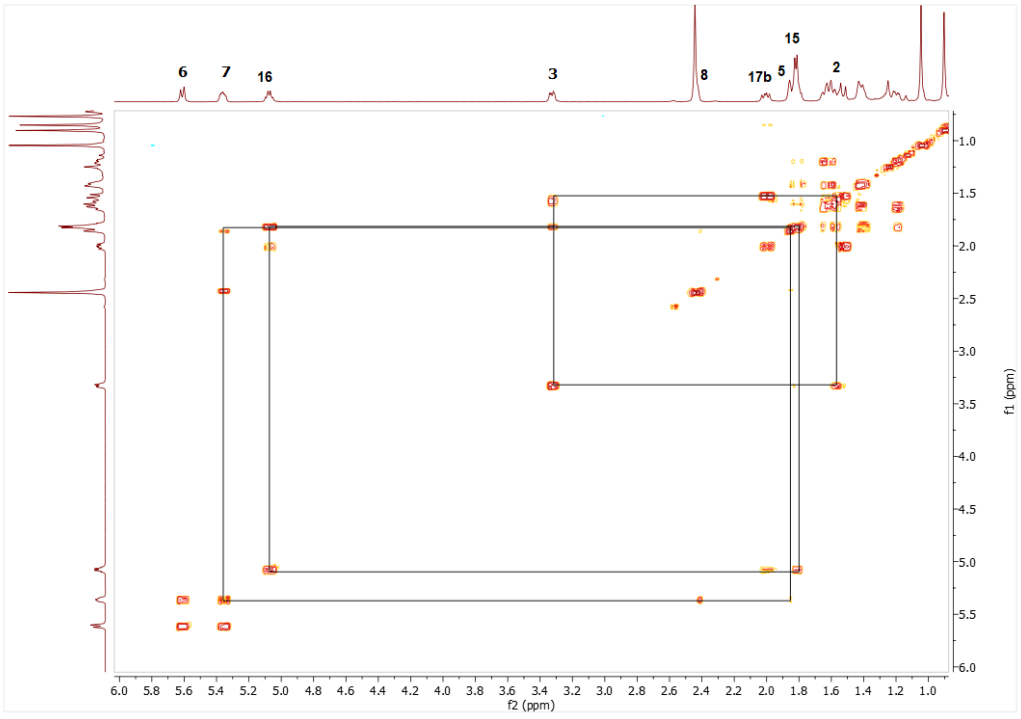

Spectrum 86. COSY spectrum of SCG-05.

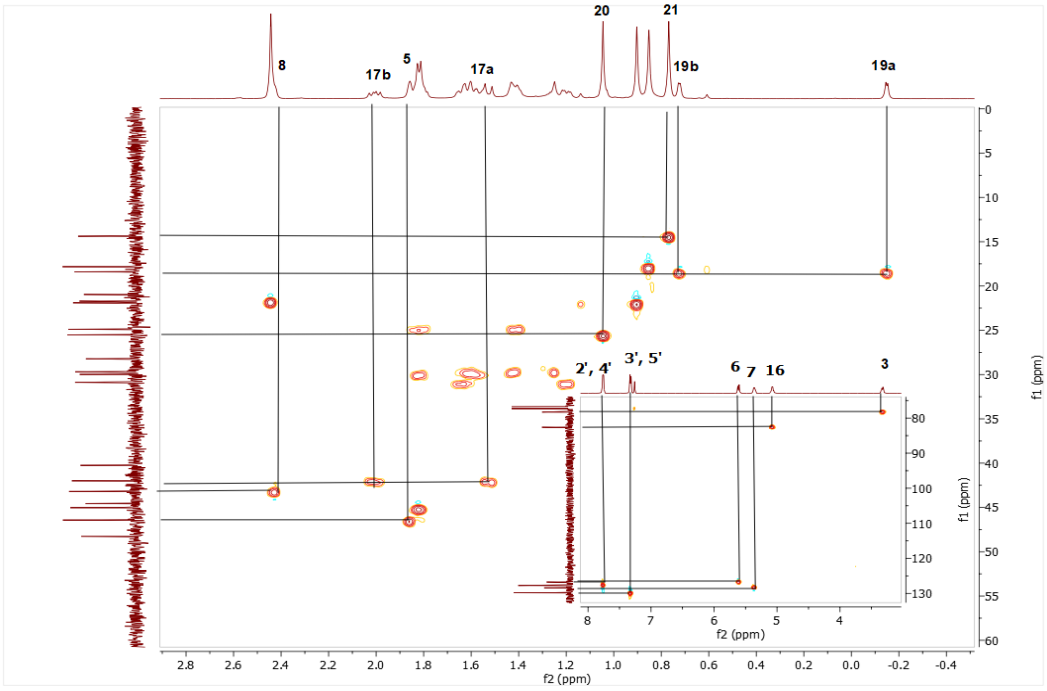

Spectrum 87. HMQC spectrum of SCG-05.

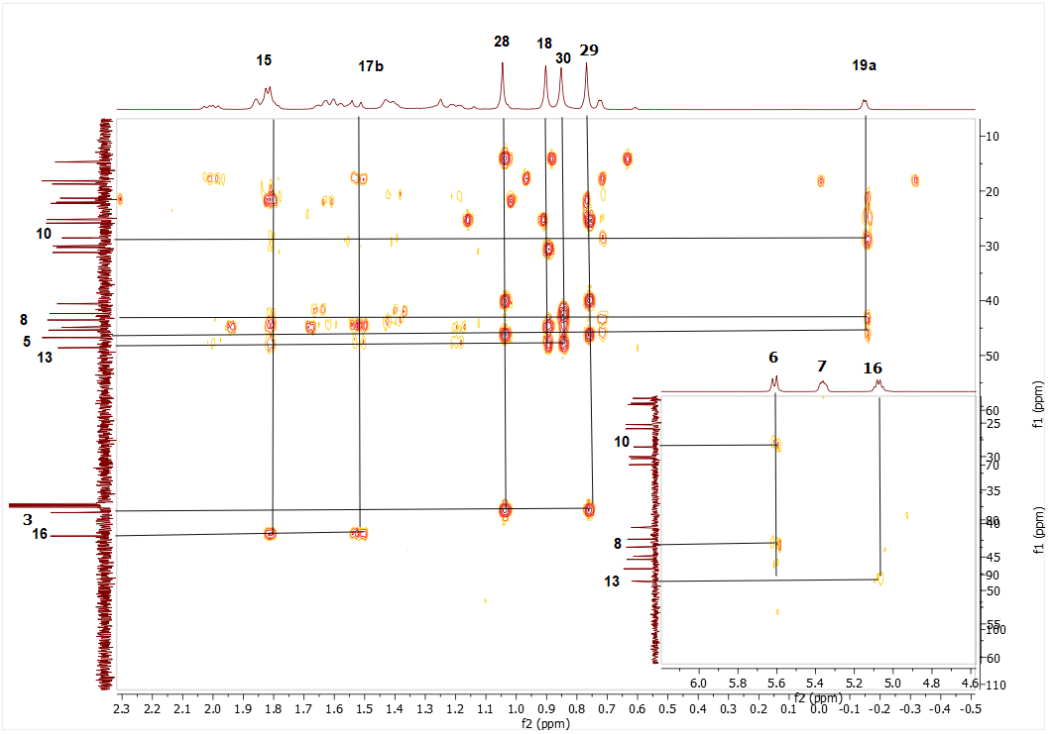

Spectrum 88. HMBC spectrum of SCG-05.

3.2.14. Structural Elucidation of Compound SCG-06

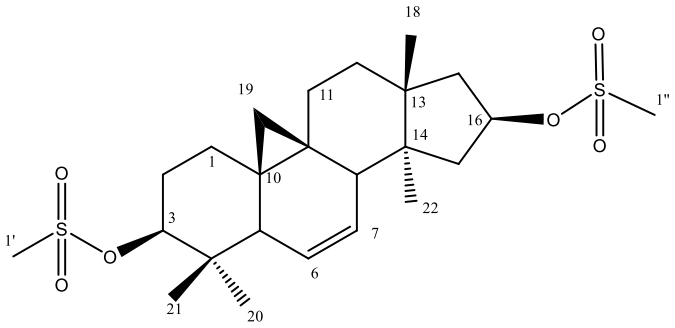

Figure 33. Chemical Structure of SCG-06

Compound SCG-06 was obtained from reaction of SCG with Mscl. Initial inspection of the ^{1}H NMR spectrum revealed two additional methyl group at low-field which shown two mesylate group in structure. Also, disubstituted double bond system was apparent in the ^{1}H, ^{13}C NMR and DEPT135 spectra (δ_C 129.2, d and 125.9, d; δ_H 5.61 and 5.45, each 1H). Location of the olefinic double bonds was assigned from the correlations in the HMBC spectrum. Long-range HMBC correlation from olefinic proton (H-6; δ_H 5.61) to C-10 (δ_C 27.8), C-5 (δ_C 46.7) and C-8 (δ_C 43.2) clearly demonstrated double bond at C-6. Moreover, characteristic signal of H-3 and H-16 shifted to low-field implying mesylation position. Thus, the structure of SCG-06 was identified as 6-ene-3(O),16(O)-di-mesyl-20,27-octanor cycloastragenol.

Table 17. The ^{13}C and ^{1}H NMR data of SCG-06 (*100/500 MHz, δ ppm, in $CDCl_3$).*

H/C	δ_C (ppm)	δ_H (ppm), *J* (Hz)
1	29.5 t	1.7 m, 1.92 m
2	28.1 t	1.92 m, 2.14 m
3	89.5 d	4.45 dd (12, 4.6)
4	40.0 s	-
5	46.7 d	2.0 m
6	125.9 d	5.61 d (10.5)
7	129.2 d	5.45 ddd (10.3, 6.1, 3.0)
8	43.2 d	2.51 dd (6, 2.6)
9	21.2 s	-
10	27. 8 s	-

(cont. on next page)

Table 17 (cont.).

H/C	δ_C (ppm)	δ_H (ppm), *J* (Hz)
11	25.0 t	1.43 m, 1.89 m
12	30.9 t	1.27 dd (13, 5.1), 1.69 m
13	44.7 s	-
14	48.4 s	-
15	42.3 t	1.63 m, 2.2 m
16	82.0 d	5.29 q (7.6)
17	45.2 t	1.93 m, 2.04 m
18	22.0 q	0.98 s
19	18.4 t	-007, 0.77 d (4.3)
28	15.3 q	0.86 s
29	25.8 q	1.1 s
30	17.9 q	0.87 s
1'	39.0 q*	3.03 s'
1''	38.5 q*	2.97 s'

*,': exchangeable

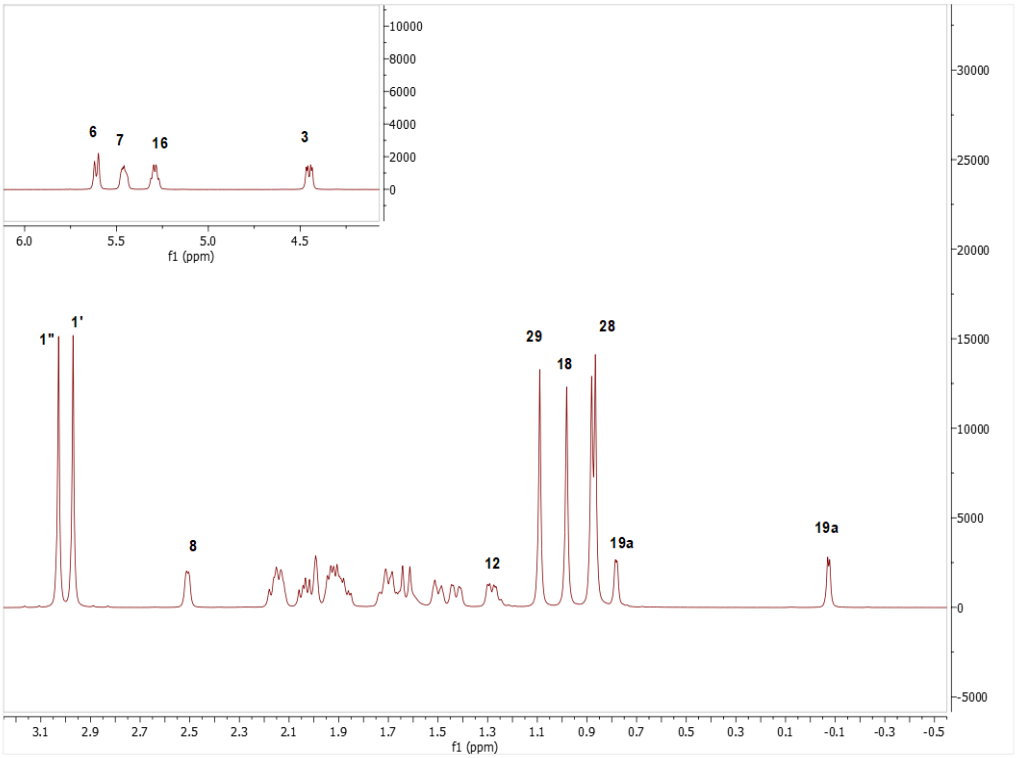

Spectrum 89. ^{1}H NMR Spectrum of SCG-06.

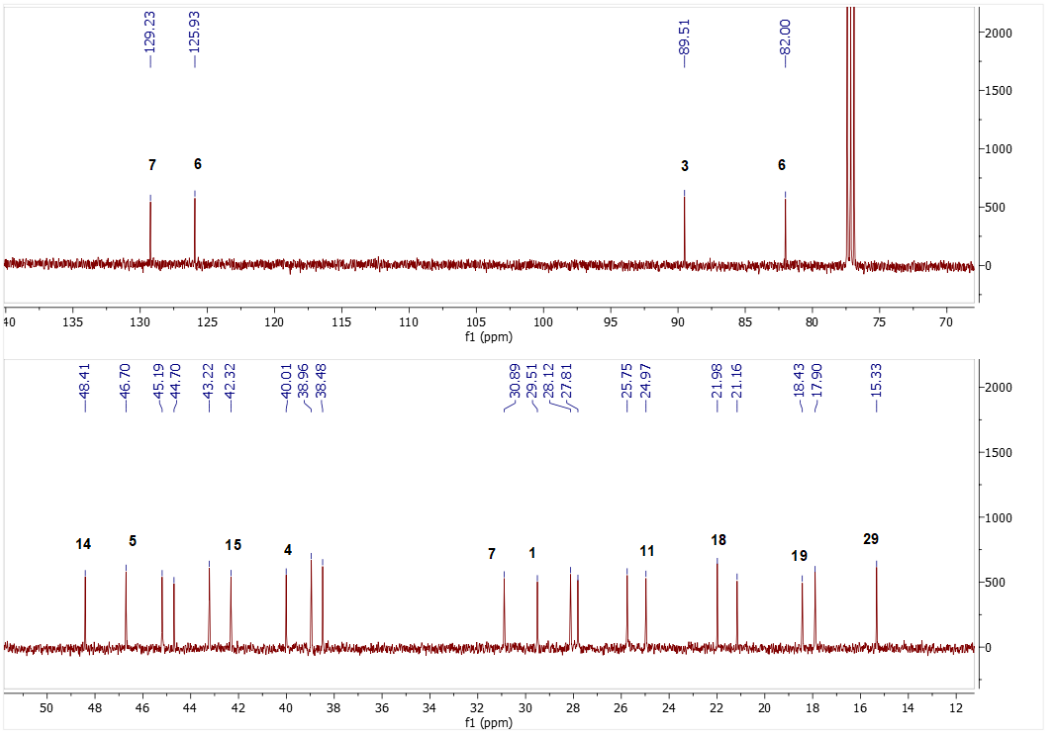

Spectrum 90. ^{13}C NMR Spectrum of SCG-06.

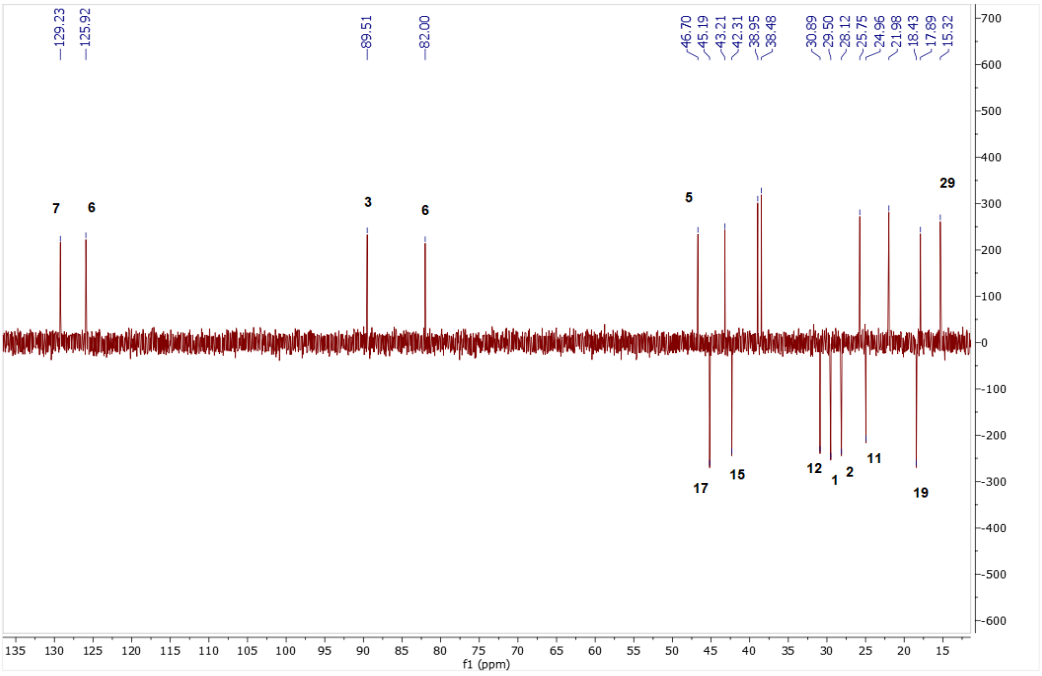

Spectrum 91. DEPT135 spectrum of SCG-06.

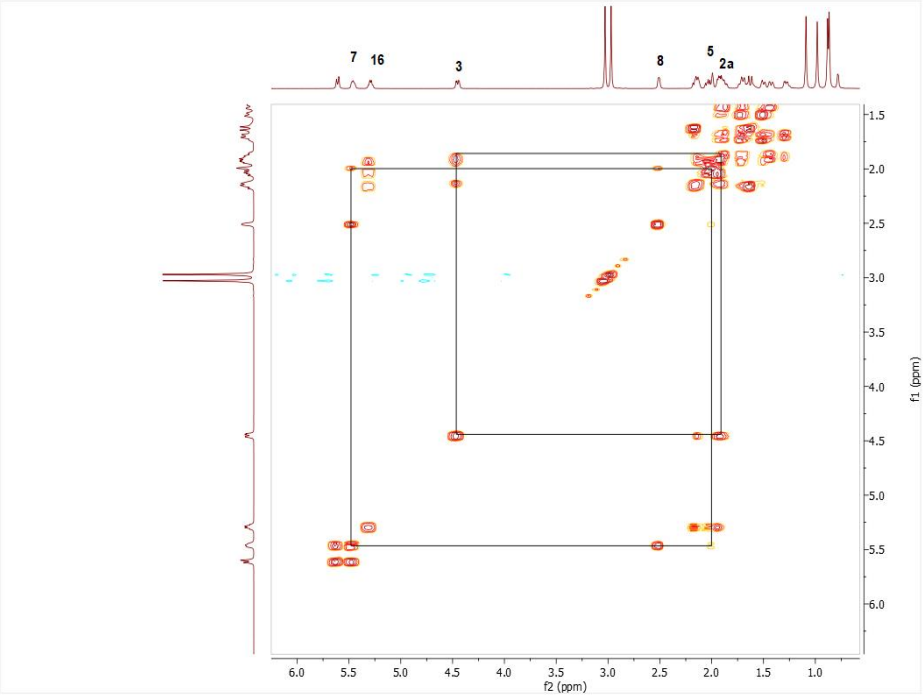

Spectrum 92. COSY spectrum of SCG-06.

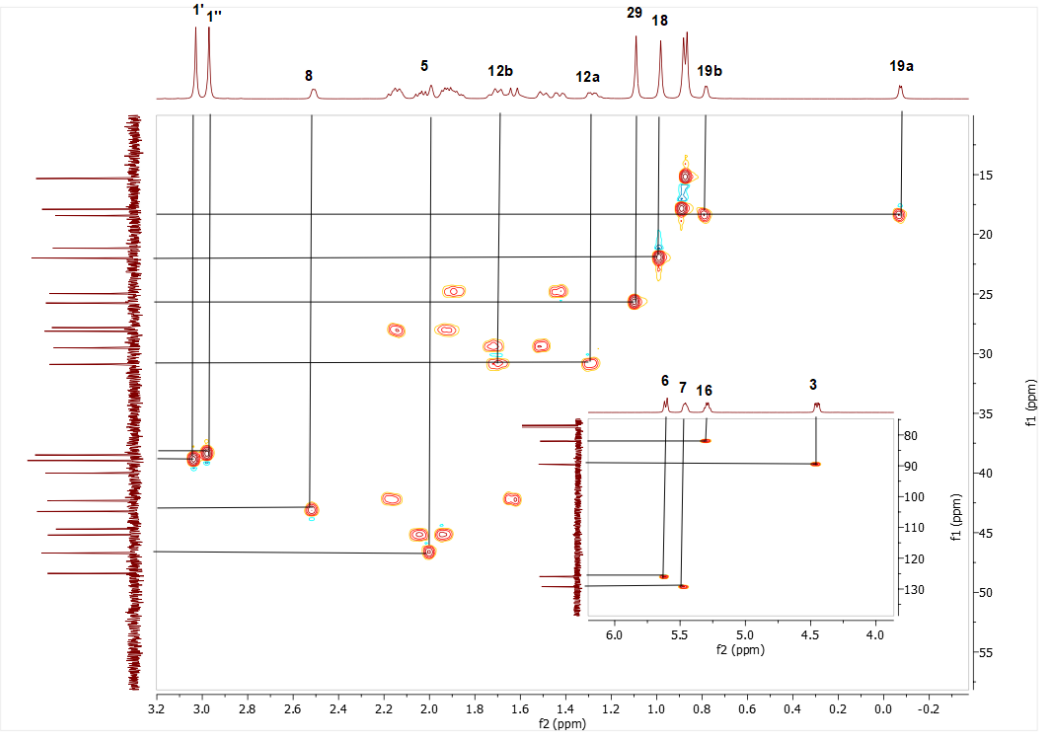

Spectrum 93. HMQC spectrum of SCG-06.

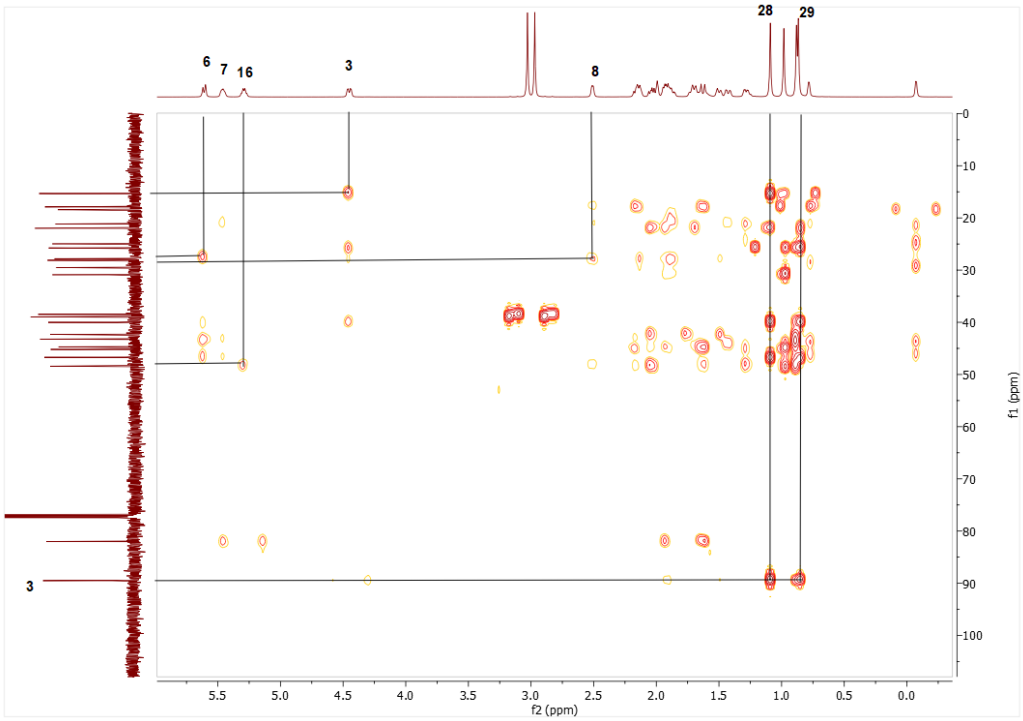

Spectrum 94. HMBC spectrum of SCG-06.

3.2.15. Structural Elucidation of Compound SCG-07

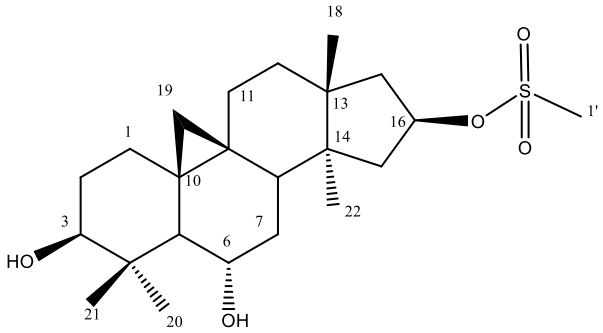

Figure 34. Chemical Structure of SCG-07.

The compound SCG-07 had a molecular formula of $C_{23}H_{38}O_5S$ based on the HR-MS data (*m/z* 449.2366 $[M + Na]^+$). When the MS data of SCG-08 was compared with SCG, 78 amu (atomic mass unit) difference suggested mesylate addition to SCG skeleton. Also, additional methyl group (δ_H 2.97) at down field supported this proposition. ^1H spectrum of SCG-07 was inspected to determine location of mesylation. Characteristic H-16 signal (δ_H 5.26) shifted to low-field suggesting position of mesylation at C-16.

Consequently, the structure of SCG-07 was established as 3,6-diene-16(O)-mesyl-20,27-octanor cycloastragenol.

Table 18. The ^{13}C and ^{1}H NMR data of SCG-07 (*100/500 MHz, δ ppm, in $CDCl_3$).*

H/C	δ_C (ppm)	δ_H (ppm), *J* (Hz)
1	31.3 t	1.26 m, 1.63 m
2	30.2 t	1.58 m, 1.8 m
3	78.48 d	3.22 dd (11.2, 4.2)
4	41.6 s	-
5	53.4 d	1.37 m
6	68.4 d	3.56 ddd (9.2, 9.2, 4.1)
7	37.6 t	1.38 m, 1.55 m
8	45.6 d	1.71 m
9	20.7 s	-
10	29.0 s	-
11	26.1 t	1.31 m, 1.97 m
12	30.3 t	1.48 m
13	44.7 s	-
14	46.0 s	-
15	44.6 t	1.79 m, 2.06 m
16	82.39 d	5.26 q (8)
17	46.2 t	2.01 m, 2.11 m
18	24.9 q	1.03 s
19	26.7 t	0.31 d, 0.5 d(4.7)
28	15.3 q	0.94 s
29	27.9 q	1.23 s
30	19.8 q	1.1 s
1'	38.5 q	2.97 s

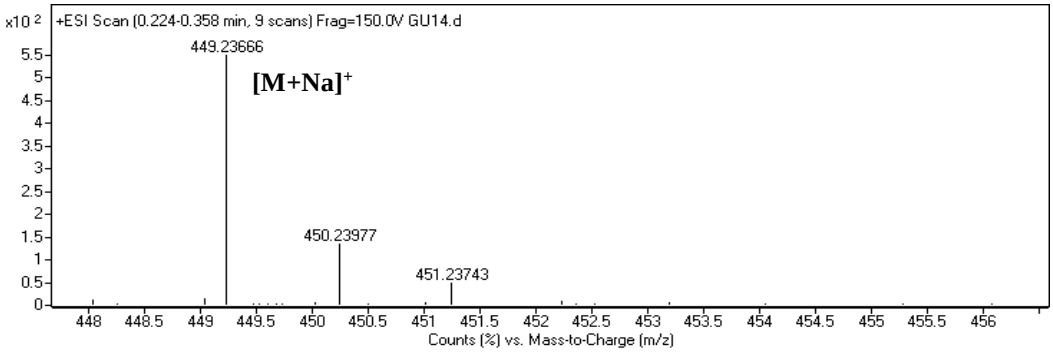

Spectrum 95. HR-ESI-MS Spectrum of SCG-07 (positive mode).

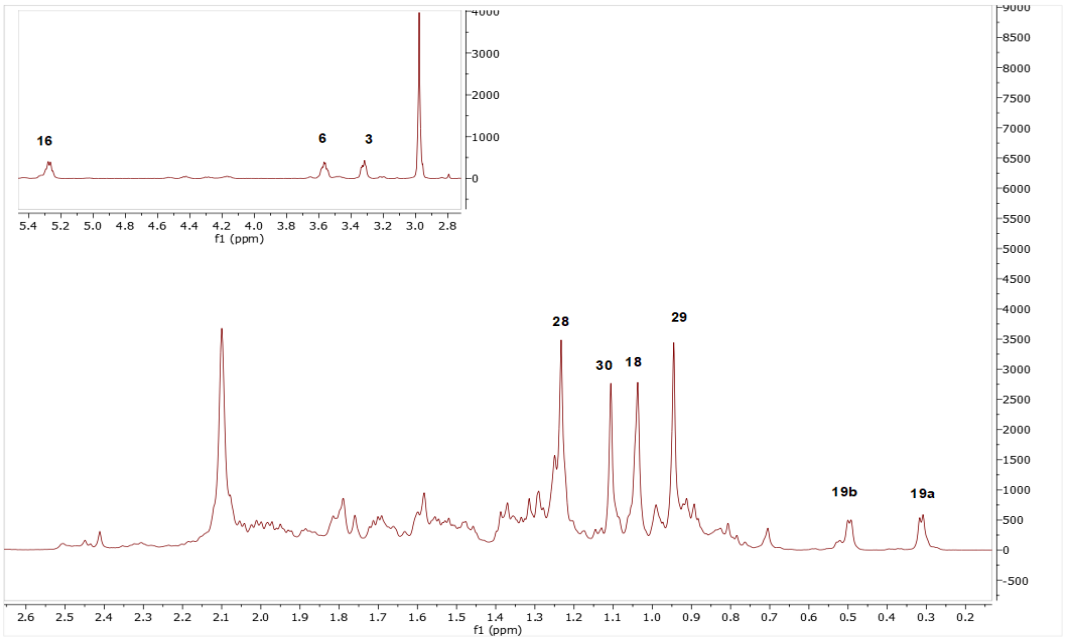

Spectrum 96. ^{1}H NMR Spectrum of SCG-07.

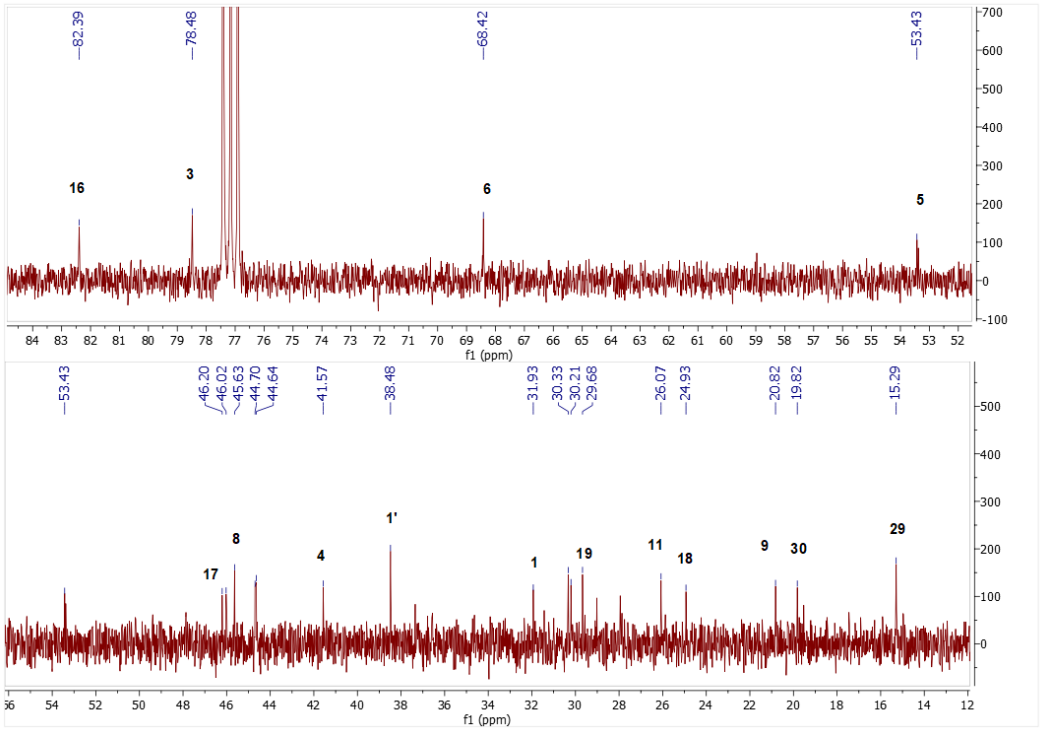

Spectrum 97. ^{13}C NMR Spectrum of SCG-07.

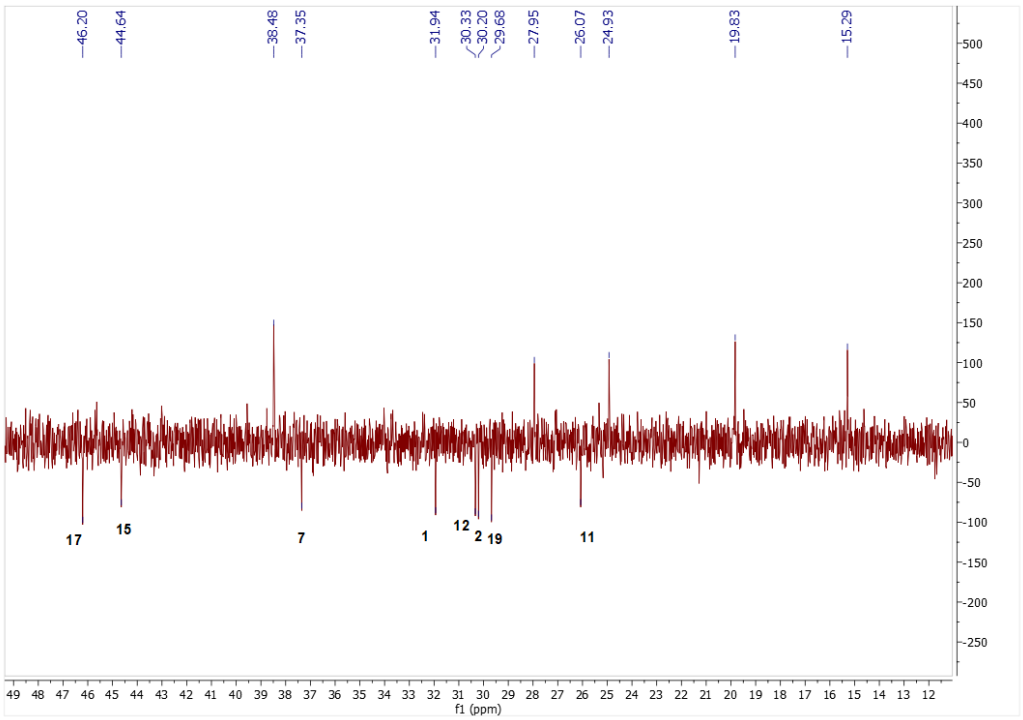

Spectrum 98. DEPT135 spectrum of SCG-07.

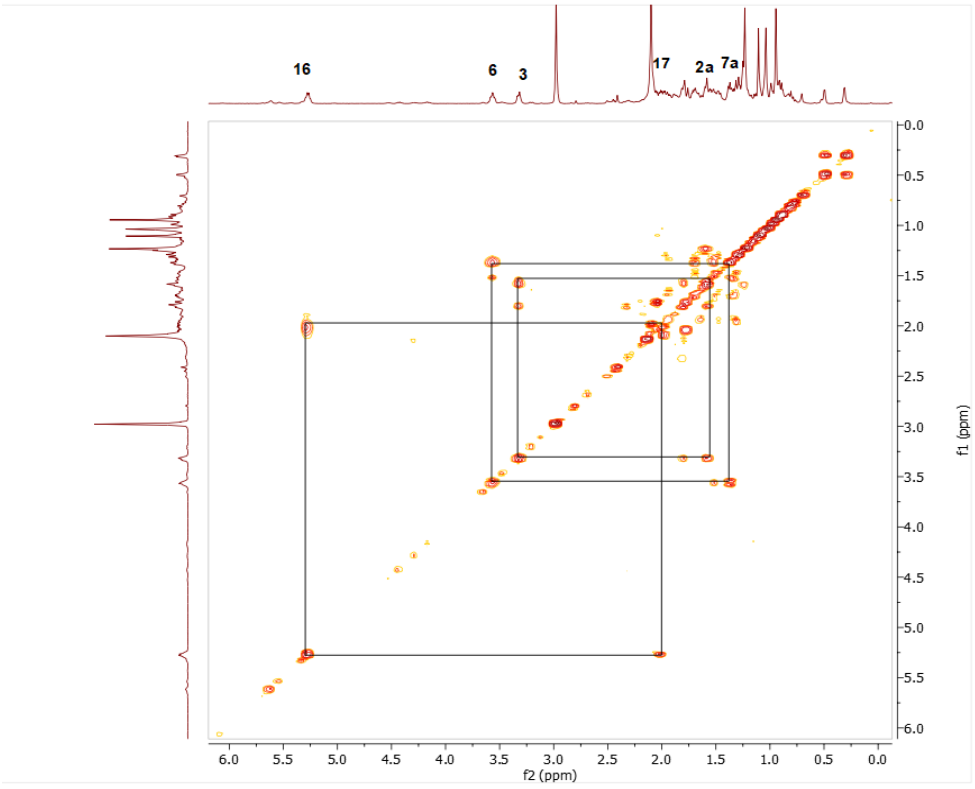

Spectrum 99. COSY spectrum of SCG-07.

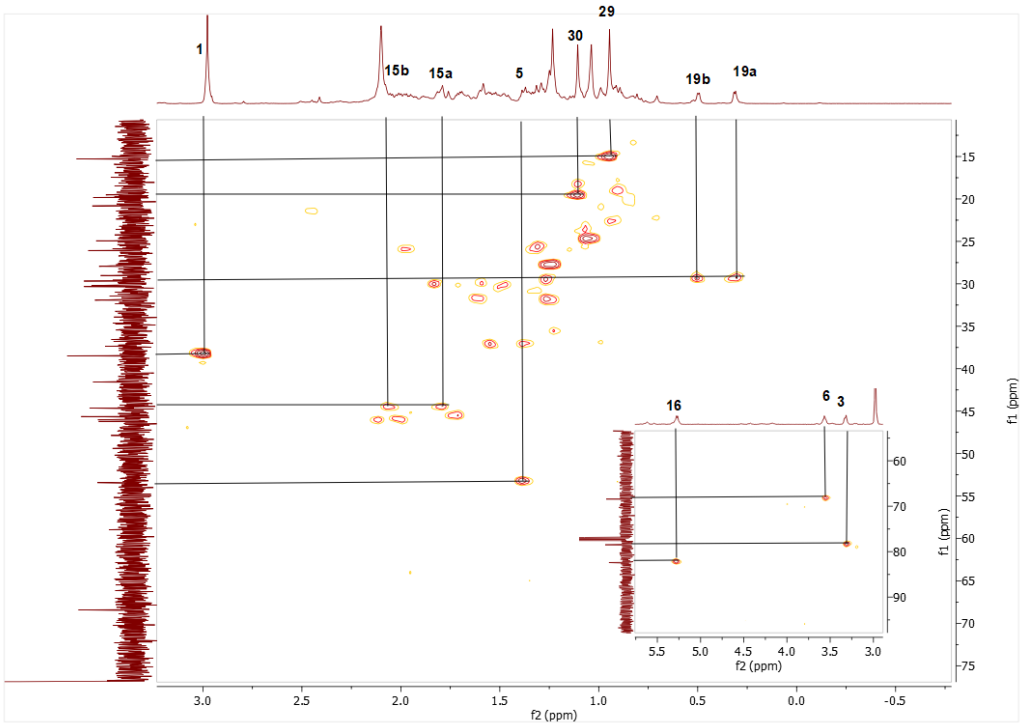

Spectrum 100. HMQC spectrum of SCG-07.

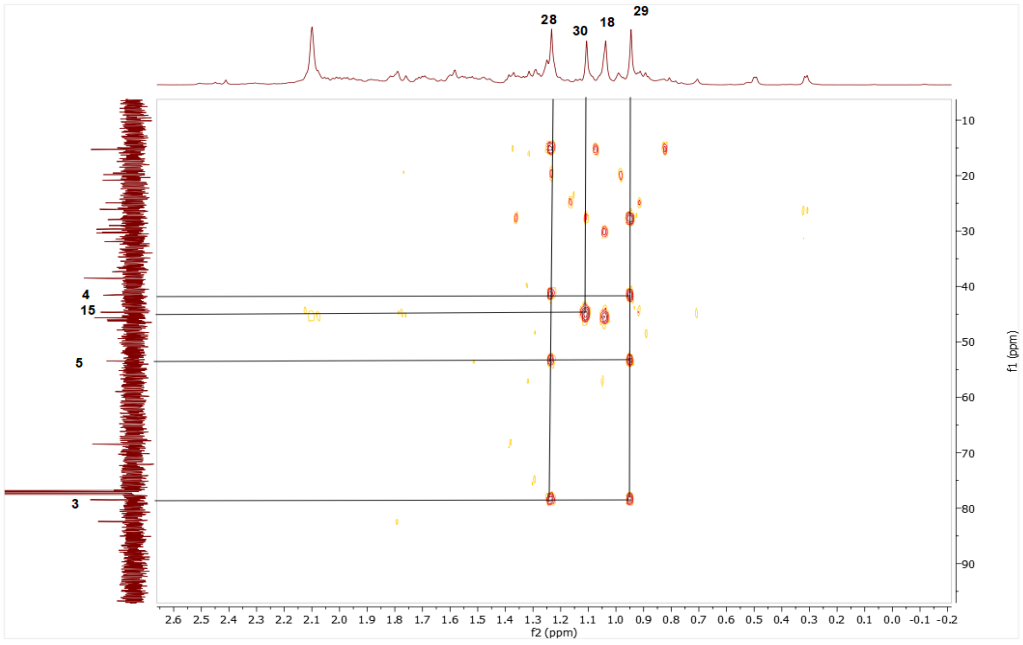

Spectrum 101. HMBC spectrum of SCG-07.

3.3. Biological Activity of AG-08 Derivatives

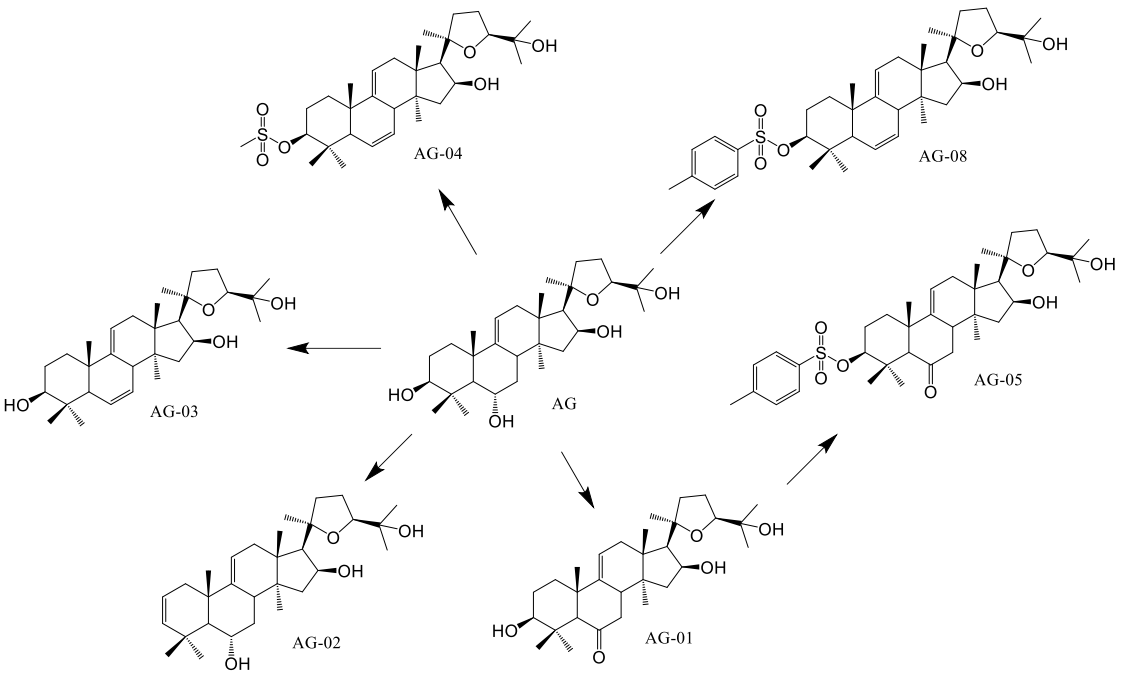

Figure 35**.** Structure of AG derivatives.

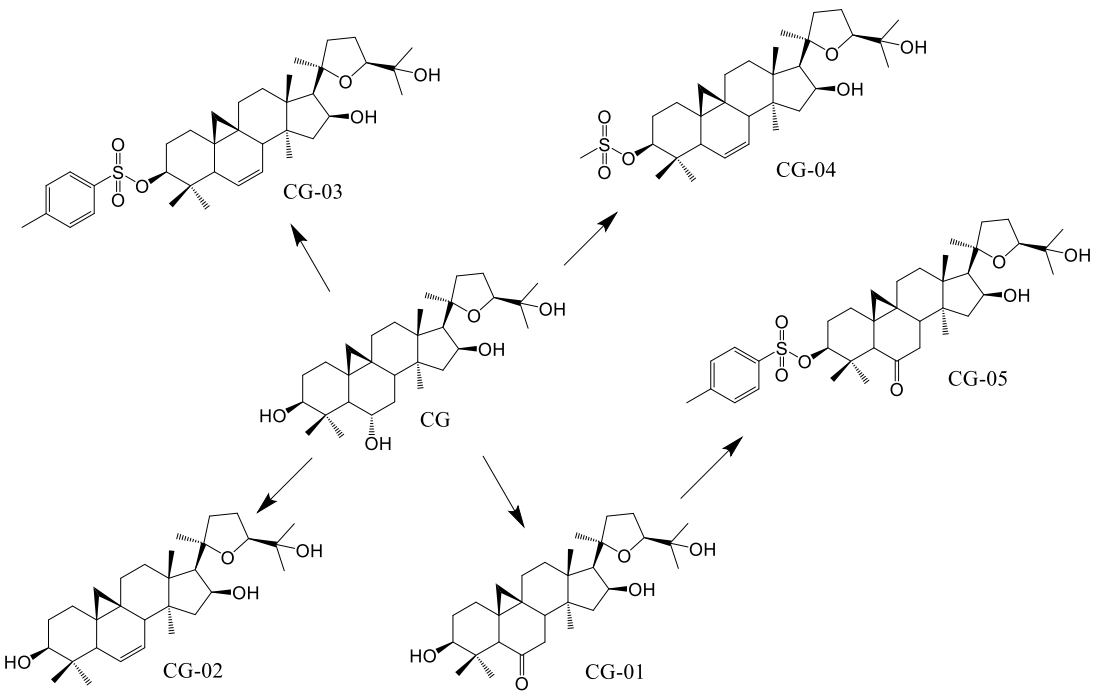

Figure 36. Structure of CG derivatives.

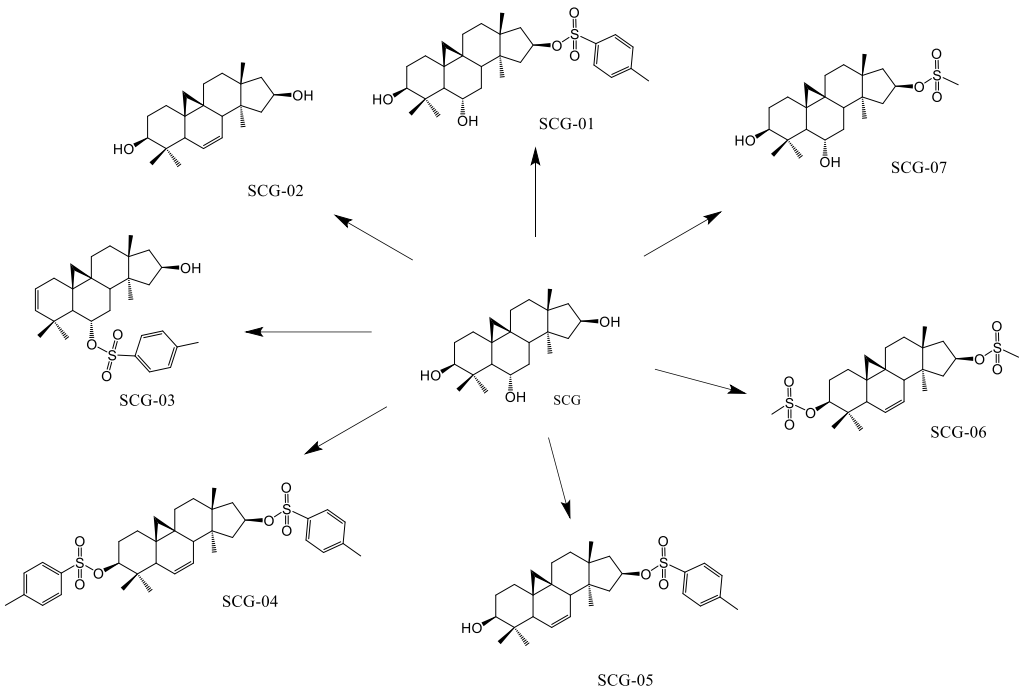

Figure 37. Structure of SCG derivatives.

In semi-synthetic studies, four AG, four CG and seven SCG derivatives were synthesized. Their structures were shown in Fig 35., Fig 36. and Fig 37., respectively. To determine their cytotoxic activities, all the analogs were screened by MTT assay. Then, further studies were conducted with the active ones to determine their toxicity mechanism

3.3.1. Cytotoxic Activity of Semi-Synthetic Derivatives

Cytotoxic activities of the semi-synthetic analogs were evaluated against four human cancer cell lines, namely HeLa, HCC1937, MCF7 and A549 as well as against MRC-5 as a normal cell line. All molecules except AG, AG-6-oxo and CG-6-oxo were used at concentrations ranging between 1 to 50 µM. AG, AG-6-oxo and CG-6-oxo were tested between 1 to 30 µM concentrations due to solubility problems. The IC_{50} values were shown in the Table 18. Molecules having lower IC_{50} values than 20 µM were regarded as cytotoxic and progressed to subsequent studies. The compounds except CG-03, AG-05, and CG-05 did not exhibit promising cytotoxicity (IC_{50} >20 µM). As CG-03, AG-05, and CG-05 compounds were more reliable for cytotoxicity, they were also tested versus four additional cell lines (HK-2, PC3, SH-SY5Y and U2OS). The expanded IC_{50}

values were given in the Table 19. Also, Table 19 includes IC_{50} values of AG-08 against the same cell lines for comparison.

CG-03 had cytotoxic activity against all cell lines with IC_{50} values ranging between 3.65 and 18.82 µM. On the other hand, cytotoxic effect of CG-03 was lower than AG-08 for all cell lines. It suggests that the cleavage of cyclopropane ring affording AG and its derivatives is significant for cytotoxicity. Similar to AG-08, CG-03 was not selective towards cancer and normal cell lines.

Table 19. IC_{50} values (µM) of analogs and parent molecules.

Cell lines	HeLa	HCC1937	MRC-5	MCF7	A549
AG-01	>30	>30	>30	>30	>30
AG-02	42.6	46.08	39.9	32.1	30.5
AG-03	33.42	20.31	24.4	21.76	25.53
AG-04	>50	>50	29.55	22.05	27.5
AG-05	5.9	4.28	1.55	2.55	2.02
CG-01	>30	>30	>30	>30	>30
CG-02	43.94	32.48	33.37	21.2	21.08
CG-03	12.87	6.13	5.29	5.5	3.65
CG-04	>50	>50	>50	>50	>50
CG-05	6.1	2.66	2.58	3.85	1.85
SCG-01	>50	>50	>50	>50	>50
SCG-02	>50	>50	>50	>50	>50
SCG-03	>50	>50	>50	>50	>50
SCG-04	>50	>50	>50	>50	>50
SCG-05	>50	>50	>50	>50	>50
SCG-06	>50	>50	>50	>50	>50
SCG-07	>50	>50	>50	>50	>50
AG	>30	>30	>30	>30	>30
CG	>50	>50	>50	>50	>50
SCG	>50	>50	>50	>50	>50

Both AG-05 and CG-05 have a carbonyl group at C-6 rather than a double bond as in AG-08. IC_{50} values of AG-05 and CG-05 ranged from 2.02 to 5.9 µM and 1.85 to 6.46 µM, respectively.

Interestingly, cytotoxicity of CG-05, a CG derivative, was almost identical with AG-05, an AG analog. Thus, the abovementioned trend in regard to cytotoxicity of CG-03 and AG-08 was not the case for CG-05 and AG-05. Thus, oxidation of C-6(OH) to carbonyl group seems to be affecting cytotoxicity reasonably in CG analogs (CG-05). The ^{1}H NMR data of CG-03 reveals that π electrons of C-6 double bond are in close proximity with the cyclopropane ring, which results in significant deshielding of one of the cyclopropane ring protons. This suggest that electron density difference over the B ring might be one of the parameters varying bioactivity of CG-03 and CG-05.

Cytotoxicity tests show that the tosyl group plays essential role in activity. First evidence was that AG-04 and CG-04, which had mesylate group at C-3 instead of tosyl, were inactive (Table 18). Additionally, AG-03 and CG-02, possessing a double bond at C-6 with no tosyl group at C-3, did not inhibit the growth of cell lines below 20 µM. This data clearly demonstrated that the presence of more bulky and aromatic sulfonic ester was required for superior cytotoxic activity. Therefore, activity of AG-08 and its derivatives essentially depend on the presence of tosyl group. The absence of significant toxicity in the case C-6 double bond containing compounds (AG-03 and CG-02) and C-6-oxo analogs (AG-01, CG-01) reveals that these modifications alone with no tosyl at C-3 are not enough to produce activity.

Similar semi-synthetic modifications were also carried out with SCG. We were not able to synthesize the similar analog of AG-08 with SCG molecule. Mono-tosylated analogs were only SCG-03 (C-2 double bond and C-6 tosylate), SCG-01 (C-16 tosylate) and SCG-05 (C-6 double bond with C-16 tosylate), whereas di-tosylated derivative was only SCG-04 (C-6 double bond and C-3/C-16 tosylate). It was seen that all SCG derivatives were inactive towards tested cell lines. As SCG does not have the side chain extending from C-17, the existence of tetrahydrofurane ring is realized to be important for activity. Additionally, it is clear that the tosyl group(s) presence on sapogenin skeleton is not sufficient to cause cellular toxicity. Therefore, the intact sapogenin skeleton together with regioselective tosylation at C-3 and dehydration/oxidation at C-6 are important structural features for superior cytotoxicity. However, analog of SCG possessing C-3(O)-tosyl and C-6 double bond must be synthesized to justify our assumptions mentioned above.

Table 20. IC_{50} values (μM) of cytotoxic analogs and AG-08. Data represents as mean ± standard error from the triplicate experiment (n: 3).

Cell lines	AG-08	CG-03	AG-05	CG-05
HeLa	5.7±0.447	12.87±0.163	5.9±0.463	6.1±0.495
HCC1937	3.81±0.272	6.13±0.449	4.28±0.48	2.66±0.293
MRC-5	2.18±0.044	5.29±0.623	1.55±0.178	2.58±0.125
MCF7	3.78±0.269	5.5±0.277	2.55±0.495	3.85±0.375
A549	2.3±0.035	3.65±0.362	2.02±0.118	1.85±0.117
SH-SY5Y	3.57±0.092	7.71±0.471	4.34±0.081	6.46±0.290
PC3	6.6±0.887	12.45±0.178	3.3±0.236	6.36±0.382
HK-2	10.18 ±0.509	16.59±0.2924	5.73±0.382	4.14±0.341
U2OS	6.49±0.7293	15.4±0.138	3.3±0.084	4.23±0.067

Consequently, none of the parent molecules (AG, CG, SCG, AG-01 and CG-01) showed cytotoxic effects. Thus, it is rationale to state that the starting compounds (CG and AG) could be turned into more prominent cytotoxic compounds via simple synthetic modifications. Based on the data presented above, further semi-synthesis studies are certainly warranted to substantiate our structure activity relationship deductions and achieve more active and/or selective molecules.

3.3.2. Molecular Mechanism of Action of Cytotoxic AG-08 Analogs

CG-03, AG-05 and CG-05 were determined as cytotoxic derivatives of AG-08. To identify characteristics of cell death induced by them, LDH assay was performed. As shown in Fig 38, all compounds caused significant release of LDH dose dependently. Massive release of LDH in response to three analogs indicated necrotic cell death in line with AG-08.

After LDH assay, immunoblotting was used to determine whether their molecular pathways were the same as AG-08. The effect of AG-08 analogs on the protein profiles of LC3, Atg-7 and caspase 3 were investigated in order to evaluate the autophagic process, the cleavage of ATGs and caspase 3 activation, respectively. It was found that,

all compounds caused increasing LC3-II and cleaved caspase 3 formation in dose dependent manner. Additionally, Atg-7 protein level was decreased with treatment of compounds.

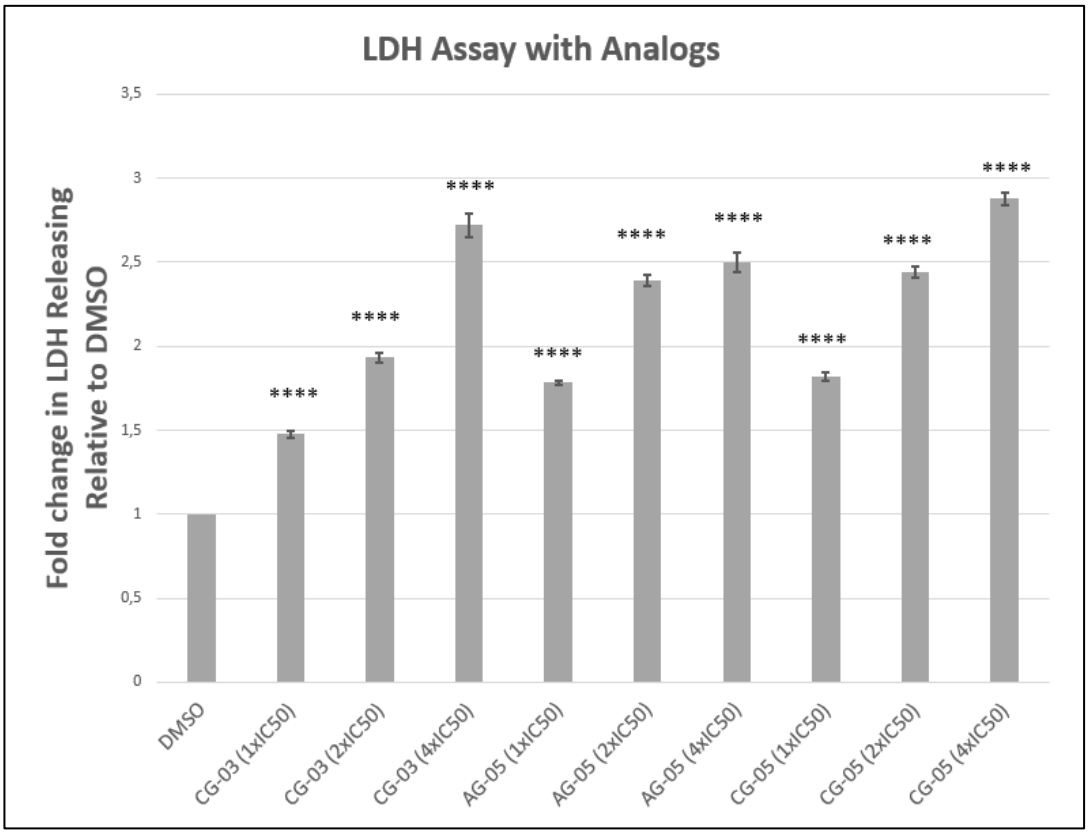

Figure 38. Release of LDH with AG-08 analogs. LDH activity were measured and amount of released LDH was calculated as fold change relative to DMSO. All compounds were used at 1, 2, and 4 times of their IC_{50} values and incubated 24 h. Error bars represent standard deviations. One-way ANOVA was used to analyze the statistical significance. The significant difference was defined between compounds and DMSO.

It was clear that cytotoxic AG-08 derivatives inhibited autophagy like AG-08 according to LC3-II accumulation and decrease in Atg-7 level. Also, caspase 3 activation was demonstrated that they induce caspase 3 involved necrosis. Consequently, CG-03, AG-05, and CG-05 induced necrotic cell death through similar activity mechanism with AG-08.

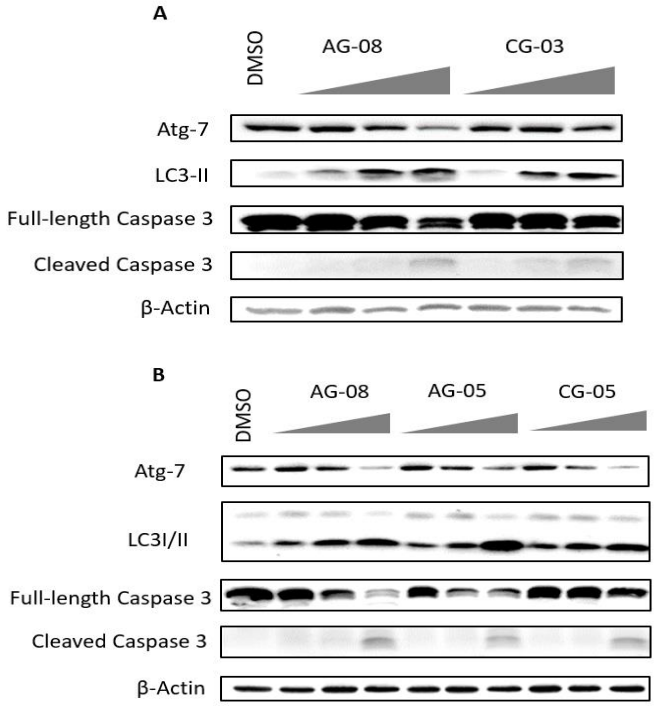

Figure 39. Immuno-blotting studies with cytotoxic analogs. β-Actin was used as the loading control. HCC1937 cells were treated with 1, 2 and 4-fold of IC_{50} value of compounds for 16 h.

CHAPTER 4

CONCLUSION

Semi-synthesis approach is applied to enhance anti-tumor activity of different types of saponins. With the same motivation, we prepared a number of analogous compounds from cycloartane-type sapogenols of *Astragalus* genus, *viz.* cycloastragenol and cyclocanthogenol (TÜBİTAK 109S345) to increase cytotoxicity of the starting compounds. One of the derivatives, namely AG-08, was turned out to be a good candidate to pursue because of its distinctive cytotoxicity profile including necrotic cell death along with autophagic inhibition. Furthermore, the immunoblotting experiments demonstrated that AG-08 promoted cleavage of various proteins such as ATGs, p62, and PARP-1. Non-canonical cell death inducing activity of AG-08 has encouraged us to design a further study. Thus, clarification of molecular mechanisms of AG-08 treatment and preparation of additional analogs to realize structure activity relationships were attempted in the context of this thesis.

As several proteins were effectively cleaved, we first investigated possible role of proteases through co-treatment of several protease inhibitors and AG-08. Results showed that inhibition of caspases, calpains and cathepsin B/L/S attenuated AG-08 inflicted cell death. Therefore, the link between proteases and AG-08 was substantiated within this study. However, revealing activity of these proteases together with their specific substrate in AG-08 exposed cells or knockdown of these proteins will help us to establish relationships between proteases and AG-08 soundly.

The effect of cathepsins inhibitor on cell death and autophagic flux inhibition prompted us to look into lysosomal condition. The lysotracker staining demonstrated that AG-08 treatment led to loss of acidity in lysosomes. The results of staining and co-treatment with cathepsins inhibitor consistently indicated lysosomal leakage. Additional tests are certainly warranted to confirm lysosomal membrane destabilization and its extent. On the other hand, lysosome membrane permeabilization might be arising from several factors such as reactive oxygen species or proteases (see literature section 1.2.). Thus, further studies are required to be performed with initiator/s of lysosomal impairment via AG-08.

Based on the accumulation of LC3-II via AG-08 treatment, we had suggested autophagic flux inhibition in the preliminary study. Herein, the lysosomal impairment also ascertained our suggestion. Moreover, in time course experiments, p62 level firstly increased and then started to decrease with treatment of AG-08 at IC_{50} dose. This finding implied that LC3-II and p62 proteins were accumulated due to autophagic flux inhibition at early point of treatment, and then proteases degraded full-length of p62 initiating decrease in the protein level. It is sound to suggest that the lysosomal impairment is responsible for autophagic flux inhibition and accumulation of these proteins. Besides, the decrease in full-length of ATG proteins were verified within this thesis. So, following vacuole accumulation by autophagic flux, vacuole formation must cease with longer exposure to AG-08 due to absence of ATGs. Consequently, autophagy is efficiently inhibited with two different steps during AG-08 treatment.

Both lysosomal dysfunction and autophagic inhibition have been reported as new targets in cancer therapy. Since cancer cells require highly active lysosomal function for invasive growth, angiogenesis, and drug resistance, targeting lysosomes is an original approach for more effective cancer therapy. Additionally, lysosomal membranes of cancer cells are more susceptible to permeabilization than normal cells. Therefore, targeting lysosome has been suggested to increase selectivity towards cancer cells (Piao and Amaravadi 2016). Morgan et al. showed that metastatic property of cancer cells relied on lysosomal function independent of autophagy. Moreover, it was reported that metastatic cells were more vulnerable to lysosomal impairment agents (Morgan et al. 2018). Damaged lysosome also offers susceptibility in cancer cells through autophagic inhibition. Because of its survival role, autophagic activation causes drug resistance in most cases. Therefore, lysosomal impairment reduces the chance of resistance development relying on autophagy, and makes cancer cells to be sensitive (Piao and Amaravadi 2016). Although our cytotoxicity results do not refer to any selectivity between cancer and normal cells, targeting lysosome as well as autophagy with AG-08 would bring susceptibility to cancer cells. Therefore, further studies are warranted utilizing co-treatment of AG-08 with well-known chemotherapeutic agents as well as involving resistant cancer cell lines.

Fifteen AG-08 analogs from AG, CG and SCG were prepared during semi-synthesis studies. Among them, CG-03, AG-05 and CG-05 were cytotoxic (Figure 39). Additional studies suggested that these compounds induce necrotic cell death in a similar manner. On the basis of activity results of AG-08 and its analogs, the following could be

stated for structure activity relationships: i) Co-existence of cyclopropane and double bond at C-6 decrease cytotoxicity, whereas double bond presence at C-6 alone does not have significant effect; ii) If it is found with a bulky/aromatic substitution (tosyl group in case of AG-08 and active analogs), the presence of sulfonic ester is crucial for activity; iii) loss of toxicity with all SCG derivatives makes clear that tosyl substitution is not sufficient for activity alone, and intact sapogenin skeleton is required including 20,24-epoxy side chain. Nevertheless, similar semi-synthesis reactions must be carried out with different sapogenin skeletons to see that cycloartane/cyclolanostane frameworks are crucial for the activity or not.

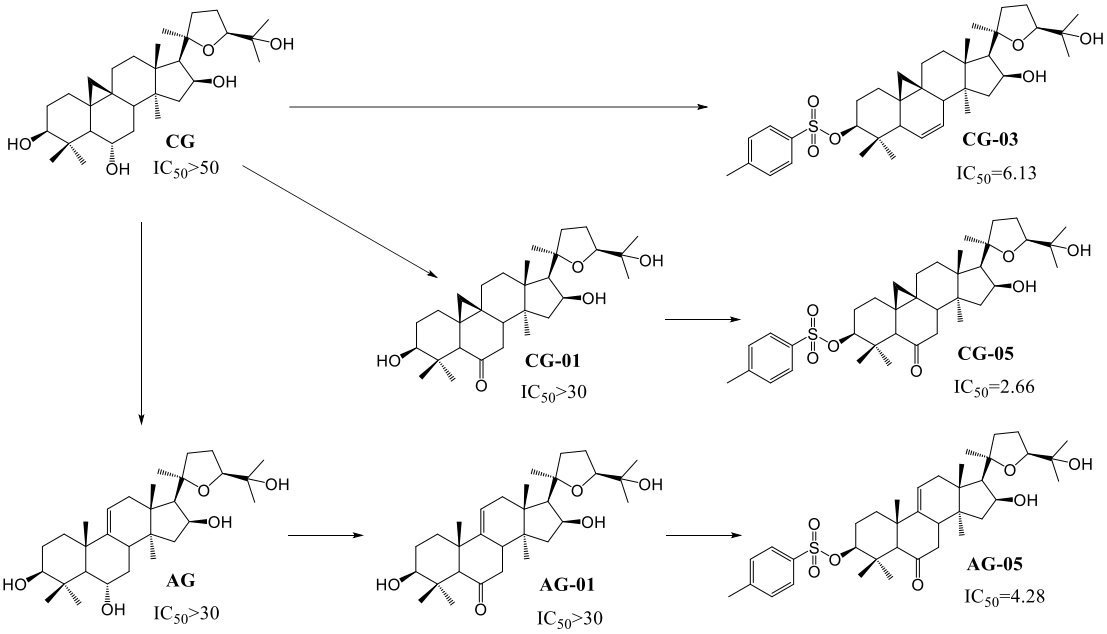

Figure 40. Structures of cytotoxic analogs and their parent compounds with their IC_{50} values (μM) versus HCC1937 cell line

Both previous and recent results demonstrate herein that AG-08 induce necrotic cell death. Furthermore, three new sapogenol derivatives leading to necrotic cell death are also prepared and reported in this thesis. Only a small number of saponins inducing necrosis have been reported in terms of molecular mechanism. B10 is one of them, shown to induce lysosomal membrane destabilization, cathepsin releasing, and also autophagic flux inhibition. Inhibition of cathepsins significantly reduced cell death (Gonzalez et al. 2012). Also, Gonzales and his co-workers revealed caspase 3 activation and alleviation of cell death upon downregulation of caspase 3, which was comparable with AG-08

results. However, the cleavage of ATGs was not observed with B10 treatment. Even, downregulation of ATGs significantly decreased caspase-3 activation, lysosomal permeabilization and cell death (Gonzalez et al. 2012). Another necrotic cell death inducer saponin is Dehydroeburicoic acid (DeEA). DeEA induced cell death depending on calpain activation and Ca^{+2} elevation. Nevertheless, inhibition of caspases did not have any effect on DeEA mediated cell death (Deng et al. 2009). Asiatic acid induced necrotic cell death in U-87 MG (human glioblastoma cells) but apoptosis in RKO (colon cancer cells). Calpain activation and Ca^{+2} elevation played important role in necrotic cell death via Asiatic acid treatment. Additionally, caspase 9 and caspase 3 were found to be activated in the same study. In contrast to AG-08, inhibition of caspases did not interfere cell death (Cho et al. 2006).

Necrosis has been believed as uncontrollable and unwanted cell death form for long time. Especially immune response to necrotic cell death is acknowledged as a negative feature as it has been reported to result in release of cellular content which recruit immune cells and exert tumor-promoting activity by inducing angiogenesis, proliferation, and invasion (Lee et al. 2018). However, the reports of regulated necrosis have provided a novel target for curing cancer. Even, the immune reaction originating from necrosis is proposed to enhance treatment possibilities through activation of defense mechanisms to cancer. To be clearer, necrotic cell death induces stimulation of naive cytotoxic CD8+ T cells that are required for tumor immunity. Sauter et al. has shown that necrosis but not apoptosis induces maturation of dendritic cells, which stimulate naive cytotoxic CD8+ T cells and consequently promote tumor immunity (Sauter et al. 2000). On the other hand, in a report, necroptosis is stated to induce immune response that stimulates both tumor promoting and anti-tumor mechanisms (Najafov, Chen, and Yuan 2017). Thus, further studies are required to find the link in regard to immune reaction upon necrosis in cancer treatment. Although immune response to necrotic cells is still under debate, demonstration of necrotic cell death by FDA-approved drugs proves that necrosis is targetable cell death type for treatment(Okada et al. 2004, Wu et al. 2015, Lachaier et al. 2014).

As mentioned above, necrosis has become area of interest as an alternative cell death mechanism to cope with drug resistance. Because resistance to apoptotic cell death is one of the main problems faced with current chemotherapeutic agents. For instance, leukemia shows resistance to most of the apoptotic anti-cancer drugs, and necroptosis is put forward as a novel therapeutic strategy for overcoming apoptosis resistance in

leukemia (Huang et al. 2018). Additionally, use of necrotic cell death initiators in combination with current chemotherapy agents is a logical alternative for drug development studies because simultaneous activation of different pathways with multiple drugs/drug candidates may cope with failure of the treatment due to intra-heterogeneity. (Dagogo-Jack and Shaw 2018, Mokhtari et al. 2017).

Finally, there is a huge need for new course of actions to prevent and/or cure cancer. Regulated necrosis has emerged as one of the promising alternatives. Our findings clearly show that it is possible to prepare cytotoxic compounds from inactive sapogenols via semi-synthesis even with new mode of actions such as induction of necrotic cell death and autophagy inhibition. Yet, molecular data provided in this thesis is just the tip of the iceberg and infer to the complex relationship between cell death modules, and further studies are warranted to understand the complete mechanism of AG-08 and its analogs.

REFERENCES

Aits, S., and M. Jaattela. 2013. "Lysosomal cell death at a glance." *J Cell Sci* 126 (Pt 9):1905-12. doi: 10.1242/jcs.091181.

Amaravadi, R. K., and C. B. Thompson. 2007. "The roles of therapy-induced autophagy and necrosis in cancer treatment." *Clin Cancer Res* 13 (24):7271-9. doi: 10.1158/1078-0432.CCR-07-1595.

Ashkenazi, A., and G. Salvesen. 2014. "Regulated cell death: signaling and mechanisms." *Annu Rev Cell Dev Biol* 30:337-56. doi: 10.1146/annurev-cellbio-100913-013226.

Azad, Meghan B, Yongqiang Chen, Elizabeth S Henson, Jeannick Cizeau, Eileen McMillan-Ward, Sara J Israels, and Spencer B Gibson. 2008. "Hypoxia induces autophagic cell death in apoptosis-competent cells through a mechanism involving BNIP3." *Autophagy* 4 (2):195-204.

Bialik, S., S. K. Dasari, and A. Kimchi. 2018. "Autophagy-dependent cell death - where, how and why a cell eats itself to death." *J Cell Sci* 131 (18). doi: 10.1242/jcs.215152.

Brojatsch, Jürgen, Heriberto Lima, Alak K Kar, Lee S Jacobson, Stefan M Muehlbauer, Kartik Chandran, and Felipe Diaz-Griffero. 2014. "A proteolytic cascade controls lysosome rupture and necrotic cell death mediated by lysosome-destabilizing adjuvants." *PloS one* 9 (6):e95032.

Cai, Xianyi, Yunlu Liu, Yiqiang Hu, Xianzhe Liu, Hongyan Jiang, Shuhua Yang, Zengwu Shao, Yun Xia, and Liming Xiong. 2018. "ROS-mediated lysosomal membrane permeabilization is involved in bupivacaine-induced death of rabbit intervertebral disc cells." *Redox biology* 18:65-76.

Cai, Zhenyu, Anling Zhang, Swati Choksi, Weihua Li, Tao Li, Xue-Min Zhang, and Zheng-Gang Liu. 2016a. "Activation of cell-surface proteases promotes necroptosis, inflammation and cell migration." *Cell Research* 26:886. doi: 10.1038/cr.2016.87

https://www.nature.com/articles/cr201687#supplementary-information.

Cai, Zhenyu, Anling Zhang, Swati Choksi, Weihua Li, Tao Li, Xue-Min Zhang, and Zheng-Gang Liu. 2016b. "Activation of cell-surface proteases promotes necroptosis, inflammation and cell migration." *Cell research* 26 (8):886.

Campbell, Kirsteen J, and Stephen WG Tait. 2018. "Targeting BCL-2 regulated apoptosis in cancer." *Open biology* 8 (5):180002.

Chaitanya, G. V., A. J. Steven, and P. P. Babu. 2010. "PARP-1 cleavage fragments: signatures of cell-death proteases in neurodegeneration." *Cell Commun Signal* 8:31. doi: 10.1186/1478-811X-8-31.

Chan, Francis Ka-Ming, Kenta Moriwaki, and María José De Rosa. 2013. "Detection of necrosis by release of lactate dehydrogenase activity." In *Immune Homeostasis*, 65-70. Springer.

Chen, Q., J. Kang, and C. Fu. 2018. "The independence of and associations among apoptosis, autophagy, and necrosis." *Signal Transduct Target Ther* 3:18. doi: 10.1038/s41392-018-0018-5.

Chen, Si, Cui Zhou, Huiyan Yu, Lingwei Tao, Yu An, Xiaona Zhang, Ying Wang, Yushan Wang, and Rong Xiao. 2019. "27-hydroxycholesterol contributes to lysosomal membrane permeabilization-mediated pyroptosis in co-cultured SH-SY5Y cells and C6 cells." *Frontiers in Molecular Neuroscience* 12.

Chen, Xin, Wan-ting He, Lichen Hu, Jingxian Li, Yuan Fang, Xin Wang, Xiaozheng Xu, Zhuo Wang, Kai Huang, and Jiahuai Han. 2016. "Pyroptosis is driven by non-selective gasdermin-D pore and its morphology is different from MLKL channel-mediated necroptosis." *Cell research* 26 (9):1007.

Chen, Xin, Wenjuan Li, Junming Ren, Deli Huang, Wan-ting He, Yunlong Song, Chao Yang, Wanyun Li, Xinru Zheng, and Pengda Chen. 2014. "Translocation of mixed lineage kinase domain-like protein to plasma membrane leads to necrotic cell death." *Cell research* 24 (1):105.

Cho, CW, DS Choi, MH Cardone, Chan Wha Kim, AJ Sinskey, and C Rha. 2006. "Glioblastoma cell death induced by asiatic acid." *Cell biology and toxicology* 22 (6):393-408.

Cho, Dong-Hyung, Yoon Kyung Jo, Jung Jin Hwang, Yoo Mee Lee, Seon Ae Roh, and Jin Cheon Kim. 2009. "Caspase-mediated cleavage of ATG6/Beclin-1 links apoptosis to autophagy in HeLa cells." *Cancer letters* 274 (1):95-100.

Cho, Yoon Jin, Jeong-Hwa Woo, Jae-Seung Lee, Dae Sik Jang, Kyung-Tae Lee, and Jung-Hye Choi. 2016. "Eclalbasaponin II induces autophagic and apoptotic cell death in human ovarian cancer cells." *Journal of pharmacological sciences* 132 (1):6-14.

Choi, Sunga, Tae Woong Kim, and Shivendra V Singh. 2009. "Ginsenoside Rh2-mediated G 1 phase cell cycle arrest in human breast cancer cells is caused by p15 Ink4B and p27 Kip1-dependent inhibition of cyclin-dependent kinases." *Pharmaceutical research* 26 (10):2280-2288.

Chua, Boon Tin, Ke Guo, and Peng Li. 2000. "Direct Cleavage by the Calcium-activated Protease Calpain Can Lead to Inactivation of Caspases." *THE JOURNAL OF BIOLOGICAL CHEMISTRY* 275 (7):5131–5135.

Conrad, M., J. P. Angeli, P. Vandenabeele, and B. R. Stockwell. 2016. "Regulated necrosis: disease relevance and therapeutic opportunities." *Nat Rev Drug Discov* 15 (5):348-66. doi: 10.1038/nrd.2015.6.

Conus, S., C. Pop, S. J. Snipas, G. S. Salvesen, and H. U. Simon. 2012. "Cathepsin D primes caspase-8 activation by multiple intra-chain proteolysis." *J Biol Chem* 287 (25):21142-51. doi: 10.1074/jbc.M111.306399.

Dagogo-Jack, Ibiayi, and Alice T Shaw. 2018. "Tumour heterogeneity and resistance to cancer therapies." *Nature reviews Clinical oncology* 15 (2):81.

David, Karen Kate, Shaida Ahmad Andrabi, Ted Murray Dawson, and Valina Lynn Dawson. 2009. "Parthanatos, a messenger of death." *Frontiers in bioscience (Landmark edition)* 14:1116.

de Castro, M. A., G. Bunt, and F. S. Wouters. 2016. "Cathepsin B launches an apoptotic exit effort upon cell death-associated disruption of lysosomes." *Cell Death Discov* 2:16012. doi: 10.1038/cddiscovery.2016.12.

Deng, Jhu-Yun, Sian-Jin Chen, Guey-Mei Jow, Chao-Wen Hsueh, and Chung-Jiuan Jeng. 2009. "Dehydroeburicoic acid induces calcium-and calpain-dependent necrosis in human U87MG glioblastomas." *Chemical research in toxicology* 22 (11):1817-1826.

Divya, Thomas, Sekar Vasudevan, and Ganapasam Sudhandiran. 2017. "Role of Proteases in Regulating Cell Death Pathways." In *Pathophysiological Aspects of Proteases*, 535-551. Springer.

Djavaheri-Mergny, M, MC Maiuri, and G Kroemer. 2010. "Cross talk between apoptosis and autophagy by caspase-mediated cleavage of Beclin 1." *Oncogene* 29 (12):1717.

Droga-Mazovec, Gabriela, Lea Bojič, Ana Petelin, Saška Ivanova, Urska Repnik, Guy S Salvesen, Veronika Stoka, Vito Turk, and Boris Turk. 2008. "Cysteine cathepsins trigger caspase-dependent cell death through cleavage of bid and antiapoptotic Bcl-2 homologues." *Journal of Biological Chemistry* 283 (27):19140-19150.

Dunlop, Rachael A, Ulf T Brunk, and Kenneth J Rodgers. 2011. "Proteins containing oxidized amino acids induce apoptosis in human monocytes." *Biochemical Journal* 435 (1):207-216.

Elmore, S. 2007. "Apoptosis: a review of programmed cell death." *Toxicol Pathol* 35 (4):495-516. doi: 10.1080/01926230701320337.

Erez, Elinor, Deborah Fass, and Eitan Bibi. 2009. "How intramembrane proteases bury hydrolytic reactions in the membrane." *Nature* 459 (7245):371.

Escobar-Sánchez, María L., Luis Sánchez-Sánchez, and Jesús Sandoval-Ramírez. 2015. "Steroidal Saponins and Cell Death in Cancer." In *Cell Death - Autophagy, Apoptosis and Necrosis*.

Fehrenbacher, Nicole, Lone Bastholm, Thomas Kirkegaard-Sørensen, Bo Rafn, Trine Bøttzauw, Christina Nielsen, Ekkehard Weber, Senji Shirasawa, Tuula Kallunki, and Marja Jäättelä. 2008. "Sensitization to the lysosomal cell death pathway by oncogene-induced down-regulation of lysosome-associated membrane proteins 1 and 2." *Cancer research* 68 (16):6623-6633.

Feltham, Rebecca, James E Vince, and Kate E Lawlor. 2017. "Caspase-8: not so silently deadly." *Clinical & translational immunology* 6 (1):e124.

Fulda, S. 2013. "Regulation of cell death in cancer-possible implications for immunotherapy." *Front Oncol* 3:29. doi: 10.3389/fonc.2013.00029.

Fulda, Simone, and Guido Kroemer. 2009. "Targeting mitochondrial apoptosis by betulinic acid in human cancers." *Drug discovery today* 14 (17-18):885-890.

Gafni, J., X. Cong, S. F. Chen, B. W. Gibson, and L. M. Ellerby. 2009. "Calpain-1 cleaves and activates caspase-7." *J Biol Chem* 284 (37):25441-9. doi: 10.1074/jbc.M109.038174.

Galluzzi, L., O. Kepp, S. Krautwald, G. Kroemer, and A. Linkermann. 2014. "Molecular mechanisms of regulated necrosis." *Semin Cell Dev Biol* 35:24-32. doi: 10.1016/j.semcdb.2014.02.006.

Galluzzi, L., I. Vitale, S. A. Aaronson, J. M. Abrams, D. Adam, P. Agostinis, E. S. Alnemri, L. Altucci, I. Amelio, D. W. Andrews, M. Annicchiarico-Petruzzelli, A. V. Antonov, E. Arama, E. H. Baehrecke, N. A. Barlev, N. G. Bazan, F. Bernassola, M. J. M. Bertrand, K. Bianchi, M. V. Blagosklonny, K. Blomgren, C. Borner, P. Boya, C. Brenner, M. Campanella, E. Candi, D. Carmona-Gutierrez, F. Cecconi, F. K. Chan, N. S. Chandel, E. H. Cheng, J. E. Chipuk, J. A. Cidlowski, A. Ciechanover, G. M. Cohen, M. Conrad, J. R. Cubillos-Ruiz, P. E. Czabotar, V. D'Angiolella, T. M. Dawson, V. L. Dawson, V. De Laurenzi, R. De Maria, K. M. Debatin, R. J. DeBerardinis, M. Deshmukh, N. Di Daniele, F. Di Virgilio, V. M. Dixit, S. J. Dixon, C. S. Duckett, B. D. Dynlacht, W. S. El-Deiry, J. W. Elrod, G. M. Fimia, S. Fulda, A. J. Garcia-Saez, A. D. Garg, C. Garrido, E. Gavathiotis, P. Golstein, E. Gottlieb, D. R. Green, L. A. Greene, H. Gronemeyer, A. Gross, G. Hajnoczky, J. M. Hardwick, I. S. Harris, M. O. Hengartner, C. Hetz, H. Ichijo, M. Jaattela, B. Joseph, P. J. Jost, P. P. Juin, W. J.

Kaiser, M. Karin, T. Kaufmann, O. Kepp, A. Kimchi, R. N. Kitsis, D. J. Klionsky, R. A. Knight, S. Kumar, S. W. Lee, J. J. Lemasters, B. Levine, A. Linkermann, S. A. Lipton, R. A. Lockshin, C. Lopez-Otin, S. W. Lowe, T. Luedde, E. Lugli, M. MacFarlane, F. Madeo, M. Malewicz, W. Malorni, G. Manic, J. C. Marine, S. J. Martin, J. C. Martinou, J. P. Medema, P. Mehlen, P. Meier, S. Melino, E. A. Miao, J. D. Molkentin, U. M. Moll, C. Munoz-Pinedo, S. Nagata, G. Nunez, A. Oberst, M. Oren, M. Overholtzer, M. Pagano, T. Panaretakis, M. Pasparakis, J. M. Penninger, D. M. Pereira, S. Pervaiz, M. E. Peter, M. Piacentini, P. Pinton, J. H. M. Prehn, H. Puthalakath, G. A. Rabinovich, M. Rehm, R. Rizzuto, C. M. P. Rodrigues, D. C. Rubinsztein, T. Rudel, K. M. Ryan, E. Sayan, L. Scorrano, F. Shao, Y. Shi, J. Silke, H. U. Simon, A. Sistigu, B. R. Stockwell, A. Strasser, G. Szabadkai, S. W. G. Tait, D. Tang, N. Tavernarakis, A. Thorburn, Y. Tsujimoto, B. Turk, T. Vanden Berghe, P. Vandenabeele, M. G. Vander Heiden, A. Villunger, H. W. Virgin, K. H. Vousden, D. Vucic, E. F. Wagner, H. Walczak, D. Wallach, Y. Wang, J. A. Wells, W. Wood, J. Yuan, Z. Zakeri, B. Zhivotovsky, L. Zitvogel, G. Melino, and G. Kroemer. 2018. "Molecular mechanisms of cell death: recommendations of the Nomenclature Committee on Cell Death 2018." *Cell Death Differ* 25 (3):486-541. doi: 10.1038/s41418-017-0012-4.

Gao, M., P. Monian, Q. Pan, W. Zhang, J. Xiang, and X. Jiang. 2016. "Ferroptosis is an autophagic cell death process." *Cell Res* 26 (9):1021-32. doi: 10.1038/cr.2016.95.

Giraldo, Ana M Villamil, Hanna Appelqvist, Thomas Ederth, and Karin Öllinger. 2014. Lysosomotropic agents: impact on lysosomal membrane permeabilization and cell death. Portland Press Limited.

Gobeil, S, CC Boucher, D Nadeau, and GG Poirier. 2001. "Characterization of the necrotic cleavage of poly(ADP-ribose) polymerase (PARP-1): implication of lysosomal proteases." *Cell Death and Differentiation* 8:588-594.

Gonzalez, P., I. Mader, A. Tchoghandjian, S. Enzenmuller, S. Cristofanon, F. Basit, K. M. Debatin, and S. Fulda. 2012. "Impairment of lysosomal integrity by B10, a glycosylated derivative of betulinic acid, leads to lysosomal cell death and converts autophagy into a detrimental process." *Cell Death Differ* 19 (8):1337-46. doi: 10.1038/cdd.2012.10.

Goodall, Megan L, Brent E Fitzwalter, Shadi Zahedi, Min Wu, Diego Rodriguez, Jean M Mulcahy-Levy, Douglas R Green, Michael Morgan, Scott D Cramer, and Andrew Thorburn. 2016. "The autophagy machinery controls cell death switching between apoptosis and necroptosis." *Developmental cell* 37 (4):337-349.

Guicciardi, M Eugenia, Jan Deussing, Hideyuki Miyoshi, Steven F Bronk, Phyllis A Svingen, Christoph Peters, Scott H Kaufmann, and Gregory J Gores. 2000. "Cathepsin B contributes to TNF-α–mediated hepatocyte apoptosis by

promoting mitochondrial release of cytochrome c." *The Journal of clinical investigation* 106 (9):1127-1137.

Gump, Jacob M, and Andrew Thorburn. 2011. "Autophagy and apoptosis: what is the connection?" *Trends in cell biology* 21 (7):387-392.

Gyrd-Hansen, Mads, Thomas Farkas, Nicole Fehrenbacher, Lone Bastholm, Maria Høyer-Hansen, Folmer Elling, David Wallach, Richard Flavell, Guido Kroemer, and Jesper Nylandsted. 2006. "Apoptosome-independent activation of the lysosomal cell death pathway by caspase-9." *Molecular and cellular biology* 26 (21):7880-7891.

Hanahan, Douglas, and Robert A Weinberg. 2011. "Hallmarks of cancer: the next generation." *cell* 144 (5):646-674.

Honeychurch, Jamie, Waleed Alduaij, Mahsa Azizyan, Eleanor J Cheadle, Helene Pelicano, Andrei Ivanov, Peng Huang, Mark S Cragg, and Tim M Illidge. 2012. "Antibody-induced nonapoptotic cell death in human lymphoma and leukemia cells is mediated through a novel reactive oxygen species-dependent pathway." *Blood* 119 (15):3523-3533.

Hou, W., J. Han, C. Lu, L. A. Goldstein, and H. Rabinowich. 2010. "Autophagic degradation of active caspase-8: a crosstalk mechanism between autophagy and apoptosis." *Autophagy* 6 (7):891-900. doi: 10.4161/auto.6.7.13038.

Hsu, Keng-Fu, Chao-Liang Wu, Soon-Cen Huang, Ching-Ming Wu, Jenn-Ren Hsiao, Yi-Te Yo, Yu-Hung Chen, Ai-Li Shiau, and Cheng-Yang Chou. 2009. "Cathepsin L mediates resveratrol-induced autophagy and apoptotic cell death in cervical cancer cells." *Autophagy* 5 (4):451-460.

Huang, Xianbo, Feng Xiao, Yuan Li, Wenbin Qian, Wei Ding, and Xiujin Ye. 2018. "Bypassing drug resistance by triggering necroptosis: recent advances in mechanisms and its therapeutic exploitation in leukemia." *Journal of Experimental & Clinical Cancer Research* 37 (1):310.

Ivanov, Andrei, Stephen A Beers, Claire A Walshe, Jamie Honeychurch, Waleed Alduaij, Kerry L Cox, Kathleen N Potter, Stephen Murray, Claude HT Chan, and Tetyana Klymenko. 2009. "Monoclonal antibodies directed to CD20 and HLA-DR can elicit homotypic adhesion followed by lysosome-mediated cell death in human lymphoma and leukemia cells." *The Journal of clinical investigation* 119 (8):2143-2159.

Izzo, Valentina, José Manuel Bravo-San Pedro, Valentina Sica, Guido Kroemer, and Lorenzo Galluzzi. 2016. "Mitochondrial permeability transition: new findings and persisting uncertainties." *Trends in cell biology* 26 (9):655-667.

Jacobson, L. S., H. Lima, Jr., M. F. Goldberg, V. Gocheva, V. Tsiperson, F. S. Sutterwala, J. A. Joyce, B. V. Gapp, V. A. Blomen, K. Chandran, T. R. Brummelkamp, F. Diaz-Griffero, and J. Brojatsch. 2013. "Cathepsin-mediated necrosis controls the adaptive immune response by Th2 (T helper type 2)-associated adjuvants." *J Biol Chem* 288 (11):7481-91. doi: 10.1074/jbc.M112.400655.

Jacobson, Lee S, Heriberto Lima, Michael F Goldberg, Vasilena Gocheva, Vladislav Tsiperson, Fayyaz S Sutterwala, Johanna A Joyce, Bianca V Gapp, Vincent A Blomen, and Kartik Chandran. 2013. "Cathepsin-mediated necrosis controls the adaptive immune response by Th2 (T helper type 2)-associated adjuvants." *Journal of Biological Chemistry* 288 (11):7481-7491.

Jacquin, E., S. Leclerc-Mercier, C. Judon, E. Blanchard, S. Fraitag, and O. Florey. 2017. "Pharmacological modulators of autophagy activate a parallel noncanonical pathway driving unconventional LC3 lipidation." *Autophagy* 13 (5):854-867. doi: 10.1080/15548627.2017.1287653.

Jiang, Hong-Yan, Yang Yang, Yuan-Yuan Zhang, Zhen Xie, Xue-Yan Zhao, Yu Sun, and Wei-Jia Kong. 2018. "The dual role of poly (ADP-ribose) polymerase-1 in modulating parthanatos and autophagy under oxidative stress in rat cochlear marginal cells of the stria vascularis." *Redox biology* 14:361-370.

Jin, Zhaoyu, and Wafik S. El-Deiry. 2014. "Overview of cell death signaling pathways." *Cancer Biology & Therapy* 4 (2):147-171. doi: 10.4161/cbt.4.2.1508.

Johansson, A. C., H. Appelqvist, C. Nilsson, K. Kagedal, K. Roberg, and K. Ollinger. 2010. "Regulation of apoptosis-associated lysosomal membrane permeabilization." *Apoptosis* 15 (5):527-40. doi: 10.1007/s10495-009-0452-5.

Jorgensen, Ine, and Edward A Miao. 2015. "Pyroptotic cell death defends against intracellular pathogens." *Immunological reviews* 265 (1):130-142.

Kågedal, Katarina, Ann-Charlotte Johansson, Uno Johansson, Gerd Heimlich, Karin Roberg, Nancy S Wang, Juliane M Jürgensmeier, and Karin Öllinger. 2005. "Lysosomal membrane permeabilization during apoptosis-involvement of Bax?" *International journal of experimental pathology* 86 (5):309-321.

Kaminskyy, V., and B. Zhivotovsky. 2012. "Proteases in autophagy." *Biochim Biophys Acta* 1824 (1):44-50. doi: 10.1016/j.bbapap.2011.05.013.

Katunuma, N., A. Matsui, Q.T. Le, K. Utsumi, G. Salvesen, and A. Ohash. 2001. "NOVEL PROCASPASE-3 ACTIVATING CASCADE MEDIATED BY LYSOAPOPTASES AND ITS BIOLOGICAL SIGNIFICANCES IN APOPTOSIS." *Advan. Enzyme Regul.* 42:237–250.

Kavcic, N., K. Pegan, and B. Turk. 2017. "Lysosomes in programmed cell death pathways: from initiators to amplifiers." *Biol Chem* 398 (3):289-301. doi: 10.1515/hsz-2016-0252.

Kessler, Jan H, Franziska B Mullauer, Guido M de Roo, and Jan Paul Medema. 2007. "Broad in vitro efficacy of plant-derived betulinic acid against cell lines derived from the most prevalent human cancer types." *Cancer letters* 251 (1):132-145.

Kim, BM. 2017. "The Implications of Several Forms of Programmed Necrosis for Cancer Therapy." *J Cancer Sci Ther* 9:630-635.

Klionsky, D. J., K. Abdelmohsen, A. Abe, M. J. Abedin, H. Abeliovich, A. Acevedo Arozena, H. Adachi, C. M. Adams, P. D. Adams, K. Adeli, P. J. Adhihetty, S. G. Adler, G. Agam, R. Agarwal, M. K. Aghi, M. Agnello, P. Agostinis, P. V. Aguilar, J. Aguirre-Ghiso, E. M. Airoldi, S. Ait-Si-Ali, T. Akematsu, E. T. Akporiaye, M. Al-Rubeai, G. M. Albaiceta, C. Albanese, D. Albani, M. L. Albert, J. Aldudo, H. Algul, M. Alirezaei, I. Alloza, A. Almasan, M. Almonte-Beceril, E. S. Alnemri, C. Alonso, N. Altan-Bonnet, D. C. Altieri, S. Alvarez, L. Alvarez-Erviti, S. Alves, G. Amadoro, A. Amano, C. Amantini, S. Ambrosio, I. Amelio, A. O. Amer, M. Amessou, A. Amon, Z. An, F. A. Anania, S. U. Andersen, U. P. Andley, C. K. Andreadi, N. Andrieu-Abadie, A. Anel, D. K. Ann, S. Anoopkumar-Dukie, M. Antonioli, H. Aoki, N. Apostolova, S. Aquila, K. Aquilano, K. Araki, E. Arama, A. Aranda, J. Araya, A. Arcaro, E. Arias, H. Arimoto, A. R. Ariosa, J. L. Armstrong, T. Arnould, I. Arsov, K. Asanuma, V. Askanas, E. Asselin, R. Atarashi, S. S. Atherton, J. D. Atkin, L. D. Attardi, P. Auberger, G. Auburger, L. Aurelian, R. Autelli, L. Avagliano, M. L. Avantaggiati, L. Avrahami, S. Awale, N. Azad, T. Bachetti, J. M. Backer, D. H. Bae, J. S. Bae, O. N. Bae, S. H. Bae, E. H. Baehrecke, S. H. Baek, S. Baghdiguian, A. Bagniewska-Zadworna, H. Bai, J. Bai, X. Y. Bai, Y. Bailly, K. N. Balaji, W. Balduini, A. Ballabio, R. Balzan, R. Banerjee, G. Banhegyi, H. Bao, B. Barbeau, M. D. Barrachina, E. Barreiro, B. Bartel, A. Bartolome, D. C. Bassham, M. T. Bassi, R. C. Bast, Jr., A. Basu, M. T. Batista, H. Batoko, M. Battino, K. Bauckman, B. L. Baumgarner, K. U. Bayer, R. Beale, J. F. Beaulieu, G. R. Beck, Jr., C. Becker, J. D. Beckham, P. A. Bedard, P. J. Bednarski, T. J. Begley, C. Behl, C. Behrends, G. M. Behrens, K. E. Behrns, E. Bejarano, A. Belaid, F. Belleudi, G. Benard, G. Berchem, D. Bergamaschi, M. Bergami, B. Berkhout, L. Berliocchi, A. Bernard, M. Bernard, F. Bernassola, A. Bertolotti, A. S. Bess, S. Besteiro, S. Bettuzzi, S. Bhalla, S. Bhattacharyya, S. K. Bhutia, C. Biagosch, M. W. Bianchi, M. Biard-Piechaczyk, V. Billes, C. Bincoletto, B. Bingol, S. W. Bird, M. Bitoun, I. Bjedov, C. Blackstone, L. Blanc, G. A. Blanco, H. K. Blomhoff, E. Boada-Romero, S. Bockler, M. Boes, K. Boesze-Battaglia, L. H. Boise, A. Bolino, A. Boman, P. Bonaldo, M. Bordi, J. Bosch, L. M. Botana, J. Botti, G. Bou, M. Bouche, M. Bouchecareilh, M. J. Boucher, M. E. Boulton, S. G. Bouret, P. Boya, M. Boyer-Guittaut, P. V. Bozhkov, N. Brady, V. M. Braga, C. Brancolini, G. H. Braus, J. M. Bravo-San Pedro, L. A. Brennan, E. H. Bresnick, P. Brest, D. Bridges, M. A. Bringer, M. Brini, G. C. Brito, B. Brodin, P. S. Brookes, E. J. Brown, K. Brown, H. E. Broxmeyer, A. Bruhat, P. C. Brum, J. H. Brumell, N. Brunetti-Pierri, R. J. Bryson-Richardson, S. Buch, A. M. Buchan, H. Budak, D. V. Bulavin, S. J. Bultman, G. Bultynck, V.

Bumbasirevic, Y. Burelle, R. E. Burke, M. Burmeister, P. Butikofer, L. Caberlotto, K. Cadwell, M. Cahova, D. Cai, J. Cai, Q. Cai, S. Calatayud, N. Camougrand, M. Campanella, G. R. Campbell, M. Campbell, S. Campello, R. Candau, I. Caniggia, L. Cantoni, L. Cao, A. B. Caplan, M. Caraglia, C. Cardinali, S. M. Cardoso, J. S. Carew, L. A. Carleton, C. R. Carlin, S. Carloni, S. R. Carlsson, D. Carmona-Gutierrez, L. A. Carneiro, O. Carnevali, S. Carra, A. Carrier, B. Carroll, C. Casas, J. Casas, G. Cassinelli, P. Castets, S. Castro-Obregon, G. Cavallini, I. Ceccherini, F. Cecconi, A. I. Cederbaum, V. Cena, S. Cenci, C. Cerella, D. Cervia, S. Cetrullo, H. Chaachouay, H. J. Chae, A. S. Chagin, C. Y. Chai, G. Chakrabarti, G. Chamilos, E. Y. Chan, M. T. Chan, D. Chandra, P. Chandra, C. P. Chang, R. C. Chang, T. Y. Chang, J. C. Chatham, S. Chatterjee, S. Chauhan, Y. Che, M. E. Cheetham, R. Cheluvappa, C. J. Chen, G. Chen, G. C. Chen, G. Chen, H. Chen, J. W. Chen, J. K. Chen, M. Chen, M. Chen, P. Chen, Q. Chen, Q. Chen, S. D. Chen, S. Chen, S. S. Chen, W. Chen, W. J. Chen, W. Q. Chen, W. Chen, X. Chen, Y. H. Chen, Y. G. Chen, Y. Chen, Y. Chen, Y. Chen, Y. J. Chen, Y. Q. Chen, Y. Chen, Z. Chen, Z. Chen, A. Cheng, C. H. Cheng, H. Cheng, H. Cheong, S. Cherry, J. Chesney, C. H. Cheung, E. Chevet, H. C. Chi, S. G. Chi, F. Chiacchiera, H. L. Chiang, R. Chiarelli, M. Chiariello, M. Chieppa, L. S. Chin, M. Chiong, G. N. Chiu, D. H. Cho, S. G. Cho, W. C. Cho, Y. Y. Cho, Y. S. Cho, A. M. Choi, E. J. Choi, E. K. Choi, J. Choi, M. E. Choi, S. I. Choi, T. F. Chou, S. Chouaib, D. Choubey, V. Choubey, K. C. Chow, K. Chowdhury, C. T. Chu, T. H. Chuang, T. Chun, H. Chung, T. Chung, Y. L. Chung, Y. J. Chwae, V. Cianfanelli, R. Ciarcia, I. A. Ciechomska, M. R. Ciriolo, M. Cirone, S. Claerhout, M. J. Clague, J. Claria, P. G. Clarke, R. Clarke, E. Clementi, C. Cleyrat, M. Cnop, E. M. Coccia, T. Cocco, P. Codogno, J. Coers, E. E. Cohen, D. Colecchia, L. Coletto, N. S. Coll, E. Colucci-Guyon, S. Comincini, M. Condello, K. L. Cook, G. H. Coombs, C. D. Cooper, J. M. Cooper, I. Coppens, M. T. Corasaniti, M. Corazzari, R. Corbalan, E. Corcelle-Termeau, M. D. Cordero, C. Corral-Ramos, O. Corti, A. Cossarizza, P. Costelli, S. Costes, S. L. Cotman, A. Coto-Montes, S. Cottet, E. Couve, L. R. Covey, L. A. Cowart, J. S. Cox, F. P. Coxon, C. B. Coyne, M. S. Cragg, R. J. Craven, T. Crepaldi, J. L. Crespo, A. Criollo, V. Crippa, M. T. Cruz, A. M. Cuervo, J. M. Cuezva, T. Cui, P. R. Cutillas, M. J. Czaja, M. F. Czyzyk-Krzeska, R. K. Dagda, U. Dahmen, C. Dai, W. Dai, Y. Dai, K. N. Dalby, L. Dalla Valle, G. Dalmasso, M. D'Amelio, M. Damme, A. Darfeuille-Michaud, C. Dargemont, V. M. Darley-Usmar, S. Dasarathy, B. Dasgupta, S. Dash, C. R. Dass, H. M. Davey, L. M. Davids, D. Davila, R. J. Davis, T. M. Dawson, V. L. Dawson, P. Daza, J. de Belleroche, P. de Figueiredo, R. C. de Figueiredo, J. de la Fuente, L. De Martino, A. De Matteis, G. R. De Meyer, A. De Milito, M. De Santi, W. de Souza, V. De Tata, D. De Zio, J. Debnath, R. Dechant, J. P. Decuypere, S. Deegan, B. Dehay, B. Del Bello, D. P. Del Re, R. Delage-Mourroux, L. M. Delbridge, L. Deldicque, E. Delorme-Axford, Y. Deng, J. Dengjel, M. Denizot, P. Dent, C. J. Der, V. Deretic, B. Derrien, E. Deutsch, T. P. Devarenne, R. J. Devenish, S. Di Bartolomeo, N. Di Daniele, F. Di Domenico, A. Di Nardo, S. Di Paola, A. Di Pietro, L. Di Renzo, A. DiAntonio, G. Diaz-Araya, I. Diaz-Laviada, M. T. Diaz-Meco, J. Diaz-Nido, C. A. Dickey, R. C. Dickson, M. Diederich, P. Digard, I. Dikic, S. P. Dinesh-Kumar, C. Ding, W. X. Ding, Z. Ding, L. Dini, J. H. Distler, A. Diwan, M. Djavaheri-Mergny, K. Dmytruk, R. C. Dobson, V. Doetsch, K. Dokladny, S. Dokudovskaya, M. Donadelli, X. C. Dong, X. Dong, Z. Dong, T. M. Donohue, Jr., K. S. Doran, G.

D'Orazi, G. W. Dorn, 2nd, V. Dosenko, S. Dridi, L. Drucker, J. Du, L. L. Du, L. Du, A. du Toit, P. Dua, L. Duan, P. Duann, V. K. Dubey, M. R. Duchen, M. A. Duchosal, H. Duez, I. Dugail, V. I. Dumit, M. C. Duncan, E. A. Dunlop, W. A. Dunn, Jr., N. Dupont, L. Dupuis, R. V. Duran, T. M. Durcan, S. Duvezin-Caubet, U. Duvvuri, V. Eapen, D. Ebrahimi-Fakhari, A. Echard, L. Eckhart, C. L. Edelstein, A. L. Edinger, L. Eichinger, T. Eisenberg, A. Eisenberg-Lerner, N. T. Eissa, W. S. El-Deiry, V. El-Khoury, Z. Elazar, H. Eldar-Finkelman, C. J. Elliott, E. Emanuele, U. Emmenegger, N. Engedal, A. M. Engelbrecht, S. Engelender, J. M. Enserink, R. Erdmann, J. Erenpreisa, R. Eri, J. L. Eriksen, A. Erman, R. Escalante, E. L. Eskelinen, L. Espert, L. Esteban-Martinez, T. J. Evans, M. Fabri, G. Fabrias, C. Fabrizi, A. Facchiano, N. J. Faergeman, A. Faggioni, W. D. Fairlie, C. Fan, D. Fan, J. Fan, S. Fang, M. Fanto, A. Fanzani, T. Farkas, M. Faure, F. B. Favier, H. Fearnhead, M. Federici, E. Fei, T. C. Felizardo, H. Feng, Y. Feng, Y. Feng, T. A. Ferguson, A. F. Fernandez, M. G. Fernandez-Barrena, J. C. Fernandez-Checa, A. Fernandez-Lopez, M. E. Fernandez-Zapico, O. Feron, E. Ferraro, C. V. Ferreira-Halder, L. Fesus, R. Feuer, F. C. Fiesel, E. C. Filippi-Chiela, G. Filomeni, G. M. Fimia, J. H. Fingert, S. Finkbeiner, T. Finkel, F. Fiorito, P. B. Fisher, M. Flajolet, F. Flamigni, O. Florey, S. Florio, R. A. Floto, M. Folini, C. Follo, E. A. Fon, F. Fornai, F. Fortunato, A. Fraldi, R. Franco, A. Francois, A. Francois, L. B. Frankel, I. D. Fraser, N. Frey, D. G. Freyssenet, C. Frezza, S. L. Friedman, D. E. Frigo, D. Fu, J. M. Fuentes, J. Fueyo, Y. Fujitani, Y. Fujiwara, M. Fujiya, M. Fukuda, S. Fulda, C. Fusco, B. Gabryel, M. Gaestel, P. Gailly, M. Gajewska, S. Galadari, G. Galili, I. Galindo, M. F. Galindo, G. Galliciotti, L. Galluzzi, L. Galluzzi, V. Galy, N. Gammoh, S. Gandy, A. K. Ganesan, S. Ganesan, I. G. Ganley, M. Gannage, F. B. Gao, F. Gao, J. X. Gao, L. Garcia Nannig, E. Garcia Vescovi, M. Garcia-Macia, C. Garcia-Ruiz, A. D. Garg, P. K. Garg, R. Gargini, N. C. Gassen, D. Gatica, E. Gatti, J. Gavard, E. Gavathiotis, L. Ge, P. Ge, S. Ge, P. W. Gean, V. Gelmetti, A. A. Genazzani, J. Geng, P. Genschik, L. Gerner, J. E. Gestwicki, D. A. Gewirtz, S. Ghavami, E. Ghigo, D. Ghosh, A. M. Giammarioli, F. Giampieri, C. Giampietri, A. Giatromanolaki, D. J. Gibbings, L. Gibellini, S. B. Gibson, V. Ginet, A. Giordano, F. Giorgini, E. Giovannetti, S. E. Girardin, S. Gispert, S. Giuliano, C. L. Gladson, A. Glavic, M. Gleave, N. Godefroy, R. M. Gogal, Jr., K. Gokulan, G. H. Goldman, D. Goletti, M. S. Goligorsky, A. V. Gomes, L. C. Gomes, H. Gomez, C. Gomez-Manzano, R. Gomez-Sanchez, D. A. Goncalves, E. Goncu, Q. Gong, C. Gongora, C. B. Gonzalez, P. Gonzalez-Alegre, P. Gonzalez-Cabo, R. A. Gonzalez-Polo, I. S. Goping, C. Gorbea, N. V. Gorbunov, D. R. Goring, A. M. Gorman, S. M. Gorski, S. Goruppi, S. Goto-Yamada, C. Gotor, R. A. Gottlieb, I. Gozes, D. Gozuacik, Y. Graba, M. Graef, G. E. Granato, G. D. Grant, S. Grant, G. L. Gravina, D. R. Green, A. Greenhough, M. T. Greenwood, B. Grimaldi, F. Gros, C. Grose, J. F. Groulx, F. Gruber, P. Grumati, T. Grune, J. L. Guan, K. L. Guan, B. Guerra, C. Guillen, K. Gulshan, J. Gunst, C. Guo, L. Guo, M. Guo, W. Guo, X. G. Guo, A. A. Gust, A. B. Gustafsson, E. Gutierrez, M. G. Gutierrez, H. S. Gwak, A. Haas, J. E. Haber, S. Hadano, M. Hagedorn, D. R. Hahn, A. J. Halayko, A. Hamacher-Brady, K. Hamada, A. Hamai, A. Hamann, M. Hamasaki, I. Hamer, Q. Hamid, E. M. Hammond, F. Han, W. Han, J. T. Handa, J. A. Hanover, M. Hansen, M. Harada, L. Harhaji-Trajkovic, J. W. Harper, A. H. Harrath, A. L. Harris, J. Harris, U. Hasler, P. Hasselblatt, K. Hasui, R. G. Hawley, T. S. Hawley, C. He, C. Y. He, F. He, G. He, R. R. He, X. H. He, Y. W. He, Y. Y. He, J. K. Heath, M. J. Hebert,

R. A. Heinzen, G. V. Helgason, M. Hensel, E. P. Henske, C. Her, P. K. Herman, A. Hernandez, C. Hernandez, S. Hernandez-Tiedra, C. Hetz, P. R. Hiesinger, K. Higaki, S. Hilfiker, B. G. Hill, J. A. Hill, W. D. Hill, K. Hino, D. Hofius, P. Hofman, G. U. Hoglinger, J. Hohfeld, M. K. Holz, Y. Hong, D. A. Hood, J. J. Hoozemans, T. Hoppe, C. Hsu, C. Y. Hsu, L. C. Hsu, D. Hu, G. Hu, H. M. Hu, H. Hu, M. C. Hu, Y. C. Hu, Z. W. Hu, F. Hua, Y. Hua, C. Huang, H. L. Huang, K. H. Huang, K. Y. Huang, S. Huang, S. Huang, W. P. Huang, Y. R. Huang, Y. Huang, Y. Huang, T. B. Huber, P. Huebbe, W. K. Huh, J. J. Hulmi, G. M. Hur, J. H. Hurley, Z. Husak, S. N. Hussain, S. Hussain, J. J. Hwang, S. Hwang, T. I. Hwang, A. Ichihara, Y. Imai, C. Imbriano, M. Inomata, T. Into, V. Iovane, J. L. Iovanna, R. V. Iozzo, N. Y. Ip, J. E. Irazoqui, P. Iribarren, Y. Isaka, A. J. Isakovic, H. Ischiropoulos, J. S. Isenberg, M. Ishaq, H. Ishida, I. Ishii, J. E. Ishmael, C. Isidoro, K. Isobe, E. Isono, S. Issazadeh-Navikas, K. Itahana, E. Itakura, A. I. Ivanov, A. K. Iyer, J. M. Izquierdo, Y. Izumi, V. Izzo, M. Jaattela, N. Jaber, D. J. Jackson, W. T. Jackson, T. G. Jacob, T. S. Jacques, C. Jagannath, A. Jain, N. R. Jana, B. K. Jang, A. Jani, B. Janji, P. R. Jannig, P. J. Jansson, S. Jean, M. Jendrach, J. H. Jeon, N. Jessen, E. B. Jeung, K. Jia, L. Jia, H. Jiang, H. Jiang, L. Jiang, T. Jiang, X. Jiang, X. Jiang, X. Jiang, Y. Jiang, Y. Jiang, A. Jimenez, C. Jin, H. Jin, L. Jin, M. Jin, S. Jin, U. K. Jinwal, E. K. Jo, T. Johansen, D. E. Johnson, G. V. Johnson, J. D. Johnson, E. Jonasch, C. Jones, L. A. Joosten, J. Jordan, A. M. Joseph, B. Joseph, A. M. Joubert, D. Ju, J. Ju, H. F. Juan, K. Juenemann, G. Juhasz, H. S. Jung, J. U. Jung, Y. K. Jung, H. Jungbluth, M. J. Justice, B. Jutten, N. O. Kaakoush, K. Kaarniranta, A. Kaasik, T. Kabuta, B. Kaeffer, K. Kagedal, A. Kahana, S. Kajimura, O. Kakhlon, M. Kalia, D. V. Kalvakolanu, Y. Kamada, K. Kambas, V. O. Kaminskyy, H. H. Kampinga, M. Kandouz, C. Kang, R. Kang, T. C. Kang, T. Kanki, T. D. Kanneganti, H. Kanno, A. G. Kanthasamy, M. Kantorow, M. Kaparakis-Liaskos, O. Kapuy, V. Karantza, M. R. Karim, P. Karmakar, A. Kaser, S. Kaushik, T. Kawula, A. M. Kaynar, P. Y. Ke, Z. J. Ke, J. H. Kehrl, K. E. Keller, J. K. Kemper, A. K. Kenworthy, O. Kepp, A. Kern, S. Kesari, D. Kessel, R. Ketteler, C. Kettelhut Ido, B. Khambu, M. M. Khan, V. K. Khandelwal, S. Khare, J. G. Kiang, A. A. Kiger, A. Kihara, A. L. Kim, C. H. Kim, D. R. Kim, D. H. Kim, E. K. Kim, H. Y. Kim, H. R. Kim, J. S. Kim, J. H. Kim, J. C. Kim, J. H. Kim, K. W. Kim, M. D. Kim, M. M. Kim, P. K. Kim, S. W. Kim, S. Y. Kim, Y. S. Kim, Y. Kim, A. Kimchi, A. C. Kimmelman, T. Kimura, J. S. King, K. Kirkegaard, V. Kirkin, L. A. Kirshenbaum, S. Kishi, Y. Kitajima, K. Kitamoto, Y. Kitaoka, K. Kitazato, R. A. Kley, W. T. Klimecki, M. Klinkenberg, J. Klucken, H. Knaevelsrud, E. Knecht, L. Knuppertz, J. L. Ko, S. Kobayashi, J. C. Koch, C. Koechlin-Ramonatxo, U. Koenig, Y. H. Koh, K. Kohler, S. D. Kohlwein, M. Koike, M. Komatsu, E. Kominami, D. Kong, H. J. Kong, E. G. Konstantakou, B. T. Kopp, T. Korcsmaros, L. Korhonen, V. I. Korolchuk, N. V. Koshkina, Y. Kou, M. I. Koukourakis, C. Koumenis, A. L. Kovacs, T. Kovacs, W. J. Kovacs, D. Koya, C. Kraft, D. Krainc, H. Kramer, T. Kravic-Stevovic, W. Krek, C. Kretz-Remy, R. Krick, M. Krishnamurthy, J. Kriston-Vizi, G. Kroemer, M. C. Kruer, R. Kruger, N. T. Ktistakis, K. Kuchitsu, C. Kuhn, A. P. Kumar, A. Kumar, A. Kumar, D. Kumar, D. Kumar, R. Kumar, S. Kumar, M. Kundu, H. J. Kung, A. Kuno, S. H. Kuo, J. Kuret, T. Kurz, T. Kwok, T. K. Kwon, Y. T. Kwon, I. Kyrmizi, A. R. La Spada, F. Lafont, T. Lahm, A. Lakkaraju, T. Lam, T. Lamark, S. Lancel, T. H. Landowski, D. J. Lane, J. D. Lane, C. Lanzi, P. Lapaquette, L. R. Lapierre, J. Laporte, J. Laukkarinen, G. W. Laurie, S. Lavandero, L. Lavie,

M. J. LaVoie, B. Y. Law, H. K. Law, K. B. Law, R. Layfield, P. A. Lazo, L. Le Cam, K. G. Le Roch, H. Le Stunff, V. Leardkamolkarn, M. Lecuit, B. H. Lee, C. H. Lee, E. F. Lee, G. M. Lee, H. J. Lee, H. Lee, J. K. Lee, J. Lee, J. H. Lee, J. H. Lee, M. Lee, M. S. Lee, P. J. Lee, S. W. Lee, S. J. Lee, S. J. Lee, S. Y. Lee, S. H. Lee, S. S. Lee, S. J. Lee, S. Lee, Y. R. Lee, Y. J. Lee, Y. H. Lee, C. Leeuwenburgh, S. Lefort, R. Legouis, J. Lei, Q. Y. Lei, D. A. Leib, G. Leibowitz, I. Lekli, S. D. Lemaire, J. J. Lemasters, M. K. Lemberg, A. Lemoine, S. Leng, G. Lenz, P. Lenzi, L. O. Lerman, D. Lettieri Barbato, J. I. Leu, H. Y. Leung, B. Levine, P. A. Lewis, F. Lezoualc'h, C. Li, F. Li, F. J. Li, J. Li, K. Li, L. Li, M. Li, M. Li, Q. Li, R. Li, S. Li, W. Li, W. Li, X. Li, Y. Li, J. Lian, C. Liang, Q. Liang, Y. Liao, J. Liberal, P. P. Liberski, P. Lie, A. P. Lieberman, H. J. Lim, K. L. Lim, K. Lim, R. T. Lima, C. S. Lin, C. F. Lin, F. Lin, F. Lin, F. C. Lin, K. Lin, K. H. Lin, P. H. Lin, T. Lin, W. W. Lin, Y. S. Lin, Y. Lin, R. Linden, D. Lindholm, L. M. Lindqvist, P. Lingor, A. Linkermann, L. A. Liotta, M. M. Lipinski, V. A. Lira, M. P. Lisanti, P. B. Liton, B. Liu, C. Liu, C. F. Liu, F. Liu, H. J. Liu, J. Liu, J. J. Liu, J. L. Liu, K. Liu, L. Liu, L. Liu, Q. Liu, R. Y. Liu, S. Liu, S. Liu, W. Liu, X. D. Liu, X. Liu, X. H. Liu, X. Liu, X. Liu, X. Liu, Y. Liu, Y. Liu, Z. Liu, Z. Liu, J. P. Liuzzi, G. Lizard, M. Ljujic, I. J. Lodhi, S. E. Logue, B. L. Lokeshwar, Y. C. Long, S. Lonial, B. Loos, C. Lopez-Otin, C. Lopez-Vicario, M. Lorente, P. L. Lorenzi, P. Lorincz, M. Los, M. T. Lotze, P. E. Lovat, B. Lu, B. Lu, J. Lu, Q. Lu, S. M. Lu, S. Lu, Y. Lu, F. Luciano, S. Luckhart, J. M. Lucocq, P. Ludovico, A. Lugea, N. W. Lukacs, J. J. Lum, A. H. Lund, H. Luo, J. Luo, S. Luo, C. Luparello, T. Lyons, J. Ma, Y. Ma, Y. Ma, Z. Ma, J. Machado, G. M. Machado-Santelli, F. Macian, G. C. MacIntosh, J. P. MacKeigan, K. F. Macleod, J. D. MacMicking, L. A. MacMillan-Crow, F. Madeo, M. Madesh, J. Madrigal-Matute, A. Maeda, T. Maeda, G. Maegawa, E. Maellaro, H. Maes, M. Magarinos, K. Maiese, T. K. Maiti, L. Maiuri, M. C. Maiuri, C. G. Maki, R. Malli, W. Malorni, A. Maloyan, F. Mami-Chouaib, N. Man, J. D. Mancias, E. M. Mandelkow, M. A. Mandell, A. A. Manfredi, S. N. Manie, C. Manzoni, K. Mao, Z. Mao, Z. W. Mao, P. Marambaud, A. M. Marconi, Z. Marelja, G. Marfe, M. Margeta, E. Margittai, M. Mari, F. V. Mariani, C. Marin, S. Marinelli, G. Marino, I. Markovic, R. Marquez, A. M. Martelli, S. Martens, K. R. Martin, S. J. Martin, S. Martin, M. A. Martin-Acebes, P. Martin-Sanz, C. Martinand-Mari, W. Martinet, J. Martinez, N. Martinez-Lopez, U. Martinez-Outschoorn, M. Martinez-Velazquez, M. Martinez-Vicente, W. K. Martins, H. Mashima, J. A. Mastrianni, G. Matarese, P. Matarrese, R. Mateo, S. Matoba, N. Matsumoto, T. Matsushita, A. Matsuura, T. Matsuzawa, M. P. Mattson, S. Matus, N. Maugeri, C. Mauvezin, A. Mayer, D. Maysinger, G. D. Mazzolini, M. K. McBrayer, K. McCall, C. McCormick, G. M. McInerney, S. C. McIver, S. McKenna, J. J. McMahon, I. A. McNeish, F. Mechta-Grigoriou, J. P. Medema, D. L. Medina, K. Megyeri, M. Mehrpour, J. L. Mehta, Y. Mei, U. C. Meier, A. J. Meijer, A. Melendez, G. Melino, S. Melino, E. J. de Melo, M. A. Mena, M. D. Meneghini, J. A. Menendez, R. Menezes, L. Meng, L. H. Meng, S. Meng, R. Menghini, A. S. Menko, R. F. Menna-Barreto, M. B. Menon, M. A. Meraz-Rios, G. Merla, L. Merlini, A. M. Merlot, A. Meryk, S. Meschini, J. N. Meyer, M. T. Mi, C. Y. Miao, L. Micale, S. Michaeli, C. Michiels, A. R. Migliaccio, A. S. Mihailidou, D. Mijaljica, K. Mikoshiba, E. Milan, L. Miller-Fleming, G. B. Mills, I. G. Mills, G. Minakaki, B. A. Minassian, X. F. Ming, F. Minibayeva, E. A. Minina, J. D. Mintern, S. Minucci, A. Miranda-Vizuete, C. H. Mitchell, S. Miyamoto, K. Miyazawa, N. Mizushima,

K. Mnich, B. Mograbi, S. Mohseni, L. F. Moita, M. Molinari, M. Molinari, A. B. Moller, B. Mollereau, F. Mollinedo, M. Mongillo, M. M. Monick, S. Montagnaro, C. Montell, D. J. Moore, M. N. Moore, R. Mora-Rodriguez, P. I. Moreira, E. Morel, M. B. Morelli, S. Moreno, M. J. Morgan, A. Moris, Y. Moriyasu, J. L. Morrison, L. A. Morrison, E. Morselli, J. Moscat, P. L. Moseley, S. Mostowy, E. Motori, D. Mottet, J. C. Mottram, C. E. Moussa, V. E. Mpakou, H. Mukhtar, J. M. Mulcahy Levy, S. Muller, R. Munoz-Moreno, C. Munoz-Pinedo, C. Munz, M. E. Murphy, J. T. Murray, A. Murthy, I. U. Mysorekar, I. R. Nabi, M. Nabissi, G. A. Nader, Y. Nagahara, Y. Nagai, K. Nagata, A. Nagelkerke, P. Nagy, S. R. Naidu, S. Nair, H. Nakano, H. Nakatogawa, M. Nanjundan, G. Napolitano, N. I. Naqvi, R. Nardacci, D. P. Narendra, M. Narita, A. C. Nascimbeni, R. Natarajan, L. C. Navegantes, S. T. Nawrocki, T. Y. Nazarko, V. Y. Nazarko, T. Neill, L. M. Neri, M. G. Netea, R. T. Netea-Maier, B. M. Neves, P. A. Ney, I. P. Nezis, H. T. Nguyen, H. P. Nguyen, A. S. Nicot, H. Nilsen, P. Nilsson, M. Nishimura, I. Nishino, M. Niso-Santano, H. Niu, R. A. Nixon, V. C. Njar, T. Noda, A. A. Noegel, E. M. Nolte, E. Norberg, K. K. Norga, S. K. Noureini, S. Notomi, L. Notterpek, K. Nowikovsky, N. Nukina, T. Nurnberger, V. B. O'Donnell, T. O'Donovan, P. J. O'Dwyer, I. Oehme, C. L. Oeste, M. Ogawa, B. Ogretmen, Y. Ogura, Y. J. Oh, M. Ohmuraya, T. Ohshima, R. Ojha, K. Okamoto, T. Okazaki, F. J. Oliver, K. Ollinger, S. Olsson, D. P. Orban, P. Ordonez, I. Orhon, L. Orosz, E. J. O'Rourke, H. Orozco, A. L. Ortega, E. Ortona, L. D. Osellame, J. Oshima, S. Oshima, H. D. Osiewacz, T. Otomo, K. Otsu, J. H. Ou, T. F. Outeiro, D. Y. Ouyang, H. Ouyang, M. Overholtzer, M. A. Ozbun, P. H. Ozdinler, B. Ozpolat, C. Pacelli, P. Paganetti, G. Page, G. Pages, U. Pagnini, B. Pajak, S. C. Pak, K. Pakos-Zebrucka, N. Pakpour, Z. Palkova, F. Palladino, K. Pallauf, N. Pallet, M. Palmieri, S. R. Paludan, C. Palumbo, S. Palumbo, O. Pampliega, H. Pan, W. Pan, T. Panaretakis, A. Pandey, A. Pantazopoulou, Z. Papackova, D. L. Papademetrio, I. Papassideri, A. Papini, N. Parajuli, J. Pardo, V. V. Parekh, G. Parenti, J. I. Park, J. Park, O. K. Park, R. Parker, R. Parlato, J. B. Parys, K. R. Parzych, J. M. Pasquet, B. Pasquier, K. B. Pasumarthi, D. Patschan, C. Patterson, S. Pattingre, S. Pattison, A. Pause, H. Pavenstadt, F. Pavone, Z. Pedrozo, F. J. Pena, M. A. Penalva, M. Pende, J. Peng, F. Penna, J. M. Penninger, A. Pensalfini, S. Pepe, G. J. Pereira, P. C. Pereira, V. Perez-de la Cruz, M. E. Perez-Perez, D. Perez-Rodriguez, D. Perez-Sala, C. Perier, A. Perl, D. H. Perlmutter, I. Perrotta, S. Pervaiz, M. Pesonen, J. E. Pessin, G. J. Peters, M. Petersen, I. Petrache, B. J. Petrof, G. Petrovski, J. M. Phang, M. Piacentini, M. Pierdominici, P. Pierre, V. Pierrefite-Carle, F. Pietrocola, F. X. Pimentel-Muinos, M. Pinar, B. Pineda, R. Pinkas-Kramarski, M. Pinti, P. Pinton, B. Piperdi, J. M. Piret, L. C. Platanias, H. W. Platta, E. D. Plowey, S. Poggeler, M. Poirot, P. Polcic, A. Poletti, A. H. Poon, H. Popelka, B. Popova, I. Poprawa, S. M. Poulose, J. Poulton, S. K. Powers, T. Powers, M. Pozuelo-Rubio, K. Prak, R. Prange, M. Prescott, M. Priault, S. Prince, R. L. Proia, T. Proikas-Cezanne, H. Prokisch, V. J. Promponas, K. Przyklenk, R. Puertollano, S. Pugazhenthi, L. Puglielli, A. Pujol, J. Puyal, D. Pyeon, X. Qi, W. B. Qian, Z. H. Qin, Y. Qiu, Z. Qu, J. Quadrilatero, F. Quinn, N. Raben, H. Rabinowich, F. Radogna, M. J. Ragusa, M. Rahmani, K. Raina, S. Ramanadham, R. Ramesh, A. Rami, S. Randall-Demllo, F. Randow, H. Rao, V. A. Rao, B. B. Rasmussen, T. M. Rasse, E. A. Ratovitski, P. E. Rautou, S. K. Ray, B. Razani, B. H. Reed, F. Reggiori, M. Rehm, A. S. Reichert, T. Rein, D. J. Reiner, E. Reits, J. Ren, X. Ren, M. Renna, J. E. Reusch, J. L. Revuelta, L.

Reyes, A. R. Rezaie, R. I. Richards, D. R. Richardson, C. Richetta, M. A. Riehle, B. H. Rihn, Y. Rikihisa, B. E. Riley, G. Rimbach, M. R. Rippo, K. Ritis, F. Rizzi, E. Rizzo, P. J. Roach, J. Robbins, M. Roberge, G. Roca, M. C. Roccheri, S. Rocha, C. M. Rodrigues, C. I. Rodriguez, S. R. de Cordoba, N. Rodriguez-Muela, J. Roelofs, V. V. Rogov, T. T. Rohn, B. Rohrer, D. Romanelli, L. Romani, P. S. Romano, M. I. Roncero, J. L. Rosa, A. Rosello, K. V. Rosen, P. Rosenstiel, M. Rost-Roszkowska, K. A. Roth, G. Roue, M. Rouis, K. M. Rouschop, D. T. Ruan, D. Ruano, D. C. Rubinsztein, E. B. Rucker, 3rd, A. Rudich, E. Rudolf, R. Rudolf, M. A. Ruegg, C. Ruiz-Roldan, A. A. Ruparelia, P. Rusmini, D. W. Russ, G. L. Russo, G. Russo, R. Russo, T. E. Rusten, V. Ryabovol, K. M. Ryan, S. W. Ryter, D. M. Sabatini, M. Sacher, C. Sachse, M. N. Sack, J. Sadoshima, P. Saftig, R. Sagi-Eisenberg, S. Sahni, P. Saikumar, T. Saito, T. Saitoh, K. Sakakura, M. Sakoh-Nakatogawa, Y. Sakuraba, M. Salazar-Roa, P. Salomoni, A. K. Saluja, P. M. Salvaterra, R. Salvioli, A. Samali, A. M. Sanchez, J. A. Sanchez-Alcazar, R. Sanchez-Prieto, M. Sandri, M. A. Sanjuan, S. Santaguida, L. Santambrogio, G. Santoni, C. N. Dos Santos, S. Saran, M. Sardiello, G. Sargent, P. Sarkar, S. Sarkar, M. R. Sarrias, M. M. Sarwal, C. Sasakawa, M. Sasaki, M. Sass, K. Sato, M. Sato, J. Satriano, N. Savaraj, S. Saveljeva, L. Schaefer, U. E. Schaible, M. Scharl, H. M. Schatzl, R. Schekman, W. Scheper, A. Schiavi, H. M. Schipper, H. Schmeisser, J. Schmidt, I. Schmitz, B. E. Schneider, E. M. Schneider, J. L. Schneider, E. A. Schon, M. J. Schonenberger, A. H. Schonthal, D. F. Schorderet, B. Schroder, S. Schuck, R. J. Schulze, M. Schwarten, T. L. Schwarz, S. Sciarretta, K. Scotto, A. I. Scovassi, R. A. Screaton, M. Screen, H. Seca, S. Sedej, L. Segatori, N. Segev, P. O. Seglen, J. M. Segui-Simarro, J. Segura-Aguilar, E. Seki, C. Sell, I. Seiliez, C. F. Semenkovich, G. L. Semenza, U. Sen, A. L. Serra, A. Serrano-Puebla, H. Sesaki, T. Setoguchi, C. Settembre, J. J. Shacka, A. N. Shajahan-Haq, I. M. Shapiro, S. Sharma, H. She, C. K. Shen, C. C. Shen, H. M. Shen, S. Shen, W. Shen, R. Sheng, X. Sheng, Z. H. Sheng, T. G. Shepherd, J. Shi, Q. Shi, Q. Shi, Y. Shi, S. Shibutani, K. Shibuya, Y. Shidoji, J. J. Shieh, C. M. Shih, Y. Shimada, S. Shimizu, D. W. Shin, M. L. Shinohara, M. Shintani, T. Shintani, T. Shioi, K. Shirabe, R. Shiri-Sverdlov, O. Shirihai, G. C. Shore, C. W. Shu, D. Shukla, A. A. Sibirny, V. Sica, C. J. Sigurdson, E. M. Sigurdsson, P. S. Sijwali, B. Sikorska, W. A. Silveira, S. Silvente-Poirot, G. A. Silverman, J. Simak, T. Simmet, A. K. Simon, H. U. Simon, C. Simone, M. Simons, A. Simonsen, R. Singh, S. V. Singh, S. K. Singh, D. Sinha, S. Sinha, F. A. Sinicrope, A. Sirko, K. Sirohi, B. J. Sishi, A. Sittler, P. M. Siu, E. Sivridis, A. Skwarska, R. Slack, I. Slaninova, N. Slavov, S. S. Smaili, K. S. Smalley, D. R. Smith, S. J. Soenen, S. A. Soleimanpour, A. Solhaug, K. Somasundaram, J. H. Son, A. Sonawane, C. Song, F. Song, H. K. Song, J. X. Song, W. Song, K. Y. Soo, A. K. Sood, T. W. Soong, V. Soontornniyomkij, M. Sorice, F. Sotgia, D. R. Soto-Pantoja, A. Sotthibundhu, M. J. Sousa, H. P. Spaink, P. N. Span, A. Spang, J. D. Sparks, P. G. Speck, S. A. Spector, C. D. Spies, W. Springer, D. S. Clair, A. Stacchiotti, B. Staels, M. T. Stang, D. T. Starczynowski, P. Starokadomskyy, C. Steegborn, J. W. Steele, L. Stefanis, J. Steffan, C. M. Stellrecht, H. Stenmark, T. M. Stepkowski, S. T. Stern, C. Stevens, B. R. Stockwell, V. Stoka, Z. Storchova, B. Stork, V. Stratoulias, D. J. Stravopodis, P. Strnad, A. M. Strohecker, A. L. Strom, P. Stromhaug, J. Stulik, Y. X. Su, Z. Su, C. S. Subauste, S. Subramaniam, C. M. Sue, S. W. Suh, X. Sui, S. Sukseree, D. Sulzer, F. L. Sun, J. Sun, J. Sun, S. Y. Sun, Y. Sun, Y. Sun, Y. Sun, V. Sundaramoorthy, J. Sung,

H. Suzuki, K. Suzuki, N. Suzuki, T. Suzuki, Y. J. Suzuki, M. S. Swanson, C. Swanton, K. Sward, G. Swarup, S. T. Sweeney, P. W. Sylvester, Z. Szatmari, E. Szegezdi, P. W. Szlosarek, H. Taegtmeyer, M. Tafani, E. Taillebourg, S. W. Tait, K. Takacs-Vellai, Y. Takahashi, S. Takats, G. Takemura, N. Takigawa, N. J. Talbot, E. Tamagno, J. Tamburini, C. P. Tan, L. Tan, M. L. Tan, M. Tan, Y. J. Tan, K. Tanaka, M. Tanaka, D. Tang, D. Tang, G. Tang, I. Tanida, K. Tanji, B. A. Tannous, J. A. Tapia, I. Tasset-Cuevas, M. Tatar, I. Tavassoly, N. Tavernarakis, A. Taylor, G. S. Taylor, G. A. Taylor, J. P. Taylor, M. J. Taylor, E. V. Tchetina, A. R. Tee, F. Teixeira-Clerc, S. Telang, T. Tencomnao, B. B. Teng, R. J. Teng, F. Terro, G. Tettamanti, A. L. Theiss, A. E. Theron, K. J. Thomas, M. P. Thome, P. G. Thomes, A. Thorburn, J. Thorner, T. Thum, M. Thumm, T. L. Thurston, L. Tian, A. Till, J. P. Ting, V. I. Titorenko, L. Toker, S. Toldo, S. A. Tooze, I. Topisirovic, M. L. Torgersen, L. Torosantucci, A. Torriglia, M. R. Torrisi, C. Tournier, R. Towns, V. Trajkovic, L. H. Travassos, G. Triola, D. N. Tripathi, D. Trisciuoglio, R. Troncoso, I. P. Trougakos, A. C. Truttmann, K. J. Tsai, M. P. Tschan, Y. H. Tseng, T. Tsukuba, A. Tsung, A. S. Tsvetkov, S. Tu, H. Y. Tuan, M. Tucci, D. A. Tumbarello, B. Turk, V. Turk, R. F. Turner, A. A. Tveita, S. C. Tyagi, M. Ubukata, Y. Uchiyama, A. Udelnow, T. Ueno, M. Umekawa, R. Umemiya-Shirafuji, B. R. Underwood, C. Ungermann, R. P. Ureshino, R. Ushioda, V. N. Uversky, N. L. Uzcategui, T. Vaccari, M. I. Vaccaro, L. Vachova, H. Vakifahmetoglu-Norberg, R. Valdor, E. M. Valente, F. Vallette, A. M. Valverde, G. Van den Berghe, L. Van Den Bosch, G. R. van den Brink, F. G. van der Goot, I. J. van der Klei, L. J. van der Laan, W. G. van Doorn, M. van Egmond, K. L. van Golen, L. Van Kaer, M. van Lookeren Campagne, P. Vandenabeele, W. Vandenberghe, I. Vanhorebeek, I. Varela-Nieto, M. H. Vasconcelos, R. Vasko, D. G. Vavvas, I. Vega-Naredo, G. Velasco, A. D. Velentzas, P. D. Velentzas, T. Vellai, E. Vellenga, M. H. Vendelbo, K. Venkatachalam, N. Ventura, S. Ventura, P. S. Veras, M. Verdier, B. G. Vertessy, A. Viale, M. Vidal, H. L. Vieira, R. D. Vierstra, N. Vigneswaran, N. Vij, M. Vila, M. Villar, V. H. Villar, J. Villarroya, C. Vindis, G. Viola, M. T. Viscomi, G. Vitale, D. T. Vogl, O. V. Voitsekhovskaja, C. von Haefen, K. von Schwarzenberg, D. E. Voth, V. Vouret-Craviari, K. Vuori, J. M. Vyas, C. Waeber, C. L. Walker, M. J. Walker, J. Walter, L. Wan, X. Wan, B. Wang, C. Wang, C. Y. Wang, C. Wang, C. Wang, C. Wang, D. Wang, F. Wang, F. Wang, G. Wang, H. J. Wang, H. Wang, H. G. Wang, H. Wang, H. D. Wang, J. Wang, J. Wang, M. Wang, M. Q. Wang, P. Y. Wang, P. Wang, R. C. Wang, S. Wang, T. F. Wang, X. Wang, X. J. Wang, X. W. Wang, X. Wang, X. Wang, Y. Wang, Y. Wang, Y. Wang, Y. J. Wang, Y. Wang, Y. Wang, Y. T. Wang, Y. Wang, Z. N. Wang, P. Wappner, C. Ward, D. M. Ward, G. Warnes, H. Watada, Y. Watanabe, K. Watase, T. E. Weaver, C. D. Weekes, J. Wei, T. Weide, C. C. Weihl, G. Weindl, S. N. Weis, L. Wen, X. Wen, Y. Wen, B. Westermann, C. M. Weyand, A. R. White, E. White, J. L. Whitton, A. J. Whitworth, J. Wiels, F. Wild, M. E. Wildenberg, T. Wileman, D. S. Wilkinson, S. Wilkinson, D. Willbold, C. Williams, K. Williams, P. R. Williamson, K. F. Winklhofer, S. S. Witkin, S. E. Wohlgemuth, T. Wollert, E. J. Wolvetang, E. Wong, G. W. Wong, R. W. Wong, V. K. Wong, E. A. Woodcock, K. L. Wright, C. Wu, D. Wu, G. S. Wu, J. Wu, J. Wu, M. Wu, M. Wu, S. Wu, W. K. Wu, Y. Wu, Z. Wu, C. P. Xavier, R. J. Xavier, G. X. Xia, T. Xia, W. Xia, Y. Xia, H. Xiao, J. Xiao, S. Xiao, W. Xiao, C. M. Xie, Z. Xie, Z. Xie, M. Xilouri, Y. Xiong, C. Xu, C. Xu, F. Xu, H. Xu, H. Xu, J. Xu, J. Xu, J. Xu, L. Xu, X. Xu, Y. Xu, Y. Xu, Z. X. Xu,

Z. Xu, Y. Xue, T. Yamada, A. Yamamoto, K. Yamanaka, S. Yamashina, S. Yamashiro, B. Yan, B. Yan, X. Yan, Z. Yan, Y. Yanagi, D. S. Yang, J. M. Yang, L. Yang, M. Yang, P. M. Yang, P. Yang, Q. Yang, W. Yang, W. Y. Yang, X. Yang, Y. Yang, Y. Yang, Z. Yang, Z. Yang, M. C. Yao, P. J. Yao, X. Yao, Z. Yao, Z. Yao, L. S. Yasui, M. Ye, B. Yedvobnick, B. Yeganeh, E. S. Yeh, P. L. Yeyati, F. Yi, L. Yi, X. M. Yin, C. K. Yip, Y. M. Yoo, Y. H. Yoo, S. Y. Yoon, K. Yoshida, T. Yoshimori, K. H. Young, H. Yu, J. J. Yu, J. T. Yu, J. Yu, L. Yu, W. H. Yu, X. F. Yu, Z. Yu, J. Yuan, Z. M. Yuan, B. Y. Yue, J. Yue, Z. Yue, D. N. Zacks, E. Zacksenhaus, N. Zaffaroni, T. Zaglia, Z. Zakeri, V. Zecchini, J. Zeng, M. Zeng, Q. Zeng, A. S. Zervos, D. D. Zhang, F. Zhang, G. Zhang, G. C. Zhang, H. Zhang, H. Zhang, H. Zhang, H. Zhang, J. Zhang, J. Zhang, J. Zhang, J. Zhang, J. P. Zhang, L. Zhang, L. Zhang, L. Zhang, L. Zhang, M. Y. Zhang, X. Zhang, X. D. Zhang, Y. Zhang, Y. Zhang, Y. Zhang, Y. Zhang, Y. Zhang, M. Zhao, W. L. Zhao, X. Zhao, Y. G. Zhao, Y. Zhao, Y. Zhao, Y. X. Zhao, Z. Zhao, Z. J. Zhao, D. Zheng, X. L. Zheng, X. Zheng, B. Zhivotovsky, Q. Zhong, G. Z. Zhou, G. Zhou, H. Zhou, S. F. Zhou, X. J. Zhou, H. Zhu, H. Zhu, W. G. Zhu, W. Zhu, X. F. Zhu, Y. Zhu, S. M. Zhuang, X. Zhuang, E. Ziparo, C. E. Zois, T. Zoladek, W. X. Zong, A. Zorzano, and S. M. Zughaier. 2016. "Guidelines for the use and interpretation of assays for monitoring autophagy (3rd edition)." *Autophagy* 12 (1):1-222. doi: 10.1080/15548627.2015.1100356.

Kovacs, Stephen B, and Edward A Miao. 2017. "Gasdermins: effectors of pyroptosis." *Trends in cell biology* 27 (9):673-684.

Lachaier, Emma, Christophe Louandre, Corinne Godin, Zuzana Saidak, Maxime Baert, Momar Diouf, Bruno Chauffert, and Antoine Galmiche. 2014. "Sorafenib induces ferroptosis in human cancer cell lines originating from different solid tumors." *Anticancer research* 34 (11):6417-6422.

Lawen, A. 2003. "Apoptosis-an introduction." *Bioessays* 25 (9):888-96. doi: 10.1002/bies.10329.

Lee, Su Yeon, Min Kyung Ju, Hyun Min Jeon, Eui Kyong Jeong, Yig Ji Lee, Cho Hee Kim, Hye Gyeong Park, Song Iy Han, and Ho Sung Kang. 2018. "Regulation of Tumor Progression by Programmed Necrosis." *Oxidative medicine and cellular longevity* 2018.

Li, J, and J Yuan. 2008. "Caspases in apoptosis and beyond." *Oncogene* 27 (48):6194.

Li, Wei, XiMing Yuan, Gunnar Nordgren, Helge Dalen, Gene M Dubowchik, Raymond A Firestone, and Ulf T Brunk. 2000. "Induction of cell death by the lysosomotropic detergent MSDH." *FEBS letters* 470 (1):35-39.

Li, X, AB Roginsky, X-Z Ding, C Woodward, P Collin, RA Newman, Jr Bell, RH, and TE Adrian. 2008. "Review of the Apoptosis Pathways in Pancreatic Cancer and the Anti-apoptotic Effects of the Novel Sea Cucumber Compound, Frondoside A." *Annals of the New York Academy of Sciences* 1138 (1):181-198.

Lieberman, Judy. 2010. "Granzyme A activates another way to die." *Immunological reviews* 235 (1):93-104. doi: 10.1111/j.0105-2896.2010.00902.x.

Lima, H., Jr., L. S. Jacobson, M. F. Goldberg, K. Chandran, F. Diaz-Griffero, M. P. Lisanti, and J. Brojatsch. 2013. "Role of lysosome rupture in controlling Nlrp3 signaling and necrotic cell death." *Cell Cycle* 12 (12):1868-78. doi: 10.4161/cc.24903.

Lin, Yizhi, David L Epstein, and Paloma B Liton. 2010. "Intralysosomal iron induces lysosomal membrane permeabilization and cathepsin D–mediated cell death in trabecular meshwork cells exposed to oxidative stress." *Investigative ophthalmology & visual science* 51 (12):6483-6495.

Lin, Yong, Anne Devin, Yolanda Rodriguez, and Zheng-gang Liu. 1999. "Cleavage of the death domain kinase RIP by caspase-8 prompts TNF-induced apoptosis." *Genes & development* 13 (19):2514-2526.

Liu, Lu, Na Zhang, Yueying Dou, Genxiang Mao, Chongwen Bi, Weiqiang Pang, Xiaojia Liu, Danqing Song, and Hongbin Deng. 2017. "Lysosomal dysfunction and autophagy blockade contribute to IMB-6G-induced apoptosis in pancreatic cancer cells." *Scientific reports* 7:41862.

Louandre, Christophe, Zakaria Ezzoukhry, Corinne Godin, Jean-Claude Barbare, Jean-Claude Mazière, Bruno Chauffert, and Antoine Galmiche. 2013. "Iron-dependent cell death of hepatocellular carcinoma cells exposed to sorafenib." *International journal of cancer* 133 (7):1732-1742.

Lu, Tao, Ying Xu, Maura T Mericle, and Ronald L Mellgren. 2002. "Participation of the conventional calpains in apoptosis." *Biochimica et Biophysica Acta (BBA)-Molecular Cell Research* 1590 (1-3):16-26.

Lv, Linlin, Lingli Zheng, Deshi Dong, Lina Xu, Lianhong Yin, Youwei Xu, Yan Qi, Xu Han, and Jinyong Peng. 2013. "Dioscin, a natural steroid saponin, induces apoptosis and DNA damage through reactive oxygen species: a potential new drug for treatment of glioblastoma multiforme." *Food and chemical toxicology* 59:657-669.

Man, Si Ming, Rajendra Karki, and Thirumala-Devi Kanneganti. 2017. "Molecular mechanisms and functions of pyroptosis, inflammatory caspases and inflammasomes in infectious diseases." *Immunological reviews* 277 (1):61-75.

Masaldan, Shashank, Sharnel AS Clatworthy, Cristina Gamell, Peter M Meggyesy, Antonia-Tonia Rigopoulos, Sue Haupt, Ygal Haupt, Delphine Denoyer, Paul A Adlard, and Ashley I Bush. 2018. "Iron accumulation in senescent cells is coupled with impaired ferritinophagy and inhibition of ferroptosis." *Redox biology* 14:100-115.

McIlwain, David R, Thorsten Berger, and Tak W Mak. 2013. "Caspase functions in cell death and disease." *Cold Spring Harbor perspectives in biology* 5 (4):a008656.

Messner, Barbara, Christian Ploner, Günther Laufer, and David Bernhard. 2012. "Cadmium activates a programmed, lysosomal membrane permeabilization-dependent necrosis pathway." *Toxicology letters* 212 (3):268-275.

Meurette, O., A. Rebillard, L. Huc, G. Le Moigne, D. Merino, O. Micheau, D. Lagadic-Gossmann, and M. T. Dimanche-Boitrel. 2007. "TRAIL induces receptor-interacting protein 1-dependent and caspase-dependent necrosis-like cell death under acidic extracellular conditions." *Cancer Res* 67 (1):218-26. doi: 10.1158/0008-5472.CAN-06-1610.

Meurette, Olivier, Laurence Huc, Amelie Rebillard, Gwenaelle Le Moigne, DOMINIQUE LAGADIC-GOSSMANN, and MARIE-THERESE DIMANCHE-BOITREL. 2005. "TRAIL (TNF-Related Apoptosis-Inducing Ligand) Induces Necrosis-Like Cell Death in Tumor Cells at Acidic Extracellular pH." *Annals of the new York Academy of Sciences* 1056 (1):379-387.

Mishra, Abhay P., Bahare Salehi, Mehdi Sharifi-Rad, Raffaele Pezzani, Farzad Kobarfard, Javad Sharifi-Rad, and Manisha Nigam. 2018. "Programmed Cell Death, from a Cancer Perspective: An Overview." *Molecular Diagnosis & Therapy* 22 (3):281-295. doi: 10.1007/s40291-018-0329-9.

Mizushima, N. 2007a. "Autophagy: process and function." *Genes Dev* 21 (22):2861-73. doi: 10.1101/gad.1599207.

Mizushima, Noboru. 2007b. "Autophagy: process and function." *Genes & development* 21 (22):2861-2873.

Mizushima, Noboru, and Masaaki Komatsu. 2011. "Autophagy: renovation of cells and tissues." *Cell* 147 (4):728-741.

Mokhtari, Reza Bayat, Tina S Homayouni, Narges Baluch, Evgeniya Morgatskaya, Sushil Kumar, Bikul Das, and Herman Yeger. 2017. "Combination therapy in combating cancer." *Oncotarget* 8 (23):38022.

Morgan, M. J., B. E. Fitzwalter, C. R. Owens, R. K. Powers, J. L. Sottnik, G. Gamez, J. C. Costello, D. Theodorescu, and A. Thorburn. 2018. "Metastatic cells are preferentially vulnerable to lysosomal inhibition." *Proc Natl Acad Sci U S A* 115 (36):E8479-E8488. doi: 10.1073/pnas.1706526115.

Moses, Tessa, Kalliope K Papadopoulou, and Anne Osbourn. 2014. "Metabolic and functional diversity of saponins, biosynthetic intermediates and semi-synthetic derivatives." *Critical reviews in biochemistry and molecular biology* 49 (6):439-462.

Najafov, Ayaz, Hongbo Chen, and Junying Yuan. 2017. "Necroptosis and cancer." *Trends in cancer* 3 (4):294-301.

Nakagawa, Takashi, Shigeomi Shimizu, Tetsuya Watanabe, Osamu Yamaguchi, Kinya Otsu, Hirotaka Yamagata, Hidenori Inohara, Takeshi Kubo, and Yoshihide Tsujimoto. 2005. "Cyclophilin D-dependent mitochondrial permeability transition regulates some necrotic but not apoptotic cell death." *Nature* 434 (7033):652.

Nikoletopoulou, V., M. Markaki, K. Palikaras, and N. Tavernarakis. 2013. "Crosstalk between apoptosis, necrosis and autophagy." *Biochim Biophys Acta* 1833 (12):3448-59. doi: 10.1016/j.bbamcr.2013.06.001.

Norman, Joanna M., Gerald M. Cohen, and Edward T. W. Bampton. 2014. "The in vitro cleavage of the hAtg proteins by cell death proteases." *Autophagy* 6 (8):1042-1056. doi: 10.4161/auto.6.8.13337.

Okada, Masayuki, Souichi Adachi, Tsuyoshi Imai, Ken-ichiro Watanabe, Shin-ya Toyokuni, Masaki Ueno, Antonis S Zervos, Guido Kroemer, and Tatsutoshi Nakahata. 2004. "A novel mechanism for imatinib mesylate–induced cell death of BCR-ABL–positive human leukemic cells: caspase-independent, necrosis-like programmed cell death mediated by serine protease activity." *Blood* 103 (6):2299-2307.

Oral, Ozlem, Devrim Oz-Arslan, Zeynep Itah, Atabak Naghavi, Remziye Deveci, Sabire Karacali, and Devrim Gozuacik. 2012. "Cleavage of Atg3 protein by caspase-8 regulates autophagy during receptor-activated cell death." *Apoptosis* 17 (8):810-820.

Pacheco, Fabio J, Jacqueline Servin, David Dang, Jim Kim, Christine Molinaro, Tracy Daniels, Terry A Brown-Bryan, Mizue Imoto-Egami, and Carlos A Casiano. 2005. "Involvement of lysosomal cathepsins in the cleavage of DNA topoisomerase I during necrotic cell death." *Arthritis & Rheumatism* 52 (7):2133-2145.

Pajak, B, B Gajkowska, and A Orzechowski. 2005. "Cycloheximide-mediated sensitization to TNF-alpha-induced apoptosis in human colorectal cancer cell line COLO 205; role of FLIP and metabolic inhibitors." *Journal of physiology and pharmacology* 56:101.

Piao, S., and R. K. Amaravadi. 2016. "Targeting the lysosome in cancer." *Ann N Y Acad Sci* 1371 (1):45-54. doi: 10.1111/nyas.12953.

Podolak, I., A. Galanty, and D. Sobolewska. 2010. "Saponins as cytotoxic agents: a review." *Phytochem Rev* 9 (3):425-474. doi: 10.1007/s11101-010-9183-z.

Rayamajhi, Manira, Yue Zhang, and Edward A Miao. 2013. "Detection of pyroptosis by measuring released lactate dehydrogenase activity." In *The Inflammasome*, 85-90. Springer.

Reiser, J., B. Adair, and T. Reinheckel. 2010. "Specialized roles for cysteine cathepsins in health and disease." *J Clin Invest* 120 (10):3421-31. doi: 10.1172/JCI42918.

Repnik, U., M. H. Cesen, and B. Turk. 2016. "The Use of Lysosomotropic Dyes to Exclude Lysosomal Membrane Permeabilization." *Cold Spring Harb Protoc* 2016 (5). doi: 10.1101/pdb.prot087106.

Repnik, U., M. Hafner Cesen, and B. Turk. 2014. "Lysosomal membrane permeabilization in cell death: concepts and challenges." *Mitochondrion* 19 Pt A:49-57. doi: 10.1016/j.mito.2014.06.006.

Repnik, Urska, Marita Borg Distefano, Martin Tobias Speth, Matthew Yoke Wui Ng, Cinzia Progida, Bernard Hoflack, Jean Gruenberg, and Gareth Griffiths. 2017. "LLOMe does not release cysteine cathepsins to the cytosol but inactivates them in transiently permeabilized lysosomes." *J Cell Sci*:jcs. 204529.

Saleem, M. 2009. "Lupeol, a novel anti-inflammatory and anti-cancer dietary triterpene." *Cancer Lett* 285 (2):109-15. doi: 10.1016/j.canlet.2009.04.033.

Sanman, Laura E, and Matthew Bogyo. 2014. "Activity-based profiling of proteases." *Annual review of biochemistry* 83:249-273.

Saraste, A. , and K. Pulkki. 2000. "Morphologic and biochemical hallmarks of apoptosis." *Cardiovascular Research* 45:528–537.

Sauter, B., M. L. Albert, L. Francisco, M. Larsson, S. Somersan, and N. Bhardwaj. 2000. "Consequences of Cell Death: Exposure to Necrotic Tumor Cells, but Not Primary Tissue Cells or Apoptotic Cells, Induces the Maturation of Immunostimulatory Dendritic Cells." *Journal of Experimental Medicine* 191 (3):423-434. doi: 10.1084/jem.191.3.423.

Serrano-Puebla, A., and P. Boya. 2016. "Lysosomal membrane permeabilization in cell death: new evidence and implications for health and disease." *Ann N Y Acad Sci* 1371 (1):30-44. doi: 10.1111/nyas.12966.

Serrano-Puebla, A., and P. Boya. 2018. "Lysosomal membrane permeabilization as a cell death mechanism in cancer cells." *Biochem Soc Trans* 46 (2):207-215. doi: 10.1042/BST20170130.

Shalini, Sonia, L Dorstyn, S Dawar, and S Kumar. 2015. "Old, new and emerging functions of caspases." *Cell death and differentiation* 22 (4):526.

Shi, Jianjin, Yue Zhao, Yupeng Wang, Wenqing Gao, Jingjin Ding, Peng Li, Liyan Hu, and Feng Shao. 2014. "Inflammatory caspases are innate immune receptors for intracellular LPS." *Nature* 514 (7521):187.

Shimizu, S., T. Yoshida, M. Tsujioka, and S. Arakawa. 2014. "Autophagic cell death and cancer." *Int J Mol Sci* 15 (2):3145-53. doi: 10.3390/ijms15023145.

Shimizu, Shigeomi, Akimitsu Konishi, Yuya Nishida, Takeshi Mizuta, Hiroshi Nishina, Akitsugu Yamamoto, and Yoshihide Tsujimoto. 2010. "Involvement of JNK in the regulation of autophagic cell death." *Oncogene* 29 (14):2070.

Soriano, Jorge, Inma Mora-Espí, María Elisa Alea-Reyes, Lluïsa Pérez-García, Leonardo Barrios, Elena Ibáñez, and Carme Nogués. 2017. "Cell death mechanisms in tumoral and non-tumoral human cell lines triggered by photodynamic treatments: apoptosis, necrosis and parthanatos." *Scientific reports* 7:41340.

Stoka, Veronika, Boris Turk, Sharon L Schendel, Tae-Hyoung Kim, Tina Cirman, Scott J Snipas, Lisa M Ellerby, Dale Bredesen, Hudson Freeze, and Magnus Abrahamson. 2001. "Lysosomal protease pathways to apoptosis cleavage of Bid, not pro-caspases, is the most likely route." *Journal of Biological Chemistry* 276 (5):3149-3157.

Storr, Sarah J, Neil O Carragher, Margaret C Frame, Tim Parr, and Stewart G Martin. 2011. "The calpain system and cancer." *Nature Reviews Cancer* 11 (5):364.

Suzuki, Koichi, Shoji Hata, Yukiko Kawabata, and Hiroyuki Sorimachi. 2004. "Structure, activation, and biology of calpain." *Diabetes* 53 (suppl 1):S12-S18.

Suzuki, Y., K. Takahashi-Niki, T. Akagi, T. Hashikawa, and R. Takahashi. 2003. "Mitochondrial protease Omi/HtrA2 enhances caspase activation through multiple pathways." *Cell Death And Differentiation* 11:208. doi: 10.1038/sj.cdd.4401343.

Tait, S. W., G. Ichim, and D. R. Green. 2014. "Die another way--non-apoptotic mechanisms of cell death." *J Cell Sci* 127 (Pt 10):2135-44. doi: 10.1242/jcs.093575.

Torii, Seiji, Ryosuke Shintoku, Chisato Kubota, Makoto Yaegashi, Ryoko Torii, Masaya Sasaki, Toshinobu Suzuki, Masanobu Mori, Yuhei Yoshimoto, and Toshiyuki Takeuchi. 2016. "An essential role for functional lysosomes in ferroptosis of cancer cells." *Biochemical Journal*:BJ20150658.

Trapani, Joseph A, and Mark J Smyth. 2002. "Functional significance of the perforin/granzyme cell death pathway." *Nature Reviews Immunology* 2 (10):735.

Turk, Vito. 1999. *Proteases: new perspectives*: Springer Science & Business Media.

Vakifahmetoglu, H, M Olsson, and B Zhivotovsky. 2008. "Death through a tragedy: mitotic catastrophe." *Cell death and differentiation* 15 (7):1153.

Vallecillo-Hernández, Jorge, Maria Dolores Barrachina, Dolores Ortiz-Masiá, Sandra Coll, Juan Vicente Esplugues, Sara Calatayud, and Carlos Hernández. 2018. "Indomethacin disrupts Autophagic flux by inducing lysosomal dysfunction in gastric Cancer cells and increases their sensitivity to cytotoxic drugs." *Scientific reports* 8 (1):3593.

Vegliante, R., and M. R. Ciriolo. 2018. "Autophagy and Autophagic Cell Death: Uncovering New Mechanisms Whereby Dehydroepiandrosterone Promotes Beneficial Effects on Human Health." *Vitam Horm* 108:273-307. doi: 10.1016/bs.vh.2018.01.006.

Villalpando Rodriguez, G. E., and A. Torriglia. 2013. "Calpain 1 induce lysosomal permeabilization by cleavage of lysosomal associated membrane protein 2." *Biochim Biophys Acta* 1833 (10):2244-53. doi: 10.1016/j.bbamcr.2013.05.019.

Vincken, J. P., L. Heng, A. de Groot, and H. Gruppen. 2007. "Saponins, classification and occurrence in the plant kingdom." *Phytochemistry* 68 (3):275-97. doi: 10.1016/j.phytochem.2006.10.008.

Vosler, PS, CS Brennan, and J Chen. 2008. "Calpain-mediated signaling mechanisms in neuronal injury and neurodegeneration." *Molecular neurobiology* 38 (1):78-100.

Wang, F., R. Gomez-Sintes, and P. Boya. 2018. "Lysosomal membrane permeabilization and cell death." *Traffic* 19 (12):918-931. doi: 10.1111/tra.12613.

Wang, Fengjuan, Anna Salvati, and Patricia Boya. 2018. "Lysosome-dependent cell death and deregulated autophagy induced by amine-modified polystyrene nanoparticles." *Open biology* 8 (4):170271.

Wang, Yingfei, Ran An, George K Umanah, Hyejin Park, Kalyani Nambiar, Stephen M Eacker, BongWoo Kim, Lei Bao, Maged M Harraz, and Calvin Chang. 2016. "A nuclease that mediates cell death induced by DNA damage and poly (ADP-ribose) polymerase-1." *Science* 354 (6308):aad6872.

Watanabe, Shunsuke, Tatuya Suzuki, Fujio Hara, Toshihiro Yasui, Naoko Uga, and Atuki Naoe. 2017. "Polyphyllin D, a steroidal saponin in Paris polyphylla, induces apoptosis and necroptosis cell death of neuroblastoma cells." *Pediatric surgery international* 33 (6):713-719.

Watson, Ronald Ross. 2011. *Complementary and Alternative Therapies and the Aging Population: An Evidence-based Approach*: Academic Press.

Wei, Gaofei, Jiahong Sun, Zhuang Hou, Weijing Luan, Shuai Wang, Shanshan Cui, Maosheng Cheng, and Yang Liu. 2018. "Novel antitumor compound optimized from natural saponin Albiziabioside A induced caspase-dependent apoptosis and ferroptosis as a p53 activator through the mitochondrial pathway." *European journal of medicinal chemistry* 157:759-772.

Werneburg, Nathan W, M Eugenia Guicciardi, Steven F Bronk, and Gregory J Gores. 2002. "Tumor necrosis factor-α-associated lysosomal permeabilization is cathepsin B dependent." *American Journal of Physiology-Gastrointestinal and Liver Physiology* 283 (4):G947-G956.

Wu, P., X. Zhu, W. Jin, S. Hao, Q. Liu, and L. Zhang. 2015. "Oxaliplatin triggers necrosis as well as apoptosis in gastric cancer SGC-7901 cells." *Biochem Biophys Res Commun* 460 (2):183-90. doi: 10.1016/j.bbrc.2015.03.003.

Xia, Hong-guang, Lihong Zhang, Gang Chen, Tao Zhang, Junli Liu, Mingzhi Jin, Xiuquan Ma, Dawei Ma, and Junying Yuan. 2010. "Control of basal autophagy by calpain1 mediated cleavage of ATG5." *Autophagy* 6 (1):61-66.

Xie, Y, W Hou, X Song, Y Yu, J Huang, X Sun, R Kang, and D Tang. 2016. "Ferroptosis: process and function." *Cell death and differentiation* 23 (3):369.

Xu, Mei-Ying, Dong Hwa Lee, Eun Ji Joo, Kun Ho Son, and Yeong Shik Kim. 2013. "Akebia saponin PA induces autophagic and apoptotic cell death in AGS human gastric cancer cells." *Food and chemical toxicology* 59:703-708.

Xu, Yang, Jen-Fu Chiu, Qing-Yu He, and Feng Chen. 2009. "Tubeimoside-1 exerts cytotoxicity in HeLa cells through mitochondrial dysfunction and endoplasmic reticulum stress pathways." *Journal of proteome research* 8 (3):1585-1593.

Yamashima, T. 2004. "Ca2+-dependent proteases in ischemic neuronal death: a conserved 'calpain-cathepsin cascade' from nematodes to primates." *Cell Calcium* 36 (3-4):285-93. doi: 10.1016/j.ceca.2004.03.001.

Yamashima, T., A. B. Tonchev, T. Tsukada, T. C. Saido, S. Imajoh-Ohmi, T. Momoi, and E. Kominami. 2003. "Sustained calpain activation associated with lysosomal rupture executes necrosis of the postischemic CA1 neurons in primates." *Hippocampus* 13 (7):791-800. doi: 10.1002/hipo.10127.

Yang, W. S., and B. R. Stockwell. 2016. "Ferroptosis: Death by Lipid Peroxidation." *Trends Cell Biol* 26 (3):165-176. doi: 10.1016/j.tcb.2015.10.014.

Yousefi, S., R. Perozzo, I. Schmid, A. Ziemiecki, T. Schaffner, L. Scapozza, T. Brunner, and H. U. Simon. 2006. "Calpain-mediated cleavage of Atg5 switches autophagy to apoptosis." *Nat Cell Biol* 8 (10):1124-32. doi: 10.1038/ncb1482.

Zaffagnini, G., and S. Martens. 2016. "Mechanisms of Selective Autophagy." *J Mol Biol* 428 (9 Pt A):1714-24. doi: 10.1016/j.jmb.2016.02.004.

Zhang, D. M., H. G. Xu, L. Wang, Y. J. Li, P. H. Sun, X. M. Wu, G. J. Wang, W. M. Chen, and W. C. Ye. 2015. "Betulinic Acid and its Derivatives as Potential Antitumor Agents." *Med Res Rev* 35 (6):1127-55. doi: 10.1002/med.21353.

Zhang, Yin, Nai-Di Yang, Fan Zhou, Ting Shen, Ting Duan, Jing Zhou, Yin Shi, Xin-Qiang Zhu, and Han-Ming Shen. 2012. "(−)-Epigallocatechin-3-gallate induces non-apoptotic cell death in human cancer cells via ROS-mediated lysosomal membrane permeabilization." *PloS one* 7 (10):e46749.

Zhu, Yushan, Lixia Zhao, Lei Liu, Ping Gao, Weili Tian, Xiaohui Wang, Haijing Jin, Haidong Xu, and Quan Chen. 2010. "Beclin 1 cleavage by caspase-3 inactivates autophagy and promotes apoptosis." *Protein & cell* 1 (5):468-477.

APPENDIX A

PREVIOUS RESULTS OF AG-08

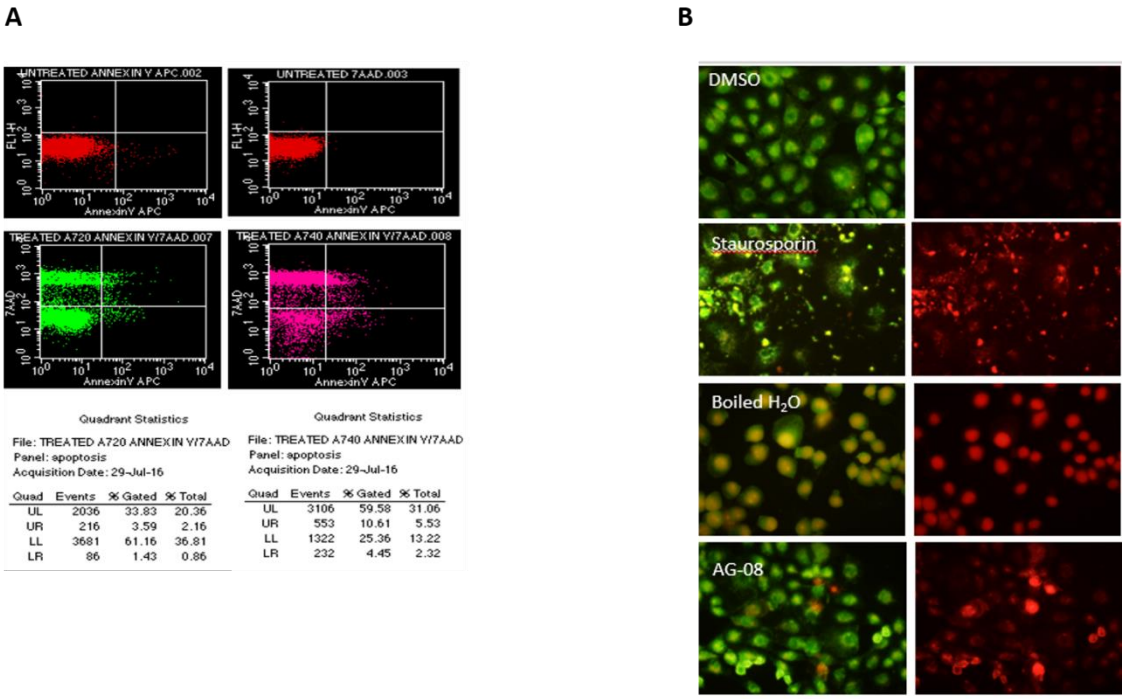

Figure 41. 7-AAD/ Annexin V staining in flow cytometry (A) and acridine orange/ethidium bromide fluorescent staining (B) of AG-08 treated HCC1937 cells. Boiled water was used as necrotic cell death inducer whereas staurosporin was used as apoptotic inducer.

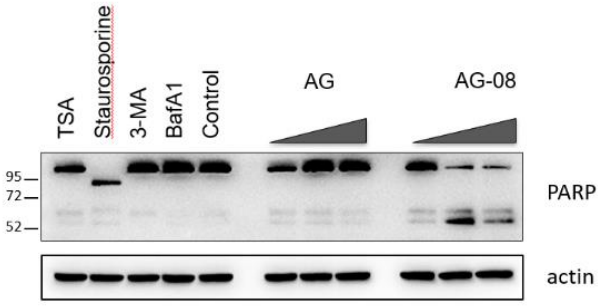

Figure 42. Immunoblotting image which show cleavage of PARP-1 with AG-08 into approximately 50 kDa. Baf A1 and 3-MA (3-metiladenin) was used as autophagic inhibitor, while TSA (trichostatin A) was used as histoneacetylase inhibitor

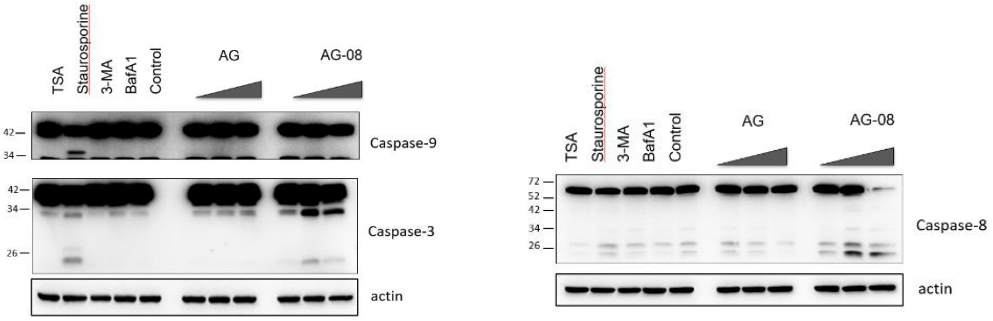

Figure 43. Investigation of caspases activation with AG-08

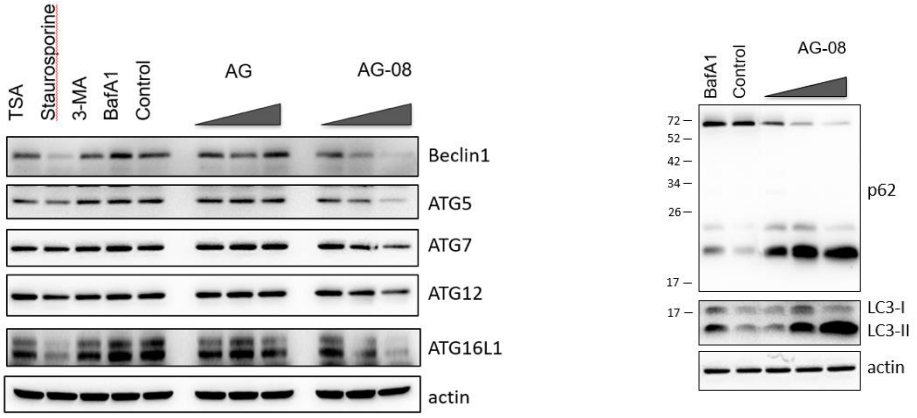

Figure 44. Effect of AG-08 on autophagic marker